



University of Strathclyde

Department of Pure and Applied Chemistry

Nanoparticle Probes for the Study of Biomolecular Interactions

by

Fiona McKenzie

A thesis presented in fulfilment of the requirements for the degree of Doctor of
Philosophy

2010

This thesis is the result of the author's original research. It has been composed by the author and has not been previously submitted for examination which has led to the award of a degree. The copyright of this thesis belongs to the author under the terms of the United Kingdom Copyright Acts as qualified by University of Strathclyde Regulation 3.50. Due acknowledgement must always be made of the use of any material contained in, or derived from, this thesis.

Acknowledgements

I would like to thank my supervisors Prof. Duncan Graham and Dr. Karen Faulds for their advice and discussions throughout my Ph.D research.

I thank Dr. Andrew Ingram for the synthesis of the linker molecule used for the antibody conjugations; Dr. Emma MacFarlane from the Strathclyde Institute of Pharmaceutical and Biological Sciences for cell incubation experiments; and Vivienne Gibson from the Centre of Biophotonics for flow cytometry.

I would like to say a big thank you to Jennifer Dougan for our in-depth discussions and ponderings about oligonucleotide nanoparticles, and all non-science related conversations too! I thank Charlotte, Colette and Jane for making me laugh and Aaron for coming back.

My biggest thank you is to Dr. Robert Stokes for all his advice regarding spectroscopy and nanoscience, but most importantly for always being there to listen and keep me going.

Abstract

There is a growing requirement to be able to detect interactions between biological molecules to develop our understanding of disease expression and progression and for improvement of patient diagnosis in medical applications. One of the most effective ways this can be achieved is to label biomolecules with optically active reporters. To date this has been performed using fluorescent dyes; however there has been recent interest in the use of noble metal nanoparticles due to their large extinction coefficients and near-field properties. This research details the preparation of oligonucleotide functionalised gold and silver nanoparticles for the detection of single and double stranded DNA sequences. The oligonucleotides are modified to incorporate locked nucleic acid (LNA) ribose sugars, affording highly advantageous affinity and selectivity properties. Hybridisation of the probes with the target sequence was monitored colorimetrically and by extinction spectroscopy. Double stranded DNA was targeted through formation of a triple-stranded DNA structure *via* Hoogsteen hydrogen bonding. The nanoparticle probes were further utilised for detection by surface enhanced resonance Raman scattering (SERRS). This method of detection enables multiple DNA sequences to be detected simultaneously due to the molecularly specific and narrow emission spectral profiles obtained. As such, the multiplexing capabilities of this detection method were investigated, indicating that as many as five dye-labelled oligonucleotides could be identified within one spectrum without application of chemometric techniques. A novel method for the incorporation of a SERRS label into oligonucleotide nanoparticle probes was developed which was found to be compatible with a number of commercially available dyes, increasing their potential in multiplexed analysis. Biomolecular SERRS detection was also extended towards cellular analysis using antibody functionalised gold nanoparticles for targeting cell surface receptors. Conjugation was achieved using a novel linker incorporating a chromophore excitable by near-infrared radiation. Using SERRS line mapping, numerous cells could be analysed and were shown to exhibit discrete areas of receptor expression which was quantified by inspection of SERRS intensity and the number of active pixels in the SERRS map.

Abbreviations

A	Adenine
BODIPY TR-X	6-(((4-(4,4-Difluoro-5-(2-thienyl)-4-bora-3a,4a-diaza-s-indacene-3-yl)phenoxy)acetyl)amino)hexanoic acid
C	Cytosine
CCD	Charge Coupled Device
CCL2	Chemokine Receptor 2
CCR2	Chemokine Ligand 2
CD	Circular Dichroism
cDNA	Complementary DNA
CPG	Controlled Pore Glass
CTAB	Cetyltrimethylammonium Bromide
Cy	Cyanine
d	Deoxy
D	Dimensional
DABT PA	3,5-Dimethoxy-4-(6'-azobenzotriazolyl)phenylamine
DLVO	Derjaguin–Landau–Verwey–Overbeek
DMTr	Dimethoxytrityl
DNA	Deoxyribonucleic Acid
DTT	Dithiothreitol
EDC	<i>N</i> -(3-Dimethylaminopropyl)- <i>N'</i> -ethylcarbodiimide hydrochloride
EDTA	Ethylenediaminetetraacetic Acid
ENA	Ethylene Nucleic Acid
FACS	Fluorescence Activated Cell Sorting
FAM	5-(and 6)-Carboxyfluorescein
FBS	Fetal Bovine Serum
FITC	Fluorescein isothiocyanate
FRET	Förster Resonance Energy Transfer
G	Guanine
GM-CSF	Granulocyte-Macrophage Colony-Stimulating Factor
HEG	Hexaethylene Glycol

HEPES	4-(2-Hydroxyethyl)-1-piperazineethanesulfonic acid
HEX	6-Carboxy-2',4,4',5',7,7'-hexachlorofluorescein
HPLC	High Performance Liquid Chromatography
ICAM-1	Intercellular Adhesion Molecule-1
ICG	Indocyanine Green
Ig	Immunoglobulin
iNOS	Inducible Nitric Oxide Synthase
ITC	Isothiocyanate
IU	International Unit
LFA-1	Lymphocyte Function Associated Antigen-1
LNA	Locked Nucleic Acid
LPS	Lipopolysaccharide
^m C	5-methylcytosine
MG	Malachite Green
MHC	Major Histocompatibility Complex
MWCO	Molecular Weight Cut-Off
NHS	<i>N</i> -hydroxysuccinimide
NIR	Near-Infrared
PBS	Phosphate Buffered Saline
PCR	Polymerase Chain Reaction
PE	Phycoerythrin
PEG	Poly(ethylene)glycol
PNA	Peptide Nucleic Acid
PSA	Prostate Specific Antigen
R6G	Rhodamine 6G
RCF	Relative Centrifugal Force
RNA	Ribonucleic Acid
ROX	X-Rhodamine
rpm	Revolutions Per Minute
SAM	Self-Assembled Monolayer
SAXS	Small Angle X-ray Scattering
SEM	Scanning Electron Microscopy

SERRS	Surface Enhanced Resonance Raman Scattering
SERS	Surface Enhanced Raman Scattering
SET	Surface Energy Transfer
SNP	Single Nucleotide Polymorphism
SPR	Surface Plasmon Resonance
SWNT	Single Walled Nanotubes
T	Thymine
TAMRA	5-(and-6)-Carboxytetramethylrhodamine
TET	6-Carboxy-2',4,7,7'-tetrachlorofluorescein
TFO	Triplex Forming Oligonucleotide
T _m	Melting Temperature
TRITC	TAMRA Isothiocyanate
tRNA	Transfer Ribose Nucleic Acid
U	Uracil
UV	Ultra Violet
XPS	X-ray Photoelectron Spectroscopy

Contents

1	Introduction	1
1.1	Nanoparticles	2
1.1.1	Surface Plasmon Resonance	2
1.1.2	Surface-Enhanced Raman Scattering	3
1.1.3	Nanoparticle Aggregation	8
1.1.4	Self-Assembled Monolayers	9
1.2	DNA	11
1.2.1	DNA Oligonucleotides	12
1.2.2	Oligonucleotide Modifications	15
1.2.3	Triplex Forming Oligonucleotides	18
1.2.4	Oligonucleotide Nanoparticle Conjugates	22
1.2.5	SERS Analysis of Oligonucleotides	30
1.3	Nanoparticle Functionalisation with Protein Structures	34
1.3.1	Protein Functionalised Nanoparticles in Detection Assays	37
1.3.2	SERS Measurements from Cells	38
2	Aims	42
3	Experimental	43
3.1	Gold Nanoparticle Synthesis	43
3.2	Silver Nanoparticle Synthesis	43
3.3	LNA Functionalised Nanoparticles	44
3.4	SERRS Analysis of DNA	46
3.4.1	Multiplexed SERRS Analysis	46
3.4.2	Propargylamine Modified Oligonucleotides	47
3.4.3	In-Sequence Labelling	48
3.4.4	Nanoparticle Labelling	49
3.4.5	Mixed Metal Nanoparticle Duplex	51

3.4.6 SERRS Triplex	53
3.5 Antibody Functionalised Nanoparticles	54
3.5.1 Antibody Conjugation	55
3.5.2 Streptavidin Bead Capture	55
3.5.3 Antibody Quantitation	56
3.5.4 Cell Incubation	56
3.5.5 Cell Analysis	56
4 Nanoparticle Modified Oligonucleotides	58
4.1 LNA Functionalised Nanoparticles	58
4.2 LNA Functionalised Nanoparticles Triplexes	67
4.3 Polyethylene Glycol Spacing	72
4.4 Conclusions	77
5 DNA Detection by SERRS	79
5.1 SERRS Analysis of DNA Oligonucleotides	79
5.2 In-Sequence Labelling	88
5.3 Nanoparticle Labelling	91
5.4 Mixed Metal Analysis	109
5.5 SERRS Labelled Triplex	114
5.6 Conclusions	120
6 SERRS Analysis of Cells	122
6.1 Antibody Functionalised Nanoparticles	122
6.2 Cell Mapping	134
6.3 Lipopolysaccharide Stimulation	140
6.4 CD40 Target	143
6.5 Conclusions	145
7 Conclusions	147

8 Further Work	150
References	153
Appendix	162
A1 Cell Preparation Experimental	162
A2 T-test Calculations from Chapter 6	164
A3 Publications	168
Quantitative Simultaneous Multianalyte Detection of DNA by Dual-Wavelength Surface-Enhanced Raman Scattering	168
Evaluation of the Number of Modified Bases Required for Quantitative SERRS from Labelled DNA	171
Sequence-Specific DNA Detection Using High-Affinity LNA- Functionalized Gold Nanoparticles	174
LNA Functionalized Gold Nanoparticles as Probes for Double Stranded DNA through Triplex Formation	177
SERRS Coded Nanoparticles for Biomolecular Labelling with Wavelength-Tunable Discrimination	180
Rapid Cell Mapping using Nanoparticles and SERRS	188
Quantitation of Biomolecules Conjugated to Nanoparticles by Enzyme Hydrolysis	194
Controlled Assembly of SERRS Active Oligonucleotide- Nanoparticle Conjugates	197

1. Introduction

The completion of the Human Genome Project in 2003 can be considered one of the most significant scientific achievements in recent history. The project set out to completely identify all of the genes within human DNA and determine their DNA sequences.^{1,2} This has led to significant advances in gene testing technologies which enable diagnosis of and identification of whether a patient may be predisposed to genetic diseases. The large scale study of proteins, proteomics, is also underway which aims to identify and investigate the function of the full protein complement expressed by an organism in an effort to understand the role of specific proteins in disease. Investigation into gene and protein expression demands specific biological interactions to be probed and identified. This may be achieved through labelling the biomolecule with a component possessing certain properties to allow it to be detected within a biological system, whether *in vitro* and *in vivo*. Optical detection is one of several transduction techniques that are utilised for monitoring the occurrence of ligand-receptor binding reactions. Fluorescence spectroscopy is the most commonly used optical method for monitoring DNA hybridisation events in the polymerase chain reaction (PCR) and microarray technologies and confocal fluorescence microscopy is an established technique employed in many research labs for cellular analysis. The disadvantages to utilising fluorophores for biomolecule labelling, such as photobleaching, limited multiplexing potential and expensive detection equipment, has prompted research into the development of nanoparticle-based detection systems. Metal nanoparticles have extinction coefficients many orders of magnitudes larger than organic fluorescent dyes, providing a highly sensitive, colorimetric response when analysed by transmission extinction spectroscopy. Nanoparticles can also be used for Raman scattering enhancement (surface enhanced Raman spectroscopy, SERS) and coupled with a resonant dye yields surface enhanced resonance Raman spectroscopy (SERRS). Other detection strategies involving metallic nanoparticles include gravimetric^{3, 4} and electrochemical⁵ methods.

The functionalisation of metallic nanoparticles with biomolecules for monitoring biological interactions using optical detection techniques is reported herein. This work is not a fundamental study of the optical properties of nanomaterials. For this, the reader is directed to the work of Käll,⁶⁻⁸ Kneipp,^{9, 10} and Moskovits.^{11, 12} This work approaches the control and application of nanomaterials within the context of applied molecular biology.

1.1 Nanoparticles

1.1.1 Surface Plasmon Resonance

Noble metal nanoparticles are increasingly finding applications in bioanalytical science due to their near-field and far-field optical properties. Metal nanoparticles exhibit a maximum extinction termed the plasmon resonance band; a property that is not associated with the bulk metal. Application of an external electromagnetic field results in polarisation of the nanoparticle surface electrons which is succeeded by a linear restorative force arising from the coulombic repulsion of the electrons. This results in a collective oscillation of the electrons which is characterised by the resonance band in the UV-visible spectrum of the metal (figure 1.1). For many metals, including Pb, Hg, Sn, the plasmon resonance frequency lies in the UV region and therefore they cannot be employed for use in colorimetric applications, whereas the coinage metals, Cu, Ag and Au find greater use due to the plasmon resonance being of visible wavelength. These metals are also nobler and less susceptible to oxidation.¹³ Mie theory¹⁴ describes the extinction of metallic nanoparticles and specifies that the dielectric constant of the metal and the surrounding medium, as well as the size, shape and monodispersity of the nanoparticles all have an effect on the resultant spectrum. It is the sensitivity of the surface plasmon resonance (SPR) to changes in the local refractive index surrounding the nanoparticles that makes metallic nanoparticles ideal candidates for biosensing. The far-field properties of nanoparticles may be exploited in two ways for biosensing applications. Firstly, intra-particle SPR may be utilised which involves conjugating receptor biomolecules

to nanoparticles and then binding the target molecule which will result in a change in the dielectric constant of the immediate surroundings.

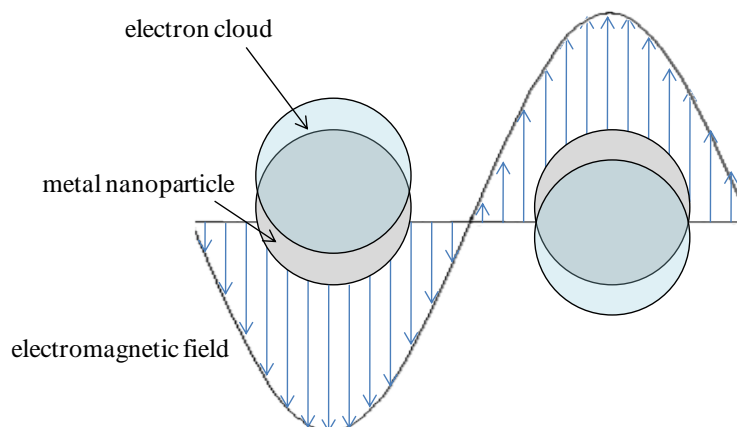


Figure 1.1 Electron displacement under the influence of an electromagnetic field

Whereas, inter-particle SPR involves conjugating both receptor and target molecules to nanoparticles which will interact and generate nanoparticle aggregates. Aggregated nanoparticles are able to interact with each other through a dipole coupling mechanism affording optical properties associated with a single larger particle. The plasmon resonance is red-shifted giving rise to a broad plasmon band at much longer wavelengths and is of a lower intensity. Factors such as the size of the aggregate and interparticle spacing will affect the extent to which the extinction maximum is altered.

1.1.2 Surface-Enhanced Raman Scattering^{15, 16}

The optical properties of nanoparticles can also be exploited in the enhancement of Raman scattering signals. Raman scattering is a form of vibrational spectroscopy and is concerned with the inelastic scattering of light from a molecule. The majority of light scattered by molecules is termed Rayleigh scattering; an elastic process that does not induce any molecular energy changes. However, one in every 10^6 - 10^8

photons involves a change in energy and is termed Raman scattering. In this process, incident light will interact with a molecule resulting in polarisation of the electron clouds surrounding the nuclei, this is accompanied by a transfer of energy from the incoming photons into the electrons to form a highly unstable species referred to as a virtual state. The light energy is released almost immediately as scattered radiation. Molecular energy changes will occur if the nuclei begin to move on generation of the virtual state. In such instances, the scattered light will be of an altered energy to the incident light. Raman scattering from a molecule which was initially in the ground vibrational state leads to Stokes Raman lines, whereas a molecule in a vibrationally excited state will generate anti-Stokes lines (figure 1.2). The energy gained and subsequently lost is equal to the energy of the vibration and hence a unique Raman spectrum is obtained for each molecule.

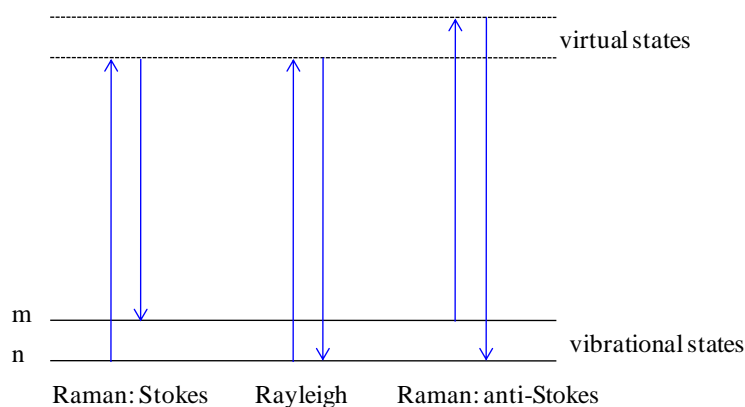


Figure 1.2 Vibrational transitions involved in light scattering

Due to the extremely low number of photons that are Raman scattered, Raman spectroscopy is often thought of as a relatively insensitive analytical technique. However, the sensitivity can be greatly improved by use of surface-enhanced Raman scattering (SERS), with signal intensities increasing by up to 6 orders of magnitude over conventional Raman scattering. Albrecht and Creighton¹⁷ and separately, Van Duyne and Jeanmaire¹⁸ attributed the increased Raman signals observed by Fleischmann *et al.*¹⁹ to an enhancement of the Raman signal instead of an increased surface area for analyte adsorption as a result of roughening of the electrode. Other

examples of suitable metal surfaces that have been used for surface enhancement purposes include metal nanoparticles,^{20, 21} roughened electrodes,¹⁷ metal island films^{22, 23} and lithographically prepared nanoparticle arrays.^{7, 24} There are two proposed mechanisms for the observed increases in signal intensities which have been related to the molecular polarisability and applied electric field parameters used to define the intensity of Raman scattering. The electric field parameter has been used to formulate the electromagnetic enhancement theory. When the excitation wavelength is resonant with the surface plasmons on the metal surface, light characteristic of the dipolar radiation is emitted, significantly increasing the applied electric field experienced by the molecule. Enhancement associated with the polarisability parameter is known as chemical enhancement. In its simplest terms, chemical enhancement theory describes the transfer of charge from the metal surface to the analyte meaning a greater degree of polarisation can occur. The electric field radiated by the metal particle (E_S) and experienced by the Raman active molecule can be represented as:

$$E_S = gE_0 \quad (1.1)$$

where g is the enhancement factor and E_0 is the incident field. Therefore the Raman scattered light (E_R) will be proportional to E_S and the polarisability of the molecule (α_R):

$$E_R \propto \alpha_R E_S \propto \alpha_R g E_0 \quad (1.2)$$

It should be noted that although α_R is referred to as the polarisability of the Raman active molecule, for SERS this is actually the polarisability of the scatterer and since the molecule is adsorbed to the metal surface, the metal will contribute particularly if a charge transfer event has occurred as is the case for chemical enhancement.

In addition to the incident light, the Raman scattered light is also enhanced by the metal particle; in effect there are two opportunities for surface enhancement to occur. As such the SERS field (E_{SERS}) becomes:

$$E_{SERS} \propto \alpha_R g g' E_0 \quad (1.3)$$

Where g' denotes the enhancement factor associated with the Raman scattered light. The intensity of the SERS light is the square modulus of E_{SERS} so that:

$$I_{SERS} \propto |\alpha_R|^2 |gg'|^2 I_0 \quad (1.4)$$

For low frequency bands, $g \cong g'$ therefore I_{SERS} becomes proportional to the fourth power of the enhancement of the incident field.

It is sometimes difficult to relate a SERS spectrum to its corresponding Raman spectrum. A common observation is the appearance of new bands, often arising due to a change in the molecule's centre of symmetry on adsorption to the metal surface. Another problem that may be encountered is a non-linear relationship between analyte concentration and signal intensity. This may come about due to the molecules adopting different orientations on the surface as monolayer coverage concentrations are approached.

SERRS is a combination of surface enhanced and resonance enhancement factors. Resonance Raman scattering involves Raman scattering from a molecule incorporating a chromophore, resulting in signal enhancements of up to 10^6 .¹⁶ Similar to electronic absorption, electrons are promoted to an excited electronic state (not a virtual state as for non-resonant Raman scattering), however the time the electrons exist in the excited state is considerably shorter for resonant scattering compared with absorption. The scattering process does not allow for the nuclei to reach equilibrium positions in the excited state whereas equilibrium geometry is reached for absorption processes. For analysis of a sample by resonance Raman scattering, a laser should be chosen with an excitation wavelength as close to the absorption maximum of the coloured molecule as possible. SERRS, although possibly occurs as one process, can be considered as the combination of two enhancement factors. The enhancement provided by SERRS is greater than the additive effect of surface and resonance enhancement, with increases in signal intensities of up to 10^{14} .^{9, 25, 26} With resonance Raman scattering, a large proportion of incident light is absorbed and can lead to fluorescence interference, due to the

occurrence of fluorescence emission in the Stokes region of the spectrum. However fluorescence is quenched by the metal surface in SERRS analyses resulting in considerably reduced background signals. It has been reported that fluorescence quenching by nanoparticles occurs through a dipole-surface energy transfer process (SET) similar to the dipole-dipole interactions in Förster resonance energy transfer (FRET).²⁷ The quenching efficiency is inversely proportional to the fourth power of the distance from the nanoparticle surface and quenching has been observed up to 250 Å from the nanoparticle surface for a 1.4 nm Au cluster. SERRS spectra are also less likely to show the presence of contaminants, a problem sometimes encountered in SERS spectra, due to the additional resonant enhancement of the target chromophore.

In nanoparticle-based analyses, the SE(R)RS signals can be enhanced furthermore by aggregation of the nanoparticles. Nanoparticle aggregation increases SE(R)RS intensities for two reasons: firstly, the plasmon resonance wavelength of the nanoparticles is red-shifted which may improve its coincidence with the absorption maximum of the dye (in the case of SERRS) and laser excitation wavelength, depending on which experimental conditions are employed;²⁸ and secondly, highly intense electromagnetic fields are present at the junction of aggregated nanoparticles, often referred to as 'hot spots'. Studies by Khan *et al.* have shown that less than 10 % of single citrate-reduced silver nanoparticles are SERS active, emphasising the necessity for aggregation. They showed that as the number of particles in the aggregate increases, the percentage of species that exhibit SERRS activity dramatically increases.^{29, 30} M^cMahon *et al.* have performed a comprehensive investigation into the electromagnetic enhancements at different nanoparticle separations using finite element calculations, a computational electrodynamics method used to predict spectral output.³¹ It was shown that as the edge-to-edge distance decreased from 1 to 0.5 nm, the enhancement increased from 10^8 to 10^{10} , and when the nanoparticle edges were touching (0 nm), the enhancement reached 10^{14} . The maximum electromagnetic enhancements were found at the nanoparticle junction along the dipolar axis, and coincided with peaks in the extinction spectra of multipole resonances. This was unexpected since multipoles are not orientated along

this axis however was attributed to the possibility of hybrid multipole-dipole resonances and the fact that the dimer behaves as an antenna for focusing the electromagnetic field towards the interparticle junction. The probability distributions of electromagnetic enhancement were determined for nanoparticles coated with a monolayer of molecules of varying diameters. Enhancements of lower magnitudes were calculated for the larger molecules, presumably because the molecules cannot fit into the interparticle crevice as easily. For all nanoparticle spacings and molecule sizes, it was found that 3 % of molecules are responsible for greater than 90 % of the SERS signal.

1.1.3 Nanoparticle Aggregation

Metal nanoparticles are susceptible to uncontrolled aggregation in solution, limiting their practical applicability, unless their surface chemistry is carefully regulated. Colloidal nanoparticles are thermodynamically unstable relative to their bulk, however are kinetically stable due to steric and/or electrostatic barriers on the surface of the nanoparticle.

One of the most common preparation methods for noble metal nanoparticles involves the reduction of the metal salt. Commonly used reducing agents include citrate,²⁰ borohydride,²⁰ and EDTA.³² During the latter stages of synthesis, unoxidised reducing agent adsorbs onto the nanoparticle surface, rendering the particle negatively charged. The sphere incorporating the noble metal nanoparticle and the layer of negative charge is termed the radius of shear. Surrounding this is another layer of mobile ions of opposite charge. Collectively they are referred to as the electrical double layer. The total free energy of interaction as described by Derjaguin–Landau–Verwey–Overbeek (DLVO) theory is:

$$G = G_{\text{van der Waals}} + G_{\text{electrostatic}} \quad (1.5)$$

Since the nanoparticles possess negative charges on their surface, the electrostatic component will be a repulsive force, whereas Van der Waals will be attractive. Non-

DLVO forces comprise of steric, hydrophobic and solvation effects and also significantly contribute towards colloidal stability.

To initiate nanoparticle aggregation, the stabilising electrostatic component needs to be reduced. This can be achieved by neutralisation of the anionic surface charge afforded by surface-bound reducing agent.²⁸ There have been several investigations into the most effective aggregating agent to use^{21, 33} where it has been found that while NaCl and HNO₃ give rise to the strongest SERS intensities upon addition, the reproducibility of the signal is best achieved when the organic agents, poly-L-lysine and spermine are employed.³³ It should also be noted that the addition of some dyes to metal colloids will induce aggregation³⁴ due to either their hydrophobic or electrostatic properties.

Aggregation is a dynamic process and a point in time will be reached where the nanoparticle aggregates grow so large that they precipitate out of solution; an undesirable consequence for solution-based experiments. Therefore it is essential that the extent of aggregation can be controlled. Indeed, for non-SE(R)RS analyses, aggregation may be unwanted entirely. As such, it is necessary to manipulate the nanoparticle surface chemistry to fit the requirements of the experiment. The free energy equation can be modified to incorporate non-DLVO forces which comprises of steric, hydrophobic and solvation forces. Steric protection is achieved by functionalisation of the nanoparticles with a species that has an affinity for the nanoparticle surface. This has been extensively reported in the literature using alkane thiols.

1.1.4 Self-Assembled Monolayers (SAMS)

Alkanethiols spontaneously self-assemble on gold surfaces to form an organised layer. The thiol group chemisorbs onto the gold surface resulting in a gold-alkane thiolate complex with a binding energy of between 40-45 kcal mol⁻¹.³⁵ The exact mechanism by which this occurs is still debated, although the adsorption process is likely to also involve displacement of the stabilising anionic layer formed in the reduction step of nanoparticle synthesis.^{36, 37} Adsorption of thiols onto gold

nanoparticle surfaces can be considered as similar to the generation of SAMS on planar surfaces however nanoparticle surface ligands can pack together more densely due to the curvature of the nanoparticle surface. It has been reported that the density of immobilised thiol-modified oligonucleotides on nanoparticle surfaces approaches the density of that on planar surfaces the larger the nanoparticle is and experimentally has been found to occur for diameters above 60 nm.³⁸ It can be assumed that sulfur-containing molecules approach the surface as thiols due to their high pKa values (10-11) although there has been conflicting evidence as to whether the thiol hydrogen is released as H₂ or H⁺ upon adsorption.³⁶ The oxidation state of the gold metal in the resultant complex is also ambiguous; Brust has presented X-ray photoelectron spectroscopy (XPS) evidence that suggests the gold exists primarily as Au (0);³⁹ whereas Sandroff and Herschbach concluded that Au (I) and Au (0) sites co-exist on the nanoparticle surface.⁴⁰ The crystal structure of a *p*-mercaptobenzoic acid protected gold nanoparticle has recently been solved by Jadzinsky *et al.*⁴¹ They report that the majority of the gold atoms form a densely packed core however there is an outershell of gold atoms that binds strongly to the gold (I) thiolate species. There have been investigations into the fate of the thiolated ligand upon adsorption onto the nanoparticle surface. Murray *et al.* investigated the mechanism for ligand exchange using alkane thiols on monolayer protected clusters. They reported that in the presence of oxygen or under high temperatures, an equilibrium exists between surface-bound alkane thiols and dissociated Au (I) thiolates and that Au (I) SR behaves as a catalyst towards exchange of bound and free ligands.⁴² Chechik and co-workers employed electron paramagnetic resonance to investigate lateral diffusion of a disulfide ligand on Au nanoparticles. They suggested that lateral diffusion was negligible and ligand rearrangement was more likely to be the result of desorption and readsorption.⁴³

Modification of thiol ligands with biomolecules largely affects their packing on the surface due to steric and electrostatic factors. As such, the ligands may not self assemble at all due to secondary interactions of the biomolecule with the gold surface. Recently there has been significant research into the functionalisation of nanoparticles with biomolecules, namely DNA, proteins and antibodies.

1.2 DNA

DNA is composed of many nucleotide units arranged in a linear chain. A single nucleotide consists of a deoxyribose sugar, a heterocyclic base, and a phosphate ester residue.

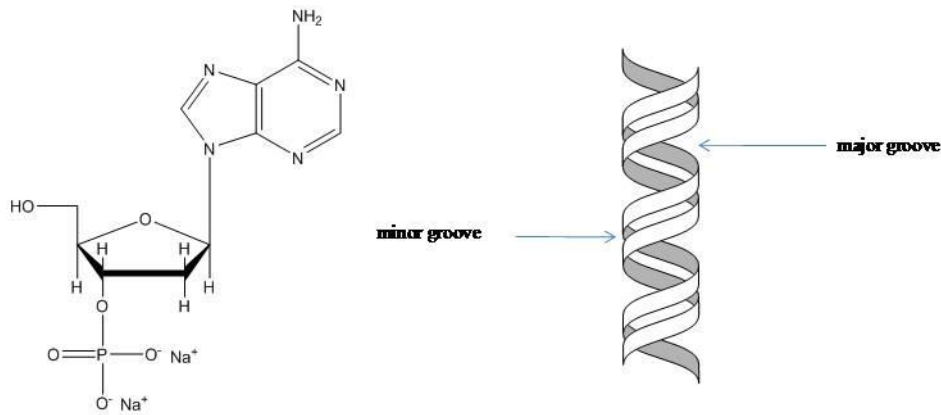


Figure 1.3 DNA nucleotide (deoxyadenosine 3' phosphate) and the DNA double helix

The heterocyclic bases are adenine, thymine, cytosine and guanine, each having specific hydrogen donating and accepting sites. The hydrogen bonding nature of the bases allows the DNA chains to organise into its secondary structure, an anti-parallel double helix featuring a major and minor groove. This is the predominant form of DNA in the human body. Adenine bases will only bond with thymine; and cytosine only bonds with guanine meaning that single strands hybridise in a highly specific manner.

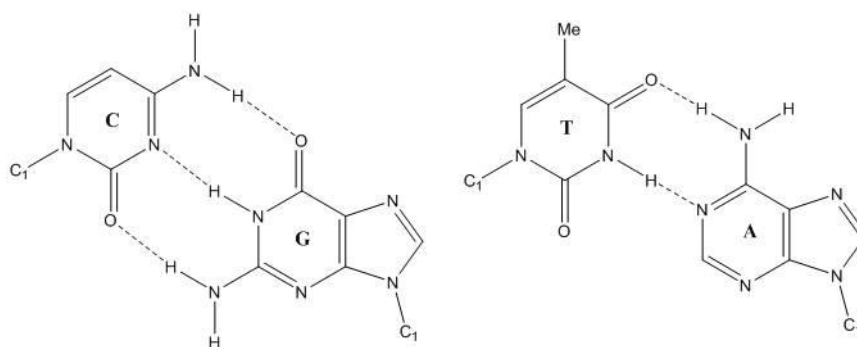


Figure 1.4 Watson-Crick base pairing of cytosine with guanine and thymine with adenine. C₁ refers to carbon 1 on the ribose sugar.

Figure 1.4 illustrates the Watson-Crick base pairing of the DNA bases. Although Watson-Crick base pairing is the most dominant pairing between single stranded DNA, other patterns exist such as wobble pairs which are present in tRNA and Hoogsteen base pairings which occur in triple-stranded DNA structures.

1.2.1 DNA Oligonucleotides

DNA can be synthesised artificially *ex vivo* to produce relatively short strands termed oligonucleotides. Oligonucleotide synthesis is performed on a solid support, controlled pore glass (CPG), and involves the introduction of phosphoramidites to a growing chain of nucleotides using an orthogonal protection strategy (figure 1.5). Unlike natural DNA synthesis involving enzymes which occurs in a 5' to 3' direction, oligonucleotide synthesis takes place in a 3' to 5' direction. The first step of the synthetic cycle is to deprotect the 5' hydroxyl group which is achieved by hydrolysis of the dimethoxytrityl group using dichloroacetic acid. This then allows coupling with the incoming phosphoramidite featuring the next base in the resultant oligonucleotide sequence. Approximately 1 % of the hydroxyl groups are not successfully coupled with the phosphoramidites and so they need to be capped to prevent unwanted side reactions. This is achieved using acetic anhydride and *N*-methylimidazole. The final step of the cycle is oxidation of the phosphorous in the DNA backbone from P³⁺ to P⁵⁺. The oligonucleotide sequence is cleaved from the CPG alongside deprotection of the bases using ammonium hydroxide.

The ability to synthesise oligonucleotides is highly advantageous for diagnostic applications. If the oligonucleotide sequence is modified to incorporate a label, then the complementary target sequence can be detected through hybridisation of the two strands. Oligonucleotides have found much use commercially in microarray formats for the identification of genetic diseases within biological DNA samples. As such, there has been significant effort towards improving the stability of the oligonucleotide-DNA target duplex.

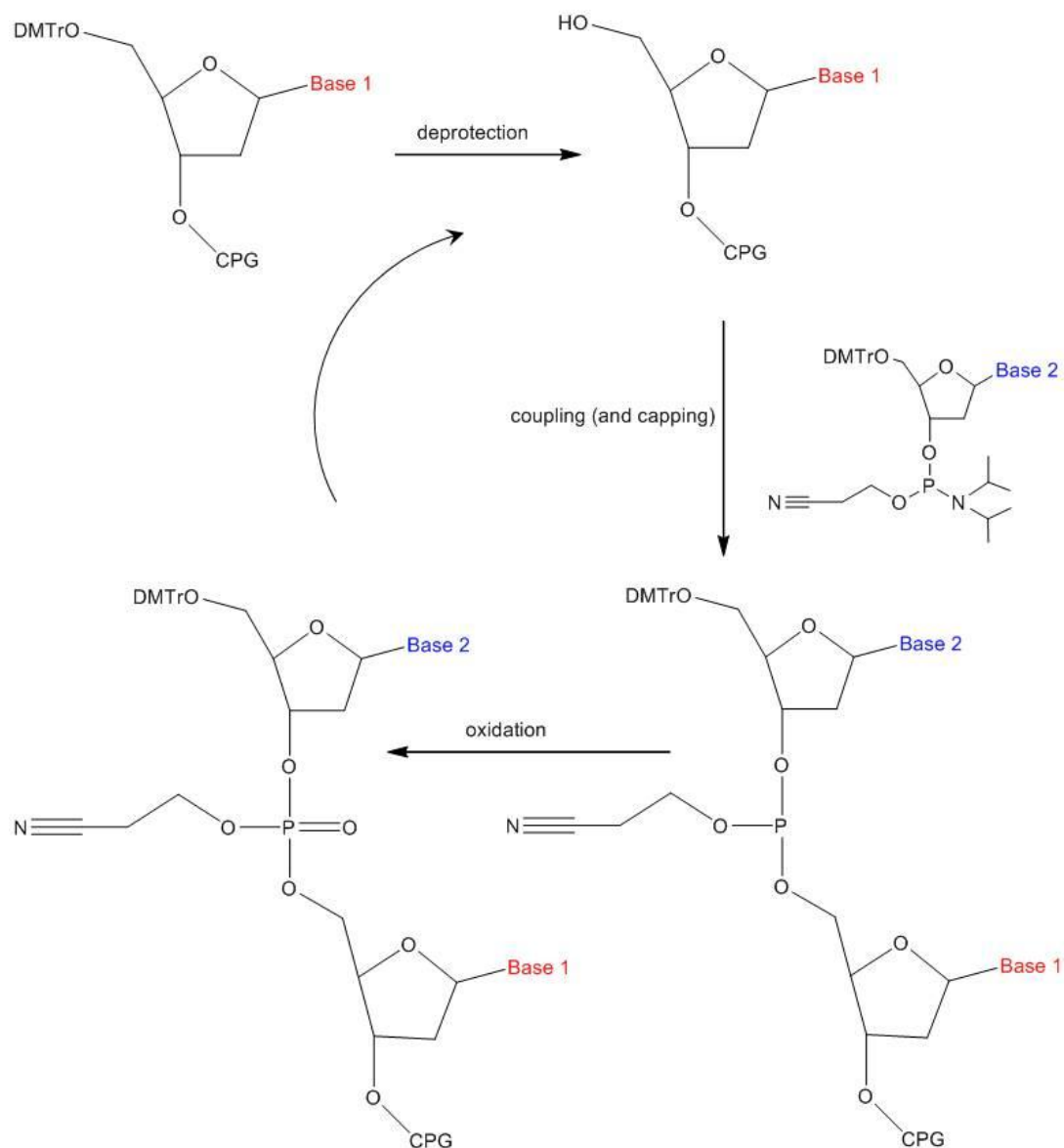


Figure 1.5 DNA oligonucleotide synthesis

One of the prime methods for determining the thermal stability of the duplex is to use UV-visible spectroscopy by exploiting DNA hyperchromicity. The double helix may be denatured by the application of heat or changes in pH and the subsequent transition of double stranded DNA to single stranded may be monitored by inspection of a UV melting curve (figure 1.6). It is only the nucleotide bases that significantly contribute to the absorption of UV light above 230 nm, with molar

extinction values of around $10^4 \text{ dm}^3 \text{ cm}^{-1} \text{ mol}^{-1}$. Upon hybridisation, the Π interactions that exist between the bases when they stack face-to-face affect the dipoles of the bases, resulting in a decrease in absorption at 260 nm. This phenomenon is known as hypochromicity and is reversible by denaturing the hybridised duplex, that is, the DNA will exhibit hyperchromicity.⁴⁴ The sigmoidal shape is characteristic of the cooperative melting process. Regions rich in AT content melt first, due to weaker stabilisation between the base pairs compared with CG, which in turn destabilises adjacent helical structure. The result is a concerted denaturation of the double stranded helix. The point of inflection is referred to as the melting temperature (T_m); the greater the melting temperature, the greater the stability of the duplex.

There are several factors affecting the stability, namely the length and GC content of the oligonucleotide, and the electrolyte concentration. DNA strands of greater lengths and GC base pairs have more hydrogen bonding sites and will confer stability to the double stranded DNA. Often electrolyte solutions, for example NaCl, are used to reduce electrostatic repulsion occurring between the negatively-charged phosphate backbones so the greater the abundance of positive counter-ions, the more stable the double stranded DNA.

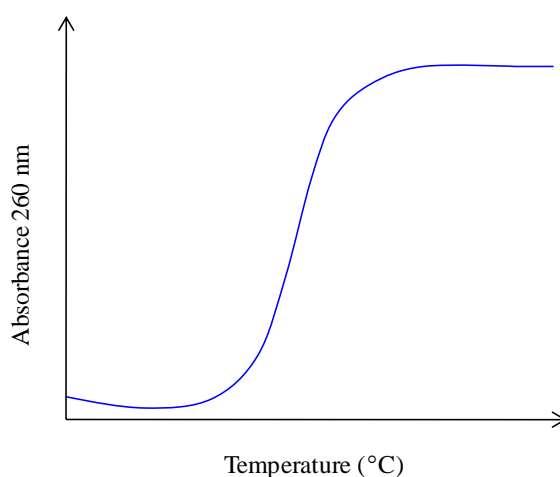


Figure 1.6 UV DNA melting curve

1.2.2 Oligonucleotide Modifications

Probe oligonucleotides may be modified in several ways to improve duplex thermal stability. Base stacking interactions contribute a significant amount of the favourable enthalpy necessary for duplex formation⁴⁵ and so pyrimidine nucleobases have been modified to improve these interactions (dipole-dipole and dipole-induced dipole) by the addition of a polarisable group, such as propyne⁴⁶ to the nucleotide base. Incorporation of the adenine analogue, 2,6 diaminopurine into oligonucleotides increases duplex thermal stability due to the additional hydrogen bond provided by an amino group located in the minor groove of AT and AU base pairs.⁴⁷ It has been proposed that the stacking interactions are also improved due to the increased dipole moment of diaminopurine-thymine base pairs (2.3 compared with 1.7 of AT base pairs). Another base modification employed for increasing thermal stability is 5-methylcytosine, due to an increased enthalpic contribution towards hybridisation.⁴⁸ 5-methylcytosine has also been incorporated into oligonucleotides designed for hybridising to double stranded DNA, that is, formation of triple-stranded DNA (section 1.2.3).

There have been several attempts to reduce the destabilisation caused by electrostatic repulsion from the negatively charged phosphate groups on the DNA backbone. Peptide nucleic acid (PNA) possesses no formal charge and is able to form stable duplexes with DNA and RNA.⁴⁹ Charge neutralisation may also be achieved by introduction of positive charges to the oligonucleotide for example, incorporation of O-amino alkyl groups at the 2' position on the pentose sugar.⁵⁰ Other modifications employed include morpholino backbones,⁵¹ methylphosphonates,⁵² and phosphorodithioates⁵³ illustrated in figure 1.7.

DNA structure may be preorganised into conformations favourable towards duplex formation. This can be achieved by forcing the ribose sugar to adopt a C3' endo conformation. DNA that possesses C3' endo pucker is referred to as A-DNA; C2' endo is associated with B-DNA (figure 1.8).

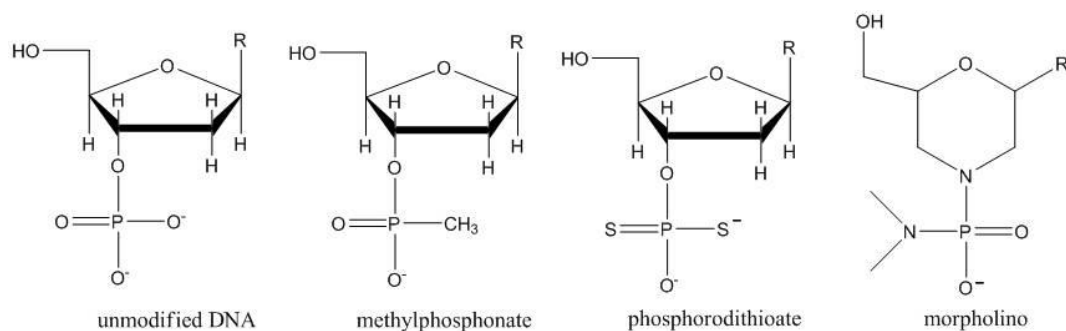


Figure 1.7 Examples of DNA backbone modifications

A-DNA has a broader shape with the major groove narrowing and deepening, and the minor groove becoming broader and shallow. Locked nucleic acid (LNA) is a commercially available oligonucleotide that incorporates a 2'O, 4'C methylene bridge across the ribose sugar (figure 1.9) resulting in C3' endo pucker. Its synthesis was first reported independently by Obika *et al.*⁵⁴ and Wengel.⁵⁵ In 1998, LNA was labelled as the most thermally stable nucleic acid duplex yet discovered⁵⁶ and has been shown to increase thermal stabilities by up to 7 °C *per monomer*.⁵⁷

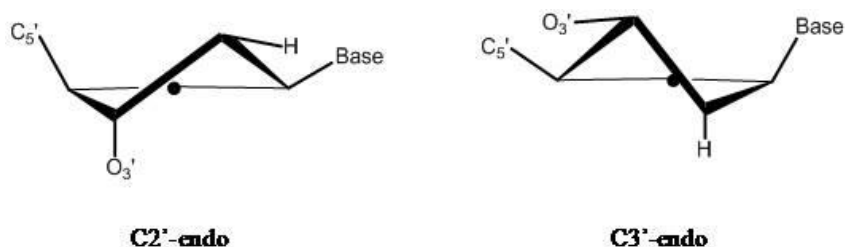


Figure 1.8 C2' and C3' sugar conformations.

It has been likened to RNA due to its A-form character which has reportedly been observed by introducing only one LNA monomer into a 10-mer oligonucleotide.⁵⁸ The source of stabilisation has been the subject of much discussion; it seems that whether an enthalpic or entropic component is responsible is dependent on the oligonucleotide sequence.

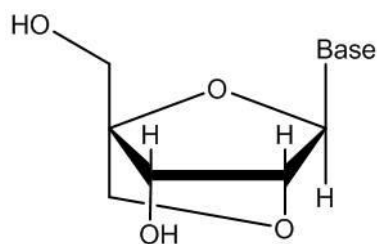


Figure 1.9 LNA

Enthalpic stabilisation is brought about by increased base stacking interactions and hydrogen-bonding, whereas entropic stabilisation can be attributed to the preorganised LNA structure. McTigue *et al.*⁵⁹ performed a comprehensive investigation into the thermodynamic parameters of modified duplexes with LNA modifications in different locations throughout the sequence. They discovered that stabilisation was the result of either enthalpic or entropic contributions, but not both at the same time and that LNA duplexes exhibited enthalpy/entropy compensation, that is the two components are inversely proportional to one another. They report that for most duplexes, entropy is the dominant factor but for oligonucleotides with the highest thermal stabilities, enthalpy is responsible. LNA pyrimidines were determined to confer greater stability than purines in the order of: C > T > G >> A however stabilisation effects are context-dependent. Although LNA purines afford less stability, a purine adjacent to an LNA pyrimidine will enhance stability. Nielsen *et al.*⁶⁰ used ¹H spectroscopy to determine the solution structure of LNA. They noted a structural strain between the A-type LNA and B-type DNA which was relaxed upon conformational rearrangements of the phosphate backbone to favour increased base stacking. Egli *et al.*⁵⁸ solved an X-ray crystal structure of an LNA duplex and identified water molecules hydrogen bonded to the oxygen in the ribose bridge. They commented that hydration of hydrogen bonding sites and acceptors is usually accompanied by an increase in thermal stabilisation however were unable to establish the contribution this would have on the overall observed stability. The effects of counterion content and hydration on the thermodynamics of LNA duplex formation has been studied by Kaur *et al.*⁶¹ It was found that LNA duplexes uptake more sodium ions compared to unmodified duplexes which has been attributed to the

higher charge density of A-DNA. This could account for observed decreases in entropy. It was also found that less water molecules were associated with the LNA duplex which is consistent with A-type geometry structures.

LNA has found much use recently as a triplex forming oligonucleotide (TFO). LNA oligonucleotides are able to form stable hybrids with double stranded DNA resulting in triple-stranded structures.^{62, 63}

1.2.3 Triplex Forming Oligonucleotides

There has been considerable effort into developing synthetic oligonucleotides for binding to double stranded DNA for antigene applications, that is, the interruption of genetic transcription. The ability to target double stranded DNA would also be beneficial in terms of diagnostic applications. At present, DNA microarrays and solution-based assays employed for the detection of gene sequences make use of oligonucleotide hybridisation to single stranded DNA. This method requires denaturation of the double stranded sample DNA prior to hybridisation with the labelled probe. The ability to target duplex DNA would allow the removal of this step.

There are several limitations associated with the formation of triplex DNA. At present, only polypurine DNA strands can be targeted. Cytosine and thymine have only one hydrogen bonding site in the major groove and hence makes targeting a polypyrimidine region of duplex DNA, or strand of mixed purine and pyrimidine bases, problematic. Accessibility of thymine bases is also hampered due to the steric clash provided by the methyl group at C5. A triplex-forming oligonucleotide (TFO) will bind to a polypurine strand in the major groove of the DNA duplex through Hoogsteen hydrogen bonds. A polypurine TFO will bind anti-parallel to the purine strand; a polypyrimidine TFO will bind parallel. Parallel binding TFOs require protonation of N3 on cytosine to form a Hoogsteen hydrogen bond with the N7 on guanine; as such, acidic conditions are often employed. Anti-parallel TFOs will form

triplexes independent of pH but have been shown to form less stable triplexes at neutral pH compared with parallel TFOs at pH 5.5.⁶⁴ Association of guanine-rich anti-parallel TFOs towards duplexes is also inhibited by physiological concentrations of monovalent cations.^{65, 66}

There are three prominent areas addressed for improving triplex formation. First is increasing the thermal stability of the triplex. RNA forms triplexes with double stranded DNA of increased stability compared with DNA. It has been proposed that this is attributable to its A-type structure, that is, the ribose sugar adopts a C3'-endo conformation. Utilisation of RNA analogues LNA,^{62, 63} α -L-LNA,⁶⁷ and ENA (ethylene nucleic acid),⁶⁸ have found merit as a consequence of this observation.

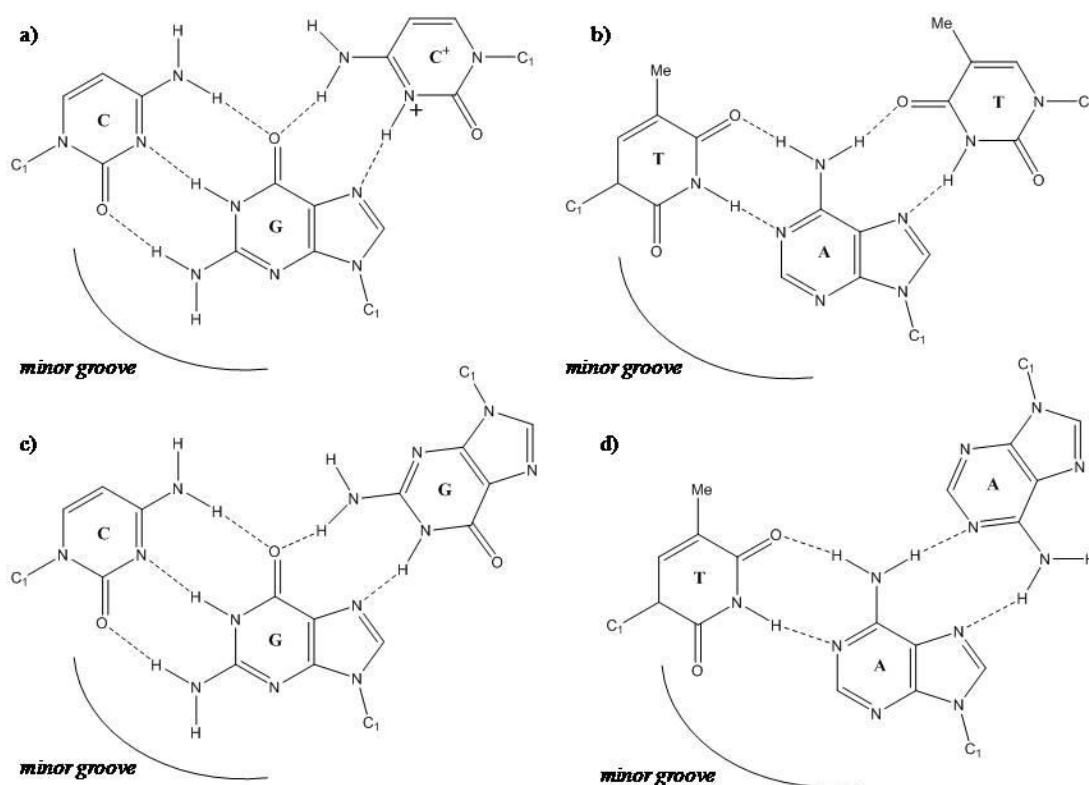


Figure 1.10 Hoogsten bonding between a) CG · C⁺ b) TA · T and reversed Hoogsten bonding between c) CG · G d) TAA

Likewise for LNA duplexes, there have been investigations into whether enthalpic or entropic stabilisation is responsible for the observed increases in thermal stability. Sun *et al.* suggest that stabilisation of the triplex through LNA modification is less enthalpy-driven than unmodified triplexes due to a less pronounced triple to double stranded DNA melting transition. They performed molecular modelling studies of the triplex which led them to comment on the far displacement of the LNA TFO bases compared to the unmodified TFO in the molecular modelling studies which was attributed to the high puckering amplitude of the ribose sugars. It was suggested that if the bases remained at the centre of the helical axis, there would be very little base stacking and significant steric hindrance between the sugars and bases.⁶² It has been found that oligonucleotides fully modified with LNA ribose sugars do not form triplexes,^{62, 63} suggesting that an optimal structural rigidity exists. Sun *et al.*⁶² reported that the LNA complement deforms upon LNA hybridisation and have suggested this to be the reason for fully modified LNA inhibiting hybridisation. Interestingly, fully modified α -L-LNA and ENA have been shown to exhibit triplex formation^{67, 68} possibly due to a lowered puckering amplitude. Torigoe *et al.* assessed the values of K_a ($K_{\text{association}}/ K_{\text{dissociation}}$) to explain the increased stabilities of LNA triplexes. The LNA TFOs yielded much larger values of K_a in comparison with unmodified TFOs and reported this was due to a lower value of $K_{\text{dissociation}}$.⁶⁹ It is believed that the LNA modifications slow the collapse of the nucleation intermediate. This was also supported by Christensen *et al.* who investigated the kinetics of a LNA duplex.⁷⁰

Oligonucleotides possessing neutral backbones, for example PNA⁷¹ and morpholino-DNA⁷² have also found use as TFOs. The non-charged backbone removes electrostatic repulsion arising from the incoming TFO and the duplex DNA. Positive charges introduced by 2'-aminoethoxy groups on the ribose sugar can strengthen triplex stability by increasing the number of interactions occurring between the TFO and DNA.⁷³ At physiological pH, the amino functionality is protonated, allowing the formation of an additional hydrogen bond between the TFO ribose sugar and the non-bridging phosphate oxygen from the underlying purine strand. Aminoalkyl

chains have also been introduced at C4' but have limited increased thermal stability compared with oligonucleotides modified at 2' position.⁷⁴

Another area of development is pH independent TFOs. Methylation of cytosine at the 5 position (5-methyldeoxycytosine) has been reported to aid triplex formation at physiological pHs due to the increased pKa of 5-methylcytosine compared with cytosine (pKa 4.5).⁷⁵ However, it should be realised that 5-methylcytosine has a pKa value only 0.1- 0.2 units higher than cytosine and that this difference is maintained when the bases are incorporated within the triplex structure. Oligonucleotides incorporating 5-methylcytosine have shown greater stability than non-modified oligonucleotides when the cytosines are fully protonated at acidic pHs, suggesting that the increased stability afforded by the modified base is most likely the result of improved base stacking interactions due to an increased polarisability.⁷⁶ Cytosine has also been replaced by pseudoisocytosine⁷⁷ when incorporated into PNA, 8-oxoadenine⁷⁸ and a 6-keto derivative of cytosine.⁷⁹



Figure 1.11 Cytosine and its replacements for incorporation into TFOs.

It is important to be able to target regions of double stranded DNA containing pyrimidine bases, whether for diagnostic or therapeutic applications. Recognition of pyrimidine inversions using natural bases may be achieved forming GTA and TCG base triplets, yet these are unstable, particularly if multiple inversions are present.⁸⁰ Significant effort has been applied to synthesising non-natural bases with Fox and co-workers reporting four base recognition of double stranded DNA at physiological pH. Unfortunately, there is a lack of selectivity for some base sequences, namely those containing TA inversions.^{81, 82}

There are several analytical techniques for detecting triplex formation. In terms of therapeutic applications, restriction enzyme assays and DNase I footprinting may be employed. This indicates the region of DNA that is protected by the TFO from enzyme activity. This is a particularly useful analytical technique to employ for antisense oligonucleotide research as it is a clear indication whether the TFO is disrupting gene translation or not. Another technique used is circular dichroism which allows identification of biological structures that have altered conformational structures. The chirality of C-1' on the ribose sugar means that right-handed and left-handed circularly polarised UV light is absorbed to different extents. The difference in left-handed and right-handed molar extinction coefficients as a function of wavelength will vary depending on the conformational structure of the nucleic acid. TFO hybridisation results in conformational changes that are indicative of triplex formation when compared with double stranded DNA alone. Although UV-visible spectroscopy is a valuable technique in determining melting temperatures of double stranded DNA structures, its application is limited for triplexes. This is because of the broad overlapping melting transitions between the triplex to duplex and duplex to random coil structures. Analysis of anti-parallel triplexes by UV-visible spectroscopy has proven to be even more so problematic than parallel triplexes since the purine TFO remains to be stacked in the free state.^{64, 83}

Employment of oligonucleotides in biodiagnostic applications ordinarily requires the probe oligonucleotide to be labelled so that the hybridisation event can be identified by the appropriate detection technique. Oligonucleotide microarrays utilise fluorescent labelled oligonucleotides so that they can be detected by fluorescence spectroscopy. Recently, there has been significant effort towards developing oligonucleotides that have been modified with nanoparticles for near-field and far-field detection strategies.

1.2.4 Oligonucleotide Nanoparticle Conjugates

The use of oligonucleotide nanoparticle conjugates for detection of specific DNA sequences was pioneered by Mirkin in 1996.⁸⁴ The conjugates are usually prepared

by adsorption of a thiol-modified oligonucleotide sequence onto the nanoparticle surface. The nanoparticle plasmon resonance is very sensitive to changes in the dielectric constant of the environment surrounding the nanoparticle and so this property can be exploited to identify a DNA hybridisation event. One of the most effective methods for detecting a target sequence is using a split probe technique where the probes are complementary in sequence to the target (figure 1.12). Hybridisation of the probes through Watson-Crick base pairing forces the nanoparticles to come into close proximity to one another, resulting in the formation of a nanoparticle aggregate. The change in the dielectric results in a significant red-shift of the plasmon resonance wavelength which is accompanied by a visible colour change from red to blue.

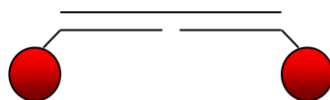


Figure 1.12 Gold nanoparticle modified oligonucleotide probes hybridised to a target DNA sequence.

The red colour will be regenerated upon heating the resultant probe-target DNA complex above its melting temperature, and as such, inspection of plasmon resonance wavelength over a temperature range allows identification of the melting temperature. The melting profiles for duplexes that have been modified with nanoparticles exhibit significantly sharper melting transitions than the analogous non-modified duplexes.⁸⁵ This is due to increased cooperative melting as a result of the large local concentration of DNA at the nanoparticle surface.⁸⁶ Since multiple DNA oligonucleotides are immobilised onto each nanoparticle, the oligonucleotides will hybridise to form 3-dimensional networks. A method for determining the number of oligonucleotides adsorbed onto each nanoparticle has been estimated for 15 nm gold nanoparticles by Demers *et al.*⁸⁷ They used mercaptoethanol to displace fluorophore-labelled oligonucleotides from the surface of the nanoparticles and used fluorescence spectroscopy for quantitative analysis.

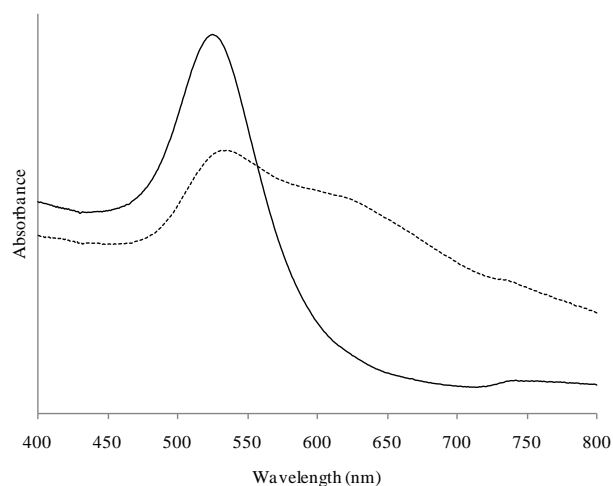


Figure 1.13 Typical UV-visible spectra of 13 nm gold nanoparticle probes before (solid line) and after hybridisation to the target DNA sequence

Circular dichroism spectroscopy has been used to show that the sharp melting transition observed when monitoring the plasmon resonance wavelength is a genuine phenomenon and not simply a “snapshot” of the latter stages of the melting process.⁸⁶ Nanoparticles with higher DNA loadings and also nanoparticles with larger diameters have been shown to exhibit sharper melting transitions due to improved cooperative effects.⁸⁶ Sharp melting transitions are highly advantageous for diagnostic applications as it means single nucleotide polymorphisms (SNPs) may be identified with increased accuracy.⁸⁸ SNPs may contribute towards the expression of genetic diseases and can influence the efficacy of a medicine for patients.

Several factors affect the melting temperature of the oligonucleotide nanoparticle network. The same trend is observed for nanoparticle oligonucleotide conjugates with increasing NaCl concentrations as for unmodified oligonucleotides, although it has been reported that nanoparticle conjugates exhibit higher absolute melting temperatures (approximately 4 °C greater). The apparent increased thermal stability of nanoparticle immobilised oligonucleotides was attributed to the increased dielectric provided for by the nanoparticle probes.⁸⁶ Conversely, Xu and Craig reported that DNA duplexes on the surface of nanoparticles were destabilised relative to free DNA in solution and that the destabilisation effect is more prominent for longer sequences. It has been suggested that the interparticle duplex bridges within a

3D network are the cause for the increased thermal stability reported by Jin *et al.*⁸⁶ however thermodynamic inspection of isolated duplexes on the nanoparticle surface indicates that they are in fact less stable than non-immobilised duplexes.⁸⁹ This was also confirmed by Chen *et al.*⁹⁰ who suggest that duplex denaturation on gold surfaces is a multi-step reaction pathway, unlike DNA in solution, resulting in lower activation energies for denaturation. They suggest that during dissociation, the denatured bases from the probe and target DNA non-specifically interact with the gold surface. It is not until the duplex is fully denatured, that the DNA is released from the nanoparticle surface. Chen *et al.*⁹⁰ have also shown that the gold nanoparticle surface affects the kinetics of hybridisation. They propose that prior to hybridisation of target DNA to the immobilised probes, the target non-specifically adsorbs to the gold nanoparticle surface and then diffuses 2-dimensionally across the nanoparticle surface followed by hybridisation with the probe strands. It is the final hybridisation process that is the rate limiting step.

The effect of interparticle distance on the melting temperature has been considered. There are three possible orientations of nanoparticle probes when employed in a split probe assay and each will give rise to a different melting temperature as a result of the interparticle distance (figure 1.14).

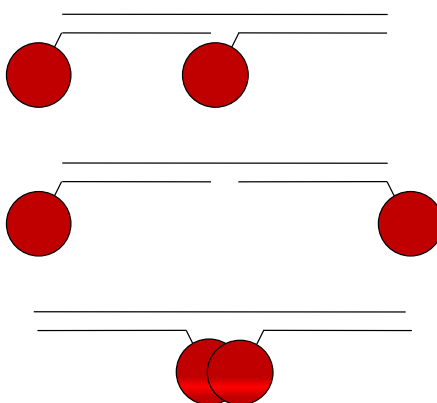


Figure 1.14 Different nanoparticle probe orientations upon hybridisation to the target DNA sequence: head-to-tail; tail-to-tail; head-to-head.

The head-to-head orientation has the lowest thermal stability, followed by head-to-tail and the tail-to-tail format has the highest.⁸⁶ This is most likely the result of high steric repulsion between the bulky nanoparticle modifications. The effect of interparticle distance on the melting temperature has also been observed when spacer groups of different lengths were employed. It is often necessary to incorporate a spacer in between the thiol terminus of the oligonucleotide sequence and the first base of the probe sequence to improve accessibility of the probe sequence to the target and to ensure complete hybridisation. This is often achieved using non-complementary DNA sequences, such as continuous runs of adenine nucleotides. It has been reported that the longer the spacer length, the higher the melting temperature.

Nanoparticles are susceptible to non-specific aggregation, particularly when in ionic buffers. To overcome this, it is necessary to gain high oligonucleotide coverage on the nanoparticle surface to provide the nanoparticle with additional steric and electrostatic protection. This is dependent on how the oligonucleotides pack together on the surface. Thiolated DNA oligonucleotides exhibit secondary interactions for the nanoparticle surface through the base residues, meaning their adsorption is not entirely comparable with alkane thiols which do not possess a competing ligand within their structure. Nucleosides can bind to the metal through either the nitrogen atoms in the heterocyclic ring and exocyclic functional groups or oxygen atoms in the ribose sugar. It has been shown using SERS, that adenosine binds to gold nanoparticles through N(7) of the heterocyclic ring and the exocyclic primary amine; cytidine binds through N(3) of the heterocyclic ring, alongside the carbonyl oxygen; guanine binds through N(1) and the carbonyl oxygen, and thymidine binds only through the C(4) carbonyl oxygen (figure 1.15).⁹¹ Thymine-rich oligonucleotides adsorb with higher surface coverages than adenine-rich oligonucleotides which has been attributed to their decreased affinity for the surface,⁸⁷ presumably since only one atom within the base structure is involved in metal coordination.⁹¹ Demers *et al.* reported that nucleosides desorb from gold surfaces at a lower temperature than the corresponding nucleobases, indicating that the ribose sugar prevents the bases from orientating themselves on the surface to allow the strongest interaction.⁹²

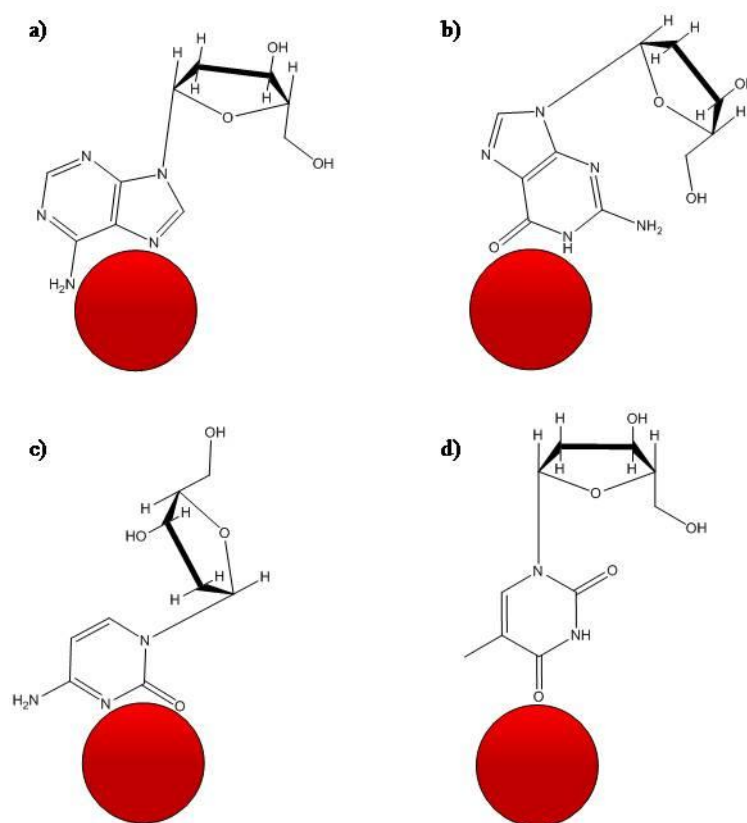


Figure 1.15 DNA nucleosides coordinated to gold nanoparticles as proposed by Jang⁹¹ (not to scale).

The less secondary interactions that exist, the more oligonucleotides can pack on the surface and protect the surface from aggregating agents. This is consistent with findings that nanoparticles functionalised with different oligonucleotides demonstrate different stabilities in the order of dT > dA > dG > dC, where dT nanoparticles are the most stable.⁹³ Incremental increases in the buffer salt concentration shields the secondary interactions encouraging the oligonucleotides to adopt an orientation perpendicular to the nanoparticle surface and pack more densely.

Alivisatos and colleagues have shown that the oligonucleotide surface coverage affects their surface conformation. It has been reported that at low surface coverages, the oligonucleotides wrap themselves around the nanoparticle surface, whereas high coverages are achieved by perpendicular packing. If sequences greater than 30 bases are adsorbed, the outer region of the oligonucleotide strands adopts a random coil

structure improving accessibility towards target sequences and subsequent hybridisation.⁹⁴ It has been shown by Demers *et al.* that incorporation of a polyadenine spacer region adjacent to the thiol group and the oligonucleotide sequence improves hybridisation efficiency by greater than a factor of 10,⁸⁷ indicating that spacer design impacts biomolecular recognition as well as nanoparticle stability. Spacer regions of poly(ethylene)glycol have also been used and have been shown to increase oligonucleotide loading by a factor of 3 which has been attributed to the lack of intermolecular repulsion between neighbouring PEG molecules and secondary interactions with the nanoparticle surface. The same study demonstrates that sonication of the nanoparticle conjugates during the salt-ageing procedure can also significantly increase oligonucleotide loading.⁹⁵

In addition to the effects of ionic salts, application of heat can also induce aggregation of nanoparticles.⁹⁶ An investigation into the mechanism by which this occurs has been conducted by Herdt *et al.*⁹⁷ who discovered that whilst the lability of the thiol-gold bond contributes to desorption of the oligonucleotides from the nanoparticle surface, the presence of the gold surface aids degradation of the oligonucleotide structure, yielding multiple decomposition products of varying oligonucleotide lengths. Their findings indicated that oxygen and ionic salts in the medium did not affect desorption and degradation of the thiol-DNA and therefore the authors reasoned that the gold surface was possibly behaving as a Lewis acid which coordinates to the DNA phosphate oxygens, resulting in cleavage of the phosphodiester bonds.

To address the problems associated with thiol-Au lability, several nanoparticle surface ligands have been synthesised that have improved resistance to the effects from heat and other competing ligands such as dithiothreitol (DTT). Letsinger and co-workers have prepared a steroidal ligand that binds to the gold surface through a disulfide moiety⁹⁸ and also a tri-thiol capped oligonucleotide,⁹⁶ and Dougan *et al.* have synthesised a surface linker based on thioctic acid.⁹⁹ The latter research group applied their linker to silver nanoparticle functionalisation which is renowned for exhibiting greater instability than gold nanoparticles.

In addition to the development of nanoparticle functionalisation techniques for biodiagnostic applications, oligonucleotide-immobilised nanoparticles are also attracting attention in the field of nanoscale assemblies. Assembly applications require the combination of building block molecules and also recognition sites so the blocks may be linked together. DNA oligonucleotides provide both these within one molecule due to its specific Watson-Crick hydrogen bonding sites along the DNA structure. Oligonucleotide length and hence interparticle distance can be altered with ease due to automated DNA synthesis and parameters such as ionic strength, temperature and pH^{84, 86, 100} may be adjusted to control initiation and reversibility of the assembly. Since the plasmon resonance wavelength of nanoparticle aggregates is sensitive to interparticle distance, plasmon rulers based on DNA functionalised nanoparticles have been described as an alternative to Förster resonance energy transfer (FRET) rulers¹⁰¹ and have been used for the quantitative measurement of nuclease activity.¹⁰² Although the nanoparticles ideally need to have a diameter of greater than 20 nm in order to sustain a surface plasmon, which is significantly larger than molecular fluorophores and so will suffer in *in vivo* applications, they can potentially be used to measure much greater distances (up to 70 nm using a 40 nm particle) than FRET (2-8 nm) with 1 nm resolution and does not suffer from photobleaching or orientation problems.¹⁰¹ El Sayed and co-workers have reported an empirical plasmon ruler equation to determine the plasmon shift of electromagnetic coupling lithographically-fabricated gold nanodiscs:¹⁰³

$$\frac{\Delta\lambda}{\lambda_0} = a \cdot e^{-\frac{s/D}{\tau}} \quad (1.6)$$

Where $\Delta\lambda/\lambda_0$ is the fractional plasmon shift, s is the edge-to-edge interparticle distance, d is the nanoparticle diameter and τ is the decay constant (0.23). The value of a is dependent on the medium dielectric constant.

Alivisatos has dedicated considerable effort towards regulation of oligonucleotide-nanoparticle assemblies and to date, has been able to manipulate the number of oligonucleotides immobilised onto the nanoparticle surface so that discrete aggregates can be formed.^{104, 105} Other advances in this field include the formation of a mixed metal assembly. Thompson *et al.* have reported the assembly of

oligonucleotides modified with gold and silver nanoparticles which results in silver nanoparticles being surrounded by the smaller gold nanoparticles in a 'halo' motif as illustrated by SEM analysis.¹⁰⁶ Small angle x-ray scattering (SAXS) has also been used for characterisation of the oligonucleotide nanoparticle networks which allows conversion of interparticle base pair distances into nanometres.¹⁰⁷⁻¹⁰⁹

Aside from analysing oligonucleotide-functionalised nanoparticles by extinction spectroscopy, which exploits the far field properties of metallic nanoparticles, surface-enhanced Raman scattering (SERS) may also be employed which takes advantage of their near-field properties. SERS spectra are molecularly unique and therefore enable detection of multiple analytes simultaneously which is highly advantageous when high throughput analysis is required.

1.2.5 SERS Analysis of Oligonucleotides

DNA bases and mononucleosides have been detected by SERS down to single-molecule detection using colloidal silver.¹⁰ Bell has also reported SERS detection of DNA mononucleotides, overcoming the electrostatic repulsion between the negatively charged phosphate backbone of the nucleotide and the citrate-reduced colloid using MgSO₄, a weak surface-binding aggregating agent.¹¹⁰ Sequences containing multiple mixed bases are difficult to differentiate by SERS due to the similarities of the observed spectra. This is a result of overwhelming SERS activity of adenine compared with the other bases^{111, 112} which has been attributed to its increased Raman cross section.¹¹² Instead, SERRS-active compounds, that is, compounds that possess a chromophore, may be used to label specific sequences. Intercalating dyes have been used to identify the presence of double stranded DNA, however labelling is non-specific and does not allow specific sequences to be detected.^{113, 114} As such, it is often preferred to label DNA sequences by covalent means, as is often employed for use in fluorescence microarrays. Commercially available fluorophores can be used as SERRS labels in solution-based assays since the metal nanoparticles quench fluorescence through a radiationless transfer of energy to the metal surface,²⁷ however, the experimental conditions employed need

to be considered for each fluorophore. One such consideration is the electrostatic nature of the dye label. Gold and silver nanoparticles are commonly prepared *via* citrate reduction of the metallic salt resulting in a physisorbed anionic citrate layer on the nanoparticle surface. Negatively charged dye labels will not efficiently adsorb to the nanoparticle due to the electrostatic repulsion between the nanoparticle and dye. This may be overcome in one of two ways. Firstly, the negative charge conferred by the fluorophore and DNA phosphate backbone can be neutralised by addition of the polyamine, spermine (figure 1.16). Not only does spermine allow effective DNA adsorption to the colloidal particle surfaces but it also behaves as an aggregating agent towards the nanoparticles.¹¹⁵ The dye-labelled DNA probe may also be modified to allow effective adsorption. Propargylamino-modified deoxyuridines can be incorporated into the DNA sequence in close proximity to the covalently attached fluorophore. The modified bases contain an aliphatic amine which is protonated at physiological pH, providing a site for electrostatic attraction between the oligonucleotide at the fluorophore terminus and the nanoparticle surface (figure 1.17).

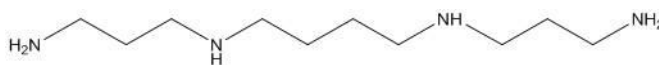


Figure 1.16 Spermine.

It is also advantageous to incorporate propargylamino bases as these have been shown to increase duplex stability due to improved base stacking interactions.¹¹⁵ A comprehensive assessment of the SERRS performance of DNA sequences labelled with commercially available fluorophores has been conducted by Faulds *et al.*^{116, 117} who have reported improved detection limits over fluorescence analysis. This work was extended by Stokes *et al.* who compared the detection limits of numerous dye labelled oligonucleotides at multiple excitation wavelengths, using silver and gold nanoparticles.¹¹⁸ Although these reports prove that SERRS is a viable method for DNA detection, they do not detail how DNA target sequences can be identified without modification of the target.

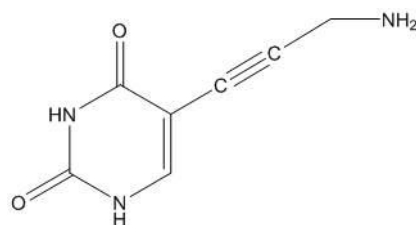


Figure 1.17 Propargylamino-modified uracil.

DNA detection can be performed in either, a homogenous or heterogeneous assay. Homogenous detection, involving nanoparticles, is advantageous due to faster reaction rates and experimental ease, whereas heterogeneous assays, akin to surface hybridisation assays, are likely to benefit from higher sensitivity since the SERS substrate and analyte is not dispersed in solution as for homogenous detection. One method of DNA detection in solution is based on a molecular beacon approach as described by Vo Dinh and colleagues.^{119, 120} The probe consists of a hairpin oligonucleotide that is labelled with a SERS active dye at one end and is attached to the nanoparticle at the other. Hybridisation with the target DNA sequence, forces the hairpin structure into an open conformation which lifts the dye off the nanoparticle surface and so SERRS signals are diminished.

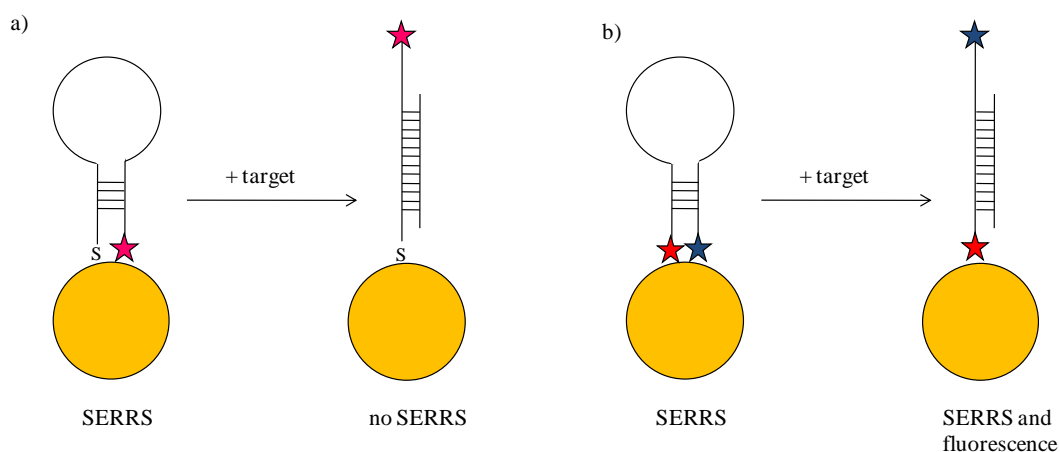


Figure 1.18 DNA detection techniques reported by a) Vo Dinh et al.¹¹⁹ and b) Faulds et al.¹²¹

A similar approach was adopted by Faulds *et al.* who labelled both ends of the probe with different SERRS active dyes which were adsorbed onto the nanoparticle surface. Upon hybridisation with the target sequence, the fluorophore is lifted off the surface and so only SERRS from the dye remaining on the nanoparticle surface is observed whereas fluorescence is obtained from the 'free' dye label.¹²¹ MacAskill *et al.* have reported multiplexed homogenous detection of DNA sequences corresponding to hospital-acquired infections using dye-labelled LNA probes. They exploited their observation that double stranded DNA had a lower affinity for the metal surface than single stranded DNA to detect whether hybridisation had occurred between the probe and target sequences. Hybridisation between complementary sequences to form double stranded DNA meant a decrease in SERRS signal intensities was observed compared with probe spectra in the absence of complementary target.¹²² Graham *et al.*¹²³ and Qian *et al.*¹²⁴ have exploited the electromagnetic coupling between nanoparticles within an aggregate to detect a target DNA sequence. Both reports involve labelling split probe oligonucleotide sequences with nanoparticles and hybridising to the target in a sandwich assay. Lee and Irudayaraj have investigated the enhancement effects afforded by 3-D DNA linked nanoparticle networks and concluded that additional enhancement was provided in comparison with 2-D arrays (10-100 times greater) due to the added dimensionality of the nanoparticle system.¹²⁵

Literature detailing DNA sequence detection in a heterogeneous assay includes the development of an assay to detect a fragment of the breast cancer susceptibility gene, BRCA1 on a silver surface²³ and Stokes *et al.* performed oligonucleotide sequence detection on a gold nanostructured surface, manipulating the more developed surface chemistry for gold substrates.¹²⁶ The multiplexing capabilities of SERRS have been demonstrated by Mirkin and co-workers by using dye-labelled gold nanoparticle oligonucleotide probes to hybridise to target DNA strands immobilized onto a chip. The probes were identified by coating the gold nanoparticles with silver, increasing the surface-enhancement potential of the system.¹²⁷ Other examples of multiplexed analysis by SERRS include multiplexed genotyping of a cystic fibrosis gene using

SERRS labelled primers¹²⁸ and analysis of an oligonucleotide 6-plex using multivariate analysis.¹²⁹

1.3 Nanoparticle Functionalisation with Protein Structures

Nanoparticles may be used to probe other biomolecular events such as protein or antibody interactions. The role of proteins in biology is of significant importance. They are involved in many biological processes including enzyme catalysis, transport and storage and immune protection. The basic unit of a protein is an amino acid which is zwitterionic at neutral pH (exists as a dipolar ion).

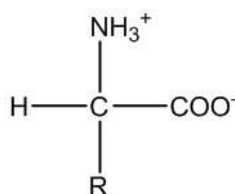


Figure 1.19 amino acid structure

R represents one of 20 side groups which affect the amino acids properties due to either their hydrophobic or hydrophilic nature. The peptide chain sequence itself, constructed by the condensation reaction between the terminal carboxylic acid and amine, has little biological function but instead dictates folding of the peptides into higher ordered structures. Although the peptide bond is rigid and planar, the bonds on either side have rotational freedom. Secondary structure is afforded by intramolecular hydrogen bonding to yield either α -helices or β -sheets. Folding to produce tertiary and quaternary structure also relies on hydrogen bonding, in addition to hydrophobic, disulfide and Van der Waals interactions.

Antibodies are proteins synthesised by animals in response to a foreign substance in the body and are frequently used in immunoassays due to their high specificity for target molecules. Target recognition occurs through the F_{ab} region (antigen-binding fragments). Immunoglobulin G, IgG, the major antibody in serum, has two identical F_{ab} regions which are hinged to the F_c region to allow flexible movement for complexing to a multivalent antigen. Monoclonal antibodies of almost any desired specificity can be readily prepared permitting their use as biofunctional tags for the detection of target molecules. Labelling proteins and antibodies with nanoparticles can largely affect their structure and therefore their biological activity. An important consideration is secondary interactions between amino acid residues and the nanoparticle surface. The nanoparticle surface is covered with excess anionic reducing agent, for example citrate groups, and as such the possibility for secondary electrostatic interactions is high. Consequently, this may lead to protein unfolding. The biological activity of proteins is largely dependent on their tertiary structure and disruption of such can affect protein function.

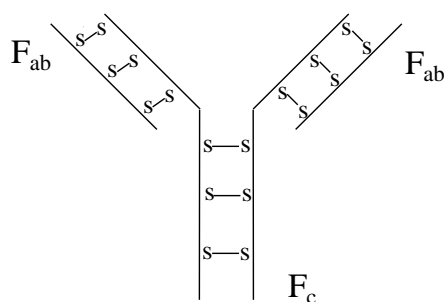


Figure 1.20 Antibody structure illustrating the F_{ab} and F_c regions

It has been shown that the structure of leucine-rich peptide was affected by adsorption onto gold nanoparticles and flat surfaces. As the nanoparticle diameter was reduced, hence increasing the curvature of the nanoparticle surface, the α -helix content decreased dramatically and β -sheet structure was more predominant.¹³⁰ Loss of activity of lysozyme adsorbed onto silica nanoparticles has been reported and has been attributed to losses in α -helix content. Greater losses were observed for lysozyme adsorbed onto larger nanoparticles, further supporting evidence that

bioactivity is dependent on surface curvature.¹³¹ The structure of cytochrome c has been investigated using nanoparticle ligands of different charges. Denaturation was observed when aminoethanethiol and bis (*p*-sulfonatophenyl)phenylphosphine were employed which are positively and negatively charged, respectively, however structure was maintained when a neutral PEG ligand was utilised.¹³² It should be noted that sometimes protein activity can be enhanced upon nanoparticle immobilisation. Protein folding of cytochrome c at high surface coverages was shown to improve on CoFe₂O₄ nanoparticles¹³³ and the activity and selectivity of certain lipases was also increased when adsorbed onto polymeric nanoparticles.¹³⁴

Nanoparticle functionalisation with protein structures can be achieved in a number of ways, namely electrostatic attachment, through a nanoparticle surface ligand, and by a direct covalent linkage with the nanoparticle surface. Attachment *via* electrostatic attraction is routinely used in histology for producing electron dense markers.¹³⁵ Proteins immobilised in this way are more likely to retain their structure although it is likely that the protein can bind in a number of different orientations due to the non-specific nature of the interaction. Nanoparticle surface ligands are frequently used for covalent attachment to the protein. Commonly, this is achieved by reacting carboxylic acid terminating linkers with lysine residues within the protein, utilising EDC and sulfoNHS chemistry.^{136, 137} Maleimide terminating linkers have also been reacted with thiols from protein cysteine residues.¹³⁸ Cobalt¹³⁹ and nickel¹⁴⁰ nitriloacetate ligands have been used to react with histidine tags which can be introduced into the protein sequence through genetic cloning. This method of attachment is advantageous as it enables site-specific labelling of the protein which means greater control can be exerted over ensuring the protein is available for biomolecular interactions. Consideration should be given to the nature of the ligand employed; ligands incorporating charged end groups have been shown to denature proteins due to electrostatic effects.¹³² Poly(ethylene)glycol is often featured in nanoparticle ligands due to its ability to prevent non-specific adsorption^{132, 141} and improve biodistribution^{142, 143}. Use of nanoparticle ligands is sometimes undesirable, for instance for FRET measurements which requires strict control to reduce any movement of the biomolecule which may affect the distance between the biomolecule and the nanoparticle. Direct attachment of the protein to the

nanoparticle surface and omission of linkers will also reduce the size of the resultant nanoparticle conjugate which is beneficial for improved distribution around the body for *in vivo* applications. Direct attachment has been reported by Aubin *et al.* who utilised a peptide cysteine residue for covalent immobilisation of Ribonuclease S onto a gold nanoparticle surface.¹⁴⁴

1.3.1 Protein Functionalised Nanoparticles in Detection Assays

Protein functionalised nanoparticles can be employed in homogenous detection assays in much the same way as for DNA functionalised nanoparticles if the target molecule is polyvalent. One of the most well-known polyvalent biomolecular interactions is that between streptavidin and the small molecule, biotin. Streptavidin features 4 biotin binding sites and so biotin functionalisation of the nanoparticles will result in aggregation upon titration with streptavidin. This has been reported by Aslan *et al.*¹⁴⁵ and Gole *et al.* who functionalised gold nanorods with biotin and used streptavidin to control the rod-rod orientation.¹⁴⁶ Brust and co-workers used avidin-functionalised gold nanoparticles to screen for kinase activity by exploiting kinase's biotinylation properties.¹⁴⁷ IgG molecules are also suitable for aggregation-based assays since they have two antigen binding sites *per* molecule. Anti-mouse IgG functionalised gold nanorods have been employed for the detection of mouse IgG¹³⁶ and anti-protein A was detected using protein A gold nanoparticles.¹⁴⁸ Yu and Irudayaraj targeted F_{ab} molecules using gold nanorods, however they did not employ nanoparticle aggregation as their means for detection. Instead, they exploited the improved sensitivity of the longitudinal plasmon resonance wavelength to changes in the refractive index in the surrounding environment to detect binding to monovalent target molecules.¹³⁷

There is little in the literature detailing homogenous protein based SERS detection; most reports involve detection on a flat surface in the classic immunoassay format.¹⁴⁹⁻¹⁵¹ Nonetheless, there has been a recent surge in the development of cell-based detection strategies, *in vitro* and *in vivo*.

1.3.2 SERS Measurements from Cells

Nanoparticles are introduced into cells most commonly by endocytotic pathways. Endocytosis involves encapsulation of an extra-cellular entity by the cell membrane which then seals off to form a vesicle. Experimentally, this is achieved simply by incubating the cells with a solution of the nanoparticles. The nanoparticle surface chemistry has been reported to affect cellular uptake, that is, nanoparticles that were functionalised with charged species were able to penetrate the cell membrane with greater ease than non-charged nanoparticles. The nanoparticles are usually dispersed throughout the cytoplasm and have been reported to cluster around the nucleus but rarely cross the nuclear membrane. To overcome this limitation, intracellular nanoparticle synthesis has been reported.^{152, 153} This involves incubation of the cells with Au^{3+} which is internalised and then converted into Au^0 using the cell's native reduction chemistry. This allowed accumulation of the nanoparticles within the nucleus although they were deemed too small for effective SERS data collection.

There have been several investigations regarding the toxicity of nanoparticles to cells. Gold nanoparticles are generally perceived as being non-cytotoxic, although there has been some conflicting reports; it was reported by Nildome *et al.* that cetyltrimethylammonium bromide (CTAB) coated nanoparticles initiated death of 80 % cells¹⁴³ whereas Murphy *et al.* found that the same surface modified nanoparticles were not cytotoxic, however non-surface bound CTAB was toxic at 10 nM concentrations.¹⁵⁴ Rotello *et al.* found that cationic 2 nm gold nanoparticles were more toxic than anionic nanoparticles which they attributed to an electrostatic interaction with the negatively charged cell membrane.¹⁵⁵ It should also be noted that cytotoxicity appears to be dependent on cell type as illustrated by Patra *et al.* who found that gold nanoparticles were compatible with baby hamster kidney and human hepatocellular liver carcinoma cells but exhibited concentration-dependent toxicity towards a human carcinoma cell line.¹⁵⁶ Silver nanoparticles, however, pose a larger threat to cell viability. Studies have shown that silver nanoparticles are cytotoxic, genotoxic¹⁵⁷ and also initiate apoptosis, which may have advantages in terms of gene therapy applications.¹⁵⁸

Raman measurements from cells are usually recorded using a mapping technique. This involves rastering the laser across the sample surface where a complete SERS image is obtained at every pixel. This differs from Raman imaging techniques which measures only one Raman band. Cellular components can be identified by utilisation of non-bioconjugated gold nanoparticles to enhance Raman signals from cellular proteins and DNA. Near-infrared (NIR) excitation wavelengths are often preferred as fluorescence background from biological samples is reduced and lower energy photons inflict less damage on the sample. NIR excitations is also advantageous since light of NIR wavelengths scatter less efficiently (equation 1.7; I is the intensity of Raman Scattering, K is a constant including the speed of light, l is the laser power, α is the polarisability of the electrons in the molecule and ω is the frequency of the incident radiation),¹⁶ thus allowing better penetration into the sample. Furthermore, absorption from haemoglobin in blood and water is minimal in the NIR spectral region.¹⁵⁹

$$I = Kl\alpha^2\omega^4 \quad (1.7)$$

Gold nanoparticles, although are generally considered less effective than silver nanoparticles for surface enhancement, have been shown to give rise to comparable enhancement factors when excited by a NIR wavelength laser²⁶ due to the plasmon resonance being of a longer wavelength and do not influence cell viability.¹⁵⁴ Kneipp and co-workers have detailed *ex vivo* utilisation of gold nanoparticles ranging between 30 and 60 nm in size for the identification of cellular proteins and DNA.^{160, 161} The latter paper determines the distribution of nanoparticles within the cell when internalised by endocytosis and the effect this has on SERS signals. Silver nanoparticles have been employed by Manfait and colleagues to detect anti-tumour drugs that had been incubated with cancer cells. SERS analysis indicated the presence of the drugs and also the interactions with their receptors.^{162, 163} Interestingly, cell viability was quoted at greater than 95 % of cells which were treated.

Nanoparticles can also be employed as Raman tags by labelling the nanoparticles with a dye. The spectra obtained are specific to the dye but may also exhibit

additional signals corresponding to the surrounding cellular environment. Kneipp *et al.* employed indocyanine green (ICG)-labelled gold nanoparticles for cell internalisation. The resulting SERS signals were indicative of the ICG label but also showed a contribution from DNA, RNA and protein structures.¹⁶⁴ Tang *et al.* investigated the uptake of R6G with 60 nm gold nanoparticles and also illustrated that SERS signals attributable to the dye and intrinsic cellular components could be recorded. The effects of fixing and air-drying cells were also investigated;¹⁶⁵ cell fixation is performed to preserve the sample so the physical and chemical properties of the cell remain unchanged. This is achieved by disabling enzymes and bacteria that may digest and damage the cell, and by conferring mechanical rigidity towards the cell to help maintain its morphology. Fixed cells are significantly more stable whilst obtaining spectroscopic measurements and so using cells in this form is advantageous over live cells. Tang *et al.* discovered that fixation and air-drying of cells resulted in SERS signals of higher intensities. It was proposed that shrinking of the cell from the drying process brought the cell components into closer proximity to the nanoparticles giving rise to greater enhancement effects.¹⁶⁵

Utilisation of biomolecule-functionalised nanoparticles has allowed specific ligand-receptor interactions to be probed. Schlücker *et al.* conjugated a prostate-specific antigen (PSA) antibody to gold nanoparticles *via* an aromatic Raman active linker to enable detection of PSA within epithelial tissue cells.¹⁶⁶ Cell surface biomarkers have also been detected using R6G labelled gold nanoparticles coated with a silver outer shell.¹⁶⁷ The bimetallic nanoparticles were functionalised with a secondary antibody specific for anti-PLC γ 1 antibodies which were incubated with the cells prior to introduction of the nanoparticle conjugates. Recently there have also been reports of extending SERS detection *in vivo*. Qian *et al.* targeted epidermal growth factor receptors on cancer cells using pegylated 60 nm gold nanoparticles labelled with malachite green. The carboxylic acid terminated PEG was conjugated to a single chain variable fragment antibody using EDC and sulfoNHS chemistry to yield specific and selective identification of cancer cells.¹⁶⁸ *In vivo* multiplexed SERS was performed by Keren *et al.* using silica coated gold nanoparticles. Single-walled

nanotubes (SWNTs) were also employed for conjugation to an arginine-glycine-aspartate peptide to detect cancerous cells in mice.¹⁶⁹

2. *Aims*

This thesis details the preparation and application of biomolecule functionalised nanoparticles for monitoring biomolecular interactions by extinction and surface enhanced resonance Raman scattering (SERRS) detection methods. The aim of the research was to:

- Prepare oligonucleotide functionalised gold and silver nanoparticles to afford improved binding affinities and selectivity for complementary DNA targets over existing oligonucleotide nanoparticle conjugates. Locked nucleic acid (LNA) was to be employed for this purpose due to its favourable properties and commercial availability. The LNA probes were intended to target single stranded DNA targets and double stranded DNA targets through triplex formation which would be monitored by means of UV-visible spectroscopy and colorimetric changes.
- Investigate the use of SERRS for DNA detection. The maximum number of dyes detectable in a multiplexed analysis was to be established exploiting the resonance selectivity of SERRS using a dual excitation wavelength approach. SERRS active nanoparticle probes were to be prepared to allow single stranded and double stranded DNA detection without modification of the target sequence. The versatility of this detection method was to be assessed using different dye labels, nanoparticles and probe orientations. The electromagnetic coupling effect was to be exploited using different DNA sequence lengths to establish the relationship between inter-nanoparticle distance and SERRS intensity.
- Prepare SERRS active antibody functionalised nanoparticles for targeting cell surface receptors. This was to be achieved using a SERRS active linker molecule that was excited upon irradiation by near-infrared wavelengths. It was necessary for the nanoparticles to be stable in biological buffers and exhibit high sensitivity. The application of SERRS for quantitative cell analysis was to be assessed.

3. Experimental

All UV-visible analysis was performed on a *Varian Cary Bio 300* spectrometer. UV-visible melting experiments were recorded at 260 nm, 410 nm, and 520 nm for unmodified, silver nanoparticle modified and gold nanoparticle modified oligonucleotides, respectively. The temperature was programmed to a heat/cool rate of 1 °C/minute. All fluorescence analysis was performed on a *Varian Cary Eclipse* spectrometer. Experimental parameters for the measurement of surface enhanced resonance Raman scattering (SERRS) are detailed in the text. Chemicals were purchased from Sigma Aldrich, UK unless otherwise stated.

3.1 Gold Nanoparticle Synthesis¹⁷⁰

All glassware was cleaned with *aqua regia* before use and rinsed thoroughly with distilled water. An aqueous solution of NaAuCl₄ (12.5 mM, 10 mL) was added to distilled water (500 mL) and heated. Upon boiling, sodium citrate (25 mM, 10 mL) was added and the solution was left to stir for 15 minutes at boiling temperature. Gold nanoparticle concentrations were determined by UV-visible spectroscopy using an extinction coefficient of $2.7 \times 10^8 \text{ M}^{-1} \text{ cm}^{-1}$ at 520 nm.⁸⁶

3.2 Silver Nanoparticle Synthesis²⁰

All glassware was cleaned with *aqua regia* before use and rinsed thoroughly with distilled water. An aqueous solution of AgNO₃ (53 mM, 10 mL) was added to distilled water (500 mL) that had been heated to 40 °C. Following further heating to 97 °C, sodium citrate (43 mM, 10 mL) was added. The temperature of the reaction mixture was maintained at 97 °C for 90 minutes. Silver nanoparticle concentrations were determined by UV-visible spectroscopy using an extinction coefficient of $2.87 \times 10^{10} \text{ M}^{-1} \text{ cm}^{-1}$ at 400 nm.¹⁷¹

3.3 LNA Functionalised Nanoparticles

DNA oligonucleotides were purchased from ATD Bio, Southampton. LNA/DNA chimera oligonucleotides were purchased from Eurogentec, Belgium.

5' thiolated and 3' thiolated oligonucleotides, table 3.1 and 3.2, were conjugated to gold and silver nanoparticles. A thiol-modified oligonucleotide solution (10 nmoles) was added to colloidal gold (17-38 nM, 1 mL) and colloidal silver (0.4 nM, 1 mL). The samples were incubated overnight at room temperature, followed by the addition of 60 mM pH 7 phosphate buffer giving a final concentration of 10 mM phosphate. Following 24 hours at room temperature, the salt concentration was brought up to 0.1 M by successive additions of NaCl over 48 hours.

Probe Sequence A (5' to 3')	Probe Sequence B (5' to 3')	Target (5' to 3')
Thiol C ₆ AAA AAA AAA AAA AAA AAA AAt ^m CT ^m c T ^m cT	^m c ^m C ^m C tTt TAA AAA AAA AAA AAA AAA AAA C ₃ Thiol	1. AAA AGG GAG AGA GA 2. AAA AGG CAG AGA GA 3. TAA AGG GAG AGA GA 4. AAA TGG GAG AGA GA 5. AAA TGG GAC AGA GA
Thiol C ₆ AAA AAA AAA AAA AAA AAA AAT CTC TCT	CCC TTT TAA AAA AAA AAA AAA AAA AAA C ₃ Thiol	AAA AGG GAG AGA GA
Thiol C ₆ AAA AAA AAA AAA AAA AAA AAt ^m CT ^m c T ^m cT	^m c ^m C ^m C tTt TAA AAA AAA AAA AAA AAA AAA C ₃ Thiol	dsDNA: AGA GAG AGG GAA AA + TTT TCC CTC TCT CT
Thiol C ₆ AAA AAA AAA ATC TCA ACT CGT A	Thiol C ₆ AAA AAA AAA ACG CAT TCA GGA T	ATC CTG AAT GCG TAC GAG TTG AGA
Thiol C ₆ HEG HEG HEG ATC TCA ACT CGT A	Thiol C ₆ HEG HEG HEG ACG CAT TCA GGA T	ATC CTG AAT GCG TAC GAG TTG AGA
Thiol C ₆ HEG HEG HEG t ^m CT ^m c T ^m cT	^m c ^m C ^m C tTt T HEG HEG HEG C ₃ Thiol	dsDNA: AGA GAG AGG GAA AA + TTT TCC CTC TCT CT

Table 3.1 List of probe sequences immobilised onto gold nanoparticles and the target sequences. Lowercase letters represent LNA modified nucleotides, ^mC represents 5-methyldeoxycytidine. HEG represents hexaethylene glycol.

Probe Sequence A (5' to 3')	Probe Sequence B (5' to 3')	Target (5' to 3')
Thiol C ₆ HEG HEG HEG t ^m CT ^m c T ^m cT	^m c ^m C ^m C tTt T HEG HEG HEG C ₃ Thiol	dsDNA: AGA GAG AGG GAA AA + TTT TCC CTC TCT CT

Table 3.2 Probe sequences immobilised onto silver nanoparticles and the target sequences. Lowercase letters represent LNA modified nucleotides, ^mC represents 5-methyldeoxycytidine. HEG represents hexaethylene glycol.

The nanoparticle conjugates were then centrifuged at 5000 rpm (RCF 2376 x g) for 20 minutes and resuspended in 0.3 M NaCl, 10 mM phosphate, pH 7 (0.3 M PBS). The concentration of the nanoparticle conjugates was determined by UV-visible spectroscopy (molar extinction coefficients are $2.87 \times 10^{10} \text{ M}^{-1} \text{ cm}^{-1}$ for silver at 400 nm¹⁷¹ and $2.7 \times 10^8 \text{ M}^{-1} \text{ cm}^{-1}$ for gold at 520 nm).⁸⁶

LNA and DNA gold nanoparticle conjugates (1 nM) were hybridised to target DNA, table 3.1, (0.1 μM) in 0.3 M PBS. LNA silver nanoparticles (20 pM) were hybridised to target DNA, table 3.2, (20 nM) in 0.3 M PBS. The melting temperatures were determined using UV-visible melting experiments by inspection of the first derivative graph.

DNA quantitation on gold nanoparticles was determined for 5' thiol C₆ AAA AAA AAA ACG CAT TCA GGA T FAM 3' and 5' thiol C₆ HEG HEG HEG CG CAT TCA GGA T FAM 3'. The nanoparticle conjugates were prepared as above. 5 replicates of each sample were prepared. The concentration of the nanoparticle conjugates in PBS was determined by UV-visible spectroscopy. DTT was added to a final concentration of 0.1 M and incubated at room temperature for 16 hours in the dark, after which time the nanoparticles had precipitated out of suspension. The samples were centrifuged twice at 5000 rpm (RCF 2376 x g), 20 minutes and the supernatant was extracted, followed by fluorescence analysis using an excitation wavelength of 492 nm. The concentration of the FAM label was calculated using a calibration graph of standard FAM-labelled DNA solutions.

3.4 SERRS Analysis of DNA

3.4.1 Multiplexed SERRS Analysis

Dye-labelled oligonucleotides were purchased from Eurogentec, Belgium, Invitrogen Paisley, and ATD Bio, Southampton.

Surface enhanced resonance Raman scattering (SERRS) spectra were recorded using *Renishaw inVIA* and *Renishaw System 2000* Raman spectrometers using excitation sources of an Argon ion laser (514.5 nm) and a He Ne laser (632.8 nm), respectively. Back-scattered light (180°) was collected using a *Leica DMLM* microscope equipped with a long-working distance objective (20x/0.4). The inelastically scattered light was analysed using a diffraction grating (*Renishaw inVIA*: 1800 lines/mm; *Renishaw System 2000*: 1200 lines/mm) centred at 1200 cm⁻¹ and a *RenCam* CCD.

The dye-labelled oligonucleotides (0.1 μM, 10 μL), sequences shown in table 3.3, were added to a solution containing silver nanoparticles (0.2 nM, 500 μL) and spermine (0.1 M, 10 μL) and analysed immediately in a microtitre plate by SERRS.

Dye Label	Oligonucleotide sequence (5' to 3')
FAM	T*CT*CT*CT*C TCC ACG TTT TCC CAG TCA CGA
TET	T*CT*CT*CT*CT*CT*C GAA GGT CCC CCT CTT TGG TCT TGC
R6G	TGC TTC TAC ACA GTC TCC T
HEX	T*CT*CT*CT*CT*CT*C GGG CGC TCA TCA TAG TCT TTC TTA
Cy3	T*CT*CT*CT*CT*CT*C ATA AAT CGC CAT TCG TTG ACT AC
TAMRA	TAA ATC GCC ATT CGT TGA CTA C
Cy3.5	T*CT*CT*CT*CT*CT*C TCC ACG TTT TCC CAG TCA CGA CGT
ROX	GCG TCA TCG TAT ACA CAG GAG CAG
BODIPY TR-X	TCC ACG TTT TCC CAG TCA CGA CGT
Cy5	T*CT*CT*CT*CT*CT*C GCG TCA TCG TAT ACA CAG GAG CAG
Cy5.5	T*CT*CT*CT*CT*CT*C TCC ACG TTT TCC CAG TCA CGA CGT

Table 3.3 Multiplex oligonucleotide sequences. T* denotes propargylamine-2'-deoxyuridine.

For multiplexed samples, a combination of dye-labelled oligonucleotides (0.1 μ M, 10 μ L) were added together and then mixed with the silver nanoparticle solution (silver colloid 0.2 nM, 500 μ L, spermine 0.1 M, 10 μ L). The multiplex was analysed quantitatively by preparation of several oligonucleotide dilutions. The oligonucleotide-silver colloid mixtures were analysed by SERRS in a cuvette using a *Ventacon* macrosampler equipped with a 20x/0.4 objective.

3.4.2 Propargylamine Modified Oligonucleotides

DNA oligonucleotides were purchased from ATD Bio, Southampton.

SERRS was recorded using a *Renishaw Probe* spectrometer with an Argon ion laser (514.5 nm) equipped with a 20x long working distance objective. The inelastically scattered light was analysed using a grating of 1800 lines/mm centred at 1200 cm^{-1} .

Oligonucleotides incorporating different numbers of propargylamine-2'-deoxyuridine, table 3.4, were prepared to several different concentrations. The oligonucleotides were added to a cuvette containing silver colloid (0.2 nM, 500 μ L) and spermine (0.1 M, 10 μ L). The final oligonucleotide concentrations ranged from 19 pM to 1.9 nM. The samples were analysed immediately by SERRS.

Number of propargylamines	Oligonucleotide sequence (5' to 3')
0	FAM TCC ACG TTT TCC CAG TCA CGA CGT
1	FAM T*C TCC ACG TTT TCC CAG TCA CGA CGT
2	FAM T*CT*C TCC ACG TTT TCC CAG TCA CGA CGT
4	FAM T*CT*CT*CT*C TCC ACG TTT TCC CAG TCA CGA
6	FAM T*CT*CT*CT*CT*CT*C TCC ACG TTT TCC CAG

Table 3.4 Propargylamine modified oligonucleotide sequences. T* denotes propargylamine-2'-deoxyuridine.

3.4.3 *In-Sequence Labelling*

Locked nucleic acid (LNA) and DNA oligonucleotides were purchased from Eurogentec, Belgium and ATD Bio, Southampton, respectively.

Silver nanoparticle conjugates were prepared using the immobilisation procedure outlined in section 3.3. The sequences used were 5' thiol HEG HEG HEG ^mc^mC^mC tTt T 3' and 5' thiol Cy 5 AAA AAA AAA ATC TCT CTC TC 3' where lowercase letters represent LNA modifications and ^mC represents 5-methyldeoxycytidine. The silver conjugates (20 pM) were hybridised to 5' AAA AGG GGA GAG AGA GA 3' at a 2 nM and 20 nM concentration in 0.3 M PBS. The conjugates were analysed before and after the addition of target DNA by UV-visible spectroscopy. SERRS spectra were recorded from a microtitre plate and obtained at 15 minute intervals for 2 hours after the addition of the target DNA. The spectra were obtained using a *Renishaw System 2000* Raman spectrometer with a He Ne laser (632.8 nm). Back-scattered light (180°) was collected using a *Leica DMLM* microscope equipped with a long-working distance objective (20x/NA 0.4). The inelastically scattered light was analysed using a grating (1200 lines/mm) centred at 1200 cm⁻¹ and a *RenCam* CCD.

DNA quantitation on the silver nanoparticles was determined for 5' thiol C₆ AAA AAA AAA ACG CAT TCA GGA T FAM 3'. 5 replicate samples were prepared as detailed in section 3.3. The concentration of the nanoparticle conjugate in PBS was determined by UV-visible spectroscopy. DTT was added to a final concentration of 0.1 M and incubated at room temperature for 16 hours in the dark, after which time the nanoparticles had precipitated out of suspension. The samples were centrifuged at 5000 rpm (RCF 2376 x g), 20 minutes and the supernatant was extracted, followed by fluorescence analysis using an excitation wavelength of 492 nm. The concentration of the FAM label was calculated using a calibration graph of standard FAM-labelled DNA solutions.

3.4.4 Nanoparticle Labelling

Locked nucleic acid (LNA) and DNA oligonucleotides were purchased from Eurogentec, Belgium and ATD Bio, Southampton, respectively. The isothiocyanate dyes were purchased from Invitrogen, Paisley and Victoria Blue was purchased from Sigma Aldrich, UK.

Silver nanoparticle conjugates were prepared using the immobilisation procedure outlined in section 3.3. The sequences used were: 5' SH C₆ (HEG)₃T^mct^mCt^mCt 3' (probe 1); 5' ^mC^mc^mcTtTt (HEG)₃ C₃ SH 3' (probe 2); 5' SH C₆ (HEG)₃ ^mC^mc^mcTtTt 3' (probe 3) where uppercase letters represent LNA modified nucleotides and ^mc or ^mC represents 5-methyldeoxycytidine. Probe 1 (500 μL, 0.67 nM) was added to 500 μL, 1 μM solution of either ROX isothiocyanate (ROX ITC), TAMRA isothiocyanate (TRITC), Victoria Blue, or 3,5-dimethoxy-4-(6'-azobenzotriazolyl)phenylamine (DABT PA). The ROX ITC dye was also added to the DNA nanoparticles at 2 μM and 10 μM concentrations. The oligonucleotide nanoparticle conjugates were incubated for 16 hours in the dark, and then centrifuged and resuspended in 0.3 M PBS. Nanoparticle assembly was initiated by addition of complementary target DNA. The combinations of probe and target sequences used are shown in table 3.5.

orientation	Probes	Target (5' to 3')
Head-to-head	Probe 1, Probe 2	AGAGAGAAAAAGGG
Head-to-tail	Probe 1, Probe 3	AAAAGGGAGAGAGA
Tail-to-tail	Probe 1, Probe 2	AAAAGGGAGAGAGA
Non-complementary	Probe 1, Probe 2	ATCCTGAATGCGTACGAGTTGAGA

Table 3.5 Target sequences added to the dye-labelled nanoparticle probes

SERRS spectra were recorded 5 minutes after the addition of the target sequence (20 nM) to the nanoparticle probes (20 pM). SERRS was performed using a *Renishaw Probe* spectrometer with a 514.5 nm argon ion laser equipped with a 20 x long

working distance objective. The inelastically scattered light was analysed using a grating (1200 lines/mm) centred at 1300 cm^{-1} .

A time study of the head-to-head orientation sequences was performed which involved collecting spectra every 2 minutes from the same sample after the target DNA had been added to the nanoparticle probes.

SERRS analysis was performed of the head-to-head duplex where both nanoparticle probes (probe 1 and probe 2, 0.67 nM) were labelled with TRITC (1 μM).

ROX labelled nanoparticle probes were assembled in a head-to-head format using different concentrations of NaCl in the PBS (0.2, 0.3, 0.5, 0.7 M). The melting temperatures were determined by inspection of the UV-visible melting profiles. SERRS spectra were recorded 5 minutes after the addition of the complementary target sequence (20 nM) to the nanoparticle probes (20 pM).

Silver nanoparticle conjugates were prepared using the immobilisation procedure outlined in section 3.3. The sequences used were: 5' SH C₆ (HEG)₃ TCT CAA CTC GTA 3' (probe 4) and 5' SH C₆ (HEG)₃ CGC ATT CAG GAT 3' (probe 5). Probe 4 (500 μL , 0.67 nM) was added to 500 μL , 1 μM solution of TRITC. The oligonucleotide nanoparticle conjugates were incubated for 16 hours in the dark, and then centrifuged and resuspended in 0.3 M PBS. Nanoparticle probe (20 pM) assembly was initiated by addition of complementary target DNA (20 nM): 5' ATC CTG AAT GCG TAC GAG TTG AGA 3' in PBS containing different concentrations of formamide (0, 5, 10, 15, 20 %). The melting temperatures were determined by inspection of the UV-visible melting profiles. SERRS spectra were recorded 10 minutes after the addition of the complementary target sequence.

To ascertain the quantity of reporter dye on the surface of the nanoparticles, 5 replicate samples of silver nanoparticles that had been functionalised with probe 1 and labelled with 1 μM TRITC were used. The concentration of the nanoparticle conjugate in PBS was determined by UV-visible spectroscopy. DTT was added to a final concentration of 0.1 M and incubated at room temperature for 16 hours in the dark, after which time the nanoparticles had precipitated out of suspension. The

samples were centrifuged at 5000 rpm (RCF 2376 x g), 20 minutes and the supernatant was extracted, followed by fluorescence analysis using an excitation wavelength of 555 nm. The concentration of the TRITC label was calculated using a calibration graph of standard TRITC solutions.

The number of DNA molecules *per* TRITC labelled silver nanoparticle was assessed using Cy5 labelled DNA: 5' thiol Cy5 (HEG)₃ TCTCTCT 3'. The concentration of the nanoparticle conjugate in PBS was determined by UV-visible spectroscopy. DTT was added to 5 replicate samples to give a final concentration of 0.1 M and incubated at room temperature for 16 hours in the dark, after which time the nanoparticles had precipitated out of suspension. The samples were centrifuged at 5000 rpm (RCF 2376 x g), 20 minutes and the supernatant was extracted, followed by fluorescence analysis using an excitation wavelength of 643 nm. The concentration of the Cy5 label was calculated using a calibration graph of standard Cy5 labelled DNA solutions.

3.4.5 Mixed Metal Nanoparticle Duplex

DNA oligonucleotides were purchased from ATD Bio, Southampton and malachite green isothiocyanate (MG ITC) was purchased from Invitrogen, Paisley. DNase I and 10 x DNase I reaction buffer was purchased from New England Biolabs, Hertfordshire.

SERRS was recorded using a *Renishaw System 2000* Raman spectrometer with a He Ne laser (632.8 nm). Back-scattered light (180°) was collected using a *Leica DMLM* microscope equipped with a long-working distance objective (20x/NA 0.4). The inelastically scattered light was analysed using a grating (1200 lines/mm) centred at 1200 cm⁻¹ and a *RenCam* CCD. The samples were analysed in a cuvette using a *Ventacon* macrosampler.

Thiol modified DNA (10 nmoles): 5' SH (HEG)₃ TCT CAA CTC GTA 3' (probe 3) and 5' SH (HEG)₃ CGC ATT CAG GAT 3' (probe 4) was added to 13 nm citrate-

reduced gold nanoparticles (1 mL, 17 nM) and 35 nm silver nanoparticles (1 mL, 0.4 nM), respectively. The nanoparticle conjugates were then prepared as in section 3.3. MG ITC, (500 μ L, 1 μ M) was added to the oligonucleotide gold nanoparticle conjugate (500 μ L, 6.7 nM) and incubated for 16 hours in the dark, followed by centrifugation and resuspension in 0.3 M PBS. The silver nanoparticle conjugate was not labelled with a dye.

The nanoparticle assembly was constructed by hybridisation of the complementary target sequence: 5' ATC CTG AAT GCG TAC GAG TTG AGA 3' (50 nM) with the MG ITC labelled oligonucleotide functionalised gold conjugate (0.5 nM) and the oligonucleotide silver conjugate (50 pM). The probes were also mixed with a non-complementary sequence: 5' CCCTTTTGACGACGACGTCTCTCT 3'. SERRS spectra were recorded 5 minutes after the addition of the target sequence. Probe 4 was also immobilised onto 13 nm gold nanoparticles and hybridised to the complementary target 5' ATC CTG AAT GCG TAC GAG TTG AGA 3' along with the MG ITC labelled gold nanoparticle probe. 0.5 nM of each probe was hybridised to 50 nM target.

5' Thiol C₆ HEG HEG HEG CG CAT TCA GGA T FAM 3' was immobilised onto 5 samples of gold nanoparticles and labelled with MG ITC to determine the number of DNA sequences on the dye-labelled nanoparticles. The concentration of the nanoparticle conjugates in distilled H₂O was determined by UV-visible spectroscopy. DNase reaction buffer was added to a final 1x concentration, followed by DNase I (125 units). The samples were incubated for 16 hours in amber 1.5 mL centrifuge tubes at 37 °C. Following centrifugation twice at 7000 rpm (RCF 4657 x g), 20 minutes, the supernatant was extracted and analysed by fluorescence spectroscopy using an excitation wavelength of 492 nm. The concentration of the FAM label was calculated using a calibration graph of standard FAM labelled DNA solutions.

3.4.6 SERRS Triplex

LNA oligonucleotides were purchased from Eurogentec, Belgium. DNA oligonucleotides were purchased from ATD Bio, Southampton and MWG, Germany. ROX ITC was purchased from Invitrogen, Paisley.

Silver nanoparticle conjugates were prepared using the immobilisation procedure outlined in section 3.3. The sequences used were: 5' SH C₆ (HEG)₃T^mctCtCt 3' (probe 1) and 5' ^mC^mc^mcTtTt (HEG)₃ thiol 3' (probe 2) where uppercase letters represent LNA modified nucleotides and ^mc represents 5-methyldeoxycytidine. Probe 1 (500 μL, 0.67 nM) was added to 500 μL, 1 μM solution ROX ITC. The oligonucleotide nanoparticle conjugates were incubated for 16 hours in the dark, and then centrifuged and resuspended in 0.3 M PBS. Head-to-head nanoparticle assembly was initiated by addition of complementary double stranded target DNA (5' GGGAAAAGAGAGA 3' and 5' TCTCTCTTTTCCC 3'). SERRS spectra were recorded 5 minutes after the addition of the target sequence (20 nM) to the nanoparticle probes (20 pM). SERRS was recorded using a *Renishaw Probe* spectrometer with a 514.5 nm argon ion laser equipped with a 20 x long working distance objective. The inelastically scattered light was analysed using a grating (1200 lines/mm) centred at 1300 cm⁻¹.

A reversibility study was performed which involved repetitively heating the triplex above its melting temperature. The assembled triplex was heated to 75 °C in a closed quartz cuvette using a peltier heating block. The UV-visible spectrum was recorded and the cuvette was then transferred to the Raman spectrometer for SERRS analysis. The sample was then cooled to 25 °C at 1 °C min⁻¹ and the SERRS and UV-visible spectra was recorded again. This was repeated 3 times.

The nanoparticle probes (20 pM) were also hybridised to double stranded sequences with non-complementary regions (20 nM). The sequences are shown in figure 3.6. The SERRS spectra were recorded 5 minutes after the addition of the target sequence.

Number of non-complementary base pairs	Target sequences (5' to 3')
0	GGGAAAAGAGAGA + TCTCTTTTTCCC
5	GGGAAAAGCTAGAGAGA + TCTCTAGCAGTTTTCCC
10	GGGAAAAGCTGCTGCTGCAGAGAGA + TCTCTGCTGCTGCTGCAGTTTTCCC
15	GGGAAAAGCTGCTGCTGCTGCTGAGAGAGA + TCTCTGCTGCTGCTGCTGCTGTTTTCCC
20	GGGAAAAGCTGCTGCTGCTGCTGCTGCTAGAGAGA + TCTCTGCTGCTGCTGCTGCTGCTGTTTTCCC
30	GGGAAAAGCTGCTGCTGCTGCTGCTGCTGCTGCTGCTGCTAGAGAGA + TCTCTGCTGCTGCTGCTGCTGCTGCTGCTGCTGCTGTTTTCCC

Table 3.6 Double stranded target sequences added to the nanoparticle probes for triplex formation

3.5 Antibody Functionalised Nanoparticles

The near-infrared linker, 3-(2-[2-(2-(2-(5-1,2-dithiolan-3-yl-pentanoylamino-6-[7-[1-ethyl-3,3-dimethyl-1,3-dihydro-benzindolylidene]-hepta-1,3,5-trienyl)-1, 1-dimethyl-1H-benz[e]indolium]-hexanoylamino)-ethoxy)-ethoxy]-ethoxy)-propionic acid,¹⁷² was dissolved in methanol to a 10^{-3} M concentration. The solution was then diluted to a concentration of 10^{-4} M in 100 mM HEPES buffer, pH 7.6 and 100 μ L was added to 1 mL gold nanoparticles (4 nM) or 1 mL silver nanoparticles (0.4 nM). The solutions were stored in the dark for 4 hours and centrifuged (5000 rpm, RCF 2376 x g, 20 mins) and resuspended in 100 mM HEPES, pH 7.6.

SERRS of nanoparticle conjugate solutions was recorded in a microtitre plate using three excitation sources: 514.5 nm Argon ion laser, 632.8 nm He Ne laser and 785 nm diode laser. The lasers were coupled with *Renishaw inVIA* (514.5 nm) and *Renishaw System 2000* (632.8 and 785 nm) Raman spectrometers. Back-scattered

light (180°) was collected using a *Leica DMLM* microscope equipped with a long-working distance objective (20x/0.4). The inelastically scattered light was analysed using a grating (*Renishaw inVIA*: 1800 lines/mm; *Renishaw System 2000*: 1200 lines/mm) and a *RenCam* CCD. The NIR-Au and NIR-Ag nanoparticles were prepared to a concentration of 2 nM and 0.2 nM in 1x PBS, respectively. A dilution study was performed by diluting the NIR-nanoparticle conjugates in distilled water to multiple concentrations between 50 fM and 6 nM.

3.5.1 Antibody Conjugation

Rat anti α -CD11a (LFA-1) was supplied by Nancy Hogg, Cancer Research UK London Research Institute; anti LFA-1 fluorescein isothiocyanate (FITC) and mouse isotype control was purchased from eBioscience, UK. Biotinylated mouse anti-rabbit was purchased from Pierce, UK. Sulfo *N*-hydroxysuccinimide (sulfoNHS) was purchased from Apollo Scientific, UK. All other chemicals were bought from Sigma Aldrich.

Either anti LFA-1 (10 μ L, 1 mg mL⁻¹), anti LFA-1 FITC (20 μ L, 0.5 mg mL⁻¹), mouse isotype control (20 μ L, 0.5 mg mL⁻¹), or biotinylated mouse anti-rabbit (20 μ L, 0.5 mg mL⁻¹) was added to a solution containing 10 μ L of 1 mM NIR linker, 10 μ L of 2 mg mL⁻¹ EDC and 10 μ L of 2 mg mL⁻¹ sulfoNHS in HEPES buffer, pH 7.6. Following 3 hours at room temperature, the conjugates were purified using centrifuge spin columns, MWCO 10,000 (Millipore, UK) and washed using 1 x PBS. The solution was added to 500 μ L gold nanoparticles (4 nM) or silver nanoparticles (0.4 nM) for 16 hours. Excess conjugate was removed by centrifugation of the nanoparticles at 5000 rpm (RCF 2376 x g), for 10 minutes. This was repeated three times.

3.5.2 Streptavidin Bead Capture

Paramagnetic streptavidin beads were purchased from New England Biolabs, Hertfordshire.

100 μL paramagnetic streptavidin beads were washed three times in 1 x PBS and resuspended with 500 μL biotinylated mouse anti-rabbit gold nanoparticle conjugates (as prepared in section 3.5.1). The solution was agitated for 1 hour, followed by bead separation using a magnet. The supernatant was extracted and analysed by UV-visible spectroscopy.

3.5.3 Antibody Quantitation

DTT (250 mM final concentration) or trypsin (final concentration 0.2 mg mL^{-1}) was added to 5 replicate samples of the anti LFA-1 FITC gold and silver nanoparticle conjugates (section 3.5.1) in 1 x PBS. The samples were left for 16 hours at $37 \text{ }^\circ\text{C}$ in amber 1.5 mL centrifuge tubes and then centrifuged. The supernatant was extracted and analysed by fluorescence spectroscopy using an excitation wavelength of 495 nm. The concentration of FITC label in the supernatant was determined using a calibration graph of standard solutions.

3.5.4 Cell Incubation

Incubation of the anti LFA-1 and mouse isotype control gold nanoparticle conjugates with murine bone marrow-derived dendritic cells was performed in the Strathclyde Institute of Pharmacy and Biomedical Sciences, University of Strathclyde by Emma McFarlane. Experimental details are included in the appendix. Confocal fluorescence microscopy and flow cytometry were performed by Vivienne Gibson in the Centre for Biophotonics, University of Strathclyde.

3.5.5 Cell Analysis

SERRS mapping was performed using a Renishaw *InVia* Raman inverted microscope system equipped with a 100x/0.75 long working distance objective. The excitation sources were a 632.8 nm He Ne and 785 nm diode laser. Line mapping was performed using a Streamline™ Raman mapping system (Renishaw, UK). A

grating of 1200 lines/mm (785 nm) and 1800 lines/mm (632.8 nm) was used with a *RenCam* CCD optimised for near infrared wavelengths.

4. Nanoparticle Modified Oligonucleotides

There has been significant interest in developing oligonucleotide hybridisation assays for biodiagnostic applications. The selectivity and specificity of single stranded DNA oligonucleotides towards a complementary sequence can be exploited for the detection of DNA sequences corresponding to genetic diseases. Modification of DNA with nanoparticles offers several advantages over unmodified DNA for diagnostic applications; the nanoparticles provide a means for monitoring DNA hybridisation colorimetrically and give rise to sharper melting transitions.⁸⁵ It is desirable for oligonucleotide probes to bind to the target DNA with high affinity and as such there has been considerable effort made in the design and synthesis of new DNA analogues. One such example is locked nucleic acid (LNA); a conformationally-restricted molecule due to the methylene bridge across the ribose sugar.^{54, 55} Gold nanoparticles were functionalised with LNA in an attempt to combine the advantages afforded by nanoparticle and ribose sugar modifications.

4.1 LNA Functionalised Nanoparticles

Gold nanoparticles (13 nm) were prepared *via* citrate reduction of sodium tetrachloroaurate.¹⁷⁰ The gold salt is reduced from a +3 to 0 oxidation state, followed by adsorption of excess citrate anions to render the nanoparticles negatively charged, providing them with electrostatic protection against irreversible aggregation. The nanoparticles were centrifuged to increase their concentration and were then functionalised with oligonucleotides. It was found that care should be taken when removing the supernatant from centrifuged gold nanoparticles as removal of too much of the excess reducing anions caused aggregation of the nanoparticles upon the addition of the oligonucleotides. Commonly, dithiothreitol (DTT) is added to

Every 2-3 nucleotides incorporated an LNA modification as this has been reported as being the optimum number for duplex stability;⁶² fully modified oligonucleotide sequences destabilise the resultant duplex.^{63, 69} In addition to LNA modifications, the cytosines were methylated. 5-methyldeoxycytidines have been shown to increase duplex stability due to improved base stacking interactions,^{173, 174} and also play an essential role for the stabilisation of parallel triplex formation at physiological pH.^{75, 175, 176}

Nanoparticle functionalisation with DNA results in a change in the refractive index of the medium surrounding the nanoparticles and as such gives rise to a shift in the plasmon resonance. Functionalisation with the LNA probe sequence resulted in a shift of 2 nm compared with unmodified nanoparticles (figure 4.2). Although the shift is slight, it provided a good indication that the thiolated sequences had successfully adsorbed onto the nanoparticle surface.

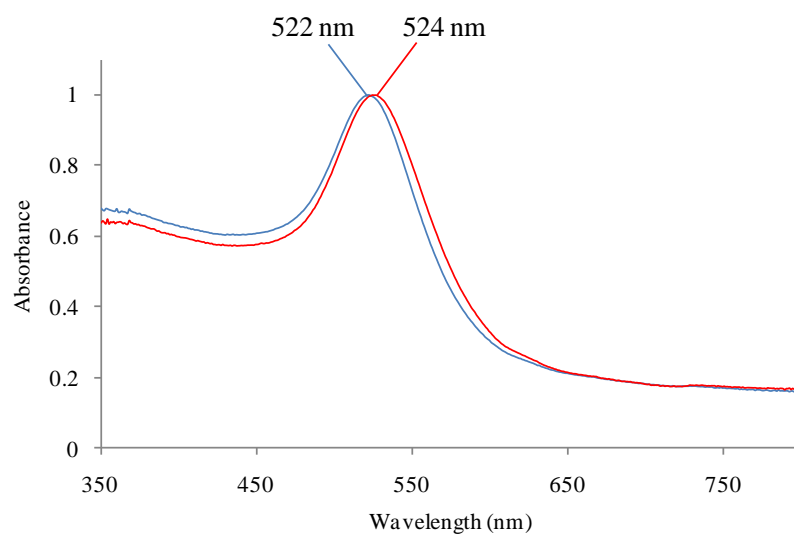


Figure 4.2 UV-visible spectra of unmodified 13 nm gold nanoparticles (blue) and LNA functionalised gold nanoparticles (red).

The probe sequences (figure 4.1) were incubated with the complementary target in phosphate buffered saline (PBS). The target sequence was used at a 100 times higher concentration compared to the nanoparticle probes as previous literature states that

the surface coverage of oligonucleotides on gold nanoparticles is 34 pmol/cm^2 ,⁸⁷ and therefore there would be 100 oligonucleotides *per* 13 nm nanoparticle. This means that the probe to target sequence concentration was approximately 1:1. Upon addition of the complementary target to the nanoparticle-modified probes, a dramatic colour change was observed from red to blue. The colour change was notable from 15 minutes after the target DNA addition. Such a colour change is indicative of the formation of larger nanoparticle aggregates and is accompanied by a broadening and red-shift in the plasmon resonance wavelength of the nanoparticles illustrated in the UV-visible spectrum (figure 4.3). Nanoparticle aggregation occurs due to hybridisation of the probes to the target sequence through Watson-Crick hydrogen bonds. Since there are two probes *per* target, probe hybridisation brings the nanoparticles into close proximity to one another which forms aggregates.

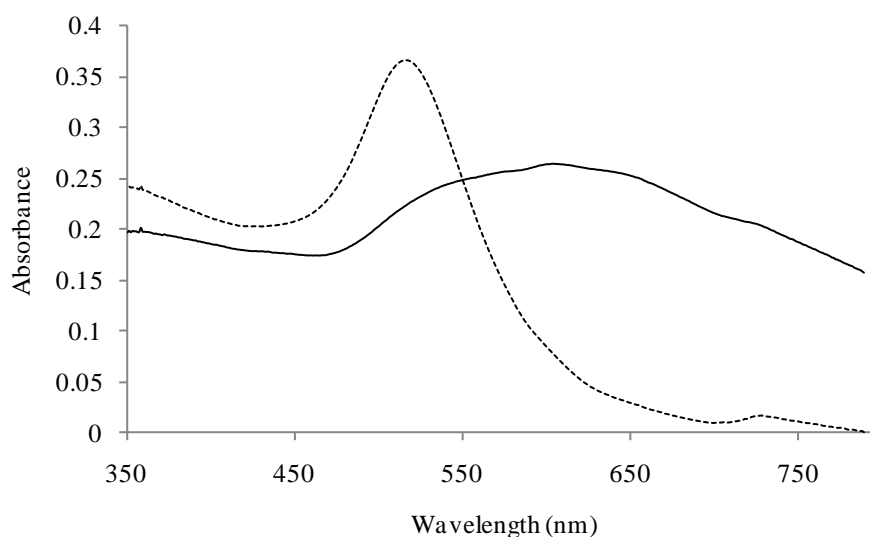
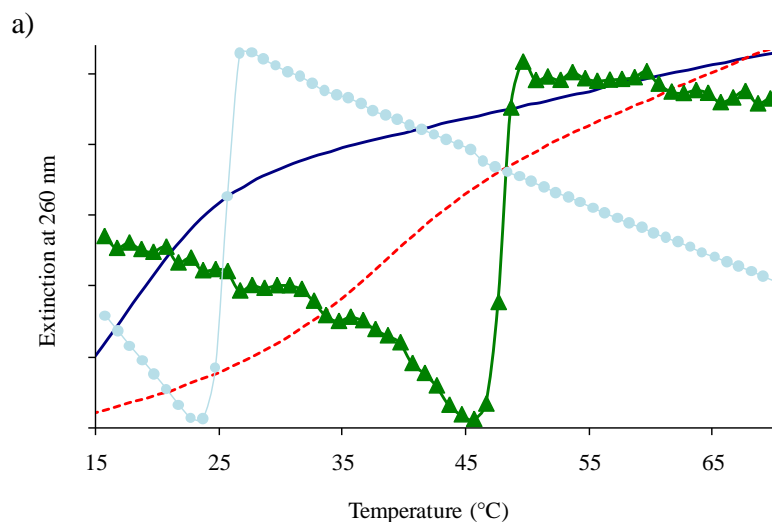


Figure 4.3 Visible spectra of the nanoparticle probes before (dashed line) and after (solid line) the addition of the complementary DNA target.

Successful hybridisation of unmodified oligonucleotide probes cannot be determined colorimetrically and so UV melting experiments are performed. Unmodified DNA sequences absorb light of UV wavelength, corresponding to the electronic transitions in the purine and pyrimidine moieties of the oligonucleotide, and so are monitored at their optical extinction maximum of 260 nm, however, since solutions of

nanoparticle-modified sequences change colour upon hybridisation, these can be monitored at the plasmon resonance wavelength (520 nm for 13 nm gold nanoparticles). The point of inflection on the sigmoidal profile is defined as the melting temperature (T_m) and is representative of the thermal stability of the duplex. The melting curves for the sequences represented in figure 4.2 are shown in figure 4.4. The melting curves were highly reproducible and the melting temperatures varied by less than 2 °C.



b)

Duplex type	T_m (°C)
DNA-DNA	19.0
LNA-DNA	38.5
Nanoparticle-modified DNA-DNA	24.5
Nanoparticle-modified LNA-DNA	47.2

Figure 4.4(a) UV melting curves obtained at 260 nm. Blue solid line: unmodified DNA-DNA duplex, red dashed line: LNA-DNA duplex, light blue circles: nanoparticle modified DNA-DNA duplex, green triangles: nanoparticle modified LNA-DNA duplex. (b) Melting temperatures for DNA and LNA/DNA duplexes. The melting temperature for the nanoparticle-modified duplex was deduced from analysis at 260 nm and 520 nm.

It is apparent from the melting curves that the incorporation of nanoparticles into the probes gives rise to much sharper melting transitions. The sigmoidal shape comes about from the double stranded DNA melting cooperatively. AT regions melt first, which in turn destabilises neighbouring GC base pairs. There are multiple oligonucleotides immobilised onto each nanoparticle and so hybridisation results in the formation of a complex 3-dimensional network. As such, the concentration of DNA at the surface of the nanoparticles is artificially high and therefore the effects of cooperativity are enhanced. Circular dichroism (CD) spectroscopy has been employed to confirm that the sharp melting transition is truly representative of the melting process or whether the observed plasmon resonance is the result of the nanoparticle dispersing as the last base pairs dissociate.⁸⁶ The CD melt indicated a melting transition over the same temperature range as the UV-visible melt and so it was assumed that the melting profile of nanoparticle modified duplexes is characteristic of the denaturation process. It is possible that the large steric repulsion from the nanoparticle modifications is also responsible for the reduced melting temperature range observed. Once the first few bases denature, the repulsive forces may significantly overcome the interstrand attractive forces afforded by remaining hydrogen bonding and base stacking and therefore melting will be accelerated. Disassembly is entropically favoured and so may also contribute to the sharp melting profile.¹⁷⁷ The sharp melting feature of nanoparticle-functionalised melting is advantageous for diagnostic applications as it allows improved discrimination between non-complementary targets.

The melting curves of the nanoparticle conjugates also show a decrease in absorbance prior to the sharp melting transition. It is possible that this is due to incomplete hybridisation of the probes to the template. To investigate this, DNA gold conjugates were allowed to hybridise to a complementary target for several hours to allow complete hybridisation and aggregation of the nanoparticles. The DNA conjugates were then melted using the normal heating/cooling rate of 1 °C *per* minute (figure 4.5).

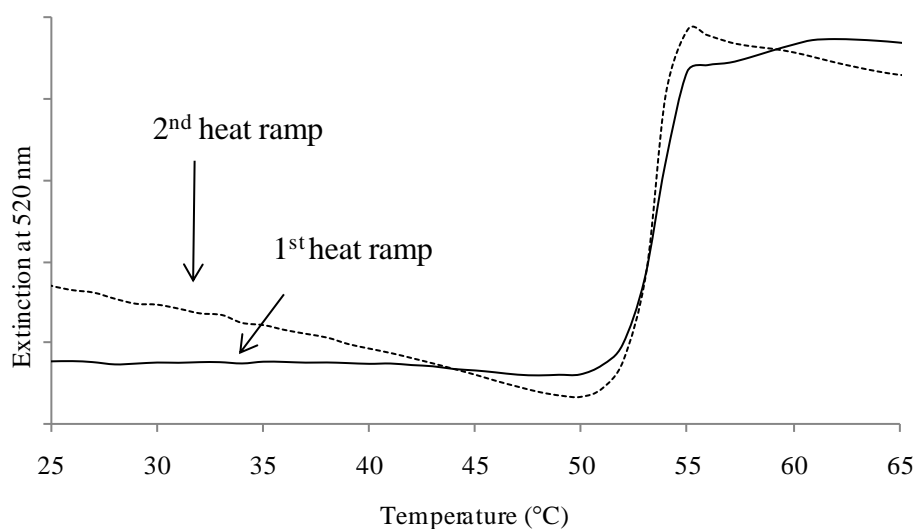


Figure 4.5. UV-visible melting curves of DNA functionalised gold nanoparticles following hybridisation over 3 hours (solid line) and following a $1\text{ }^{\circ}\text{C min}^{-1}$ cool step (dotted line).

The 1st temperature ramp to melt the duplex after complete hybridisation had occurred indicated a plateau region prior to the sharp melting transition. The conjugates were then cooled at $1\text{ }^{\circ}\text{C min}^{-1}$ and then heated again which gave rise to a decreasing absorbance before the duplex melted. This indicates that cooling the probes and target at $1\text{ }^{\circ}\text{C min}^{-1}$ is insufficient to allow complete hybridisation to take place and as a result the duplex is still hybridising during the next melt. Although this appears to have no effect on the melting temperature, it could affect the magnitude of the change in absorbance over the melting transition.

Comparison of the unmodified DNA duplex with the non-nanoparticle LNA chimera duplex in figure 4.4 indicates that the presence of LNA and 5-deoxymethylcytidine modifications increases the thermal stability of the duplex, which is consistent with previous findings in the literature; it is believed that LNA modification increases thermal stability due to either an entropic stabilisation or enthalpic stabilisation effect dependent on the oligonucleotide sequence.⁵⁹ In comparison to unmodified duplexes, enthalpic stabilisation is afforded through improved base stacking⁶⁰ and increased hydrogen bonding (with water molecules⁵⁸ or LNA complement⁶²), whereas entropic stabilisation is afforded through preorganisation of the LNA structure and the

increased numbers of free water molecules due to the more dehydrated A geometry of LNA.⁶¹ Nanoparticle modification alone also appears to increase the melting temperature (the T_m increases by 5.5 °C), although it should be noted that the optical profile obtained for nanoparticle conjugates is associated with the coupling plasmon resonance of the nanoparticles and not the hyperchromicity of the DNA bases. Mirkin and co-workers have suggested that the increase in the melting temperature observed following nanoparticle modification is due to a stabilisation of the DNA interconnects provided by the increased dielectric of the nanoparticles.⁸⁶ However, Xu and Craig reported that nanoparticle modification destabilised the stability of the DNA duplexes in comparison to free DNA in solution and attributed the observed increases in oligonucleotide nanoparticle duplex melting temperatures to multiple bridges between nanoparticles.⁸⁹ Nanoparticle modification of just one LNA probe did not provide an increase in thermal stability when measured at 260 nm, instead, a non-sigmoidal curve with a very broad melting transition was produced (data not shown). This supports Xu and Craig's claim that nanoparticle modification only affords stabilisation when the nanoparticles are linked to one another by the DNA.⁸⁹ The increase in thermal stability for the LNA chimera oligonucleotides was also seen for the nanoparticle-modified analogue, however the increase was more substantial. LNA modification affords 22.7 °C increase in stability for the nanoparticle conjugates, whereas there is only an increase of 19.5 °C for the non-nanoparticle probes, meaning 3.2 °C remains unaccounted for. At this stage, it may be assumed that LNA modification alongside nanoparticle modification results in a synergic stabilisation of the duplex. That is, the combination of these two modifications yields a greater thermal stability than that expected by the individual addition of the modifications.

The selectivity of the LNA nanoparticle probes was investigated by hybridisation of the probes to DNA targets incorporating single base pair mismatches. The sequences used and their corresponding melting profiles are shown in figure 4.6. The incorporation of a single base pair mismatch results in destabilisation of the double stranded DNA evident by the reduced melting temperatures compared with the complementary duplex. This is due to disruption of the Watson-Crick hydrogen

bonding. The extent of this destabilisation is dependent on the mismatch position within the sequence relative to the nanoparticle.

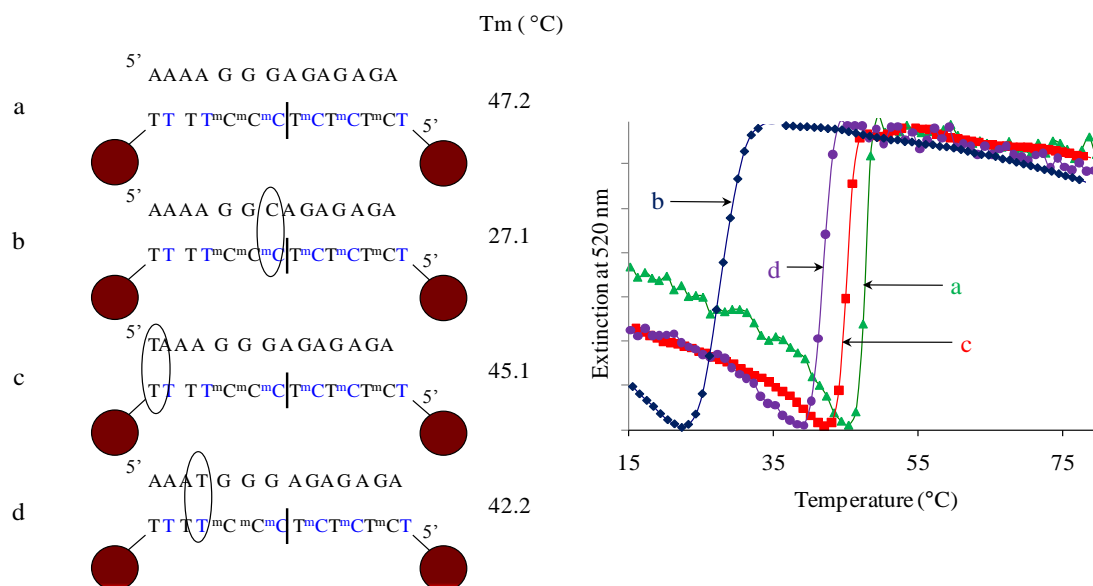


Figure 4.6 Mismatch oligonucleotide sequence melting profiles and temperatures.

A single base pair mismatch at the probe tail (furthest from the nanoparticle) gives rise to the lowest melting temperature (b), followed by mid-probe location (d). A mismatch at the probe head has the least effect on the thermal stability (c). This trend may be explained by denaturation of the double stranded DNA in close proximity to the nanoparticle. The steric bulk of the nanoparticle or secondary electrostatic interactions of the DNA bases with the surface of the nanoparticle may cause incomplete hybridisation of the probe sequences with the complementary target. Therefore, introduction of a base pair mismatch in this region is likely to have little effect on the thermal stability as hybridisation has already been compromised. Furthermore, the mismatch at the probe head was not involving an LNA modified base, and so the duplex will be destabilised to a lesser extent than for the other duplexes where the mismatches are at LNA modified locations. It should also be noted that the mismatch present at the probe tail has occurred between a cytosine and guanine base pair. This base pair has three hydrogen bonds and so disruption of such

will have a greater effect on the overall stability of the duplex compared with the adenine- thymine base pair which only has two hydrogen bonds.

Inspection of the melting curves shown in figure 4.6 enables identification of perfect complementarity between the probes and the target sequence however to ascertain whether the LNA nanoparticle probes offer extra selectivity over unmodified DNA nanoparticle probes, the melting temperatures of mismatch sequences using the latter were recorded (table 4.1).

	LNA NP conjugate		DNA NP conjugate	
	T _m (°C)	ΔT _m (°C)	T _m (°C)	ΔT _m (°C)
Complementary strand	47.2		24.5	
Probe tail mismatch	27.1	-20.1	15.3	-9.2
Probe head mismatch	45.1	-2.1	24.2	-0.3
Mid-probe mismatch	42.2	-5.0	19.3	-5.2

Table 4.1. Melting temperatures of complementary and mismatch sequences for LNA and DNA nanoparticle probes.

The difference in melting temperature between the complementary and mid-probe mismatch sequence is similar for the LNA and DNA nanoparticle conjugates, however for the probe-tail and the probe-head mismatch sequences, the LNA nanoparticle probes exhibit a marked decrease in melting temperature. This indicates that the LNA probes offer greater selectivity towards their targets.

4.2 LNA Functionalised Nanoparticle Triplexes

The LNA nanoparticle probes were used to target double stranded DNA sequences, affording a triple-stranded DNA structure or triplex. Single stranded DNA hybridisation methods require denaturation of the double stranded DNA prior to introduction of the probes, however probe hybridisation directly to double stranded

DNA means denaturation can be omitted and the probes will not be hybridising in competition with the full-length complementary sequence.

The triplex forming oligonucleotide (TFO) can hybridise in the major groove of the double stranded target DNA in either a parallel or anti-parallel orientation through Hoogsteen or reverse Hoogsteen bonding, respectively. Due to the limited accessibility of the TFO to hydrogen bonding sites, only polypurine sequences can be targeted. For parallel hybridisation, the TFO will be of polypyrimidine sequence, whereas anti-parallel hybridisation requires the TFO to be of polypurine sequence. Both hybridisation strategies have advantages and disadvantages. The TFO cytosines need to be protonated for successful parallel triplex formation which is achieved at acidic pHs (the pKa of the endocyclic nitrogen of cytosine is 4.3), however to mimic physiological conditions, the base analogue, 5-methylcytosine can be employed. 5-methylcytosine has an increased pKa, however it is only 0.1- 0.2 units higher than unmodified cytosine and so the ability for TFOs incorporating 5-methylcytosine to hybridise to double stranded DNA at neutral pH has been attributed to improved hydrophobic interactions between the bases.⁷⁶ Anti-parallel triplexes can be assembled at physiological pHs since the TFO is of polypurine sequence however they have been reported to be less thermally stable than parallel triplexes at acidic pH.⁶⁴ Analysis of anti-parallel triplexes using UV-visible melting curves has also been reported to be problematic since the triplex to duplex melting transition is often not observed.⁶⁴ Both triplex motifs benefit from the introduction of further modifications to improve thermal stability. The incorporation of LNA bases has been shown to achieve this.^{62, 69} The formation of a tri-molecular species is even more entropically challenging than formation of the double stranded DNA and so preorganisation of the TFO structure relieves some of the entropic losses that take place upon hybridisation.

Due to the increased stability of parallel triplexes, the oligonucleotide probes were designed to hybridise in a parallel orientation. The cytosines were methylated at the 5 position and every 2-3 nucleotides were modified to LNA. The complementary targets sequences were first mixed together in PBS and then added to a solution of the gold nanoparticle TFO probes. This resulted in a colour change of the

nanoparticles from red to blue, and a broadening of the plasmon resonance wavelength indicating that the TFO probes had successfully hybridised to the double stranded DNA target and induced aggregation of the nanoparticles (figure 4.7).

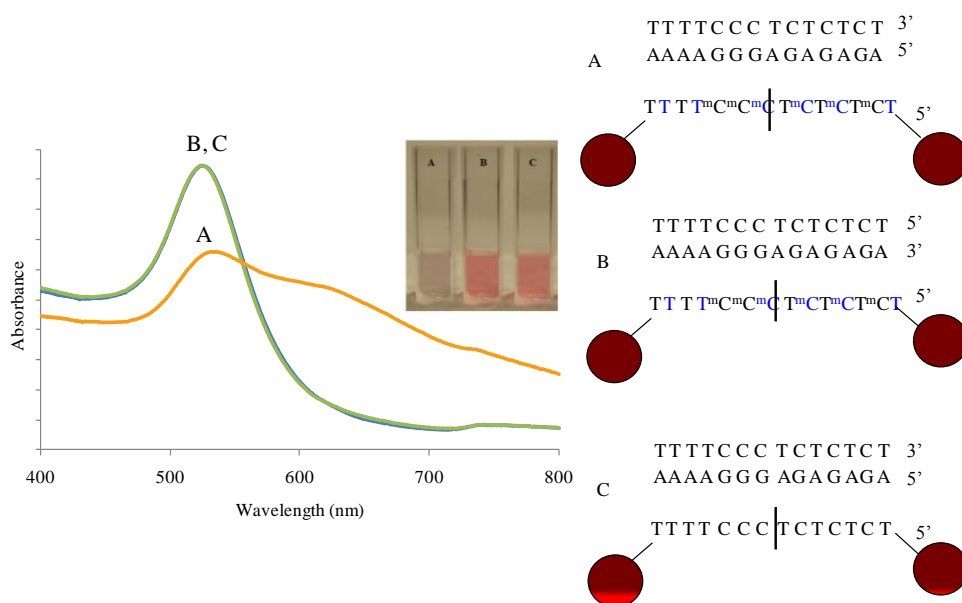


Figure 4.7 Left: UV-visible spectra of LNA nanoparticle probes upon addition of target DNA and corresponding colour change after 1 hour. Right: oligonucleotide sequences used: A) LNA TFO probes with parallel complementary sequence; B) LNA TFO probes with anti-parallel sequence; C) DNA probes with parallel complementary sequence.

Figure 4.7 also shows the control sequences incubated with the nanoparticles probes. The double stranded sequence in sample B is anti-parallel to the probes. Anti-parallel triplexes are formed *via* reverse Hoogsteen hydrogen bonds with the polypurine strand of the target duplex: CG·G and TA·A. Since reverse Hoogsteen hydrogen bonding requires the probe sequence also to be polypurine, anti-parallel triplex formation is not permitted in sample B. Despite no observation of aggregation of the nanoparticles in this sample within the time period of the experiment (1 hour), aggregation was observed after 24 hours indicating that hybridisation of the probe to the target did take place, albeit at a much slower rate. This could indicate that the probes invaded the double stranded DNA and bonded with the polypurine sequence through Watson-Crick base pairing. Strand invasion is more commonly cited as a property of peptide nucleic acid (PNA) however has also been observed for LNA.¹⁷⁸

¹⁷⁹ LNA modifications were omitted from the probe sequence in sample C.

Aggregation of the nanoparticles was not observed over any time period indicating that, in this system, triplex formation was unique to the LNA modified-nanoparticle probes only.

The melting profile obtained for the nanoparticle triplex (sample A, figure 4.7) is shown in figure 4.8. The melting temperature of the triplex was 37 °C which is 17 °C lower than that for the double stranded DNA target. This was expected as triple stranded structures are less stable than double stranded structures and indicates that the TFO probes dissociate prior to denaturation of the double stranded target.

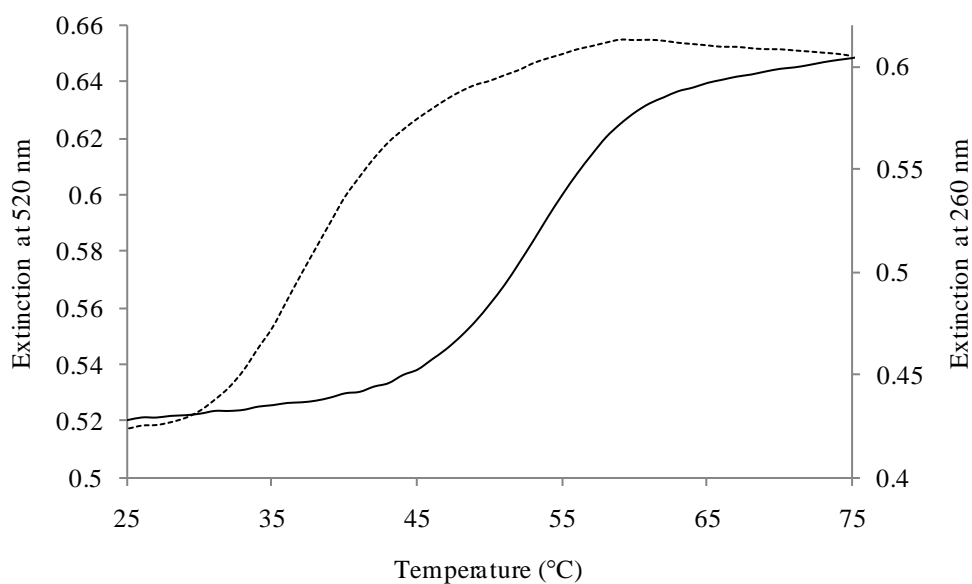


Figure 4.8 UV-visible melting curve of the nanoparticle LNA triplex at 520 nm (dotted line) and the target double stranded DNA at 260 nm (solid line).

The melting curve for the nanoparticle-modified triplex illustrates a relatively broad melting transition. This suggests that the oligonucleotide strands are not denaturing as cooperatively as for the nanoparticle-modified duplex (figure 4.4). It is possible that this is a feature of triplex melts, however due to limited literature on nanoparticle-modified triplexes it is difficult to corroborate this. Sun *et al.* noted that the triplex to double stranded DNA melting transition was less pronounced when the TFO incorporated LNA modifications and attributed this to less enthalpy driven stabilisation of the LNA modifications.⁶² Although the transition is broad, it is still a

large improvement upon non-modified triplexes. Due to overlapping transitions between triplex to duplex DNA and duplex to random coil DNA, it is often extremely difficult to ascertain the melting temperature of a triplex. The triplex to duplex melt using oligonucleotide sequences that had not been modified with nanoparticles was not identifiable at all when analysed by UV-visible spectroscopy and the duplex to random coil transition was also obscured (data not shown). This is not surprising considering the large melting transition ranges for the triplex and duplex structures (figure 4.8). Therefore, modification of the TFO probes with nanoparticles enables the melting temperature of the triplex to be determined when it was not otherwise possible by this spectroscopic method.

It was necessary to ascertain whether the selectivity of the nanoparticle probes had been compromised in exchanging a single stranded target for a double stranded target. A sequence incorporating a base pair mismatch at the probe tail was incubated with the nanoparticle probes and analysed by UV-visible spectroscopy (figure 4.9b). Over the period of 1 hour, any decrease or shift in the plasmon resonance wavelength was negligible and the colour of the sample remained red.

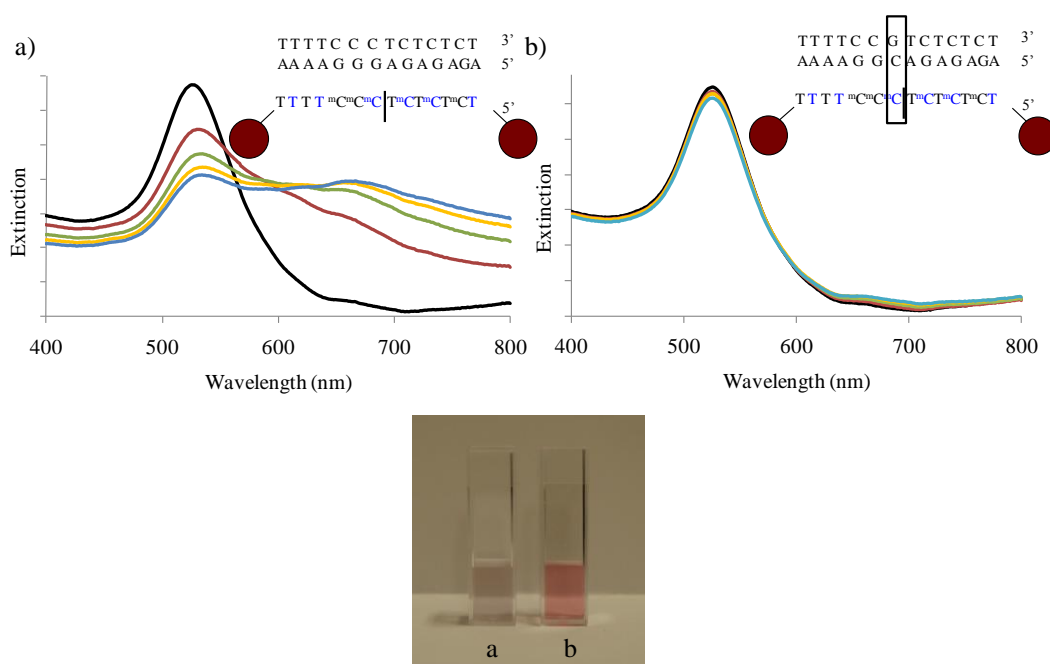


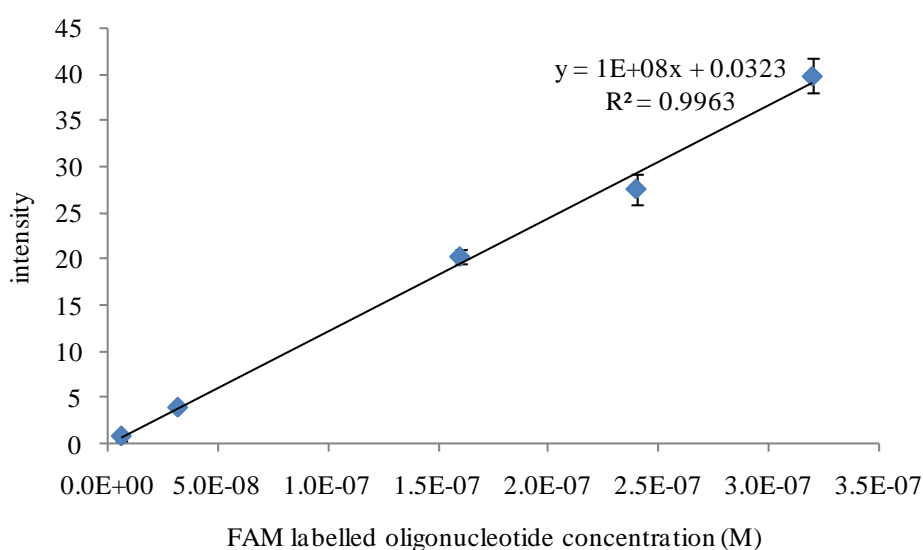
Figure 4.9 UV-visible spectra and colour of LNA nanoparticle probes after addition of complementary (a) and mismatch (b) double stranded DNA. Black: 0 minutes, red: 6 minutes, green: 12 minutes, yellow: 18 minutes, blue: 24 minutes. The boxed region of the DNA sequence in (b) highlights the mismatched base pairs.

This demonstrates that using a triplex format, LNA nanoparticle probes can be hybridised to double stranded DNA at room temperature. The probes are selective for the complementary target allowing detection of specific DNA sequences. It should be noted that the probe tail location of the mismatch within the sequence was shown to have the most destabilising effect when the nanoparticle probes were hybridised to form a duplex (figure 4.6) Therefore, it is possible that a mismatch at the probe head or mid sequence will have less of a perturbation effect on triplex formation. Fosella *et al.* have investigated the affinities of mismatch TFOs for double stranded targets and concluded that triplexes suffer greater destabilisation when the TFO contains a mismatch compared with Watson-Crick duplexes where one of the complementary strands incorporates a base pair mismatch.¹⁸⁰ It is difficult to determine if this observation is supported by the results obtained in this investigation since the LNA nanoparticle duplex was destabilised by 20 °C (table 4.1) which if extrapolated to the triplex system would mean the triplex melting temperature was 17 °C. However, the triplex mismatch experiment was conducted at room temperature; therefore it would be interesting to conduct further melting experiments to ascertain whether destabilisation was equal to or less than for the duplex.

4.3 Polyethylene Glycol Spacing

Although the oligonucleotide conjugates were effective at detecting single and double stranded DNA targets, there were often difficulties when preparing the conjugates prior to hybridisation experiments. The nanoparticles sometimes irreversibly aggregated during the salt ageing process rendering the nanoparticles unusable. It is likely this was the result of self-complementarity between the polyadenine spacer and a region of four adjacent thymines on the probe, which was unnoticed when the probes were designed. To overcome this problem, the polyadenine region was substituted with 3 hexaethylene glycol (HEG) units which collectively were of similar length to the 10 adenine region and should have no affinity with the probe sequence. It has been reported by Mirkin and co-workers that twice as many oligonucleotides are immobilised onto the nanoparticle surface if the

sequence incorporates PEG adjacent to the thiol modification⁹⁵ and so the number of oligonucleotides using both types of spacer was quantified using a displacement method first reported by Demers *et al.*⁸⁷ DTT was added to FAM-labelled oligonucleotide nanoparticle conjugates in PBS which adsorbs onto the nanoparticle surface, simultaneously displacing the thiol-modified oligonucleotides into the bulk solution. It was necessary to displace the fluorescence-labelled oligonucleotides from the nanoparticle surface prior to analysis as metal nanoparticles are able to quench²⁷ or enhance^{181, 182} fluorescence.



repeat samples	intensity	FAM oligo conc ⁿ using calibration equation (M)	FAM oligo conc ⁿ prior to sample dilution (M)	nanoparticle concentration (M)	calculated oligonucleotides per nanoparticle
A	14.64	1.46×10^{-7}	8.11×10^{-7}	2.94×10^{-8}	27.60
B	14.86	1.48×10^{-7}	8.24×10^{-7}	3.05×10^{-8}	27.02
C	13.93	1.39×10^{-7}	7.72×10^{-7}	2.67×10^{-8}	28.87
D	15.30	1.53×10^{-7}	8.48×10^{-7}	2.95×10^{-8}	28.66
E	12.48	1.24×10^{-7}	6.92×10^{-7}	2.44×10^{-8}	28.34

Figure 4.10 Fluorescence calibration graph and fluorescence quantitation for polyA oligonucleotides adsorbed onto 13 nm gold nanoparticles. The calibration graph presents the mean fluorescence intensity obtained from 5 replicate analyses. The error bars represent the standard deviation.

The addition of DTT resulted in aggregation of the nanoparticles since they were no longer protected by the oligonucleotides from the buffer ions, allowing facile extraction of the supernatant following centrifugation. The concentration of the FAM-labelled DNA was determined by correlation with a standard calibration graph which was evaluated against the original nanoparticle concentration. Using this method, the number of fluorescence-labelled oligonucleotides incorporating polyA and PEG spacers *per* 13 nm gold nanoparticle was estimated to be 28.1 ± 0.8 and 63.4 ± 3.4 , respectively. An example calculation is shown in figure 4.10 for the polyA oligonucleotides. The data supports Mirkin's findings that utilisation of PEG spacers increases the number of adsorbed oligonucleotides *per* nanoparticle.⁹⁵ This is advantageous as it means the nanoparticle conjugates are more resistant to aggregation in ionic buffers but it was also important to consider if there are any negative effects on hybridisation due to increased steric or electrostatic repulsion. The melting temperatures and hybridisation rates of nanoparticles functionalised with oligonucleotide sequences incorporating polyadenine spacers and PEG spacers were recorded and are presented in figure 4.11. There is no significant difference in aggregation rate or melting temperature between the nanoparticle probes incorporating a polyA or PEG spacer. Therefore oligonucleotide sequences used in future work were replaced to include 3 HEG units after the thiol modification.

To ascertain whether the broad triplex melt could be improved upon incorporation of the PEG spacer, the PEG spacer LNA gold nanoparticle probes were hybridised to the double stranded DNA target. The melting profile for the triplex using the gold nanoparticle probes was not improved, but interestingly, when the probes were modified with citrate-reduced silver nanoparticles a significantly sharper melting transition of higher temperature was observed (figure 4.12) suggesting that the broad transition observed in figure 4.8 is not a specific feature of triplexes. The improved hybridisation for the silver nanoparticle probes compared with the gold nanoparticle probes is possibly due to increased cooperativity arising from the greater number of oligonucleotide strands *per* silver nanoparticle compared with the number for gold nanoparticles. 35 nm silver nanoparticles have a greater available surface area for oligonucleotide adsorption which is approximately a factor of 7 greater than for 13 nm gold nanoparticles, assuming the nanoparticles are perfectly spherical.

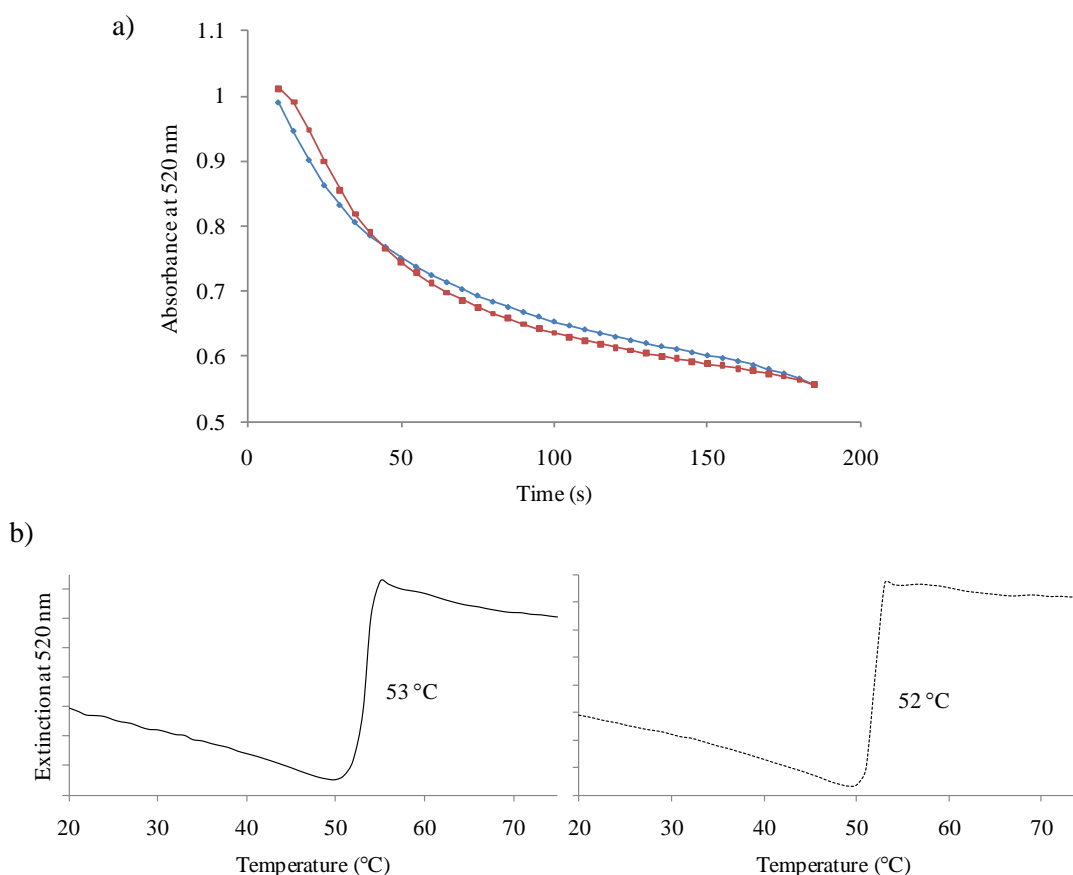


Figure 4.11 a) The change in absorbance over time during hybridisation of oligonucleotide nanoparticle probes to the complementary target. Red: polyA spacer; blue: PEG spacer. b) UV-visible melts of oligonucleotide nanoparticle probes. Solid line: polyA spacer; dashed line: PEG spacer.

Although modification of the triplex sequences with silver nanoparticles improved the melting transition, it was noted that for the subsequent heating cycle of the triplex, the melting transition became broader and exhibited an identical melting temperature as the gold triplex using polyA spacer probes, and the third melting cycle indicated that hybridisation had not occurred at all. This suggests that silver nanoparticle triplex formation is not fully reversible when a cooling rate of 1 °C *per* minute is employed. Renaturation is usually reversible for short oligonucleotides where formation of a nucleation site between the complementary strands is the rate

limiting step, whereas longer oligonucleotides are susceptible to competing base pairing interactions such as intrastrand loop formation.

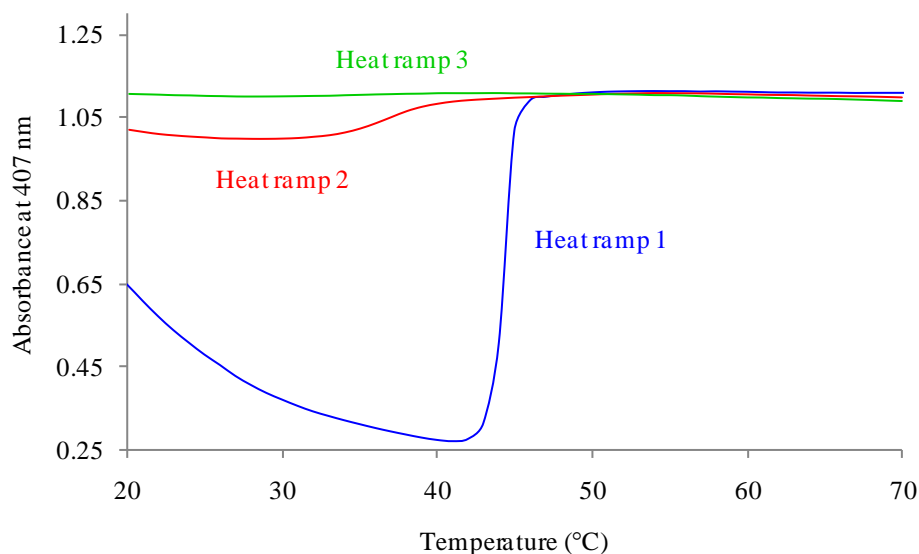


Figure 4.12 1st, 2nd and 3rd melting curves of the silver nanoparticle modified triplex.

Although the probe sequences used here are only 7-mers, a significant competing interaction is the hybridisation of the TFO probes with the polypurine strand of the target sequence through Watson-Crick hydrogen bonds, in particular the probe incorporating alternating cytosine and thymine bases which can fully hybridise to the polypurine target through both Watson-Crick and Hoogsteen hydrogen bonds. Evidence of Watson-Crick hybridisation was observed in the colorimetric experiments shown in figure 4.7 and so it is possible that hybridisation of this type is occurring after the double stranded DNA has been denatured following the first heating ramp. It should also be noted that probe hybridisation to form the triplex is tri-molecular and so nucleation will be slower than if it was a bimolecular duplex assembly. Another possible reason for non-reversibility is the lability of the thiol-silver bond. Thiolated compounds have been reported numerous times in the literature for their ability to diffuse across or desorb from a surface. Checkik and co-workers employed electron paramagnetic resonance to ascertain the mechanism for thiol mobility on a gold nanoparticle surface⁴³ and Murray and co-workers investigated ligand-exchange reactions of thiolates on gold surfaces who suggested

that nanoparticle ligand exchange occurred *via* a dissociation mechanism.⁴² In terms of DNA ligands, the gold surface has been reported to facilitate the degradation of thiolated DNA immobilised on the surface⁹⁷ and Li *et al.* reported that application of heat can cause DNA degradation.⁹⁶ Due to thiols having a reduced affinity for silver surfaces compared with gold,¹⁸³ these effects may be enhanced. Vidal *et al.* reported that oligonucleotide functionalisation of silver nanoparticles was not possible using the established salt ageing method since the nanoparticles irreversibly aggregated¹⁸⁴ and Dougan *et al.* used disulfide modified oligonucleotides on silver so that stability comparable with monothiolated oligonucleotides gold nanoparticle conjugates could be achieved.⁹⁹ Thus, it is highly probable that degradation of the silver-oligonucleotide conjugates is responsible for the observed non-reversibility of the triplex.

4.4 Conclusions

In conclusion, gold nanoparticles were functionalised with LNA modified oligonucleotides and were used to target complementary DNA sequences. This was the first report of the preparation of LNA oligonucleotide nanoparticles. Successful hybridisation was characterised by a dramatic colour change of the nanoparticle suspension from red to blue and a significant shift and broadening of the plasmon resonance wavelength. Incorporation of the LNA and nanoparticle modifications afforded a greater thermal stability of the oligonucleotide duplex than either the nanoparticle or LNA modification, separately indicating a synergic effect is produced when both modifications are employed simultaneously. The LNA nanoparticle probes were shown to effectively discriminate against DNA targets incorporating single base pair mismatches and exhibited increased selectivity for the complementary target over analogous DNA nanoparticle probes. The high affinity and selectivity for the DNA sequence, in combination with the sharp melting profiles which are feature of nanoparticle modified DNA duplexes, makes employment of LNA nanoparticle probes extremely attractive for biodiagnostic applications. The LNA nanoparticles probes were also used to target double stranded DNA by parallel

triplex formation. The probes were still shown to discriminate against a single base pair mismatch indicating that the probe selectivity had not been compromised by hybridisation through Hoogsteen hydrogen bonding instead of Watson-Crick. The melting profile for the gold nanoparticle triplex was much broader than the nanoparticle modified duplex however it was found that this was not a feature of triplexes since this was not observed for the silver nanoparticle triplex. The polyadenine spacer region was substituted for a polyethylene glycol spacer which was found to eliminate problems experienced as a result of self-complementarity and increased oligonucleotide loading which is desirable for stability in high ionic strength buffers. Nanoparticle modification of triplex structures is advantageous as it allows facile identification of the triple stranded to double stranded melting transition which is often ambiguous in non-modified triplex melts. DNA detection by triplex formation is advantageous as it means the biological sample does not need to be denatured prior to introduction of the probes however it does suffer from numerous limitations, namely decreased thermal stabilities and only polypurine sequences can be targeted.

5. DNA Detection by SERRS

5.1 SERRS Analysis of DNA Oligonucleotides

Presently, commercial oligonucleotide sequence detection is performed using fluorescence spectroscopy on microarrays and quantitative PCR. Although there are many advantages to this technique such as low limits of detection and a large number of available labels, its main drawback is broad emission profiles, limiting the number of fluorophore-labelled oligonucleotides that can be analysed at any one time. Surface enhanced resonance Raman scattering (SERRS) is considered a powerful analytical technique due to its potential to simultaneously discriminate between several targets. SERRS spectra have distinctly different characteristics which are indicative of specific molecules. The sharp, narrow bands mean peak overlap is limited and therefore structural assignments can be made at ease with little need for complex chemometric analysis. Fluorescent labels may be still be utilised in SERRS since fluorescence emission is quenched by the metal surface, an essential component for surface enhancement.

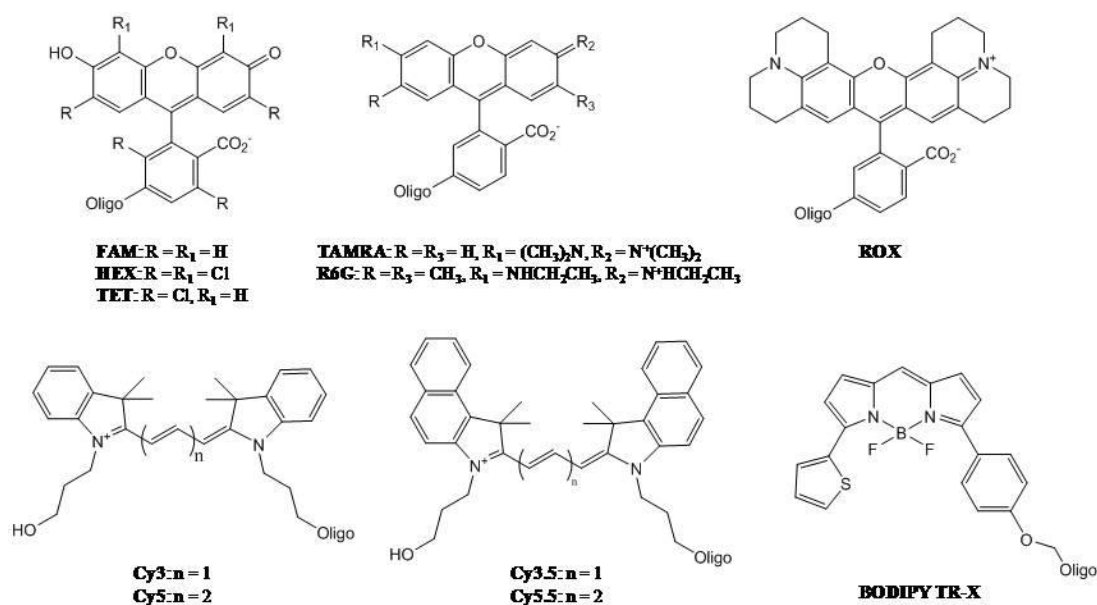


Figure 5.1 Oligonucleotide fluorescent dye labels

To investigate the multiplexing potential of SERRS, several commercially available fluorescent-labelled oligonucleotides, figure 5.1, were analysed by SERRS using laser excitation wavelengths of both 514.5 nm and 632.8 nm. Citrate-reduced silver nanoparticles were mixed with the dye-labelled oligonucleotides and aggregated using spermine immediately prior to SERRS analysis. Silver nanoparticles were used in this study as it has been reported that lower limits of detection are obtained using silver, compared with gold nanoparticles.¹¹⁸ This was attributed to the greater scattering to absorbance ratio for silver than gold and the greater polarisability of the silver electrons (the electron cloud of gold suffers from a stronger relativistic contraction¹⁸⁵) resulting in greater surface enhancement. Aggregated nanoparticles produce much stronger SERRS intensities than monodisperse nanoparticles. Only a small proportion of single nanoparticles are able to contribute to surface-enhanced scattering; it has been reported that less than 10 % of isolated nanoparticles are SERRS active.³⁰ Nanoparticle aggregation allows electromagnetic coupling between adjacent nanoparticles permitting lower energy plasmons to oscillate across the surface. As the number of particles within an aggregate increases, longer excitation wavelengths will be in resonance with the surface plasmons. Therefore, aggregation of the nanoparticles yielding different sized aggregates extends the range of wavelengths which will be in resonance with the plasmon oscillations. An aggregate of specific size can yield a wide range of SERRS intensities and therefore it may be assumed that the arrangement of the particles and localized surface features will also play a significant role in surface-enhancement.²⁹ The junctions between neighbouring nanoparticles is thought to be responsible for the generation of intense electric fields resulting in greater polarisation of the analyte's electron cloud and subsequently increased scattering. Due to the large SERRS activity observed at these junctions, the point of contact between two or more nanoparticles is referred to as a 'hot spot'. It has been shown that for nanoparticle separations of less than 0.5 nm, electromagnetic enhancements of greater than 10^{10} can be achieved.³¹ Spermine was selected as the choice of aggregating agent since it has been shown, alongside poly-L-lysine, that more reproducible SERRS signals are obtained in comparison with sodium chloride or nitric acid.³³ Aggregation is achieved through neutralisation of

the negative citrate surface layer of the nanoparticles by the protonated primary amines on the spermine.

It may be anticipated that all dyes should give increased SERRS intensities at shorter excitation wavelengths as Rayleigh theory predicts that the intensity of scattered light decreases at longer wavelengths ($I_{\text{scat}} = 1/\lambda$). However, due to the resonance contribution of SERRS, a chromophore that has a maximum absorption at a wavelength approximately coincident with the laser excitation will result in significant signal enhancement. The maximum absorbance wavelengths for each dye are shown in table 5.1.

Dye label	λ_{max} (nm) ¹¹⁸
FAM	492
TET	521
R6G	524
HEX	535
Cy3	552
TAMRA	565
Cy3.5	581
ROX	585
BODIPY TR-X	588
Cy5	643
Cy5.5	683

Table 5.1 Maximum absorbance wavelengths of oligonucleotide dye labels

The longer maximum absorbance wavelengths for Cy3.5, Cy5, Cy5.5 and BODIPY TR-X means these dyes perform better at 632.8 nm than 514.5 nm. For a given dye, the range of excitation wavelengths that result in a strong SERRS spectrum is much greater than that for absorbance. The Lorentzian shape of the resonance excitation profile means that resonance enhancement for each vibrational mode can occur at a wavelength well beyond the absorption maximum wavelength. Combining this effect with the broad resonance of the nanoparticles, necessary for the surface enhancement, allows multiple dyes to be analysed using a single wavelength.

The dye-labelled oligonucleotides were mixed together in a range of combinations, and were all used at the same concentration (0.1 μM). The most successful multiplex mixture was the addition of oligonucleotides labelled with FAM, R6G, BODIPY TR-X, Cy5.5 and ROX to the aggregated silver colloid. This combination of dye labels allows each individual dye to be identified using the two excitation wavelengths. The spectra of the individual dyes are shown below in figure 5.2.

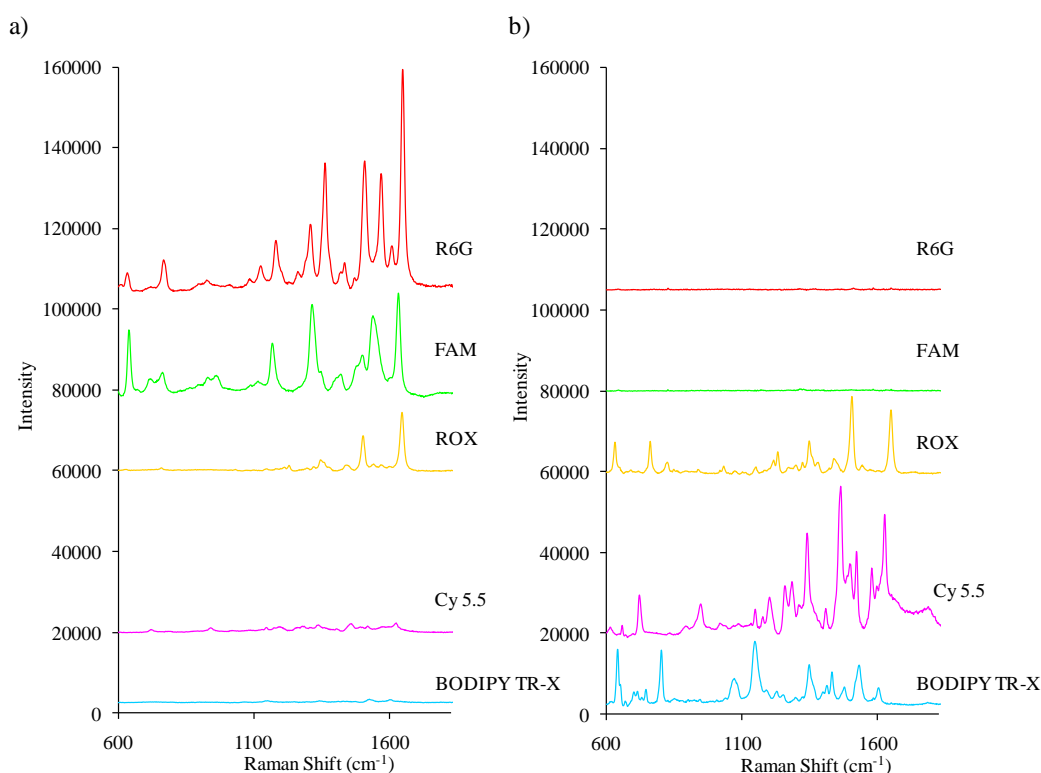


Figure 5.2 SERRS spectra of dye-labelled oligonucleotides (final concentration 1.92 nM) analysed individually using a) 514.5 nm and b) 632.8 nm excitation wavelengths

R6G and FAM can only be identified at 514.5 nm, whereas Cy 5.5 and BODIPY TR-X can only be identified at 632.8 nm. Although the strongest peak for R6G and FAM at 514.5 nm occurs at 1649 and 1631 cm^{-1} , respectively, these peaks when analysed together are too close to be resolved and therefore other peaks within the spectra must be chosen. Likewise, the strongest peak for ROX at this excitation wavelength occurs at the same wavelength as R6G and therefore identification of this dye within a multiplex would be best performed at 632.8 nm. Because the SERRS response of

the dye labels is selective for different excitation wavelengths, dual-wavelength analysis means a greater number of dyes can be analysed simultaneously without interference, for example common wavelength peaks, from other labels within the mixture.

The multiplexed mixture analysed at both wavelengths is shown in figure 5.3. Each of the dye-labelled oligonucleotides within the 5-plex can clearly be identified by eye and each labelled peak is unique to the dye within the mixture.

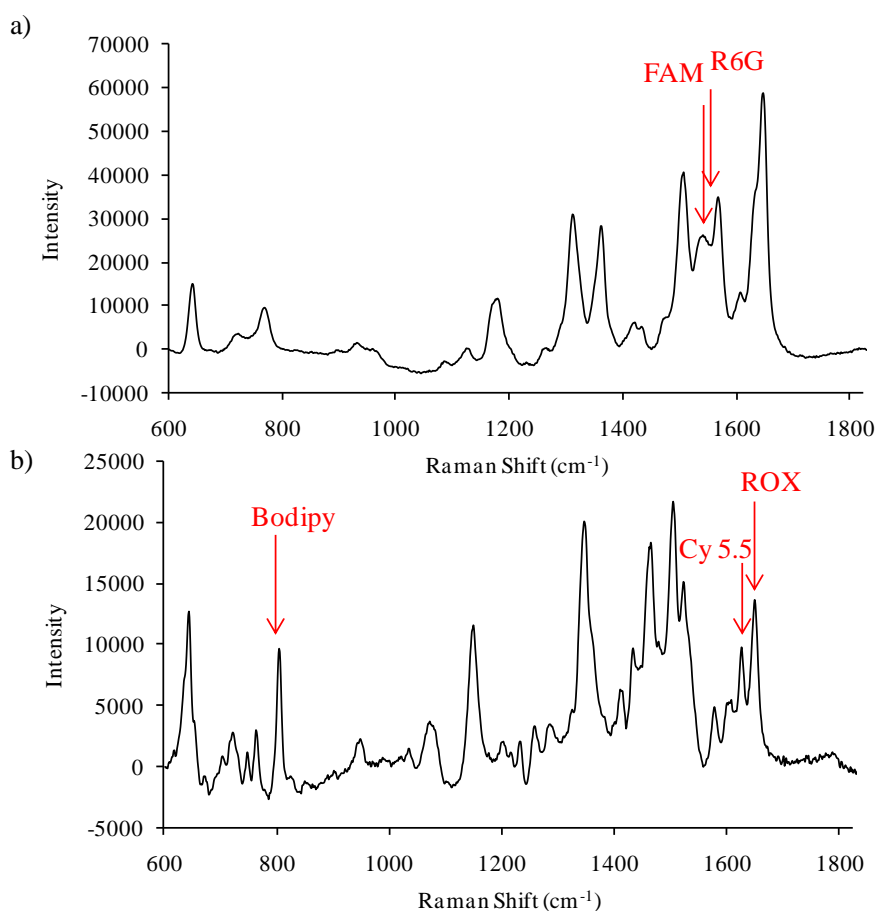


Figure 5.3 SERRS spectra of multiplex using a) 514.5 nm and b) 632.8 nm excitation wavelengths. The peaks corresponding to each dye are labelled.

It is important to consider whether the multiplexed dye-labelled oligonucleotides could be analysed quantitatively. The detection limit for the multiplex was determined by dilution of the oligonucleotide mixture and identification of each dye.

For each of the six dilutions, the mixture was analysed five times and the average intensity for each band corresponding to a particular dye-labelled oligonucleotide, was plotted (figure 5.4). The quantitative analysis was performed in a cuvette unlike the qualitative experiments that were performed using a microtitre plate. Aggregates can form at the air-water interface in microtitre plates and as such, SERRS signals can often be highly unreproducible as a result of the aggregates passing in and out of the collection voxel. Nevertheless, microtitre analysis is generally more sensitive as the laser does not have to pass through the strongly absorbing nanoparticle sample and thus lower limits of detection can be recorded.

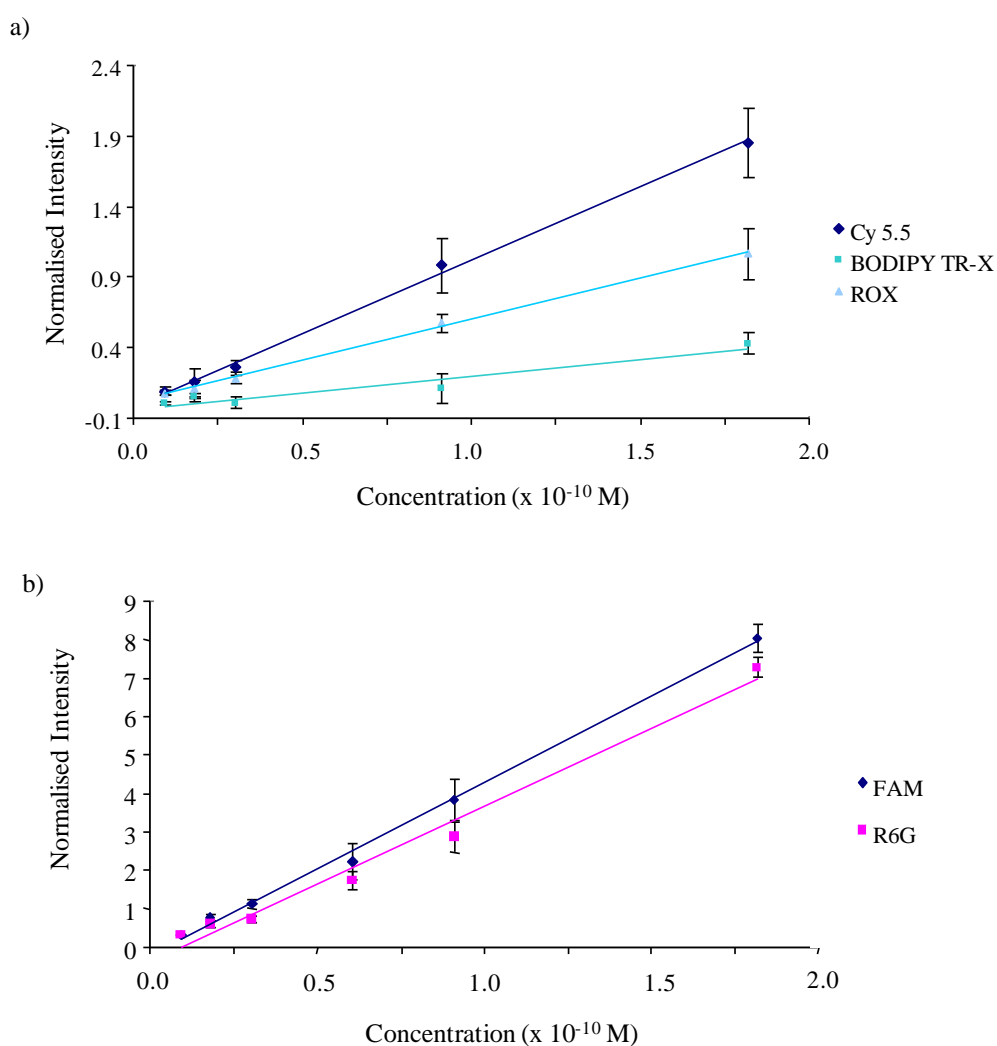


Figure 5.4 Dilution series of multiplex. The intensity of the peak corresponding to each dye label (Cy5.5: 1625 cm^{-1} ; BODIPY TR-X: 802 cm^{-1} ; ROX: 1647 cm^{-1} ; FAM: 1539 cm^{-1} ; R6G: 1568 cm^{-1}) was plotted against the concentration of the multiplex.

Linear plots were obtained for all dye labels, illustrating the multiplex may be used for quantitative purposes. The gradients of the lines for FAM and R6G are similar indicating they have a similar sensitivity, however at 632.8 nm, BODIPY TR-X has a significantly reduced sensitivity when compared with ROX and Cy5.5. The limits of detection for each dye were calculated by assigning the limiting signal intensity to be three times the standard deviation of the background signal.

	Identifying band (cm ⁻¹)	L.o.D in multiplex (M)	Individual L.o.D (M) ¹¹⁸
FAM	1539	2.91 x 10 ⁻¹²	2.7 x 10 ⁻¹²
R6G	1568	3.22 x 10 ⁻¹²	1.2 x 10 ⁻¹²
ROX	1647	1.25 x 10 ⁻¹¹	3.3 x 10 ⁻¹¹
BODIPY T-RX	802	3.08 x 10 ⁻¹¹	7.9 x 10 ⁻¹²
Cy5.5	1625	6.70 x 10 ⁻¹²	5.2 x 10 ⁻¹²

Table 5.2 Limits of detection for dye-labelled oligonucleotides in multiplex

The limits of detection presented in table 5.2 for the dye-labelled oligonucleotides that had been analysed separately were reported by Stokes *et al.*¹¹⁸ and are obtained using the same excitation wavelengths as were used in this study. The limits of detection for the multiplex are comparable to the limits of detection of individually analysed dye-labelled oligonucleotides indicating little loss in sensitivity when the dye labels are multiplexed together. It should be noted that the peaks used to determine the signal intensities are different for the two studies; for the multiplex study, the most intense peak was not inspected due to commonality of peaks between the xanthene-type dye labels. In a real biological sample, the concentration of the dye-labelled oligonucleotides will differ from one another and therefore the limits of detection will be much higher than calculated here due to increased background signal. To ascertain the limits of detection by altering the variable dye-label concentrations simultaneously, chemometric analysis would be required.

The oligonucleotides labelled with FAM and Cy5.5 incorporated several propargylamine-2'-deoxyuridine bases at the 5' end adjacent to the dye label. Propargylamine modification is employed to improve the oligonucleotides electrostatic affinity for the silver nanoparticle surface. The silver nanoparticles have a net negative charge due to adsorption of citrate which was introduced as the reducing agent in the nanoparticle synthesis.²¹ Negatively charged dye-labels will be repelled from the nanoparticle surface and therefore the Raman scattering will not benefit from surface enhancement. Propargylamine-2'-deoxyuridine has a primary amine group which will be protonated at physiological pH, hence reducing the electrostatic repulsion arising between the dye label and the silver surface. The oligonucleotides incorporating propargylamine modification used here and those reported in the literature have incorporated six bases^{116, 118} although there has been no investigation reported as to whether this is the optimum number. It would be beneficial, particularly for economic reasons, to determine if fewer bases would be equally as effective.

5' FAM-labelled oligonucleotides containing between 0 and 6 propargylamine modified bases were added to silver nanoparticles and aggregated using spermine. The SERRS response from each oligonucleotide was normalised and plotted (figure 5.5). The addition of only one propargylamine has a significant effect on the SERRS response, causing a three-fold increase in the intensity when compared with oligonucleotides containing no modified bases. Increasing the number of propargylamine bases from 1 to 4 steadily caused an increase in intensity; a result of the improved adsorption of the oligonucleotides onto the nanoparticle surface. However for most concentrations, the addition of 6 propargylamines results in a slight decrease in intensity. The maximum signal is obtained using 4 propargylamine bases for the FAM-labelled oligonucleotide meaning cost for such oligonucleotide probes may be reduced and also the probe system can be simplified with no loss of SERRS response.

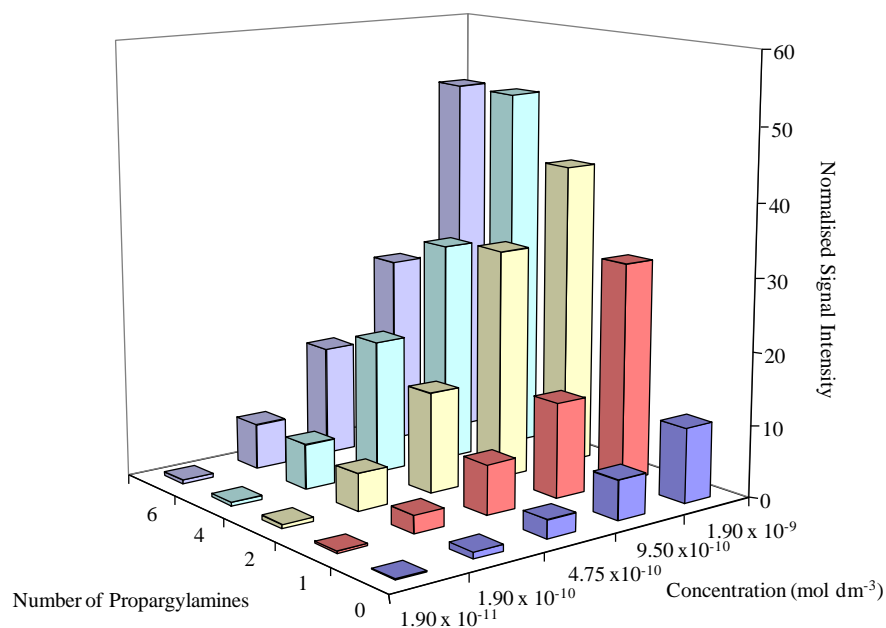


Figure 5.5 Bar chart of SERRS intensity for propargylamine modified oligonucleotides of different concentrations

In order to detect DNA sequences in a real biological sample, an approach must be developed that does not require modification of the target sequence. In solution based nanoparticle assays, this is best achieved using a split probe format (figure 5.6). Upon hybridisation of the nanoparticle modified probes to the target sequence, the nanoparticles will aggregate, allowing the plasmons of aggregated nanoparticles to electromagnetically couple with one another which significantly increases the surface enhancement component of SERRS.

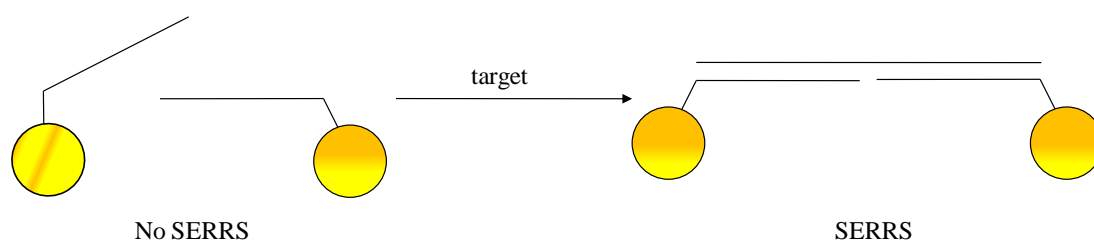


Figure 5.6 Schematic diagram illustrating the aggregation of oligonucleotide silver nanoparticle probes upon hybridisation to the target.

Furthermore, the increased range of nanoparticle plasmon resonance wavelengths permits coincidence with the laser excitation wavelength and dye absorption maximum, which is a necessary requirement for maximum SERRS intensities.²⁸ The increase in SERRS intensity can be used to identify the hybridisation event between the probes and the target and hence detect a specific oligonucleotide sequence. Since it is undesirable to modify the target sequence, the SERRS label must be introduced into the nanoparticle oligonucleotide conjugate.

5.2 *In-Sequence Labelling*

Thiol modification of the probe oligonucleotide for nanoparticle attachment can be performed at either the 3' or 5' terminus of the sequence, however placement of the dye label for SERRS detection requires more consideration. Surface enhancement of Raman signals decays exponentially with increasing distance from the nanoparticle surface^{186, 187} and so the dye label must be as close to the nanoparticle surface as possible. Therefore, it is ineffective to use a thiol modified DNA sequence that has been labelled at the other end with a dye (as in section 5.1). For in-sequence labelling, the label is best placed adjacent to the thiol modification. Such oligonucleotide sequences are commercially available and modification is achieved during oligonucleotide synthesis using a dye-labelled phosphoramidite.

Cy5 (figure 5.1) was chosen as the dye label as Cy5 labelled oligonucleotides have been shown to produce strong SERRS intensities when used in combination with gold and silver nanoparticles.¹¹⁸ Because the thiol modification behaves as the anchor point for nanoparticle surface attachment and not the dye label, less consideration needed to be given to the electrostatic charges on the dye label, therefore a propargylamine modification was not considered. The oligonucleotide sequence used was: 5' thiol C₆ Cy5 (A)₁₀ TCT CTC TCT C 3'. It was necessary for a spacer group to be introduced into the sequence to allow efficient hybridisation to the target sequence, therefore this was placed after the dye label so the Cy5 was as close to the nanoparticle as possible.

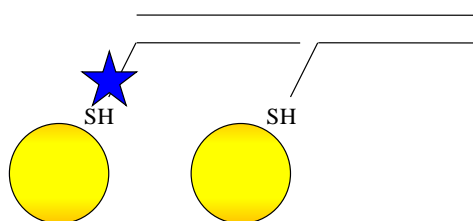


Figure 5.7 Cy5 labelled silver nanoparticle duplex. The Cy5 label is represented by the blue star and is directly followed by the polyA spacer region and then the probe sequence.

To ensure the presence of the dye label did not interfere with hybridisation of the probe to the target, a UV-visible melt was conducted of a head-to-tail duplex (figure 5.8).

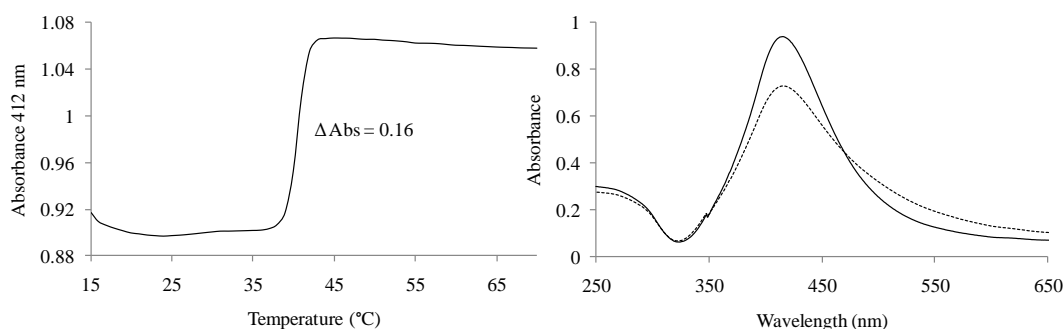


Figure 5.8 UV-visible melt of Cy5 duplex and UV-visible spectra of Cy5 duplex before (solid line) and 2 hours after (dotted line) addition of 2 nM target DNA.

A colour change from yellow to orange/brown was observed upon the addition of the target DNA. This indicated the duplex had formed since hybridisation of the probes to the target will cause the nanoparticle to aggregate resulting in a shift in the plasmon resonance wavelength and hence a colour change. The DNA melt recorded at the plasmon resonance wavelength of the silver nanoparticles also indicated duplex formation ($T_m = 40\text{ }^\circ\text{C}$) however it was noticed that the difference in absorbance corresponding to the double stranded DNA and the random coil DNA was relatively low. This was also confirmed by UV-visible spectra recorded over the full wavelength range before the addition of the target and 2 hours after the addition.

It appeared that the nanoparticles were not fully aggregated due to incomplete hybridisation.

The probes were analysed before and after the addition of the target DNA by SERRS. Cy5 has an absorbance maximum of 646 nm and so a laser excitation of 632.8 nm was used. There appeared to be little discrimination between the samples (data not shown), possibly because there were too few aggregation events for a noticeable increase in the SERRS intensity. As such, efforts were made to improve the degree of aggregation between the nanoparticle probes. The target DNA had been used at a concentration of 2 nM, which is 100 times greater than each probe concentration. Although this is the same ratio of probe to target DNA that was used in the gold nanoparticle hybridisation experiments (chapter 4), it may not be optimal for silver nanoparticle hybridisations since 35 nm diameter silver nanoparticles have a surface area more than 7 times greater than 13 nm diameter gold nanoparticles (3848 nm^2 compared with 531 nm^2 , assuming the nanoparticles are spherical), and so are likely to have a greater number of immobilised DNA strands. To quantify the number of DNA strands *per* silver nanoparticle, a DTT displacement method was used.⁸⁷ This involved immobilising thiol modified DNA labelled with FAM onto the silver nanoparticles and then displacing it from the surface by DTT to be subsequently analysed by fluorescence spectroscopy. It was necessary to displace the dye-labelled DNA prior to analysis as nanoparticles quench fluorescence emission through a surface energy transfer (SET) mechanism.²⁷ Using this method, the number of oligonucleotide strands *per* nanoparticle was determined to be 686 ± 25 . This is consistent with the findings for gold nanoparticles (chapter 4), taking into consideration the size difference for the two types of nanoparticle. Therefore, it was probable that the concentration of target DNA used for the silver nanoparticle hybridisations was insufficient. As such, the concentration of target DNA was increased from 2 nM to 20 nM (1000 times greater than the probe concentration). The melt illustrated in figure 5.9 shows an improved difference in absorbance between aggregated and non-aggregated nanoparticles, suggesting that a greater degree of hybridisation is occurring.

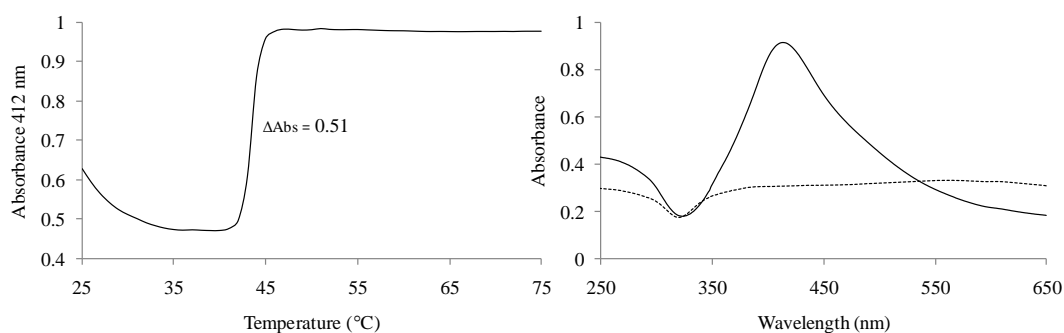


Figure 5.9 UV-visible melt of Cy5 duplex and spectra of Cy5 duplex before (solid line) and 2 hours after (dotted line) addition of 20 nM target DNA.

The SERRS spectra before and after addition of the target DNA was recorded again. There was still insufficient discrimination between the duplex and the nanoparticle probes alone and so it was theorised that the poor SERRS intensities were due to the distance between the nanoparticle surface and the dye label being too large. The thiol at the terminus of the oligonucleotide sequence is followed by a C₆ linker and then the dye label, meaning it was not directly on the nanoparticle surface. It was therefore deemed necessary to investigate an alternative method to introduce the SERRS label into the oligonucleotide nanoparticle conjugate.

5.3 Nanoparticle Labelling

Thompson and co-workers have reported the preparation of benzotriazole azo dye-labelled oligonucleotide nanoparticle conjugates.¹²³ Their method consisted of labelling silver nanoparticles first with the dye, followed by the addition of thiolated DNA. A similar approach has also been utilised by Nie and co-workers¹²⁴ who used ROX isothiocyanate (ROX ITC) as the dye label. The main benefit to these labelling methods is that the dye is adsorbed directly on the surface of the nanoparticle, although certain experimental considerations are required. The dye surface coverage needs to be controlled as there needs to be unoccupied surface sites for the oligonucleotides to adsorb.¹²⁴ Also, any electrostatic charges on the dye can be a limitation as the introduction of positive charges to the negatively charged

nanoparticle surface will induce aggregation of the nanoparticles, rendering them unusable. To overcome this, Thompson and co-workers used a non-aggregating dye and Nie and co-workers coated the nanoparticles in poly(ethylene)glycol (PEG) after oligonucleotide functionalisation to aid stabilisation of the nanoparticles in the ionic buffer.

Another way to overcome these issues would be to label the nanoparticles using a dye after oligonucleotide functionalisation. Once the nanoparticles have been functionalised with oligonucleotides, the nanoparticles are relatively stable since the DNA is conferring steric protection and the anionic charge is maintained due to the negatively charged phosphate backbone. As such an excess of dye can be added avoiding unwanted aggregation. This approach was adopted for labelling locked nucleic acid (LNA) functionalised silver nanoparticles. LNA is an RNA structural mimic that possesses a methylene bridge across the ribose sugar. It has been shown to afford large increases in thermal stability towards duplex structures as a result of either enthalpic or entropic stabilisation.⁵⁹ Detailed discussion of LNA is included in chapter 4. An excess solution of ROX ITC or TAMRA ITC (TRITC) was added to silver nanoparticles that had been pre-functionalised with LNA oligonucleotides. The ROX and TAMRA labels adsorb to the nanoparticle surface through the isothiocyanate moiety.¹⁸⁸ Only one of the oligonucleotide nanoparticle probes was labelled with the dye.

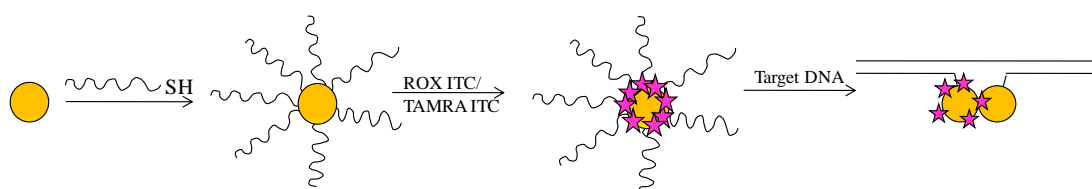


Figure 5.10 ROX ITC or TAMRA ITC labelling procedure of the oligonucleotide functionalised nanoparticles and their hybridisation to the target DNA sequence

The nanoparticles were stored in the dark for 16 hours, and then centrifuged to remove any excess dye label. It was necessary to quantify the number of oligonucleotides post-labelling to establish if any oligonucleotides had been

displaced upon introduction of the SERRS dye and hence would affect the concentration of target DNA that should be added to allow optimum aggregation of the nanoparticles. Cy5 labelled oligonucleotides were adsorbed onto silver nanoparticles for labelling with TRITC. Cy5 was selected as the oligonucleotide label since its excitation wavelength and emission profile did not coincide with the absorbance profile of TAMRA. DTT was used to displace the oligonucleotides (and the TRITC) from the nanoparticle surface for subsequent quantitation by fluorescence spectroscopy. The number of Cy5 DNA molecules *per* silver nanoparticle was found to be 1069 ± 63 if the nanoparticles had not been labelled with TRITC and 934 ± 49 if the nanoparticles had been labelled. It appears that the addition of TRITC to the nanoparticles does displace a very small proportion of the oligonucleotides from the surface however does not significantly affect the reproducibility of the surface functionalisation procedure as apparent by the similar standard deviations. The number of TRITC molecules was calculated using non-dye labelled oligonucleotide functionalised nanoparticles and was estimated to be 1205 ± 84 *per* silver nanoparticle. Since the number of oligonucleotides was still approximately 1000 *per* nanoparticle, the target DNA was added at a concentration 1000 times greater than the nanoparticle probes. The duplex was analysed by SERRS one hour after the addition of the complementary target (figure 5.11).

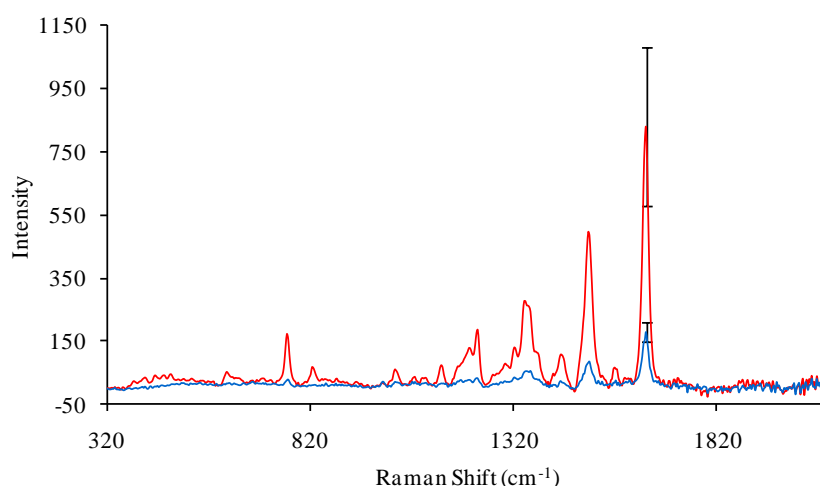


Figure 5.11 SERRS spectra using 514.5 nm excitation of ROX labelled LNA nanoparticle conjugates before (blue) and one hour after (red) addition of target DNA. The error bars represent the standard deviation of 10 replicate SERRS analyses.

Figure 5.11 shows that upon the addition of the target DNA, there is a significant increase in the SERRS intensity. This is due to aggregation of the nanoparticle probes which shifts the plasmon resonance peak to be in resonance with the laser excitation wavelength and dye absorption maximum (575 nm, figure 5.12) and gives rise to intense electromagnetic fields between adjacent nanoparticles. This was a promising initial result suggesting that oligonucleotide sequence detection is possible using SERRS.

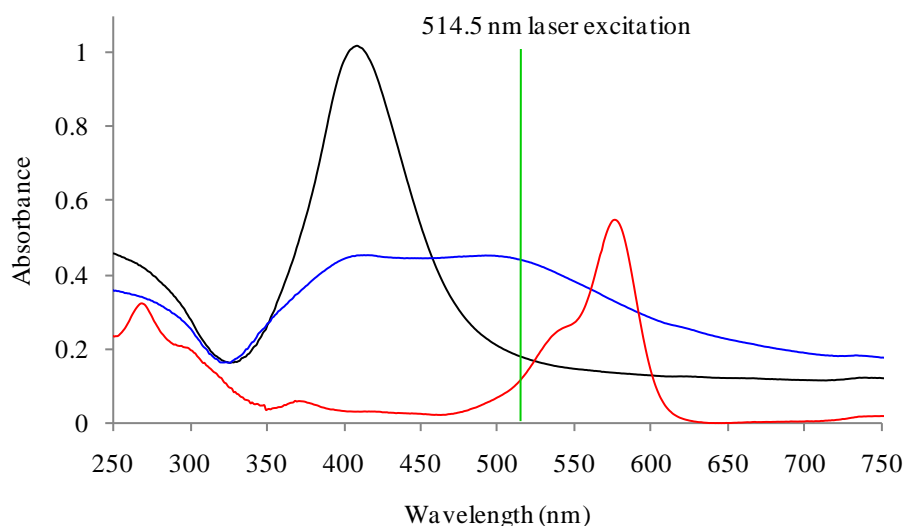


Figure 5.12 UV-visible spectra of ROX ITC (red) and the nanoparticle probes in the absence (black) and presence (blue) of the target DNA.

Nanoparticle aggregation is a dynamic process and so it is important that the time at which spectra are recorded after the addition of the target DNA is kept constant. A compromise must be made between ensuring the nanoparticles have aggregated enough for effective surface enhancement and not allowing too much aggregation so that the nanoparticles precipitate out of solution and fall to the bottom of the cuvette, meaning they are no longer in the laser beam path. Additionally, as the size of the nanoparticle aggregate increases, multipolar plasmon resonances develop meaning the dipolar resonance condition of SERS is no longer satisfied. The SERRS spectra of TRITC-labelled nanoparticle conjugates in the presence of DNA was recorded every 5 minutes over the course of an hour (figure 5.13).

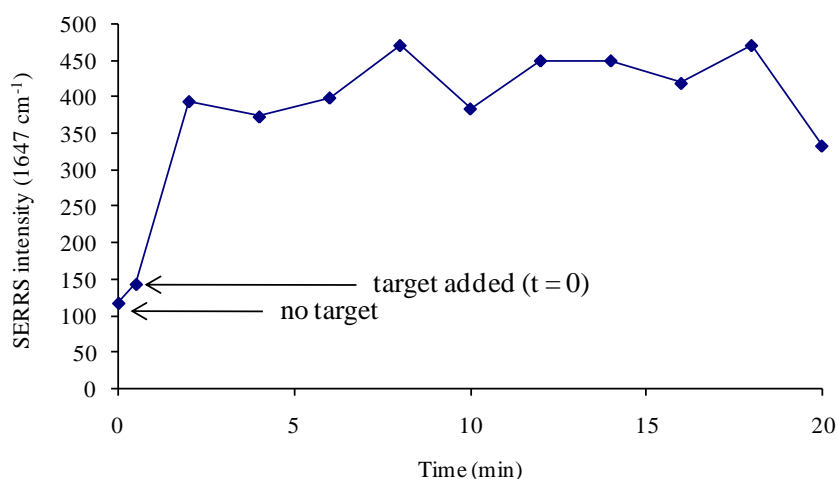


Figure 5.13 SERRS intensity at 1647 cm^{-1} following the addition of the complementary DNA sequence to TRITC ITC labelled LNA functionalised nanoparticles. Spectra were recorded every 2 minutes over a 20 minute period.

The SERRS intensity increases almost immediately after the addition of the target DNA and then plateaus, although there is a degree of signal fluctuation between 325 and 500 counts. The results suggest that spectra recorded from 2 minutes onwards are sufficient for effective detection of hybridisation. This is beneficial as it means that the detection method is not a lengthy process and a result may be obtained relatively soon after the target DNA is added.

In an effort to optimise the detection method, the concentration of dye initially incubated with the oligonucleotide conjugates was varied. Nie and colleagues state that the quantity of dye adsorbed onto the nanoparticles affected the discrimination between positive and negative controls and that it was necessary to limit the dye concentration. They also suggested this was necessary to maintain enough vacant surface sites on the nanoparticles for the oligonucleotides to adsorb.¹²⁴ Although consideration of available surface sites does not apply to this method since the dye is added after DNA functionalisation; it was worthwhile to investigate whether the discrimination between signals arising from presence and absence of target DNA could be improved. Solutions of ROX ITC ranging between 0.5 to 5 μM were added to the oligonucleotide functionalised nanoparticles. As the dye concentration increases, the SERRS intensities in the absence and presence of target DNA

increases, indicating that the number of dye molecules being adsorbed onto the surface is dependent on the dye concentration. This would be expected as the equilibrium between free dye molecules and nanoparticle-bound dye molecules will favour nanoparticle-bound molecules upon higher concentrations.

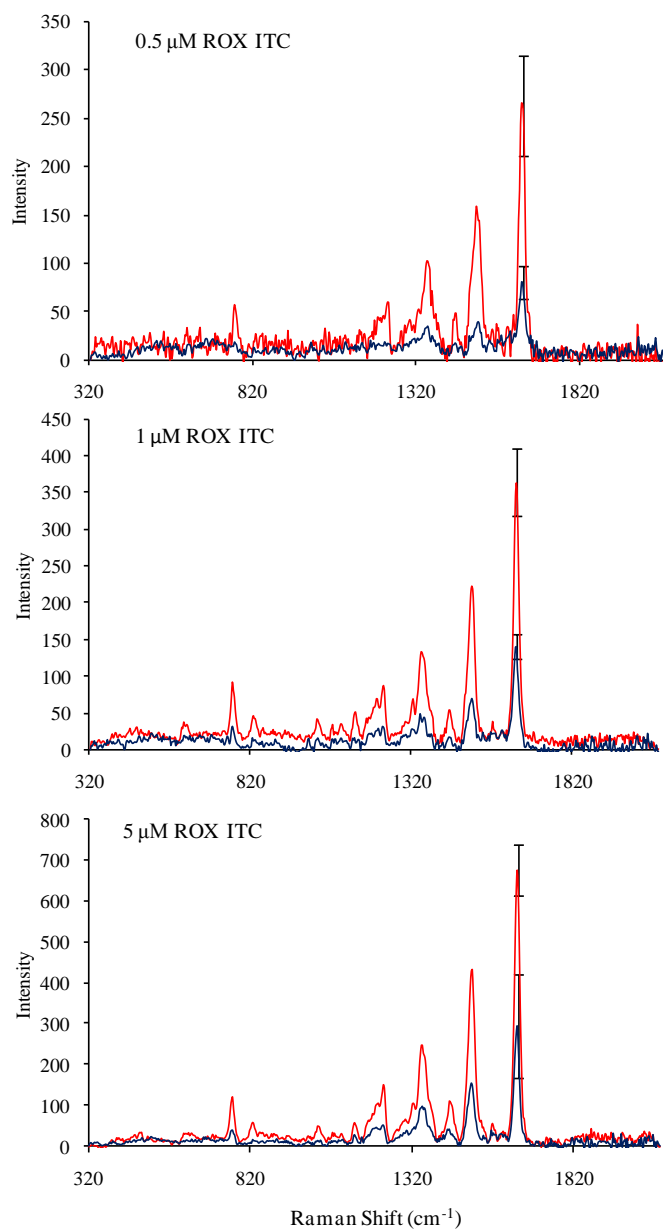


Figure 5.14 SERRS spectra before (blue) and 5 minutes after (red) the addition of the complementary target DNA of oligonucleotide nanoparticle conjugates that had been labelled using an initial concentration of 0.5 μM, 1 μM, and 5 μM ROX ITC.

It should be noted, however, that optimal signal discrimination was achieved when a concentration of 0.5 μM ROX ITC was added to the silver nanoparticles. As such, this concentration of dye was used throughout the remainder of this study.

SERRS spectra are often baseline corrected to allow effective comparison of SERRS peaks between samples however it adds extra time to the data analysis process and is difficult to automate, meaning it is often applied subjectively. In this assay, the presence of target DNA was easily identifiable even before baseline correction (figure 5.15). This is advantageous as it means post-analysis data correction is not required making the assay more attractive for employment by end-users.

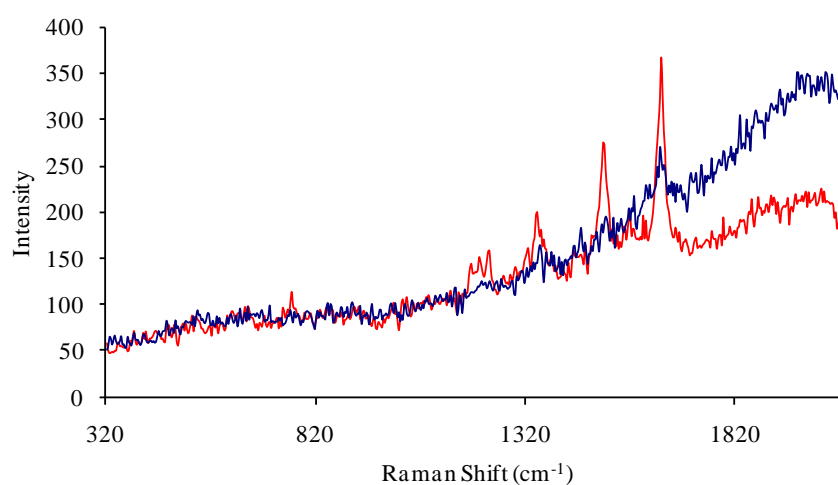


Figure 5.15 Non-baseline corrected SERRS spectra before (blue) and 5 minutes after (red) the addition of the complementary sequence to ROX ITC labelled LNA functionalised nanoparticles.

The non-baseline corrected spectra in figure 5.15 illustrate a decrease in the background signal at the higher wavelengths upon the addition of the target DNA. The background signal is likely to be the result of fluorescence. Adsorption of a fluorophore onto a nanoparticle surface can result in either surface enhancement of the fluorescence signal or quenching through a radiation-less energy transfer. The proximity of the fluorophore to the nanoparticle surface determines which one of these processes dominates. Fluorescence quenching follows a $1/d^4$ dependence, where d is distance and therefore is most efficient the closer the fluorophore is to the surface.²⁷ Maximum surface enhanced fluorescence has been reported to take place

approximately 100 Å from the surface.¹⁸¹ It is possible that the reduction in signal upon aggregation of the nanoparticles is the result of additional radiation-less quenching of the fluorescence emission due to the increased overlap of the fluorescence emission with the red-shifted nanoparticle plasmons (figure 5.16).

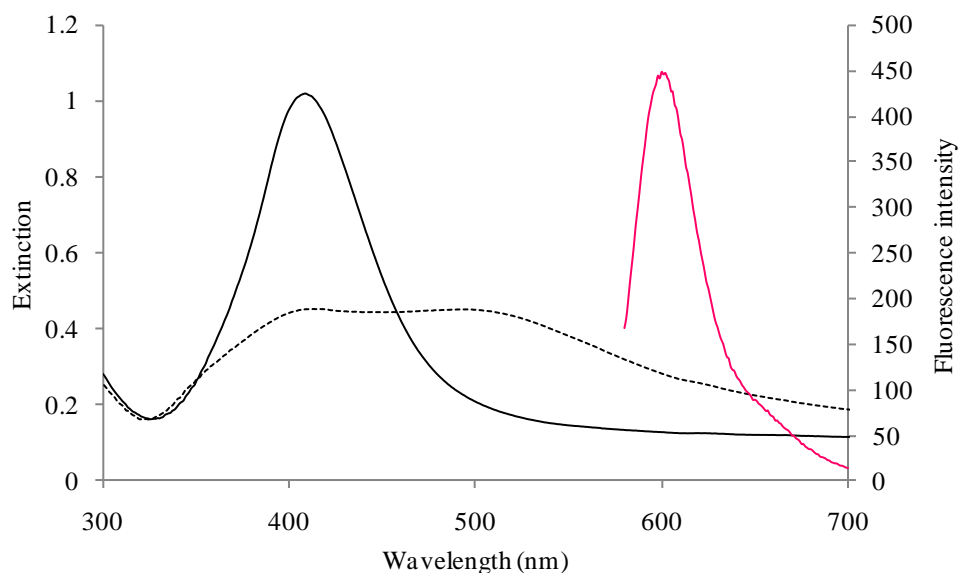


Figure 5.16. UV-visible spectra of oligonucleotide functionalised silver nanoparticle probes before (solid line) and after (dotted line) the addition of target DNA. The fluorescence emission spectrum of ROX ITC is shown in pink.

It has been shown that before the addition of the target DNA sequence, the SERRS intensities of the dye labelled nanoparticles is relatively low, however it was important to ascertain that the increase in signal intensities upon the complementary target is sequence specific. Therefore, a non-complementary DNA target was added to the nanoparticle probes and analysed by SERRS. Figure 5.17 shows that there is no increase in SERRS intensity upon the addition of the non-complementary DNA. This indicates that the increase in SERRS signal is the result of a specific interaction relying on base recognition. The target DNA does not hybridise to the nanoparticle probes and so aggregation does not occur, meaning there is no increased surface enhancement as the result of electromagnetic coupling between the nanoparticles.

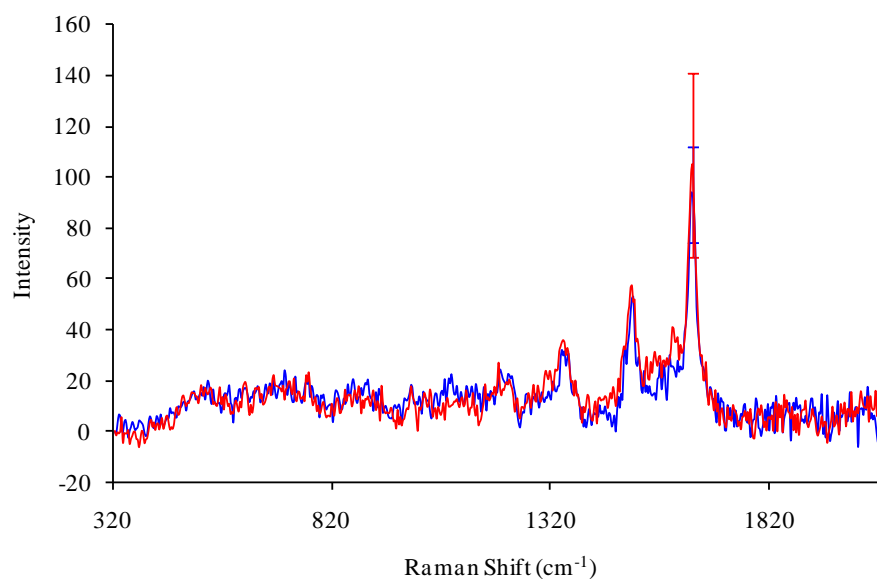


Figure 5.17 SERRS spectra of LNA nanoparticle probes before the addition of target DNA (blue) and after the addition of non-complementary DNA (red). The error bars represent the standard deviation of 5 replicate SERRS analyses.

The relatively low background signal is likely to be caused by a small number of SERRS active single particles. To investigate the degree of specificity the probes have for complementary DNA using SERRS as a detection method, the probes were hybridised to target DNA incorporating a single base pair mismatch. The location of the base mismatch within the target sequence affects the extent that the resultant double stranded DNA is destabilised. This was investigated in chapter 4 using the oligonucleotide probe sequences in a tail-to-tail arrangement. Maximum destabilisation of the tail-to-tail duplex was found to occur when a mismatch was present at the probe tail which is furthest from the nanoparticle. This was thought to occur because the nanoparticle obstructs full hybridisation of the probe sequence with the target and so a mismatch in close proximity to the nanoparticle has a negligible effect of the melting temperature. The probe arrangement for the SERRS experiments was head-to-head and so it was necessary to establish the effects different mismatches have when this format is employed. The melting temperatures obtained by the visible melting profiles are shown in figure 5.18. A single base pair mismatch at the probe head and probe tail results in thermal destabilisation when compared with the melting temperature of the complementary duplex (43 °C),

however indicates that hybridisation-induced aggregation of the nanoparticles will still occur at room temperature and therefore can be assumed to give rise to intense SERRS signals.

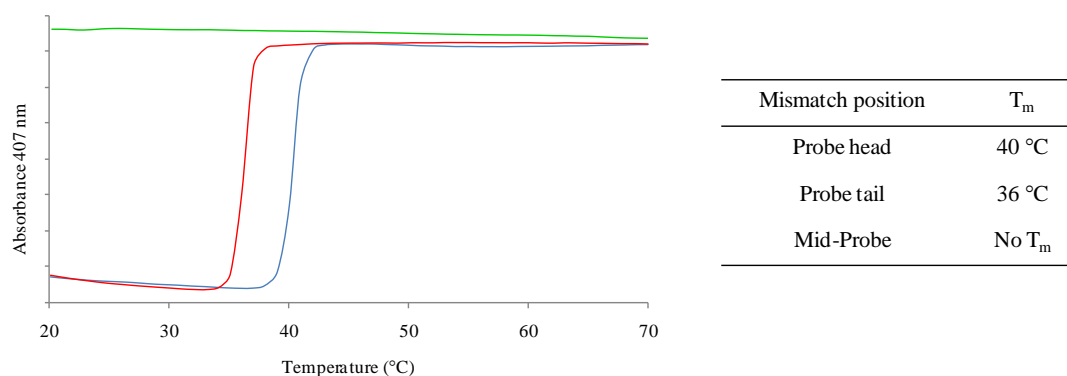


Figure 5.18 UV-visible melting profiles and temperatures of LNA silver nanoparticle probes hybridised to DNA targets incorporating a base pair mismatch at the probe head (blue), probe tail (red) and mid-probe (green).

The target sequence incorporating a mid-probe mismatch did not hybridise with the nanoparticle probes and therefore the nanoparticles did not aggregate. This sequence was used to demonstrate that single base pair mismatches can be identified by SERRS. The mid-probe mismatch sequence was added to the LNA ROX ITC labelled nanoparticles in PBS and the SERRS spectrum was recorded following 5 minutes at room temperature (figure 5.19). The addition of the mismatch sequence does not result in nanoparticle aggregation and so electromagnetic coupling effects are not observed. This illustrates that SERRS detection of DNA sequences is sensitive to non-complementary regions within the target sequence, even allowing single base pair mismatch discrimination if the melting temperature of the duplex is below room temperature.

For optimum electromagnetic coupling between nanoparticles, the nanoparticles should be in as close proximity to one another as possible. Therefore the probes and target DNA sequences were designed so that the probes were aligned in a head-to-head arrangement. There have been several reports quoting the critical interparticle

distance for electromagnetic coupling which is suggested to lie in the region of 1.25 to 2 times^{189, 190} the distance between nanoparticle centres.

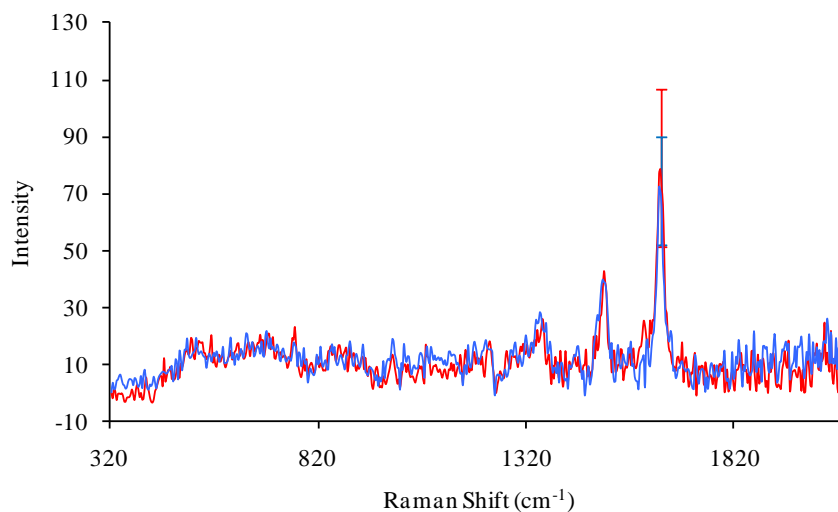


Figure 5.19 SERRS spectra of ROX ITC labelled LNA silver nanoparticle probes in the absence (red) and 5 minutes after the addition (blue) of target DNA incorporating a single base pair mismatch at a mid-probe location.

There is an exponential dependence of SERRS intensity on interparticle distance for separations smaller than the critical distance; whereas for separations of greater distances, the SERRS intensity remains approximately constant.¹⁹¹ As such, it was necessary to vary the orientation of the probes to determine if another probe arrangement where the nanoparticles are further apart is out with the effective distance for enhanced Raman scattering. It can be seen in figure 5.20 that effective discrimination between probes in the absence and presence of target DNA is achieved for all orientations. There does not appear to be much difference between SERRS intensities for the different duplex samples upon brief inspection of the spectra. This was surprising as it suggests that there is little dependence between interparticle distance and SERRS intensity. Table 5.3 presents the average SERRS intensity for probes in the presence of target DNA divided by the intensity in the absence of DNA. It can be seen that as the nanoparticles are separated by a greater distance, the SERRS intensity increases, albeit by a slight amount. This indicates that there is another variable affecting the SERRS intensity other than interparticle distance. As such, the thermal stabilities of the duplexes were considered.

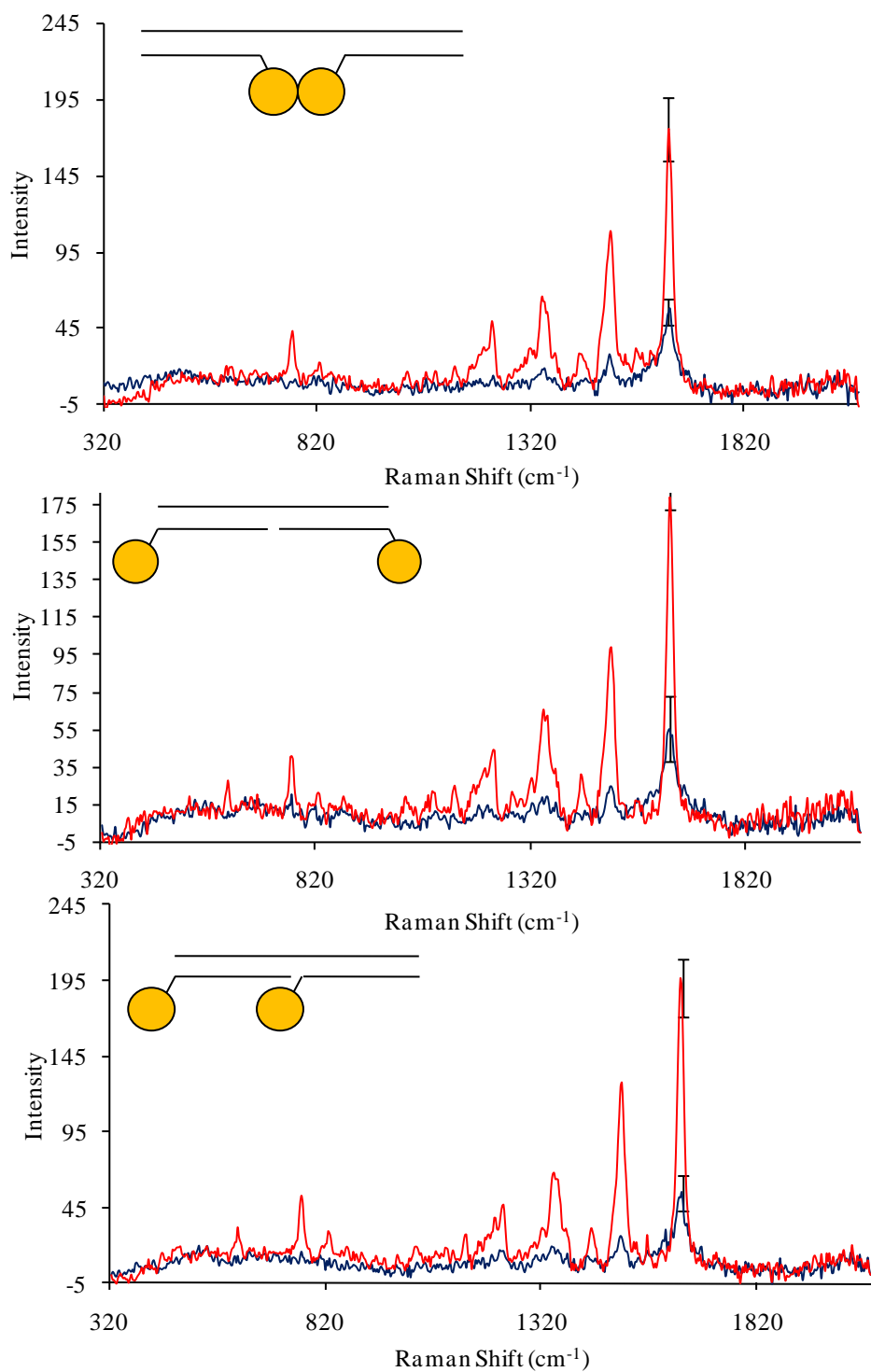


Figure 5.20 SERRS spectra of ROX labelled nanoparticle probes in different orientations before (blue) and 5 minutes after (red) the addition of target DNA.

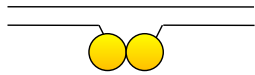
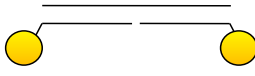
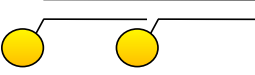
Orientation	SERRS target/SERRS no target
	3.18
	3.25
	3.45

Table 5.3 Ratio between SERRS intensities in the presence or absence of target DNA for different probe orientations.

It has been reported that the melting temperature of the duplex is dependent on probe orientation.⁸⁶ The closer together the nanoparticle modifications are to one another, the more thermally unstable the duplex due to steric repulsion from the large nanoparticles. It can be assumed that less hybridisation events occur within the analysis time frame between complementary DNA sequences that have a poor resultant stability. This could explain the observed ratios in table 5.3; although the nanoparticle plasmons can couple over a shorter distance, fewer nanoparticles aggregate in the first instance for electromagnetic coupling to take place. To investigate the effect melting temperature has on SERRS intensity, single stranded DNA sequences were mixed with NaCl of varying concentrations to produce duplexes of different melting temperatures. NaCl is necessary for effective hybridisation to allow neutralisation of DNA's negative phosphate backbone. Increasing the salt concentration means the duplexes exhibit a greater thermal stability. Each duplex was analysed by SERRS 5 minutes after the addition of the target DNA. The SERRS intensities are presented below in figure 5.21. It can be seen that as the salt concentration increases, the melting temperature increases as does the SERRS intensity. It was noticed that the nanoparticles aggregated more quickly at the higher salt concentrations when the target DNA was added, indicating that hybridisation was occurring at a faster rate.

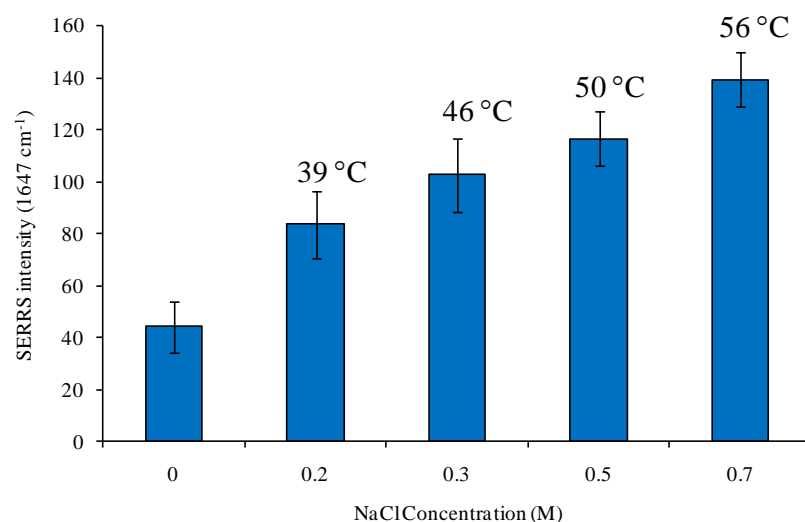


Figure 5.21 SERRS intensities of ROX ITC labelled duplex DNA in different NaCl concentrations. The melting temperatures of the duplexes are shown above the bars. The error bars represent the standard deviation of 5 replicate SERRS analyses.

It can be seen in figure 5.22 that at the time when SERRS analyses were performed (5 minutes after the addition of target DNA), the graphs corresponding to the lower salt concentrations have not yet plateaued and therefore the nanoparticles have not fully aggregated. This means that within the allowed 5 minutes prior to SERRS analysis, more hybridisation events took place at the higher salt concentrations and hence more SERRS was observed. As such, the observed SERRS intensities are not necessarily the result of the duplexes being of different stabilities but instead are due to different hybridisation and aggregation rates. To ascertain whether melting temperature has an effect on SERRS, the nanoparticle aggregation must be allowed to reach completion as it is for melting experiments. Although the 5 minute analysis time was adequate for duplexes in 0.5 and 0.7 M NaCl; full aggregation was reached at 6 minutes for the nanoparticle duplex in 0.3 M and greater than 10 minutes for 0.2 M NaCl. NaCl overcomes the electrostatic repulsion that prevents the negatively charged DNA strands from hybridising, that is the kinetic barrier. As such, using NaCl to produce duplexes of differing melting temperatures does not provide insight into whether the SERRS intensity is affected by the thermodynamic stability of the oligonucleotide nanoparticle aggregate. Further experiments needed to be performed to fully understand whether kinetics or thermodynamics are responsible for the

different SERRS intensities of nanoparticle duplexes when the interparticle distance is fixed. To assess this, oligonucleotide nanoparticle conjugates were assembled in the presence of formamide to produce duplexes of varying thermodynamic stability.

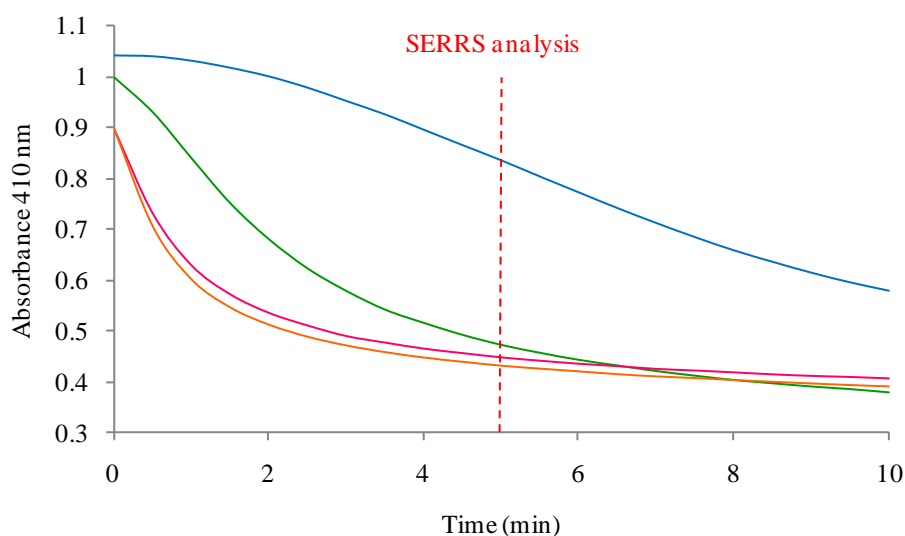


Figure 5.22 Nanoparticle aggregation profile of the nanoparticle duplexes mixed with different NaCl concentrations. The target DNA was added immediately prior to analysis by UV-visible spectroscopy. Blue: 0.2 M NaCl; green: 0.3 M NaCl; pink: 0.5 M NaCl; orange: 0.7 M NaCl.

Formamide competitively forms hydrogen bonds with the DNA bases, preventing hydrogen bond base pairing. Formamide is miscible with water and so could be incorporated into the aqueous hybridisation buffer. It was also found to be compatible with the oligonucleotide modified nanoparticles, that is, the addition of formamide did not induce non-specific irreversible aggregation. TRITC-labelled nanoparticle duplexes were analysed by UV-visible spectroscopy to determine their melting temperatures followed by SERRS measurement. Formamide is Raman active therefore it was necessary to establish that its spectrum did not interfere with the nanoparticle dye-label (figure 5.23). The strongest TRITC peak that was interrogated for quantitative identification coincided with a formamide peak which needed to be removed in the baseline correction procedure.

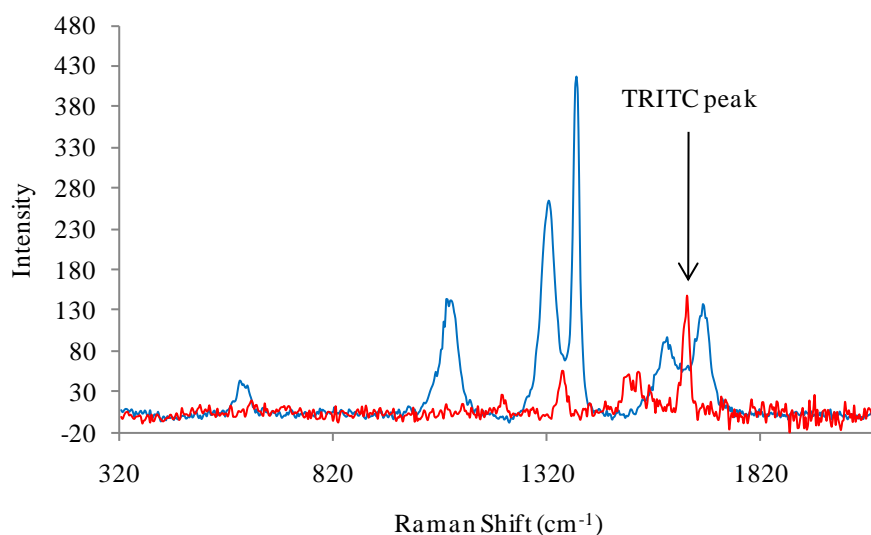


Figure 5.23 SERRS spectrum of the TRITC labelled nanoparticle duplex in the absence of formamide (red) and the Raman spectrum of 20 % formamide in water (blue).

The thermal stability of the duplex decreased as the formamide content in the hybridisation buffer was increased apparent by the melting temperatures obtained by UV-visible spectroscopy (figure 5.24).

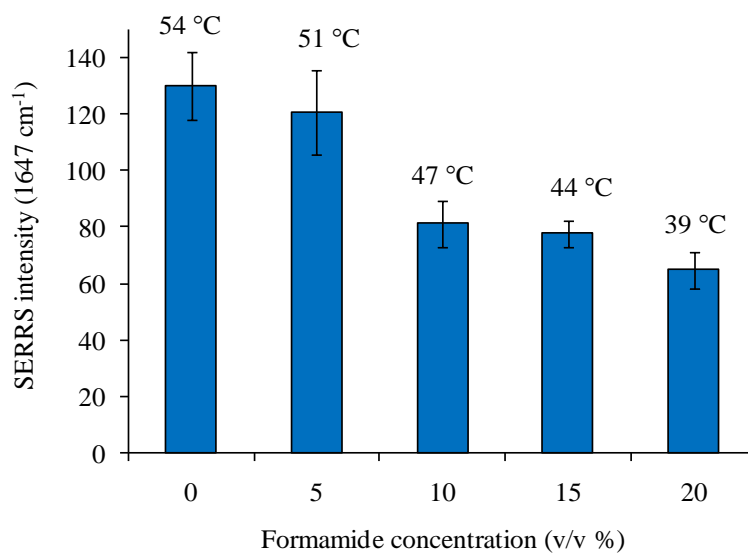


Figure 5.24 Bar graph representing the SERRS intensity of the TRITC labelled oligonucleotide nanoparticle duplex in the presence of formamide. The melting temperatures for each duplex are shown above each data point. The error bars represent the standard deviation of 5 replicate SERRS analyses.

This was also reflected in the SERRS spectra, that is, a lower SERRS intensity for the TRITC peak was observed at higher formamide concentrations. Since the formamide affects the degree of hydrogen bonding taking place between the complementary oligonucleotide sequences which is one of the factors contributing towards the oligonucleotide nanoparticle thermodynamic stability, it can be assumed that the melting temperature (thermodynamic stability) of the nanoparticle conjugates has an effect of the SERRS intensity.

A significant advantage of labelling nanoparticles post oligonucleotide functionalisation is the freedom of choice of dye. The number of available dyes is limited if the nanoparticles are labelled prior to the introduction of oligonucleotides since dyes incorporating positive electrostatic charges or hydrophobic character can induce irreversible aggregation of the nanoparticles. It is advantageous to be able to use multiple dye labels as it enables several oligonucleotide sequences to be identified simultaneously in a multiplexed analysis. To demonstrate this, Victoria Blue and an azo dye, 3,5-dimethoxy-4-(6'-azobenzotriazolyl)phenylamine, herein referred to as DABT PA, (figure 5.25) were used to label the nanoparticles in addition to the isothiocyanate dyes, ROX ITC and TRITC. Victoria Blue is likely to adsorb onto the nanoparticle surface *via* an electrostatic interaction between the positively charged nitrogen on the dye with the negatively charged citrate layer on the nanoparticles, whereas DABT PA will adsorb onto the surface through the benzotriazole moiety.¹⁹²

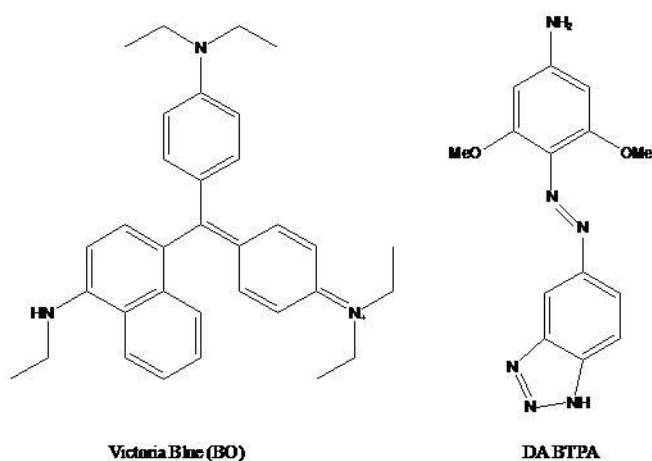


Figure 5.25 Chemical structures of Victoria Blue and DABT PA.

LNA functionalised silver nanoparticles were labelled with each dye by the same method as used for the ROX ITC and TRITC. The spectra for each labelled nanoparticle probe in solution with the corresponding non-labelled nanoparticle probe are shown in figure 5.26. The SERRS intensity increased upon the addition of target DNA for all of the SERRS labelled probes, although the discrimination between absence and presence of complementary target is significantly poorer for the DABT PA labelled duplex. This is because the DABT PA labelled probe gives rise to large SERRS signals using unaggregated nanoparticles, presumably due to the close proximity of the dye's absorbance maximum (435 nm) to the plasmon resonance wavelength of the nanoparticles (410 nm). Despite the increased background signal associated with this dye label, it has been shown that a variety of a dye labels may be employed and are not adversely affected by their means of nanoparticle surface attachment.

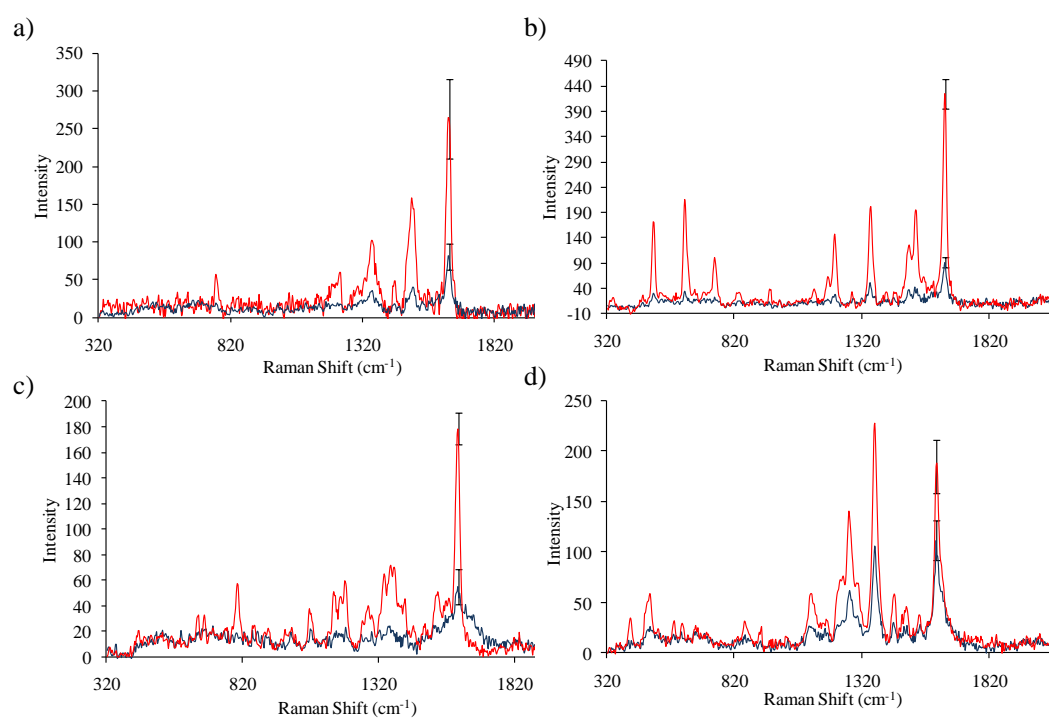


Figure 5.26 SERRS spectra of a) ROX ITC labelled probes, b) TRITC labelled probes, c) Victoria blue labelled probes and, d) DABT PA labelled probes before (blue) and after (red) the addition of the target DNA. The error bars represent the standard deviation of 5 replicate SERRS analyses.

In addition to looking at different dye labels, the effect of using probes which were both labelled with a dye was investigated. The SERRS spectra of oligonucleotide nanoparticle probes, which were both labelled with TRITC is shown in figure 5.27. There appears to be no benefit to labelling both probes with the dye. The absolute SERRS intensity has increased by a factor of approximately two (in comparison to figure 5.26b), as would be expected since the quantity of dye has doubled, however the difference between signal intensity before and after the addition of the target has not improved as the background signal also doubles (the number of SERRS active single particles has increased). Therefore, labelling one probe is sufficient for effective identification of DNA sequences which is advantageous since it means that the probes can be prepared with improved ease and less fluorophore is utilised.

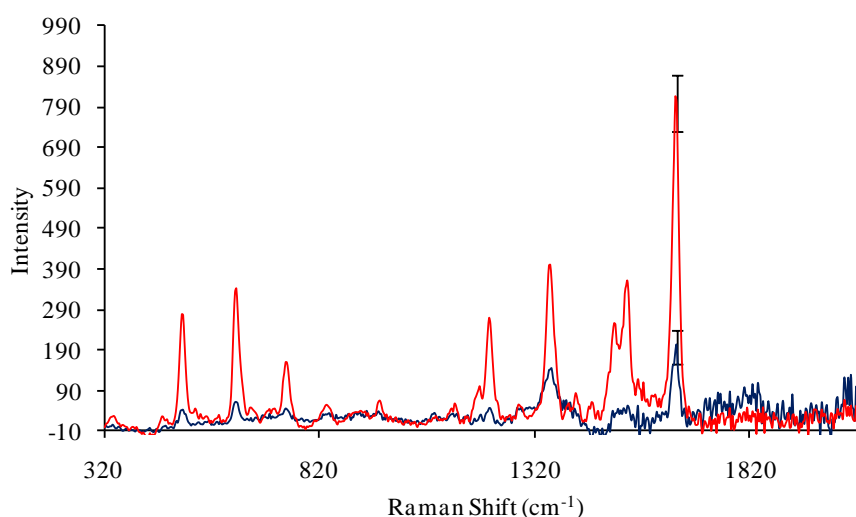


Figure 5.27 SERRS spectra of double-labelled oligonucleotide probes before (blue) and after (red) the addition of the target DNA. The error bars represent the standard deviation of 5 replicate scans.

5.4 Mixed Metal Analysis

Silver nanoparticles provide much greater surface enhancement than gold nanoparticles and so are often the preferred choice in SE(R)RS analyses, however silver nanoparticles are inherently less stable than gold nanoparticles and so their practical application can be limited, especially when modifying or functionalising the

nanoparticle surface. To demonstrate that dye-labelled 13 nm gold nanoparticles can also be utilised for SERRS analysis, a mixed metal duplex was employed that exploits the different advantages of both gold and silver nanoparticles. A split probe assay was designed so that one probe oligonucleotide was modified with the dye-labelled gold nanoparticle and the other probe oligonucleotide was modified with an unlabelled silver nanoparticle (figure 5.28).

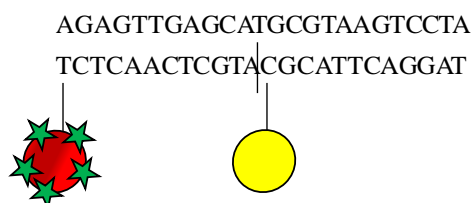


Figure 5.28 Mixed metal nanoparticle oligonucleotide probes hybridised to the complementary DNA target in a head-to-tail arrangement. The gold nanoparticle probe is coloured red and the silver nanoparticle probe is coloured yellow. The malachite green label is shown in green.

The importance of adding the correct amount of target DNA to the nanoparticle probes has already been illustrated in figure 5.8 and figure 5.9 and so careful consideration had to be given regarding the quantity of target DNA to be added to the mixed metal probes since the number of oligonucleotides on a gold nanoparticle is approximately 10 times less than for a silver nanoparticle due to its smaller surface area. An approximate 1:1 ratio of probe to target DNA was achieved by using the gold nanoparticle probes, silver nanoparticle probes and target DNA at 0.5 nM, 50 pM, and 50 nM, respectively. To ensure the nanoparticle probes effectively hybridised to the target using these concentrations to allow maximum aggregation, a UV-visible melt was performed (figure 5.29). Thompson *et al.* have shown nanoparticle aggregation using a mixed metal duplex and illustrated that numerous gold nanoparticles surround the larger silver nanoparticle in a "halo" motif.¹⁰⁶ The UV-visible spectrum of unaggregated nanoparticles predominantly displays the plasmon resonance of the silver nanoparticles with a shoulder around 520 nm corresponding to the plasmon resonance of the gold nanoparticles due to the greater extinction coefficient of silver nanoparticles. Addition of the target DNA, results in a decrease and broadening of both plasmon resonances.

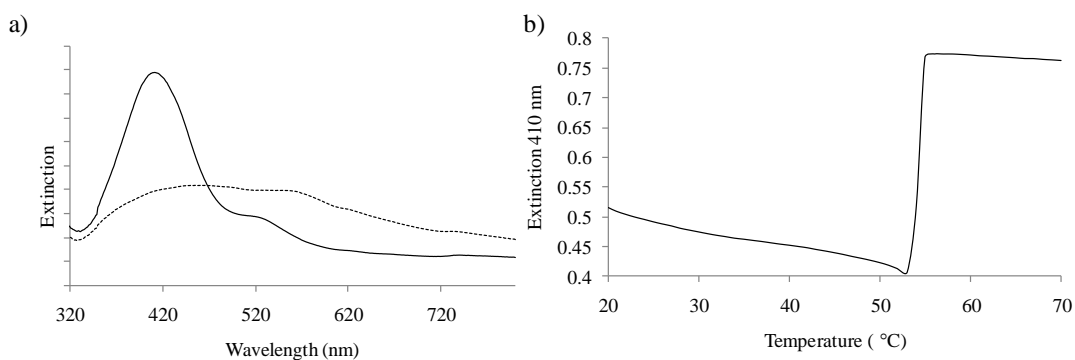


Figure 5.29 a) UV-visible spectra of the mixed metal nanoparticle probes before (solid line) and after (dotted line) the addition of the target DNA; b) UV-visible melting curve of the mixed metal duplex.

Gold nanoparticles have been shown to give poor SERRS signals at relatively short excitation wavelengths (514.5 nm) which has been attributed to absorption of the laser excitation into the bulk metal energy levels.¹¹⁸ As such, it was necessary to perform SERRS analysis at 632.8 nm and therefore tailor the choice of dye, based on its absorption maximum, accordingly. Malachite green has a broad absorbance profile with a maximum at 620 nm and is also commercially available as the isothiocyanate dye, making it an ideal choice for labelling the gold nanoparticles.

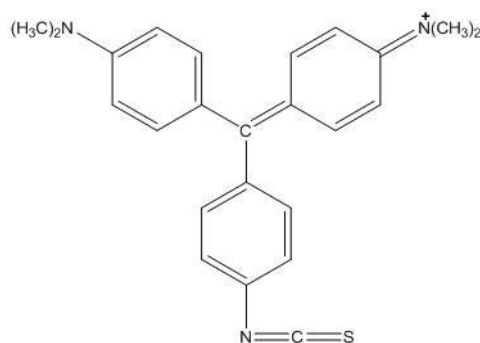


Figure 5.30 Chemical structure of malachite green (MG ITC).

SERRS spectra of the mixed metal nanoparticle probes are shown in figure 5.31 a. Upon the addition of the target DNA, there is a significant increase in the SERRS intensity brought about by aggregation of the gold and silver nanoparticles. If both

the probes are labelled with gold nanoparticles, the increase in SERRS intensity is much reduced (figure 5.31 b).

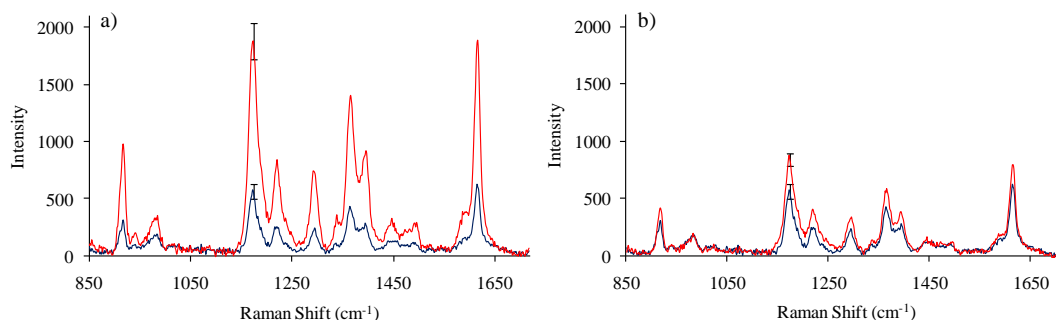


Figure 5.31 SERRS spectra using an excitation wavelength of 632.8 nm before (blue) and 5 minutes after (red) the addition of the target DNA; a) mixed metal nanoparticle duplex b) gold nanoparticle duplex. The error bars represent the standard deviation of 5 replicate SERRS analyses.

This can be attributed to their inherent poorer enhancement properties and in this experiment, their smaller size since it has been shown theoretically¹⁹³ and experimentally¹⁹¹ that surface enhancement from isolated and aggregated nanoparticles is dependent on nanoparticle size.¹⁹¹ It can therefore be seen that introduction of the second silver nanoparticle probe is highly advantageous in terms of DNA detection by SERRS, especially if gold nanoparticles of smaller diameters are desired for improved stability in functionalisation and labelling procedures. It should be noted that this study does not mean to infer that gold nanoparticles are inadequate for surface enhancement. It has been shown that surface enhancement factors comparable with silver nanoparticles can be achieved when gold particles of 60 nm diameter are utilised in parallel with a near-infrared excitation wavelength.²⁶

Quantitation of the number of MG ITC dye molecules and immobilised oligonucleotides was somewhat problematic. Previous DNA quantitations were performed using a DTT displacement protocol which results in the release of the SERRS dye and the fluorescence-labelled oligonucleotides from the nanoparticle surface. Analysis of the oligonucleotides without interference from the SERRS dye requires the fluorescence label to have an excitation wavelength that does not coincide with the absorbance of the SERRS dye and an emission profile that can not

be absorbed by the SERRS dye. The extensive absorption profile of the MG ITC across the visible region meant that no commercially available fluorophores were suitable for this purpose. Instead, an enzyme hydrolysis method was employed which would hydrolyse the DNA strands so that the fluorophore was released but left the MG ITC in contact with the surface. It has been shown that DNA quantitation by this method yields the same results as the DTT method, indicating it can be employed as a viable quantitation technique.¹⁹⁴ DNase I was added to the malachite green labelled nanoparticles functionalised with FAM labelled oligonucleotides and incubated overnight, after which the nanoparticles had aggregated indicating that the stabilising oligonucleotide layer was no longer complete. DNase I catalyses the hydrolysis of the phosphodiester linkages in the DNA backbone preferentially adjacent to pyrimidine nucleotides. Fluorescence quantitation was carried out by preparation of a calibration graph using FAM oligonucleotide standard solutions. The number of oligonucleotides *per* 13 nm gold nanoparticle that had been labelled with MG ITC was 50 ± 5 and the number of oligonucleotides *per* nanoparticle that had not been labelled with MG ITC was 52 ± 3 . Since the difference between the two values is within their error, it would seem that the MG ITC label does not significantly displace any of the oligonucleotides. It should be noted that the concentration of the MG ITC labelled oligonucleotide functionalised nanoparticles was assessed using the plasmon resonance peak of the gold nanoparticles in the UV-visible spectrum (525 nm). Since the malachite green absorbs across most of the visible region, it is likely that the concentration of the gold nanoparticles was calculated to be slightly higher than it actually was. However, the extinction coefficient of the MG ITC at 525 nm was calculated to be $4,800 \text{ M cm}^{-1}$ and even taking into consideration that there is likely to be in the region of a 1000 molecules adsorbed onto each nanoparticle (based on the value obtained for TRITC), the extinction coefficient of gold nanoparticles is over 50 times greater, and so was not considered to invalidate the experiments.

MG ITC is a non-fluorescent dye and so could not be quantified on nanoparticles using fluorescence spectroscopy. An effort was made to displace the dye from the surface by DTT and analyse by UV-visible spectroscopy however due to its relatively low extinction coefficient ($88,650 \text{ M cm}^{-1}$, 620 nm), a very concentrated

sample of the DNA functionalised nanoparticles was required, and since replicate samples needed to be analysed it meant that this method of analysis was very costly. As such, the number of MG ITC molecules *per* nanoparticle was not determined.

5.5 SERRS Labelled Triplex

Section 4.2 describes the use of triplex forming oligonucleotides (TFOs) for hybridisation to double stranded DNA. Targeting double stranded DNA means that the DNA does not have to be denatured prior to introducing the probes to the sample which means analysis times are reduced. There is also less competition between the probes and the single stranded complement for the target sequence. Introduction of SERRS labels into the TFO probes permits the identification of several double stranded sequences simultaneously. Therefore, the TRITC-labelled LNA silver nanoparticle parallel probes of pyrimidine sequence were hybridised to the double stranded target *via* Hoogsteen hydrogen bonds in a head-to-head format. Triplex melting temperatures are lower than duplex melting temperatures and so it was necessary to ensure that head-to-head hybridisation of the probes still took place at room temperature. The UV-visible melt for the triplex is shown in figure 5.32.

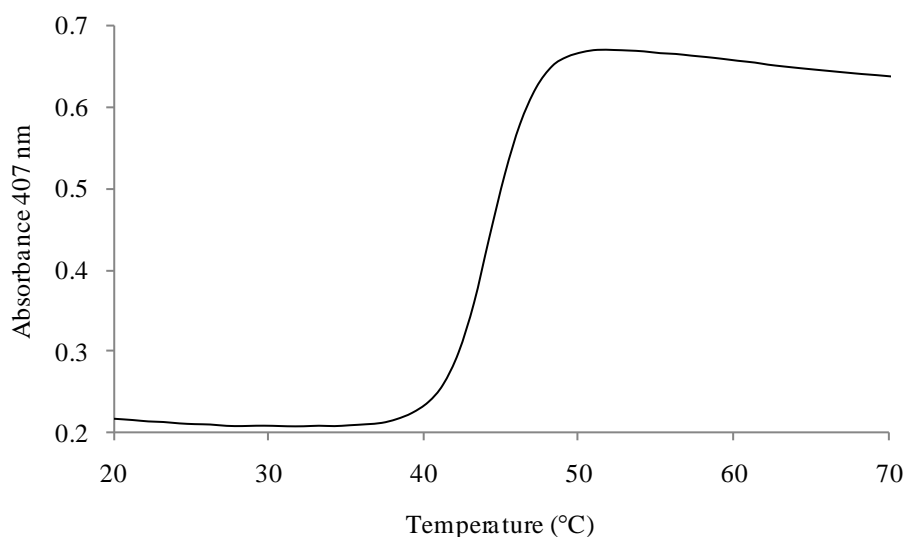


Figure 5.32 UV-visible melting curve of the head-to-head silver nanoparticle triplex.

The melting temperature is 44 °C which is the same as for the tail-to-tail triplex (figure 4.12). This indicates that changing the orientation of the probes has no effect on the stability of the triplex. This was surprising as nanoparticle duplex experiments show that the closer the nanoparticles are to one another, the lower the melting temperature presumably due to steric reasons.⁸⁶ This suggests that nanoparticle-modified triplexes are less sensitive to probe orientation effects.

The TRITC labelled nanoparticle probes were incubated with the double stranded DNA in PBS for 5 minutes and analysed by SERRS (figure 5.33). Figure 5.33 shows that upon the addition of the double stranded DNA target, there is a significant increase in SERRS intensity. The melting temperature of the triplex is above room temperature meaning that the addition of double stranded DNA causes aggregation of the nanoparticles, resulting in large surface enhancement of the TRITC Raman signals. This is the first time a double stranded DNA sequence has been identified by SERRS *via* triplex formation. DNA sequence detection by this method combines the advantages of reduced analysis times using triplex DNA formation (no denaturation required) and multiplexing using SERRS analysis.

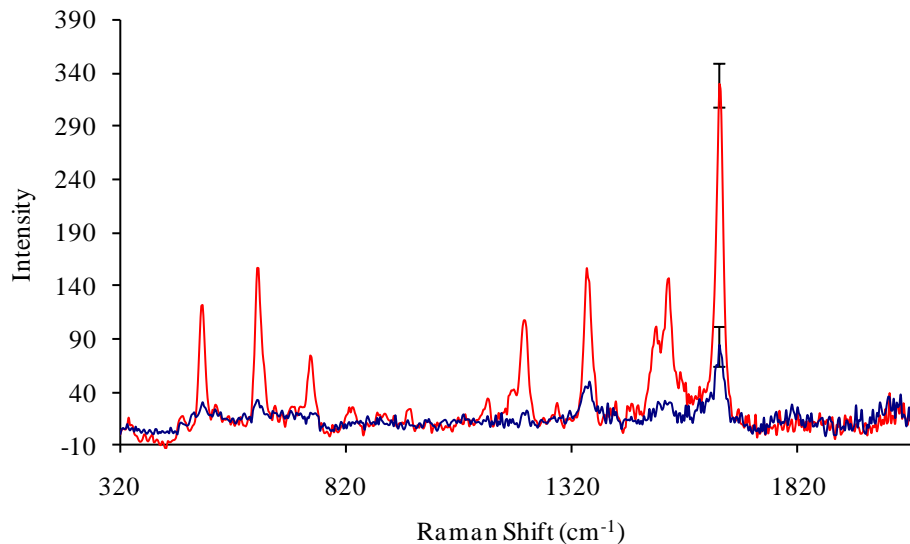


Figure 5.33 SERRS spectra before (blue) and 5 minutes after the addition of complementary double stranded DNA (red) to the TRITC-labelled LNA nanoparticle probes. The error bars represent the standard deviation of 5 replicate SERRS analyses.

Another application for nanoparticle modified oligonucleotides, aside from biodiagnostics, is their use to build nanoparticle assemblies. There are several advantages to using DNA for controlled assembly of nanoparticles: molecular recognition is inherent to the oligonucleotide structure and so they behave as both building blocks and interparticle linkers; and oligonucleotide assembly can be induced by manipulating the temperature and electrolyte concentration. A significant advantage to using DNA oligonucleotides for nanoparticle assembly is that the interparticle distance can be controlled with ease by varying the sequence length. In assembly applications, it is often desirable for the assembly to be reversible. To assess the reversibility of the triplex oligonucleotide assembly, the triplex was heated and cooled in cycles. Heat application disrupts the hydrogen bonding between the oligonucleotide strands and will result in dispersion of the nanoparticle probes. The triplex was heated to 80 °C in a peltier heating block, and then transferred to the Raman spectrometer for SERRS analysis. At the time of analysis, the temperature was recorded to be ~60 °C using a thermometer, which is above the triplex melting temperature.

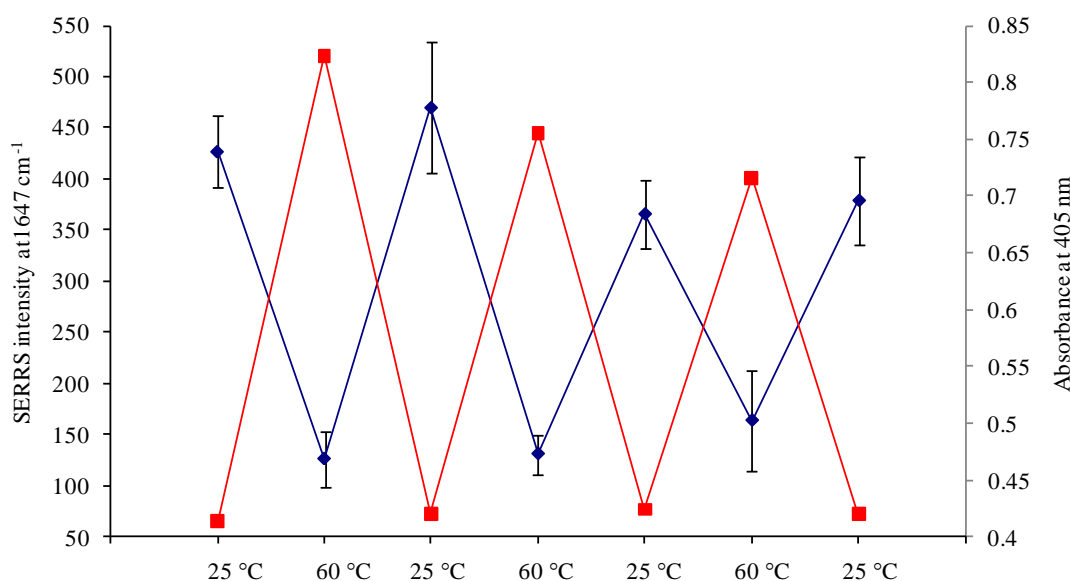


Figure 5.34 SERRS intensity (blue) and UV-visible absorbance (red) of the triplex as the temperature was cycled. The error bars represent the standard deviation of 5 replicate analyses.

UV-visible analysis indicated that the nanoparticles had dispersed, due to a high absorbance value at the plasmon resonance wavelength of unaggregated silver nanoparticles, which was also confirmed by a low SERRS intensity (figure 5.34). The nanoparticles were no longer in close proximity to each other, and therefore electromagnetic coupling would have been much poorer. Additionally, the nanoparticle plasmons were no longer in resonance with the laser excitation or dye. It can be seen that assembly of the nanoparticle probes is reversible for at least up to 3 cycles, however the difference between the values corresponding to aggregated and unaggregated nanoparticles for both UV-visible and SERRS analysis is reduced as the cycle number increases. It was also noticed that the background of the SERRS profile significantly increased by the third cycle which is often attributable to fluorescence (data not shown). It is therefore possible that the fluorophore had been irreversibly desorbed from the nanoparticle surface and so the fluorescence signal was no longer quenched. The UV-visible plasmon peak does not fully regenerate upon application of heat which could possibly be the result of dye and oligonucleotide desorption. This would cause irreversible aggregation of nanoparticles due to partial loss of their protective layer and mean that a lower concentration of the sample could be regenerated, resulting in the observed decrease in absorbance. It should be noted that the nanoparticles did appear to return to their original yellow colour upon heat application and so if irreversible aggregation is occurring it is to a small extent, undetectable to the naked eye. Elevated temperatures are known to destabilise oligonucleotide nanoparticles⁹⁶ and evidence of such for silver modified triplexes has been shown in chapter 4. Herdt *et al.* investigated the dissociation of oligonucleotides from gold nanoparticle surfaces and have found that the oligonucleotides degrade to form shorter oligonucleotide products. They commented that despite dissociation, the nanoparticles remain stable and have attributed this to adsorption of the shorter oligonucleotides onto the gold surface through the DNA bases.⁹⁷ This supports the observations of the triplex; it is possible that the isothiocyanate dye and thiol modified oligonucleotides dissociated from the nanoparticle surface followed by readsorption of shorter oligonucleotide products. Although, the nanoparticles remained predominantly stable, the hybridisation

capabilities of the nanoparticles will be reduced and irreversibly aggregated nanoparticles will eventually fall to the bottom of the cuvette, out of the laser beam.

The electromagnetic coupling effect between adjacent nanoparticles which is responsible for the increase in SERRS intensities when nanoparticles are aggregated is distance dependent. It has been reported that the closer nanoparticles are to each other, the greater the SERRS signal intensities. The critical distance between nanoparticles for surface enhancement has been suggested to be 1.25 times¹⁸⁹ or 2 times¹⁹⁰ the distance between nanoparticle centres, depending on the number of nanoparticles involved. For large interparticle spacings, the signal enhancement is almost a constant whereas for smaller spacings below the critical distance, the signal increases exponentially.¹⁹¹ Therefore, if the nanoparticles can be assembled so that there is control over the interparticle distance, the SERRS intensities can also be controlled. The effect of interparticle distance on SERRS intensity was investigated using target sequences of differing lengths.

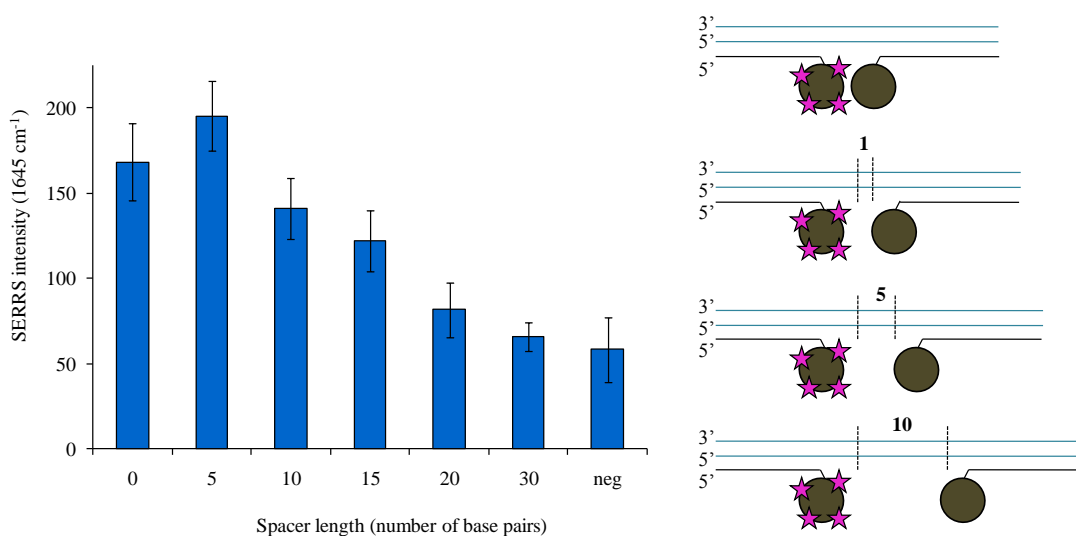


Figure 5.35 The effect of interparticle distance on SERRS intensity. The error bars represent the standard deviation of 5 replicate SERRS analyses. The diagram on the right hand side illustrates the triplexes with interparticle spacer regions of differing lengths. The target DNA is represented by the blue lines and the regions in between the dotted lines corresponds to the number of non-complementary base pairs with respect to the TFO. The TRITC label is shown in pink.

The central region of the target was non complementary with respect to the nanoparticle probes and so as the number of base pairs was increased in this region, the nanoparticle probes were expected to hybridise further apart from one another. The resultant SERRS intensities are shown in figure 5.35. In general, as the interparticle spacer increases in length, the SERRS intensity diminishes. This was expected since the plasmons have to couple over a greater distance and so enhancement is less effective. The SERRS intensity for the duplex with no interparticle spacer appears to be anomalous. However, the same trend was observed when the experiment was repeated several times. Therefore, it was deemed that another effect aside from interparticle distance was responsible for the increase in SERRS intensity as the number of interparticle base pairs increased from 0 to 5.

It was decided that the triplexes should be analysed by UV-visible spectroscopy to ascertain if the melting temperature of the triplex was responsible for the triplex sample with no interparticle spacer not fitting the trend. It was shown in figure 5.24 that thermal stability has an effect on the observed SERRS intensities. The melting temperatures of the triplexes are shown in table 5.4. The melting temperatures for triplexes with an interparticle region of greater than 15 base pairs could not be determined by UV-visible spectroscopy as the change in absorbance was very little due to the increased distance the nanoparticle plasmons were required to interact across. The plasmon resonance shift has also been shown to exhibit an exponential dependence on interparticle distance.¹⁰³ Although this was a disadvantage for this purpose, it indicates that SERRS is a more sensitive technique than UV-visible profile comparisons when the nanoparticles are separated by such distances.

Number of interparticle base pairs	T _m (°C)
0	41
5	62
10	65
15	65

Table 5.4 Melting temperatures of triplexes with different numbers of interparticle base pairs

As the number of interparticle base pairs increases from 0 to 5, the melting temperature increases by over 20 °C. It is likely that this large increase in thermal stability is the result of less steric repulsion between the nanoparticle modifications as the nanoparticles become further apart. A reduced stability indicates that less hybridisation events will take place, which will result in fewer electromagnetic coupling interactions and an overall decreased SERRS intensity. This infers that for nanoparticle triplexes suffering from large steric repulsion, the predominant effect on SERRS intensity is stability and not interparticle distance. The other triplex samples with spacer lengths greater than or equal to 5 base pairs all had very similar melting temperatures and so the interparticle distance effect could be observed.

5.6 Conclusions

To conclude, the method of DNA detection by SERRS has been investigated using dye-labelled oligonucleotide sequences. The resonance condition of SERRS was exploited using a dual-wavelength technique to increase the number of dye labelled oligonucleotides that could be detected simultaneously within a mixture. Each labelled oligonucleotide within a 5-plex could be identified and the limits of detection were determined to be similar to limits of detection obtained when the dye labelled oligonucleotides were analysed separately. The number of propargylamine bases necessary to allow effective electrostatic adsorption of oligonucleotides labelled with negatively charged dyes onto the nanoparticle surface was determined by evaluation of SERRS intensities. It was found that maximum signal intensity was obtained using 4 propargylamine bases which is less than is usually employed as standard practice. This finding is advantageous as it means oligonucleotide synthesis costs can be reduced. Efforts were made to introduce a dye label into a DNA functionalised nanoparticle conjugate. An oligonucleotide was used that had a Cy5 label incorporated adjacent to the thiol C₆ modification and prior to the spacer region. The difference in SERRS intensity upon the addition of the target DNA was negligible and so it was theorised that the Cy5 label was too far from the nanoparticle surface due to the C₆ spacer region. Another approach was adopted which involved

labelling pre-functionalised oligonucleotide nanoparticle conjugates with isothiocyanate dyes. This is an advancement of previous methods quoted in the literature which provides improved stability of the nanoparticle conjugates and versatility in terms of dye label selection. The dye concentration, analysis time and nanoparticle orientation was optimised so that the maximum SERRS signal was obtained. The dye-labelled nanoparticle probes exhibited single base pair mismatch selectivity when the melting temperature of the mismatch sequence was below room temperature however also appeared to allow discrimination between sequences of different melting temperatures above room temperature. This was further investigated using the probes at different salt concentrations however it was not possible to differentiate between the kinetic and thermodynamic effects. The nanoparticle duplex was adapted to feature mixed metal nanoparticles so that the advantages of the improved stability of gold nanoparticles could be combined with the large surface enhancements associated with silver nanoparticles. Duplex formation was extended to triplex formation using Hoogsteen hydrogen bonding silver nanoparticle probes. The advantage of using triplex formation for diagnostic applications is that the target sample does not need to be denatured prior to probe introduction. The benefit of using triplex formation for assembly purposes is the greater rigidity of the double stranded DNA target. This allowed an investigation into the effect of interparticle distance on SERRS intensity. This is the first example of using oligonucleotide nanoparticles for evaluating SERS distance effects and is an initial step towards a SERS measurement tool.

6. SERRS Analysis of Cells

6.1. Antibody Functionalised Nanoparticles

The study of biological interactions on cell surfaces using fluorescence microscopy is a relatively well-established technique, however there has been recent interest in developing surface enhanced (resonance) Raman scattering (SE(R)RS) mapping detection methods for the same purpose. The main advantages of SERRS analysis for cellular applications are its multiplexing capabilities brought about by its molecularly specific, narrow spectral lines; the resistance of SERRS substrates towards photobleaching; and near field enhancement. Cellular proteins and DNA have been identified by SERS using internalised unlabelled gold nanoparticles,^{161, 195} however conjugation of the nanoparticles to a biomolecular ligand allows a specific binding event with the corresponding receptor to be monitored. Functionalisation of nanoparticles with antibodies and proteins has been achieved using a number of methods, such as electrostatic adsorption,¹³⁵ direct attachment through protein cysteine residues,¹⁴⁴ and attachment *via* amide formation with a nanoparticle ligand.^{136, 137} For SERRS applications it is necessary for the nanoparticles to be labelled with a SERRS active molecule in addition to biomolecule conjugation. It is therefore desirable to employ a linking entity that is SERRS active and permits functionalisation with the target molecule's ligand. In an effort to achieve this, gold and silver nanoparticles were functionalised with a custom-made linker, 3-(2-[2-(2-(2-(5-1,2-dithiolan-3-yl)-pentanoylamino-6-[7-[1-ethyl-3,3-dimethyl-1,3-dihydro-benzindolylidene]-hepta-1,3,5-trienyl)-1,1-dimethyl-1H-benz[e]indolium]-hexanoylamino)-ethoxy)-ethoxy]-ethoxy)-propionic acid 7 (figure 6.1).¹⁷² The linker has several features to note. A disulfide moiety was incorporated for nanoparticle surface attachment, which has been shown to have improved binding affinities compared with monothiols.⁹⁹ This is presumably since surface dissociation would involve breaking two sulfur-metal bonds, assuming the sulfur metal interaction is covalent, instead of one for each surface-bound molecule, and the loss of entropy

upon surface attachment would be reduced for the bidentate disulfide molecule (the chelate effect).

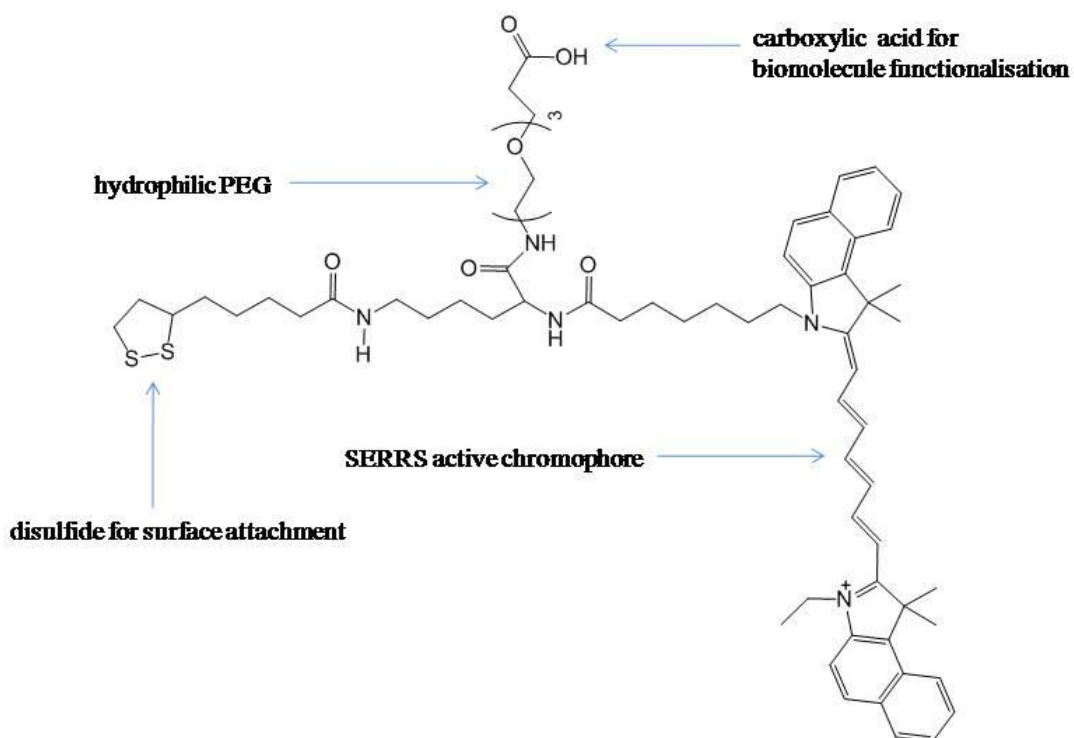


Figure 6.1 Near-infrared linker

It was necessary to include poly(ethylene) glycol (PEG) to confer hydrophilicity towards the molecule. Without such, the linker functionalised nanoparticles are insoluble in aqueous environments and aggregate, rendering them unusable. PEG also improves the steric freedom of the conjugated biomolecule improving interactions with the associated bioreceptor. The resonance Raman signal is provided by the near-infrared (NIR) dye based on a cyanine motif. Although the linker is fluorescent (figure 6.2b), once adsorbed onto the nanoparticle surface the fluorescence is quenched through a radiation-less energy transfer mechanism²⁷ and the SERRS output dominates. The linker has a broad absorption profile between 650 and 900 nm with a molar extinction coefficient of $49,000 \text{ M}^{-1} \text{ cm}^{-1}$, and has a fluorescence emission at 802 nm when using a 765 nm excitation (figure 6.2).

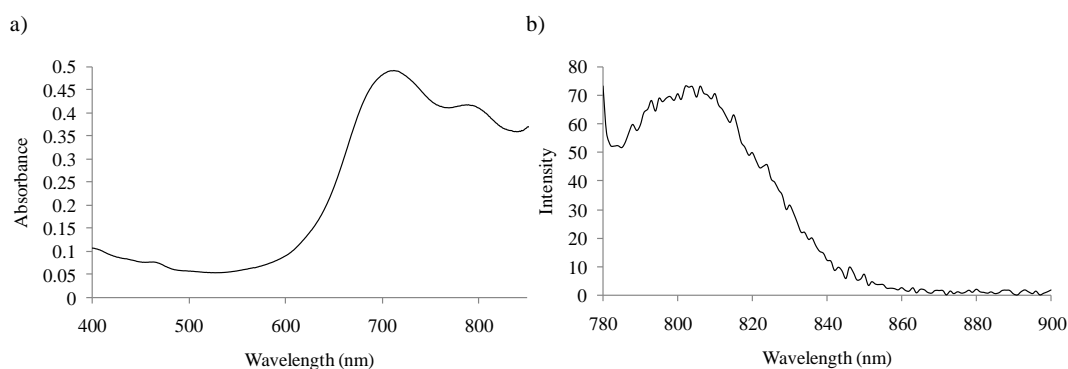


Figure 6.2 a) UV-visible spectrum and b) fluorescence spectrum of NIR linker using 765 nm excitation wavelength

Near-infrared excitation wavelengths are preferred in cell analysis as less damage is inflicted on the sample due to lower energy photons. There is also less autofluorescence from other cellular components at longer wavelengths. *In vivo* methods require NIR excitation wavelengths for increased penetration into the sample as scattering efficiency decreases with longer wavelengths, illustrated by equation 6.1 (where I is the intensity of Raman scattering, K is a constant including the speed of light, I is the laser power, α is the polarisability of the electrons in the molecule and ω is the frequency of the incident radiation),¹⁶

$$I = Kl\alpha^2\omega^4 \quad (6.1)$$

An aqueous solution of the linker was added to 13 nm gold and 35 nm silver nanoparticles for several hours to allow effective adsorption onto the nanoparticle surface. Excess linker was removed by centrifugation. Gold and silver nanoparticles functionalised with the NIR linker were analysed by UV-visible spectroscopy to assess their monodispersity (figure 6.3). The plasmon resonance peak width of the nanoparticles remains relatively narrow indicating the linker functionalised nanoparticles are tolerant to the ionic strengths used in bioconjugation buffers. The broad absorbance between 600 and 800 nm in the gold nanoparticle spectrum is due to the NIR linker which absorbs in this region. The NIR linker is more easily identified in the gold spectrum than the silver as the extinction coefficient of gold is more comparable to that of the linker. The NIR linker-modified nanoparticles are not

stable in NaCl solutions above 0.15 M without subsequent reaction with an antibody or protein. Resuspension of the nanoparticles in buffers above this salt concentration resulted in irreversible aggregation of the nanoparticles, indicated by a broadening and decrease of the plasmon resonance peak (data not shown).

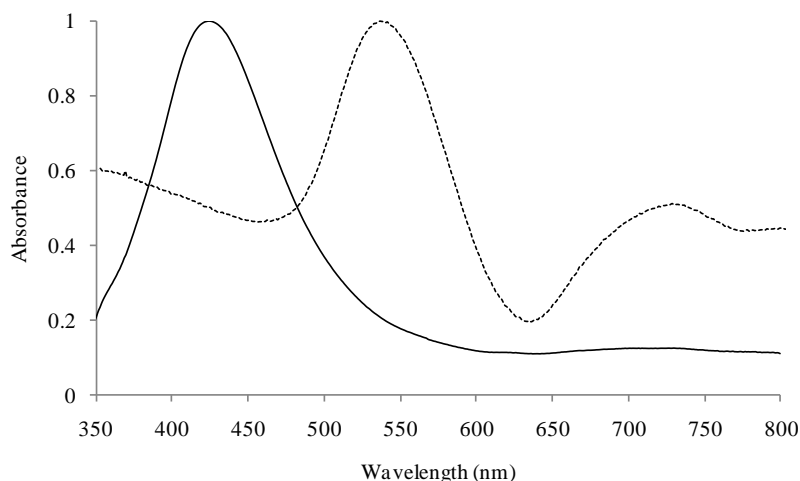


Figure 6.3 UV-visible spectra of silver (solid line) and gold (dashed line) nanoparticles functionalised with NIR linker in 1x PBS (137 mM NaCl, 10 mM phosphate, 2.7 mM KCl, pH 7.4).

The linker functionalised nanoparticles were analysed by SERRS to assess their potential as cellular SERRS substrates (figure 6.4). The linker is SERRS active at 514.5 nm, 632.8 nm, and 785 nm excitation wavelengths, however it is best suited to the longer wavelengths due to its absorbance maximum in this region. The SERRS limits of detection of the NIR linker in solution at 632.8 nm and 785 nm were calculated by analysis of multiple dilutions and are reported in figure 6.5. The limits of detection for each dye were calculated by assigning the limiting signal intensity to be three times the standard deviation of the background signal. Lower limits of detection were obtained for the NIR linker labelled silver nanoparticles compared with the labelled gold nanoparticles. This was to be expected since silver provides greater surface enhancement of Raman signals than gold.¹⁹³

The linker was reacted with a biotinylated antibody using established EDC/sulfoNHS chemistry which results in amide bond formation between the terminal carboxylic acid on the linker with amine groups from the lysine residues in the antibody (figure

6.6). It was necessary to consider the pH at which the reaction was performed since formation of the acylurea favours an acidic pH, whereas nucleophilic attack of the biomolecule on the NHS ester requires deprotonation of the primary amines which occurs at an alkaline pH. Sehgal and Vijay¹⁹⁶ state that the optimal pH is 6.5, whilst other protocols use a pH of 7-7.5.^{139, 145, 197} This reaction was performed at a pH of 7.6 using HEPES buffer. It is possible to couple the antibody to the linker in phosphate buffer, however it has been reported that phosphate will react with the EDC to form an O-phosphoisourea.¹⁹⁸ Furthermore, HEPES is an organic buffer which is more likely to solubilise the linker.

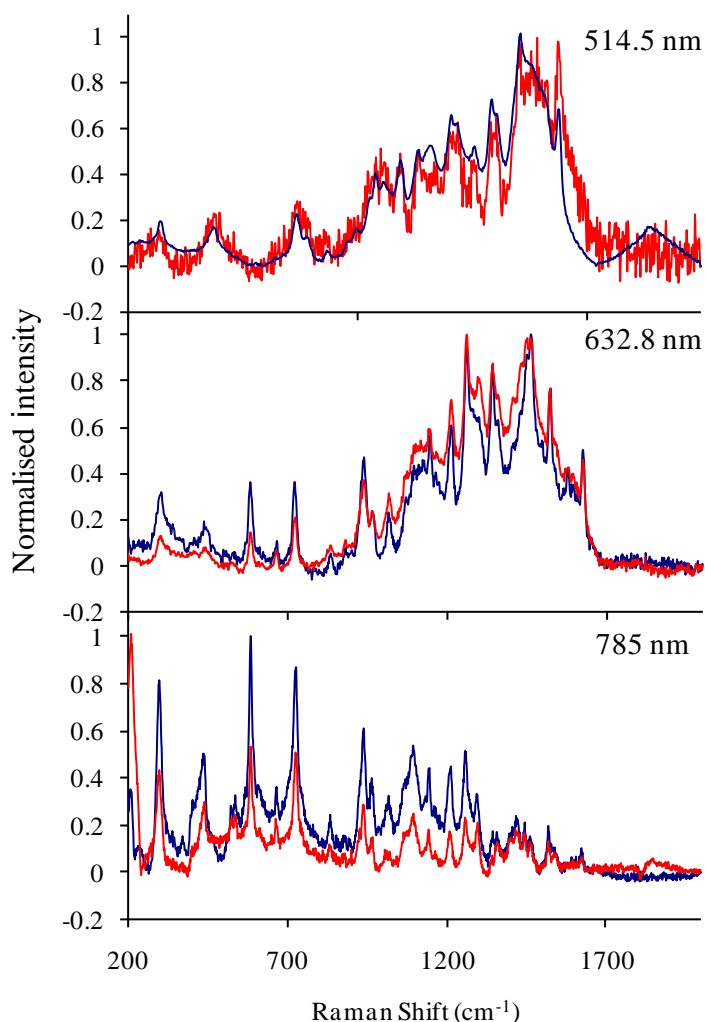
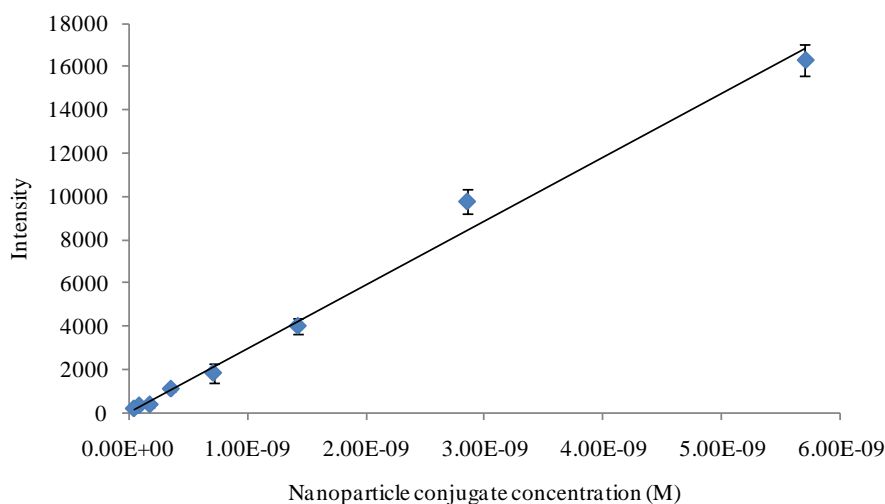


Figure 6.4 SERRS spectra of NIR linker functionalised silver (blue) and gold (red) nanoparticles at 0.2 nM and 2 nM respectively using different excitation wavelengths.



	limit of detection
Au NIR 632.8 nm	9.88×10^{-10} M
Ag NIR 632.8 nm	1.72×10^{-13} M
Au NIR 785 nm	1.81×10^{-11} M
Ag NIR 785 nm	2.28×10^{-14} M

Figure 6.5 Calibration graph showing the mean SERRS intensity of gold nanoparticles functionalised with the NIR linker analysed using 785 nm excitation wavelength. The errors bars represent the standard deviation of four replicate SERRS analyses. The theoretical limits of detection of NIR functionalised nanoparticles are presented in the table.

A solution was prepared containing the linker, the biotinylated mouse anti-rabbit, EDC and sulfoNHS in HEPES buffer and was incubated for 3 hours at room temperature. The unwanted side products of the conjugation reaction (the urea derivative of EDC and the sulfoNHS) were removed from the reaction mixture by centrifugal spin columns. Molecules with a molecular weight greater than the specified cut-off value for the columns (10,000) were retained above the membrane filter, whereas molecules of molecular weights below it passed through the filter to be later discarded. This meant that unreacted antibody was not separated from the linker-antibody conjugate at this stage. Unreacted linker could also not be removed due to its limited solubility in aqueous solutions. Although the NIR linker was soluble in the HEPES buffer, at high centrifugal speeds the linker precipitated out of

the solution and did not pass through the membrane. This meant that when the conjugate mixture was added to the nanoparticles, unreacted linker and linker-antibody conjugate was adsorbed onto the nanoparticle surface. This was advantageous as it meant that the nanoparticles were fully covered with the SERRS active dye; if the antibody-reacted linker alone was introduced to the nanoparticles then only a small number of SERRS active molecules would be immobilised due to the steric limitations of the antibody, hence the sensitivity of the detection system would be reduced. All excess reactants that had not adsorbed onto the nanoparticle surface were finally removed by centrifugation of the nanoparticles followed by removal of the supernatant and resuspension in buffer.

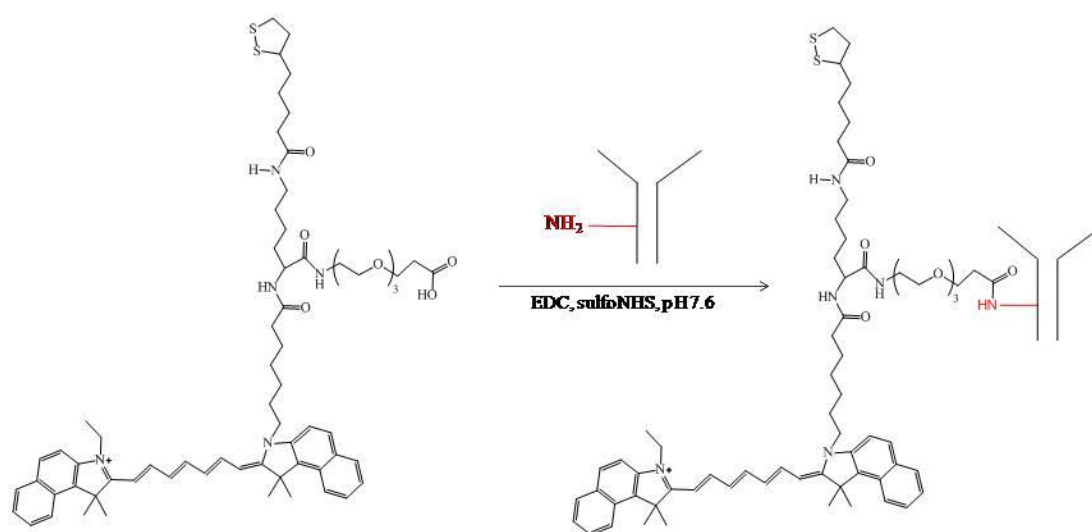


Figure 6.6 Bioconjugation of the NIR linker with an antibody

To ascertain if the biotinylated antibody was successfully conjugated to the nanoparticles, streptavidin beads were employed. Biotin is a small molecule that interacts very strongly with the tetrameric protein, streptavidin; the biotin-streptavidin interaction is one of the strongest reported in biology to-date exhibiting a dissociation constant of approximately 10^{-13} M. The biotinylated antibody nanoparticle conjugates were incubated with magnetic streptavidin beads which were then removed by a magnet. If the biotinylated antibody had been successfully

conjugated to the nanoparticles, the nanoparticles would be removed leaving a colourless solution (figure 6.7).

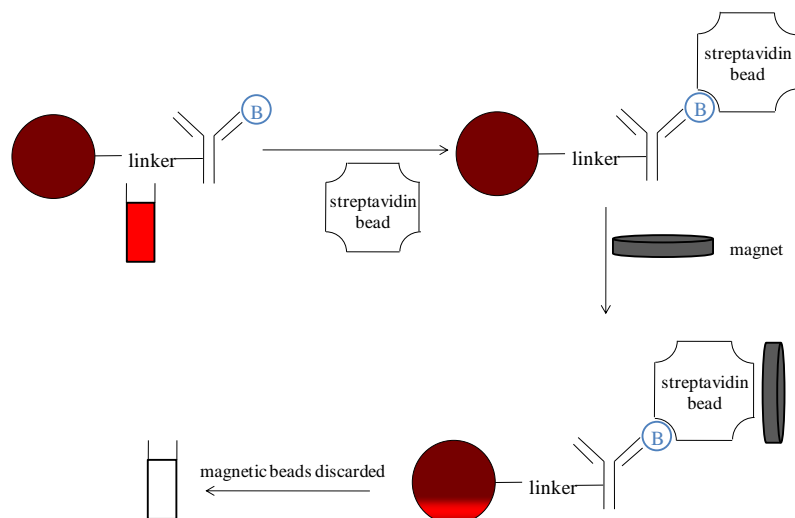


Figure 6.7 Schematic illustration of the capture of nanoparticles functionalised with biotinylated antibody by paramagnetic streptavidin beads.

Comparison of the nanoparticle plasmon absorbance before and after bead treatment indicated that the streptavidin beads had successfully captured the biotinylated conjugate (figure 6.8). Control samples were also analysed indicating that nanoparticle capture only occurs when the nanoparticle is functionalised with biotinylated antibody. This demonstrates that the antibodies were successfully conjugated to the nanoparticles using the NIR linker.

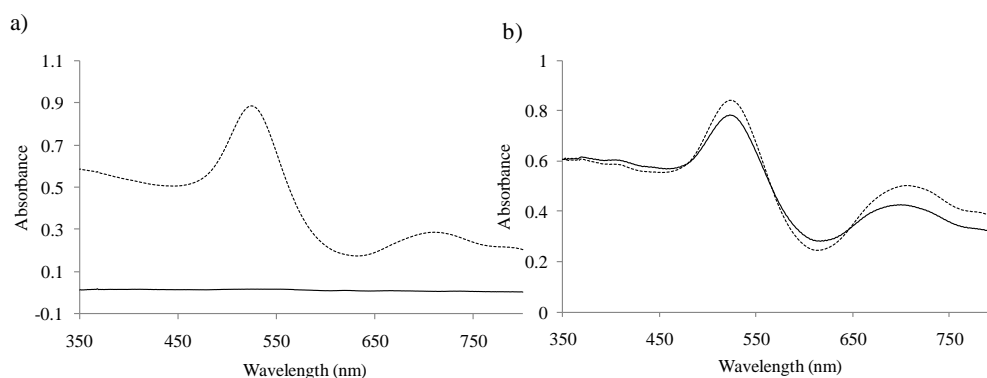


Figure 6.8 UV-visible spectra of a) biotinylated antibody functionalised NIR nanoparticles; b) NIR functionalised nanoparticles before (dashed line) and after (solid line) treatment with magnetic streptavidin beads.

The antibody employed for cellular analysis was anti-lymphocyte function associated antigen-1 (anti LFA-1), for targeting LFA-1 (lymphocyte function associated antigen-1) on dendritic cell surfaces. LFA-1 is a heterodimer comprised of two non-covalent chains: CD11a and CD18. It is a cell surface molecule expressed by all leukocytes, with the exception of some macrophages, and occupies 15,000 to 40,000 surface sites *per cell*.¹⁹⁹ LFA-1 is involved in the immune response within the body; foreign antigen material within the body is processed by antigen presenting cells such as dendritic cells, macrophages and B-cells, which is then presented on the cell surface for recognition by T-cells. The interaction between LFA-1 and its ligand intercellular adhesion molecule-1 (ICAM-1) on these cells facilitates activation of the T-cell which will ultimately differentiate into helper or cytotoxic T-cells. It should be noted that the LFA-1/ICAM-1 interaction is not exclusively responsible for T-cell activation. The predominant receptor-ligand interaction is between T-cell receptors and major histocompatibility complex molecule (MHC)-peptide complexes.²⁰⁰ In addition to T-cell activation, LFA-1 has also been shown to control T-lymphocyte migration. Monoclonal antibodies have been generated against LFA-1 and have been used to inhibit adhesion dependent leukocyte functions, indicating their specificity for the LFA-1 target.²⁰¹ They have merited interest and use as a therapeutic target for the treatment of psoriasis using humanised monoclonal antibodies.

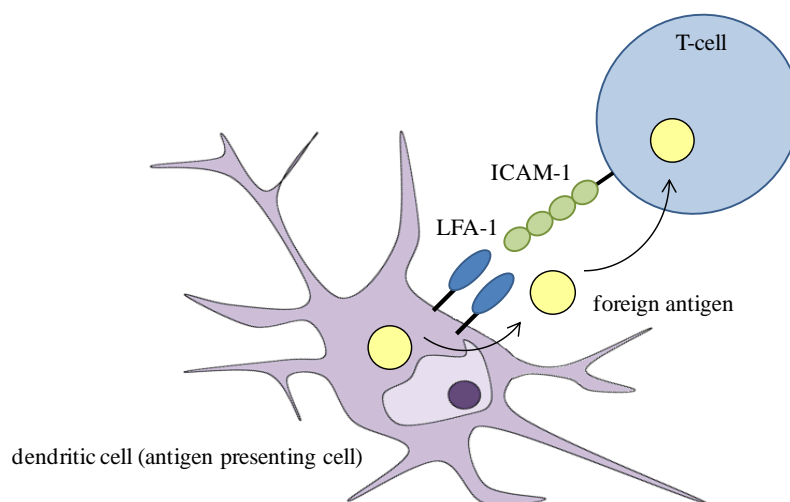
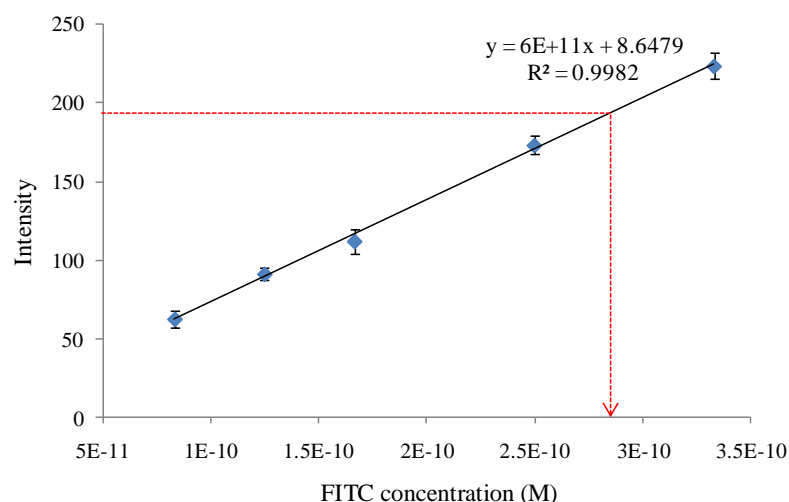


Figure 6.9 Simplified representation of the transfer of antigen material from an antigen presenting cell to a T-cell utilising the interaction between LFA-1 and ICAM-1.

Anti LFA-1 nanoparticle conjugates were prepared by the same method used for the biotinylated antibody conjugates. It should be noted that the nanoparticles may also have been conjugated to the antibodies *via* a different route involving functionalisation of the nanoparticles with the NIR linker prior to conjugation with the antibodies. This method has also been demonstrated as a viable technique¹⁷² (appendix) although was not used for the anti-LFA-1 conjugation to avoid introduction of unnecessary positive charges from the EDC towards the nanoparticles.

It was necessary to ascertain the number of biomolecules conjugated to each nanoparticle so the sensitivity of the detection method can be evaluated with respect to the biomolecule. Consideration of the maximum number of adsorbed biomolecules should also be made to limit steric crowding and any effect this may have on the functionality of the biomolecule. Quantitation of nanoparticle-bound species has been achieved for DNA by Demers *et al.*⁸⁷ using a displacement approach. Addition of a thiol-containing molecule such as mercaptoethanol or DTT to nanoparticles functionalised with fluorescence labelled thiol-DNA displaces the DNA into the bulk solution which can be isolated from the nanoparticles by centrifugation and subsequently analysed by fluorescence spectroscopy. This method was applied to gold and silver nanoparticles that had been conjugated to fluorescein isothiocyanate-labelled anti LFA-1 using the NIR linker. Addition of DTT to the nanoparticles should induce aggregation of the nanoparticles since this strips the nanoparticles of their protective layer (the linker modified biomolecules) and they are no longer able to withstand the effects of the ionic buffer. This was observed for the silver conjugates, however was not for the gold conjugates, indicating that the DTT was unsuccessful in displacing the NIR linker. This was presumably a result of the strong interaction between the disulfide moiety in the linker with the gold surface. Since thiols have a reduced affinity for the silver surface compared with gold,¹⁸³ it is not surprising that the disulfide linker was displaced from the silver nanoparticles and not the gold. Increasing the DTT concentration had no effect and so an alternative approach was employed. DTT was replaced with trypsin, an enzyme that hydrolyses amide bonds following lysine and arginine residues. It was theorised that hydrolysis of an amide bond within the antibody structure would release the fluorescence label

that was tethered to the nanoparticle surface *via* the linker modified antibody. Addition of the trypsin to the gold nanoparticles did not result in aggregation indicating that the linker and possibly a portion of the anti LFA-1 FITC remained intact with the nanoparticle surface. The fluorescence intensity was correlated with the anti LFA-1 concentration by use of a calibration prepared from standard anti LFA-1 FITC solutions which was subsequently used to estimate the number of anti LFA-1 FITC molecules *per* nanoparticle based on a previous evaluation of the nanoparticle concentration (figure 6.10).



	fluorescence intensity	FITC concentration using calibration equation (M)	concentration prior to sample dilution (M)	nanoparticle concentration (M)	antibodies <i>per</i> nanoparticle
A	205.84	3.29×10^{-10}	9.13×10^{-10}	3.87×10^{-9}	0.23
B	155.83	2.45×10^{-10}	6.81×10^{-10}	3.26×10^{-9}	0.21
C	184.21	2.93×10^{-10}	8.13×10^{-10}	4.21×10^{-9}	0.19
D	168.02	2.66×10^{-10}	7.38×10^{-10}	3.61×10^{-9}	0.20
E	195.19	3.11×10^{-10}	8.64×10^{-10}	4.05×10^{-9}	0.21

Figure 6.10 Fluorescence calibration graph of anti LFA-1 FITC and calculations corresponding to 5 replicate samples of the anti LFA-1 FITC functionalised gold nanoparticles for determining the number of antibodies *per* nanoparticle. The data points and error bars represent the mean fluorescence and standard deviation, respectively, of the replicate samples.

The calculated results are presented in table 6.1. The number of calculated antibodies on silver nanoparticles using the trypsin hydrolysis method (1.85) was corroborated

with the DTT displacement method (1.82). This indicates that enzyme hydrolysis is a valid technique for the assessment of biomolecule coverage. Therefore the number of anti LFA-1 FITC molecules *per* gold nanoparticle can be assumed to be 0.21. Since this value is between 0 and 1, it indicates that some of the nanoparticles are not functionalised with the anti LFA-1 FITC at all.

Method	Number of anti LFA-1 FITC <i>per</i> Au NP	Number of anti LFA-1 FITC <i>per</i> Ag NP
enzyme hydrolysis	0.21 ± 0.02	1.85 ± 0.50
DTT displacement	not possible	1.82 ± 0.10

Table 6.1 The number of anti LFA-1 FITC molecules per gold and silver nanoparticle using the DTT displacement method and the trypsin hydrolysis method.

This would be expected assuming functionalisation follows a discrete poisson distribution. It should be noted that this was a bulk measurement unlike quantitation methods such as stepwise fluorescence photobleaching which allow determination of the distribution of nanoparticles functionalised with different numbers of protein²⁰² and can therefore be considered a more information-rich technique. Unfortunately this method of analysis could not be applied to metallic nanoparticles since the fluorescence from the label is significantly quenched by the nanoparticle. The number of immobilised anti LFA-1 FITC on the silver nanoparticles is greater than for the gold which is consistent with the greater surface area of silver nanoparticles (3848 nm² for 35 nm silver compared with 531 nm² for 13 nm gold, assuming the nanoparticles are spherical). There have been significant efforts recently towards developing nanoparticle conjugates with high stability and resistance to displacement from other surface-seeking ligands, therefore it is essential that a method can be employed for characterisation purposes. The enzyme hydrolysis method does not rely on the competition of surface seeking species (in this instance, the disulfide NIR linker and DTT) and therefore is more effective for molecules that bind to the nanoparticle surface with high affinity.

6.2 Cell Mapping

Murine dendritic cells were incubated with the anti LFA-1 gold conjugates. Cells were also incubated with murine isotype control antibody gold nanoparticle conjugates which were believed not to interact with receptors on the cell surface and therefore serve the purpose of a negative control. The cells were then washed, fixed, and stained with a solution of Giemsa to aid cell visualisation before analysis by SERRS line mapping. Cell fixation is performed to preserve the sample so the physical and chemical properties of the cell remain unchanged. This is achieved by disabling enzymes and bacteria that may digest and damage the cell, and by conferring mechanical rigidity towards the cell to help maintain its morphology. Fixed cells are significantly more stable whilst obtaining spectroscopic measurements and so using cells in this form is advantageous over live cells. Tang *et al.* discovered that fixation and air-drying of cells resulted in SERS signals of higher intensities. It was proposed that as the cell contracts in size during the drying process, cell components are brought into closer proximity to the nanoparticles giving rise to greater enhancement effects.¹⁶⁵

Although the NIR linker is SERRS active at 632.8 and 785 nm, analysis at 785 nm was preferred as the cell stain, Giemsa, is SERRS active at 632.8 nm. Giemsa is composed of Eosin Y and methylene blue which renders the dye as fluorescent and suitable for gold and silver nanoparticle adsorption, respectively.

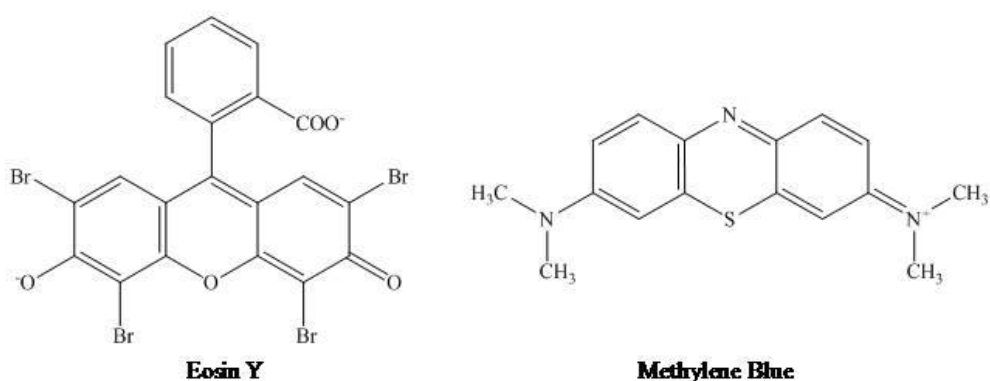


Figure 6.11 Chemical structures of Eosin Y and methylene blue

Giemsa has an absorption maximum at 627 nm (figure 6.12) and so it will be in resonance with a 632.8 nm laser excitation wavelength. The resonance Raman profile of Giemsa illustrates a relatively broad peak between 1620 and 1650 cm^{-1} (figure 6.16). Use of an excitation wavelength off-resonant with the cell stain meant the NIR linker signals would suffer less interference and possible masking. The UV-visible spectrum of Giemsa indicates that at 785 nm, there should be little resonance contributions from the cell stain and therefore would be a more suitable excitation wavelength for identifying the NIR chromophore from the antibody nanoparticle conjugates. However, it should be noted that resonance Raman excitation profiles are of a Lorentzian fashion and so some resonance enhancement will occur at wavelengths significantly removed from the absorption maximum of the dye.¹¹⁸

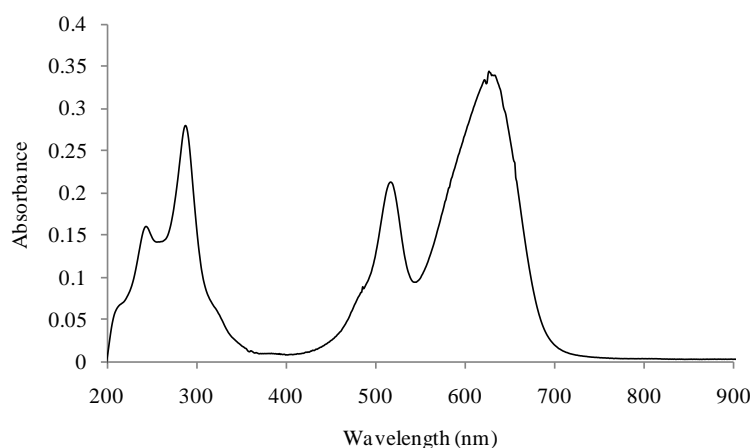


Figure 6.12 UV-visible spectrum of Giemsa

False colour images were generated based on the integrated area under the peak at 724 cm^{-1} , a characteristic peak of the NIR linker. Assigning the maximum colour intensity to the same peak area across all cell analyses allowed visual comparison of cell samples (figure 6.13). The false colour image corresponding to the anti LFA-1 conjugates in figure 6.13 appears brighter than the image of the isotype control conjugates. The spectrum from the brightest pixel in the image is also of greater intensity and has a better signal to baseline ratio than the isotype control spectrum. This indicates that the anti LFA-1 conjugates are binding in greater numbers than the isotype control conjugates. To ascertain if this result was representative of the cell

samples, 25 cells were analysed from both the anti-LFA-1 conjugate sample and the isotype control conjugate sample. The integrated peak area from the pixels comprising each cell was summed. This was a lengthy process that involved fitting each cell to a rectangle within the image and noting the x,y coordinates of each corner. The exported meta data was then sorted using the map coordinates so that only the pixels from each cell are collected and interrogated and not the blank regions in between the cells. It was necessary to assign a cut-off value to ensure only SERRS was recorded and not background signal. This ensures that the data are not skewed as a result of many small values being summed. Unfortunately, this introduces a degree of human error into the data analysis as assignment of the cut-off value is subjective and choice of a lower or higher number will have a significant effect on the data set. It was assumed that the size of the cells was uniform across the anti LFA-1 nanoparticle and control antibody nanoparticle data sets.

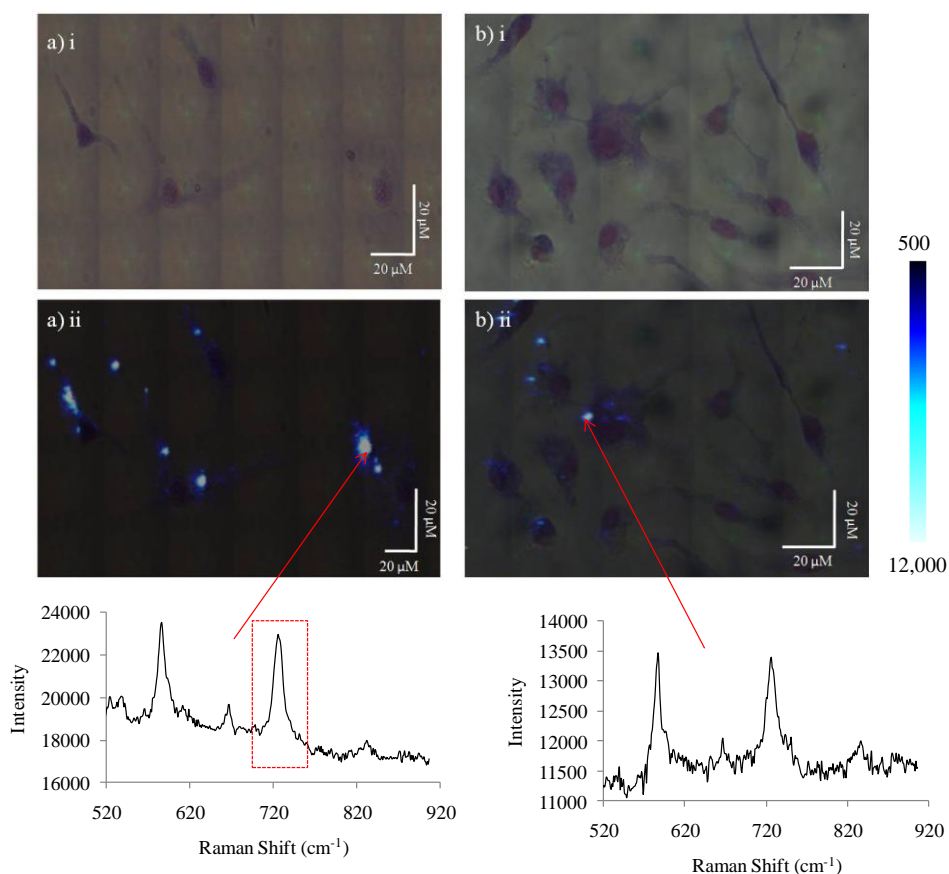


Figure 6.13 Brightfield image (i) and SERRS map superimposed on brightfield image (ii) of lipopolysaccharide (LPS) stimulated dendritic cells incubated with anti LFA-1 gold nanoparticles (a) and isotype control antibody gold nanoparticles (b). Example SERRS spectra are shown below. The red box marks the peak interrogated for generation of the false colour images.

The results are presented in figure 6.14 and illustrate there was a marked difference in SERRS intensities of cells that had been incubated with anti LFA-1 conjugates from cells incubated with isotype control conjugates, although the signal arising from the isotype control conjugates is still significant.

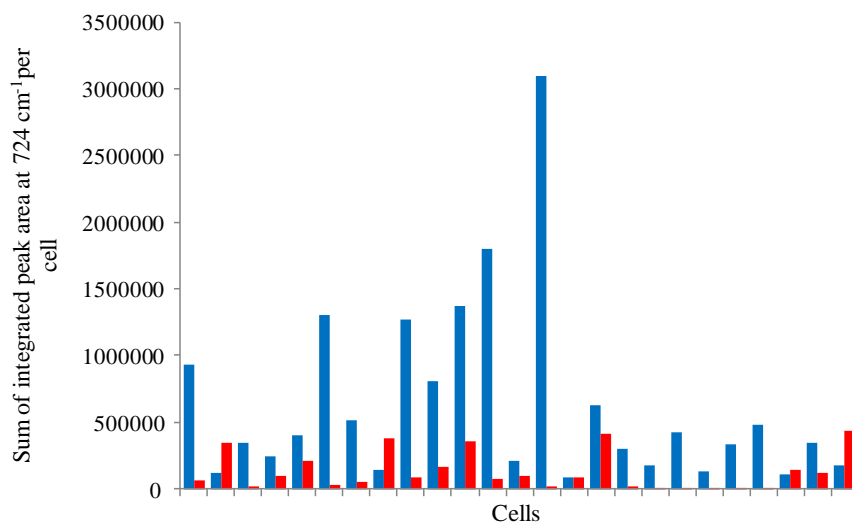


Figure 6.14 Bar chart representation of the total SERRS from 25 cells incubated with the NIR dye-labelled conjugates. Blue: anti LFA-1 conjugates; red: isotype control antibody conjugates.

Although the isotype control antibody has no known specificity for the dendritic cell surface it is possible that the conjugates are binding to the cell surface through F_c receptors. F_c receptors are present on immune system cells and bind to the crystallisable region of antibodies.

To ascertain whether the difference in signals corresponding to the anti LFA-1 and isotype control conjugates was significant, a t-test was performed (see appendix). Employing a one-tailed test at a 95 % confidence level, showed the calculated value of t to be greater than the critical value of t and so the null hypothesis was rejected (H_0 : the mean SERRS signals were not significantly different from one another). Although it may be possible to improve the discrimination between SERRS signals corresponding to the anti LFA-1 and the control conjugates, the results so far indicate a specific interaction did occur between the anti LFA-1 gold nanoparticles and the cell surface.

Gold nanoparticles labelled with the NIR linker alone (no antibody) were also incubated with the cells as means of a control. A representative cell image is shown in figure 6.15. No signal was observed from any of the cells indicating that the NIR labelled nanoparticles have a poor affinity for the cell surface. This further supports the evidence that a specific interaction took place between the anti LFA-1 conjugates and the LFA-1 receptors as illustrated in figures 6.13 and 6.14.

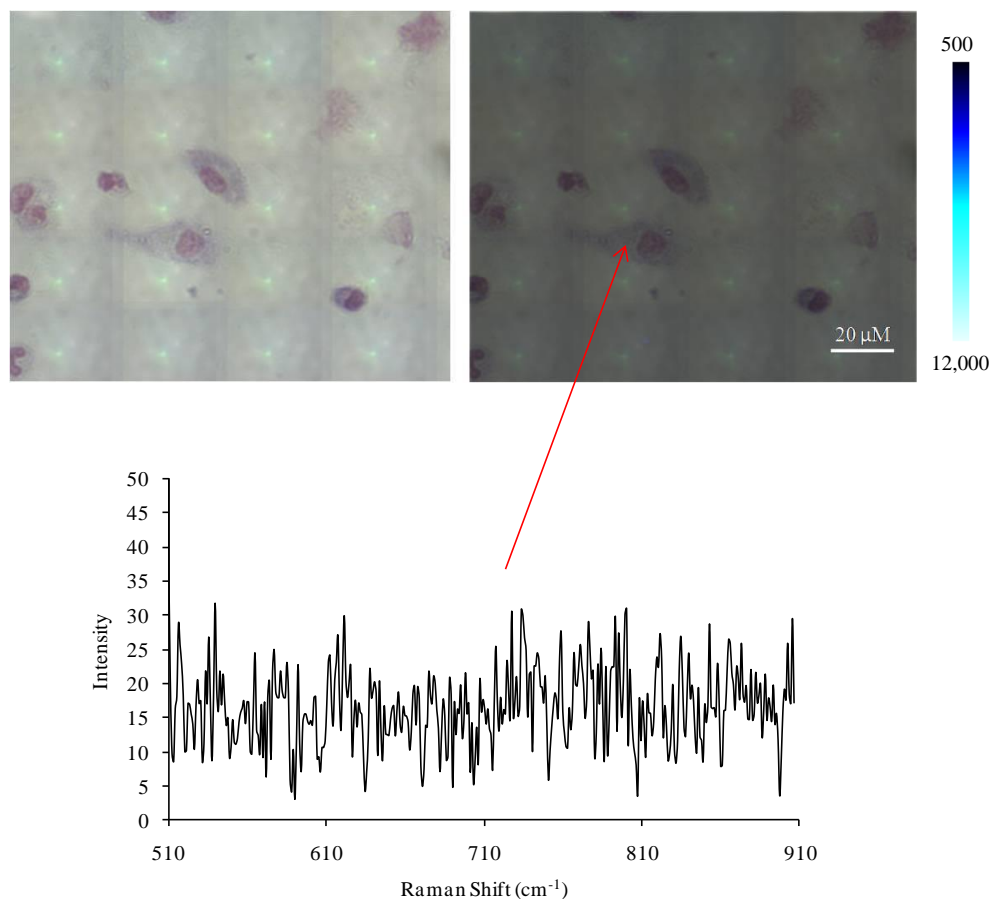


Figure 6.15 Brightfield image (left) and SERRS map superimposed on brightfield image (right) of LPS stimulated dendritic cells that had been incubated with NIR labelled gold nanoparticles (no antibody).

SERRS analysis at 632.8 nm also supports the evidence of a successful interaction between the anti LFA-1 nanoparticles and the cell surface. The presence of the NIR linker was not easily identified, however a surface enhancement contribution

provided by the nanoparticles was observed in the resonance Raman spectra of the Giemsa cell stain. SERRS analysis of cell stains has been reported by Stokes *et al.* for macrophage cells that had internalised gold and silver nanoparticles.²⁰³ The cells that had been treated with the anti LFA-1 nanoparticle conjugates illustrated SERRS signals of increased intensities compared with cells that had not been treated with nanoparticles at all, apparent by the brighter colours in the false colour images (figure 6.16). The spectra in figure 6.16 also display a reduced background signal for the cells treated with anti LFA-1 nanoparticles, which is possibly a result of fluorescence quenching.²⁷

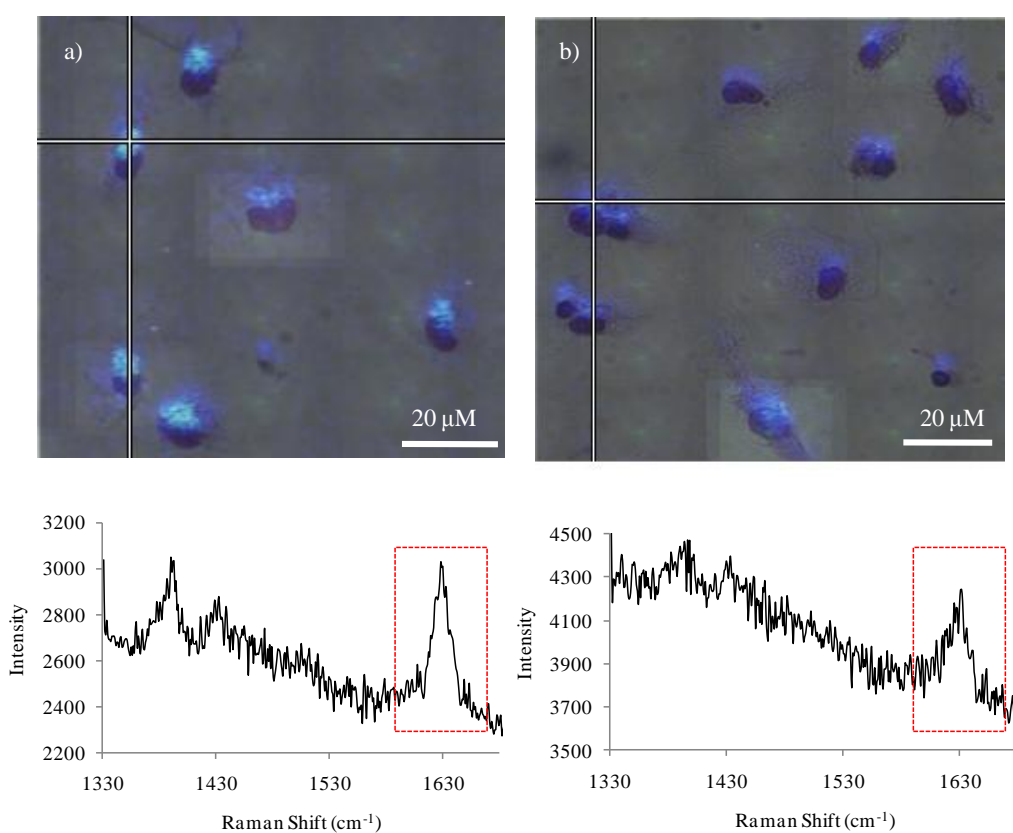


Figure 6.16 SERRS maps recorded at 632.8 nm overlaid on brightfield images of dendritic cells that had been incubated with anti LFA-1 nanoparticles (a) and cells that had not been treated with nanoparticles (b). The SERRS spectra correspond to the pixel on the images marked by the crosshairs. The region marked on the SERRS spectrum indicates the peak interrogated for generation of the false colour images.

6.3 Lipopolysaccharide Stimulation

Dendritic cells are antigen presenting cells and are found to exist in two phases: immature and mature. Immature dendritic cells exhibit high antigen uptake ability but poor T-cell stimulatory function. Upon antigen internalisation, the dendritic cells migrate to the lymph nodes where contact with microorganisms and bacterial products, such as lipopolysaccharide (LPS), initiates the transformation into mature dendritic cells which exhibit low antigen-uptake ability and high T-cell stimulatory function. Since LFA-1 is involved in T-cell stimulation, it is upregulated upon maturation. Cells can be stimulated *in vitro* by the addition of LPS. LFA-1 and ICAM-1 (the ligand to LFA-1) have been shown to be upregulated on dendritic cells following 4 hours LPS stimulation.²⁰⁴ Flow cytometry experiments performed by Vivienne Gibson, (Strathclyde Institute of Pharmacy and Biological Sciences) also indicated that LFA-1 was upregulated following LPS stimulation (figure 6.17). Flow cytometry is a fluorescence-based technique which allows analysis and sorting of microscopic particles, in this case cells, within a stream of liquid. Treatment of cells before analysis with fluorescence-labelled biomolecular ligands enables multiplexed identification and quantitation of cellular surface markers.

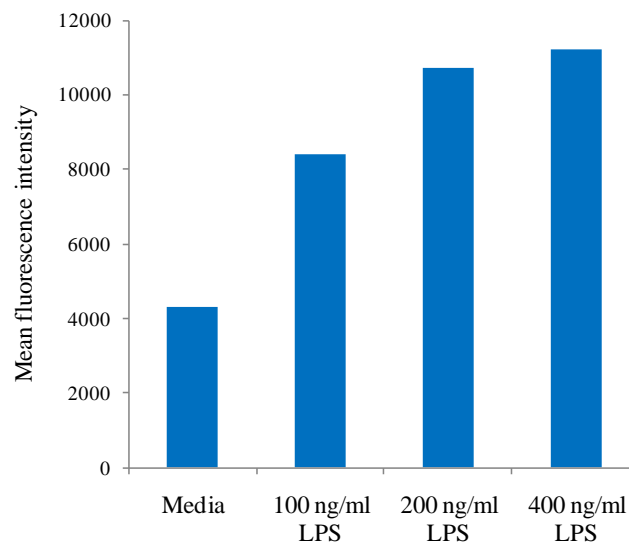


Figure 6.17 Flow cytometry data recorded by Vivienne Gibson illustrating the mean fluorescence intensities from cells that had been incubated with phycoerythrin (PE) labelled anti LFA-1.

Incubation with LPS at a 100 ng/mL concentration doubled the expression of LFA-1 on the cell surface and so incubation of LPS-stimulated cells with the anti LFA-1 nanoparticle conjugates were expected to yield increased SERRS intensities or a greater number of SERRS-active pixels across the cell map. LPS stimulated and non-stimulated cells were both treated with the nanoparticle conjugates and analysed by SERRS line mapping. The total SERRS intensity from each cell was calculated as described above and are presented in figure 6.18.

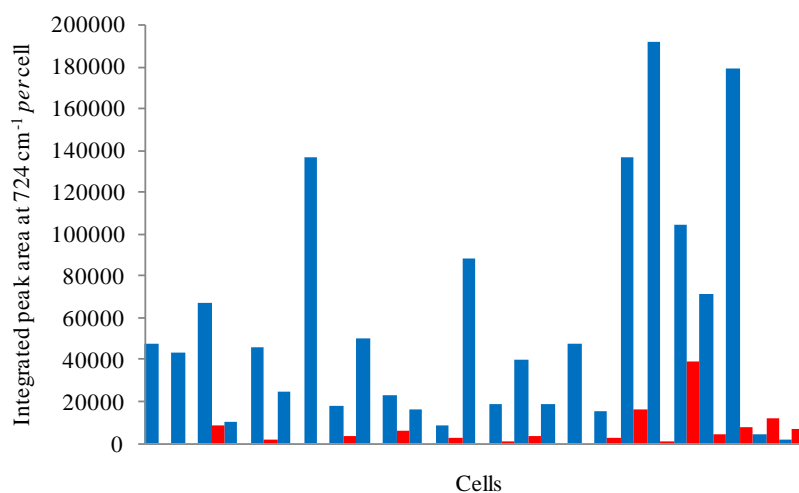


Figure 6.18 Bar chart representation of the total SERRS from 25 cells incubated with the anti LFA-1 conjugates. Blue: LPS stimulated; red: non-stimulated.

The data shown in figure 6.18 illustrates a marked increase in SERRS signals upon LPS stimulation however the figure does not provide information as to whether the differences in the total SERRS for the two samples was the result of higher SERRS intensities within each pixel or a greater number of SERRS active pixels. The number of SERRS active pixels can be compared to give an indication if the area of the cell from which SERRS was recorded was altered upon LPS stimulation. The pixel size was kept constant throughout all mapping experiments: 1.0 μM (x) by 0.5 μM (y). The total number of SERRS active pixels for 25 non-stimulated cells was 82, with an average of 5 pixels *per* cell; whereas 25 LPS stimulated cells yielded a total number of 889 SERRS active pixels and an average of 35. If the average cell size is assumed to be the same for stimulated and non-stimulated cells, then one can deduce that the absolute number of LFA-1 receptors *per* cell surface unit area has increased

upon stimulation. It should be noted that the calculated number of SERRS active pixels may be erroneously high due to poor spatial resolution on the CCD detector. If a pixel exhibits a high SERRS intensity, it is possible that surrounding pixels in the x,y plane may also appear to be SERRS active, albeit at lower intensities. This effect should be minimal in the x direction since the limit of resolution, defined by $0.6 \times \text{laser excitation wavelength} / \text{objective numerical apperture}$, is 628 nm. However, the area has been over-sampled in y since the pixel parameter was set to 1 μM , 0.5 μM (x,y).

The average SERRS intensity *per* pixel was found to be 2092 counts for LPS stimulated cells and 1441 for non-stimulated cells, indicating that not only the number of pixels has increased but also the intensities within each pixel. Since multiple binding events can take place within each pixel, it is highly likely that this is the result of the observed increase in intensities. The pixel intensities are probably not an additive effect from multiple binding events as if several anti LFA-1 functionalised nanoparticles have bound to the surface in close proximity to one another, electromagnetic coupling between adjacent nanoparticles will occur. Nanoparticle aggregates have been shown to give significantly higher SERRS intensities due to the creation of interparticle 'hotspots'³¹ and coincidence of the broadened nanoparticle plasmon resonance with the laser excitation wavelength.²⁸ This result provides some insight into the spatial arrangement of the LFA-1 receptors on the surface. It would seem that upon LPS stimulation, not only are the LFA-1 receptors distributed over a larger area of the cell surface (illustrated by the greater number of SERRS active pixels) but that the LFA-1 receptors are expressed very close together, less than one pixel apart (illustrated by the greater SERRS intensities *per* pixel).

A t-test was performed to determine whether the mean of the SERRS intensities from LPS stimulated cells were significantly greater than intensities from non-stimulated cells (see appendix for calculations). Employing a one-tailed test at a 95 % confidence level, showed the calculated value of t to be greater than the critical value of t and so the null hypothesis was rejected (H_0 : the results are not significantly

different from one another). This demonstrates that LPS stimulation of dendritic cells significantly increases the number of LFA-1 receptors as determined by SERRS.

6.4 CD40 Target

To illustrate the versatility of this technique towards other target molecules, a CD40 antibody was conjugated to nanoparticles using an identical method of that for anti LFA-1. CD40 is a 45-50 kDa, membrane-bound costimulatory protein present on antigen presenting cells, such as dendritic cells.²⁰⁵ Expression of CD40 is more abundant on mature dendritic cells for binding to T helper cells through its ligand CD40-L (or CD154).²⁰⁶ LPS has been shown to induce maturation of dendritic cells resulting in upregulation of CD40.²⁰⁴ SERRS analysis of bone-marrow derived dendritic cells illustrated up regulation of the CD40 protein molecules using the anti CD40 nanoparticle conjugates (figure 6.19). Non-stimulated cells yielded poor overall SERRS intensities and less SERRS active pixels (on average 1 pixel *per* cell compared with 8 pixels for LPS stimulated cells). It is apparent from figure 6.19 that some cells do not exhibit SERRS signals corresponding to the NIR linker at all, however the number does increase from 8 to 21 out of the 25 cells analysed.

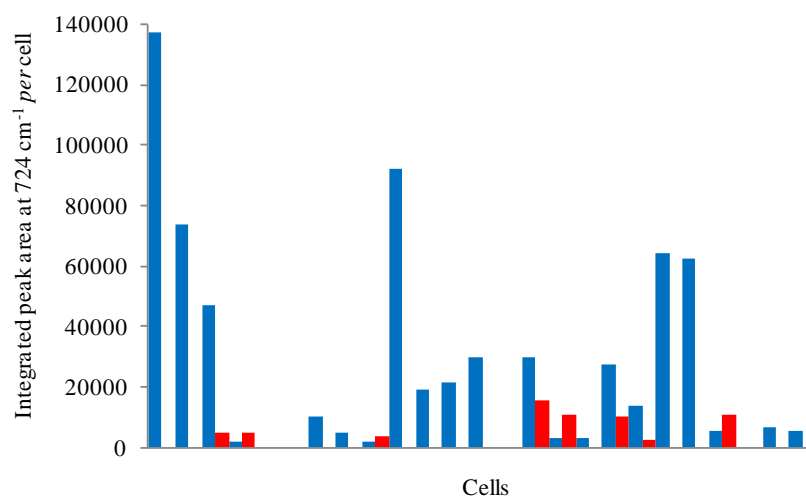


Figure 6.19 Integrated SERRS peak intensities at 724 cm⁻¹ using 785 nm excitation wavelength. Each column represents a cell. Blue: LPS stimulated cells; red: non-stimulated cells.

The SERRS results were supported by flow cytometry data indicating that expression of CD40 more than doubles when the cells were incubated with 100 ng/mL LPS (figure 6.20).

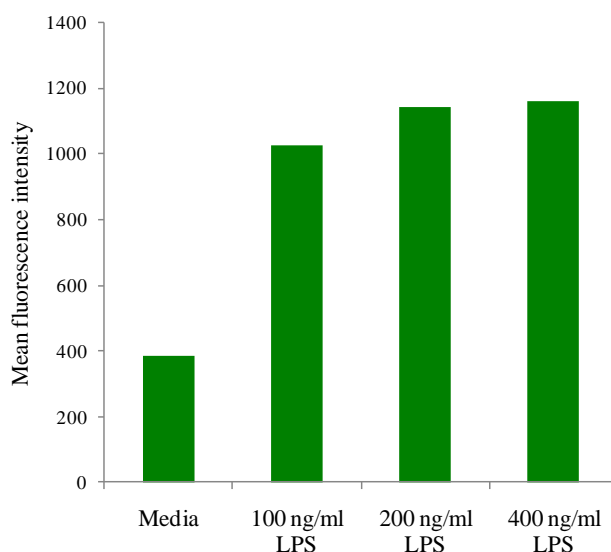


Figure 6.20 Flow cytometry data recorded by Vivienne Gibson illustrating mean fluorescence intensity from cells that had been incubated with FITC labelled anti CD40.

Another biomolecule, chemokine (CC motif) ligand 2 (CCL2), was immobilised onto nanoparticles for subsequent cell incubation. CCL2 is a cytokine belonging to the CC chemokine family. Chemokines are fundamentally involved in acute and chronic inflammatory diseases and in particular the CC chemokines attract and activate leukocytes including dendritic cells and T-cells through interaction with their corresponding cell surface receptors.^{207, 208} The receptor to CCL2 is CCR2. CCR2 has been shown to be down-regulated upon the addition of LPS to cells²⁰⁹ and so it was questioned whether the down-regulation of the CCR2 could be monitored using CCL2 conjugates akin to the up-regulation of LFA-1. The CCL2, 125 amino acid sequence was reacted with the NIR linker followed by addition to the gold nanoparticles. The gold nanoparticles aggregated immediately turning the nanoparticle solution from red to blue. It was assumed that the reason for nanoparticle aggregation was protein-specific since aggregation did not occur when the linker-modified anti LFA-1, isotype control, or anti CD40 was added to the nanoparticles. This was confirmed by direct addition of a CCL2 solution (no linker

modification) to the nanoparticles, which also resulted in aggregation. To investigate the cause for aggregation, the overall electrostatic charge of CCL2 was determined. Consideration of the number of positively charged arginine, lysine and histidine residues versus the number of negatively charged glutamate and aspartate residues indicated at physiological pH, the protein would be positively charged and further inspection of sequence using protein analysis software (ExpASY) revealed a pI value of 9.81. This suggests that although the NIR linker is able to passivate the nanoparticle surfaces in the conjugation buffers used in this investigation, it is unable to protect the nanoparticles against positive charges that may be introduced through addition of positively charged proteins.

6.5 Conclusions

In conclusion, gold and silver nanoparticles have been functionalised with a NIR dye-labelled linker to allow subsequent reaction with an antibody or protein through their lysine residues. The NIR linker nanoparticles have been shown to be stable in biological buffers and exhibit SERRS activity at 514.5 nm, 632.8 nm and 785 nm. The limits of detection were determined to be in the range of pM down to fM depending on the laser excitation wavelength and metal nanoparticle employed, allowing highly sensitive analysis. The nanoparticles were conjugated to LFA-1 antibodies *via* amide formation and the number of FITC labelled antibodies was determined using DTT displacement and a novel trypsin hydrolysis method. LFA-1 was selectively targeted on cell surfaces using the anti LFA-1 gold nanoparticle conjugates for SERRS analysis and was shown to be up-regulated upon LPS stimulation by quantitation of the SERRS intensities and number of SERRS active pixels. Successful interaction of the anti LFA-1 nanoparticles with the cell surface receptors was also verified by SERRS analysis using an excitation wavelength tailored towards the cell stain. To illustrate the versatility of the analysis technique for other targets, up-regulation of CD40 upon LPS stimulation was also monitored by SERRS using anti CD40 gold nanoparticle conjugates however it was not possible to

target the chemokine receptor CCR2, due to instability of the CCL2 nanoparticle conjugates.

7. *Conclusions*

Several advances have been made in the detection strategies of specific DNA sequences for diagnostic purposes. Nanoparticle labelling is an attractive method for identifying sequences due to the striking optical properties of nanoparticles, allowing colorimetric detection, and the sharp melting transitions produced by nanoparticle modified oligonucleotides. Locked nucleic acid (LNA) probes were immobilised onto gold nanoparticles to improve the thermal stability of the resultant duplex. This was the first report of the preparation of LNA functionalised nanoparticles. They were shown to have a greater stability than DNA functionalised nanoparticles and LNA that had not been modified with nanoparticles, and also exhibited improved selectivity for complementary sequences against sequences incorporating single base pair mismatches. The ability to discriminate against non-complementary sequences is necessary for identifying single nucleotide polymorphisms which are responsible for a person's susceptibility to certain diseases. The LNA modifications were also employed for targeting double stranded sequences by triplex formation. It was shown that hybridisation of the nanoparticle modified triplex forming oligonucleotides (TFOs) to the target by Hoogsteen hydrogen bonding was achieved at room temperature yielding the characteristic colour change of the nanoparticle solution from red to blue indicating hybridisation-induced aggregation. The selectivity of the probes for the target was maintained for triplex formation as illustrated using a double stranded target sequence with a single base pair mismatch relative to the TFO. The melting curve of the gold nanoparticle triplex was relatively broad however it was found that this was not a feature of nanoparticle modified triplexes since the silver nanoparticle triplex produced a sharp transition upon melting characteristic of nanoparticle modified oligonucleotides. DNA detection of polypurine sequences through triplex formation has been shown to be as effective as duplex formation and presents the additional advantage of not needing to denature the double stranded DNA target prior to introduction of the probes.

To further improve the detection capabilities of DNA sequences, the near field optical properties of the nanoparticle modifications was exploited for surface enhanced resonance Raman scattering (SERRS). SERRS offers numerous advantages over established fluorescence based detection strategies, namely the analyte's resistance to photobleaching, molecularly specific spectra, and narrow emission bands enabling multiplexed analysis. To illustrate the multiplexing potential of SERRS, an oligonucleotide 5-plex was analysed using a dual-wavelength approach. Exploitation of the resonance component of SERRS enabled all 5 oligonucleotide dye labels to be identified with reduced interference from each other. The spectral peaks used for analysis purposes were unique to each label and could be identified by eye with no need for chemometric analysis.

To apply SERRS as a useful detection method, it was necessary to introduce the SERRS label into the nanoparticle probes to avoid modification of the target sequence. This was achieved by labelling pre-functionalised oligonucleotide silver nanoparticle conjugates using SERRS active dyes that adsorb onto the surface through a variety of different means. This was an advancement of previous methods in the literature that require careful control of surface coverage and dye selection. Post-oligonucleotide labelling renders the nanoparticles highly stable in ionic environments and allows a large range of different dyes labels to be employed at excess concentrations. The nanoparticle duplex was adapted to incorporate mixed metal nanoparticles. Gold nanoparticles are inherently more stable than silver nanoparticles and so are more resilient to surface modification. However, it is highly desirable to employ silver nanoparticles due to their large surface enhancement properties. A mixed metal duplex consisting of a dye labelled gold nanoparticle probe and silver nanoparticle probe hybridised to a target DNA sequence is reported for the first time, illustrating the combination of advantages afforded by each metal. A SERRS active triplex was also assembled, ultimately merging the triplex-forming properties of LNA probes with SERRS detection for the first time. The increased rigidity of double stranded DNA in comparison with single stranded DNA and the ability to use DNA sequences of different lengths has enabled an investigation into the interparticle distance effect on SERRS intensity, supporting previous findings in

the literature. In the future it can be envisaged that such a system will be applied as a nano-metrology tool.

Proteins and antibodies also benefit from nano-based detection strategies which have attracted much interest for probing cellular interactions. A novel linker was designed that incorporated a disulfide anchor for nanoparticle surface attachment, carboxylic acid functionality for conjugation to a protein or antibody, and a near infrared (NIR) dye label to bestow SERRS activity upon the resultant biomolecule nanoparticle conjugate. The linker functionalised nanoparticles were shown to yield SERRS spectra at multiple excitation wavelengths, possess stability in ionic buffers, and exhibit resistance against displacing species, namely DTT. The nanoparticles were functionalised with anti lymphocyte function associated antigen-1 (LFA-1) to enable identification of LFA-1 on the surfaces of cells. LFA-1 is an important molecule involved in the immune response within the body, influencing T-cell activation and T-lymphocyte migration. Dendritic cells that had been incubated with the anti LFA-1 nanoparticles were analysed by SERRS line mapping which indicated discrete areas of nanoparticle conjugate binding across the cell surface. The up-regulation of LFA-1 upon lipopolysaccharide stimulation was monitored quantitatively by evaluation of the SERRS intensities and number of SERRS active pixels. This is the first report of quantitative cellular-based SERRS analysis. The detection strategy utilised 13 nm gold nanoparticles which are inherently more stable than gold nanoparticles of larger diameters which have been used so far in the literature. Cellular SERRS detection was also applied towards targeting another receptor, CD40, illustrating the versatility of the technique.

8. *Further Work*

LNA nanoparticle probes were used to target single and double stranded DNA with high sensitivity and selectivity. The target sequences used in the experiments were synthesised 14-mer oligonucleotides and therefore not alike to a real biological sample. The sequence targeted corresponds to the mouse inducible nitric oxide synthase (iNOS) gene which catalyses the production of nitric oxide radicals from L-arginine for immune defence purposes. Following the selection of suitable primers, the target sequence should be isolated from mouse DNA and amplified. Sequence detection will be more challenging than oligonucleotide hybridisations already conducted, due to the increased complexity of the sequence. Preliminary investigations into primer selection have indicated the shortest DNA length that can be amplified for this sequence is 150 base pairs; a significantly larger number than the 14 base pair sequence used to date in this research. The incorporation and targeting of pyrimidine sequences should also be pursued to further develop the triplex work. Fox and co-workers have dedicated significant effort towards targeting pyrimidine sequences using artificial base analogues.^{81, 82} They have also shown that natural bases can be employed although these triplexes suffer from significant destabilisation.⁸⁰

Surface enhanced resonance Raman scattering (SERRS) detection of DNA sequences using the dye-labelled oligonucleotide nanoparticle conjugates can be developed further by detecting multiple sequences simultaneously. It has been shown that the conjugates are compatible with numerous dyes and so the multiplexing capabilities of SERRS should be exploited. Consideration would need to be given to the SERS cross sections of the chosen dye labels; although two labels may have SERRS peaks that are unique to themselves, if one produces SERRS signals of much greater intensity, it may obscure the signals of the other. The SERRS duplex and triplex work indicated that melting temperature has an effect on SERRS intensities. To investigate this further, heat could be applied so that the duplex or triplex is interrogated at different stages of its melting process. This would have to be achieved

with a high degree of accuracy due to the sharp melting transition of the duplex. Utilisation of a temperature controlled Raman spectrometer would allow a SERRS melting profile to be recorded. It would be interesting to compare the profile with the UV-visible melting curve to assess the relative sensitivities of the two detection methods towards the extent of hybridisation induced aggregation. The SERRS intensities were also shown to be dependent on interparticle distance. This work should be continued to directly correlate the interparticle distance in base pairs to a value in nanometres. This has been performed for duplex systems by Park *et al.*¹⁰⁷ and Yamakoshi *et al.*¹⁰⁹ using small angle x-ray scattering (SAXS). SERRS labelling can also be applied to higher DNA structures; i-motifs and G-quadruplexes are assembled upon hydrogen bonding between four DNA strands. I-motifs are dependent on acidic pHs, much like parallel triplexes, and so a source of protons can be used as the fuel to initiate assembly. Proton dependent nanoparticle i-motif assemblies have been reported by Sharma *et al.*²¹⁰ and Wang *et al.*²¹¹ Both assemblies were shown to be reversible upon the addition of hydroxide ions.

The work involving the antibody nanoparticle conjugates could be advanced by detecting surface receptors in a multiplexed format, for example, simultaneously detecting CD40 and LFA-1. This would require the synthesis of another linking molecule featuring a SERRS active dye with a different emission spectrum. It is highly desirable that the chromophore be excited upon near-infrared radiation since longer wavelength photons are of lower energy, therefore will exert less damage upon the cells, and autofluorescence from other cell components is minimised. It would also be worthwhile investigating the feasibility of using silver nanoparticle conjugates. Silver nanoparticles provide much greater surface enhancement effects¹⁹³ however have been associated with cellular toxicity resulting in cell death.¹⁵⁷ It would therefore be necessary to stain the cells with trypan blue to determine the viability of the cells.

Cellular analysis by SERRS can be further developed by applying SERRS to flow cytometry based methods of detection for the identification of cell surface receptors. This would enable much higher throughput analysis of cells in comparison to microscopy systems however does not provide information of the spatial distribution

of the receptors across the cell surface. Current flow cytometers utilise fluorescence spectroscopy however are limited to the number of different receptors that can be identified due to the inherent broad emission profiles associated with fluorescence. The powerful multiplexing capabilities of SERRS would enable greater number of receptors to be analysed simultaneously.

References

1. I. H. G. S. Consortium, *Nature*, 2001, **409**, 860-921.
2. I. H. G. S. Consortium, *Science*, 2001, **291**, 1304-1351.
3. X. C. Zhou, S. J. O'Shea and S. F. Y. Li, *Chem. Commun.*, 2000, 953-954.
4. F. Patolsky, K. T. Ranjit, A. Lichtenstein and I. Willner, *Chem. Commun.*, 2000, 1025-1026.
5. L. Authier, C. Grossiord, P. Brossier and B. Limoges, *Anal. Chem.*, 2001, **73**, 4450-4456.
6. H. Xu, J. Aizpurua, M. Käll and P. Apell, *Phys. Rev. E*, 2000, **62**, 4318.
7. L. Gunnarsson, E. J. Bjerneld, H. Xu, S. Petronis, B. Kasemo and M. Käll, *Appl. Phys. Lett.*, 2001, **78**, 802-804.
8. P. Johansson, H. Xu and M. Käll, *Phys. Rev. B*, 2005, **72**, 035427.
9. K. Kneipp, Y. Wang, H. Kneipp, L. T. Perelman, I. Itzkan, R. R. Dasari and M. S. Feld, *Phys. Rev. Lett.*, 1997, **78**, 1667-1670.
10. K. Kneipp, H. Kneipp, I. Itzkan, R. R. Dasari and M. S. Feld, *Chem. Rev.*, 1999, **99**, 2957-2975.
11. M. Moskovits, *Rev. Mod. Phys.*, 1985, **57**, 783-823.
12. M. Moskovits, *J. Raman Spectrosc.*, 2005, **36**, 485-496.
13. S. K. Ghosh and T. Pal, *Chem. Rev.*, 2007, **107**, 4797-4862.
14. G. Mie, *Annals of Physics*, 1908, **25**, 377-445.
15. K. Kneipp, M. Moskovits and H. Kneipp, *Surface-Enhanced Raman Scattering- Physics and Applications*, Springer, Berlin, 2006.
16. W. E. Smith and G. Dent, *Modern Raman Spectroscopy; A Practical Approach*, John Wiley & Sons Ltd., Chichester, 2005.
17. M. G. Albrecht and J. A. Creighton, *J. Am. Chem. Soc.*, 1977, **99**, 5215-5217.
18. D. L. Jeanmaire and R. P. Van Duyne, *J. Electroanal. Chem.*, 1977, **84**, 1-20.
19. M. Fleischmann, P. J. Hendra and A. J. McQuillan, *Chem. Phys. Lett.*, 1974, **26**, 163-166.
20. P. C. Lee and D. Meisel, *J. Phys. Chem.*, 2002, **86**, 3391-3395.
21. C. H. Munro, W. E. Smith, M. Garner, J. Clarkson and P. C. White, *Langmuir*, 1995, **11**, 3712-3720.
22. C. A. Jennings, G. J. Kovacs and R. Aroca, *J. Phys. Chem.*, 1992, **96**, 1340-1343.
23. L. R. Allain and T. Vo-Dinh, *Anal. Chim. Acta*, 2002, **469**, 149-154.
24. C. L. Haynes and R. P. Van Duyne, *J. Phys. Chem. B*, 2003, **107**, 7426-7433.
25. S. Nie and S. R. Emory, *Science*, 1997, **275**, 1102-1106.
26. K. Kneipp, H. Kneipp, R. Manoharan, E. B. Hanlon, I. Itzkan, R. R. Dasari and M. S. Feld, *Appl. Spectrosc.*, 1998, **52**, 1493-1497.
27. C. S. Yun, A. Javier, T. Jennings, M. Fisher, S. Hira, S. Peterson, B. Hopkins, N. O. Reich and G. F. Strouse, *J. Am. Chem. Soc.*, 2005, **127**, 3115-3119.

28. D. Cunningham, R. E. Littleford, W. E. Smith, P. J. Lundahl, I. Khan, D. W. McComb, D. Graham and N. Laforest, *Faraday Discuss.*, 2006, **132**, 135–145.
29. I. Khan, D. Cunningham, D. Graham, D. W. McComb and W. E. Smith, *J. Phys. Chem. B*, 2005, **109**, 3454-3459.
30. I. Khan, D. Cunningham, R. E. Littleford, D. Graham, W. E. Smith and D. W. McComb, *Anal. Chem.*, 2006, **78**, 224-230.
31. J. M. McMahon, A.-I. Henry, K. L. Wustholz, M. J. Natan, R. G. Freeman, R. P. Van Duyne and G. C. Schatz, *Anal. Bioanal. Chem.*, 2009, **394**, 1819-1825.
32. S. M. Heard, F. Grieser, C. G. Barraclough and J. V. Sanders, *J. Colloid Interface Sci.*, 1983, **93**, 545-555.
33. J. C. Jones, C. McLaughlin, D. Littlejohn, D. A. Sadler, D. Graham and W. E. Smith, *Anal. Chem.*, 1999, **71**, 596-601.
34. K. Faulds, R. E. Littleford, D. Graham, G. Dent and W. E. Smith, *Anal. Chem.*, 2004, **76**, 592-598.
35. C. D. Bain, H. A. Biebuyck and G. M. Whitesides, *Langmuir*, 1989, **5**, 723-727.
36. C. S. Weisbecker, M. V. Merritt and G. M. Whitesides, *Langmuir*, 1996, **12**, 3763-3772.
37. S.-Y. Lin, Y.-T. Tsai, C.-C. Chen, C.-M. Lin and C.-H. Chen, *J. Phys. Chem. B*, 2004, **108**, 2134-2139.
38. H. D. Hill, J. E. Millstone, M. J. Banholzer and C. A. Mirkin, *ACS Nano*, 2009, **3**, 418-424.
39. M. Brust, M. Walker, D. Bethell, D. J. Schiffrin and R. Whyman, *J. Chem. Soc. Chem. Commun.*, 1994, 801-802.
40. C. J. Sandroff and D. R. Herschbach, *Langmuir*, 1985, **1**, 131-135.
41. P. D. Jadzinsky, G. Calero, C. J. Ackerson, D. A. Bushnell and R. D. Kornberg, *Science*, 2007, **318**, 430-433.
42. Y. Song, T. Huang and R. W. Murray, *J. Am. Chem. Soc.*, 2003, **125**, 11694-11701.
43. P. Ionita, A. Volkov, G. Jeschke and V. Chechik, *Anal. Chem.*, 2008, **80**, 95-106.
44. I. Tinoco, *J. Am. Chem. Soc.*, 1960, **82**, 4785-4790.
45. M. Petersheim and D. H. Turner, *Biochemistry*, 1983, **22**, 256-263.
46. B. C. Froehler, S. Wadwani, T. J. Terhorst and S. R. Gerrard, *Tetrahedron Lett.*, 1992, **33**, 5307-5310.
47. C. Bailly and M. J. Waring, *Nucleic Acids Res.*, 1998, **26**, 4309-4314.
48. G. T. Walker, *Nucleic Acids Res.*, 1988, **16**, 3091-3099.
49. B. Hyrup and P. E. Nielsen, *Bioorgan. Med. Chem.*, 1996, **4**, 5-23.
50. R. H. Griffey, B. P. Monia, L. L. Cummins, S. Freier, M. J. Greig, C. J. Guinosso, E. Lesnik, S. M. Manalili, V. Mohan, S. Owens, B. R. Ross, H. Sasmor, E. Wancewicz, K. Weiler, P. D. Wheeler and P. D. Cook, *J. Med. Chem.*, 1996, **39**, 5100-5109.
51. J. Summerton and D. Weller, *Antisense Nucleic A.*, 1997, **7**, 187-195.
52. P. S. Miller, M. P. Reddy, A. Murakami, K. R. Blake, S. B. Lin and C. H. Agris, *Biochemistry*, 1986, **25**, 5092-5097.

53. W. T. Wiesler and M. H. Caruthers, *J. Org. Chem.*, 1996, **61**, 4272-4281.
54. S. Obika, D. Nanbu, Y. Hari, K.-I. Morio, Y. In, T. Ishida and T. Imanishi, *Tetrahedron Lett.*, 1997, **38**, 8735-8738.
55. S. K. Singh, A. A. Koshkin, J. Wengel and P. Nielsen, *Chem. Commun.*, 1998, 455-456.
56. A. A. Koshkin, P. Nielsen, M. Meldgaard, V. K. Rajwanshi, S. K. Singh and J. Wengel, *J. Am. Chem. Soc.*, 1998, **120**, 13252-13253.
57. J. Wengel, *Accounts Chem. Res.*, 1999, **32**, 301-310.
58. M. Egli, G. Minasov, M. Teplova, R. Kumarc and J. Wengel, *Chem. Commun.*, 2001 651-652.
59. P. M. McTigue, R. J. Peterson and J. D. Kahn, *Biochemistry*, 2004, **43**, 5388-5405.
60. K. E. Nielsen, S. K. Singh, J. Wengel and J. P. Jacobsen, *Bioconjugate Chem.*, 2000, **11**, 228-238.
61. H. Kaur, A. Arora, J. Wengel and S. Maiti, *Biochemistry*, 2006, **45**, 7347-7355.
62. B. W. Sun, B. R. Babu, M. D. Sorensen, K. Zakrzewska, J. Wengel and J. S. Sun, *Biochemistry*, 2004, **43**, 4160-4169.
63. S. Obika, T. Uneda, T. Sugimoto, D. Nanbu, T. Minami, T. Doi and T. Imanishi, *Bioorgan. Med. Chem.*, 2001, **9**, 1001-1011.
64. D. Murphy, R. Eritja and G. Redmond, *Nucleic Acids Res.*, 2004, **32**, e65.
65. A. J. Cheng and M. W. Van Dyke, *Nucleic Acids Res.*, 1993, **21**, 5630-5635.
66. J. F. Milligan, S. H. Krawczyk, S. Wadwani and M. D. Matteucci, *Nucleic Acids Res.*, 1993, **21**, 327-333.
67. N. Kumar, K. E. Nielsen, S. Maiti and M. Petersen, *J. Am. Chem. Soc.*, 2006, **128**, 14-15.
68. M. Koizumi, K. Morita, M. Daigo, S. Tsutsumi, K. Abe, S. Obika and T. Imanishi, *Nucleic Acids Res.*, 2003, **31**, 3267-3273.
69. H. Torigoe, Y. Hari, M. Sekiguchi, S. Obika and T. Imanishi, *J. Biol. Chem.*, 2001, **276**, 2354-2360.
70. U. Christensen, N. Jacobsen, V. K. Rajwanshi, J. Wengel and T. Koch, *Biochem. J.*, 2001, **354**, 481-484.
71. V. V. Demidov and M. D. Frank-Kamenetskii, *Methods*, 2001, **23**, 108-122.
72. J. Basye, J. O. Trent, D. Gao and S. W. Ebbinghaus, *Nucleic Acids Res.*, 2001, **29**, 4873-4880.
73. M. J. J. Blommers, F. Natt, W. Jahnke and B. Cuenoud, *Biochemistry*, 1998, **37**, 17714-17725.
74. N. Atsumi, Y. Ueno, M. Kanazaki, S. Shuto and A. Matsuda, *Bioorgan. Med. Chem.*, 2002, **10**, 2933-2939.
75. T. J. Povsic and P. B. Dervan, *J. Am. Chem. Soc.*, 1989, **111**, 3059-3061.
76. D. Leitner, W. Schröder and K. Weisz, *Biochemistry*, 2000, **39**, 5886-5892.
77. M. Egholm, L. Christensen, K. L. Dueholm, O. Buchardt, J. Coull and P. E. Nielsen, *Nucleic Acids Res.*, 1995, **23**, 217-222.

78. P. S. Miller, G. X. Bi, S. A. Kipp, V. Fok and R. K. DeLong, *Nucleic Acids Res.*, 1996, **24**, 730-736.
79. G. Xiang and L. W. McLaughlin, *Tetrahedron*, 1998, **54**, 375-392.
80. D. M. Gowers and K. R. Fox, *Nucleic Acids Res.*, 1997, **25**, 3787-3794.
81. D. A. Rusling, L. Le Strat, V. E. C. Powers, V. J. Broughton-Head, J. Booth, O. Lack, T. Brown and K. R. Fox, *FEBS Letters*, 2005, **579**, 6616-6620.
82. D. A. Rusling, V. E. C. Powers, R. T. Ranasinghe, Y. Wang, S. D. Osborne, T. Brown and K. R. Fox, *Nucleic Acids Res.*, 2005, **33**, 3025-3032.
83. Y. He, P. V. Scaria and R. H. Shafer, *Biopolymers*, 1997, **41**, 431-441.
84. C. A. Mirkin, R. L. Letsinger, R. C. Mucic and J. J. Storhoff, *Nature*, 1996, **382**, 607-609.
85. R. Elghanian, J. J. Storhoff, R. C. Mucic, R. L. Letsinger and C. A. Mirkin, *Science*, 1997, **277**, 1078-1081.
86. R. C. Jin, G. S. Wu, Z. Li, C. A. Mirkin and G. C. Schatz, *J. Am. Chem. Soc.*, 2003, **125**, 1643-1654.
87. L. M. Demers, C. A. Mirkin, R. C. Mucic, R. A. Reynolds, R. L. Letsinger, R. Elghanian and G. Viswanadham, *Anal. Chem.*, 2000, **72**, 5535-5541.
88. J. J. Storhoff, R. Elghanian, R. C. Mucic, C. A. Mirkin and R. L. Letsinger, *J. Am. Chem. Soc.*, 1998, **120**, 1959-1964.
89. J. Xu and S. L. Craig, *J. Am. Chem. Soc.*, 2005, **127**, 13227-13231.
90. C. Chen, W. Wang, J. Ge and X. S. Zhao, *Nucleic Acids Res.*, 2009, **37**, 3756-3765.
91. N. H. Jang, *Bull. Korean Chem. Soc.*, 2002, **23**, 1790-1800.
92. L. M. Demers, M. Östblom, H. Zhang, N. H. Jang, B. Liedberg and C. A. Mirkin, *J. Am. Chem. Soc.*, 2002, **124**, 11248-11249.
93. J. J. Storhoff, R. Elghanian, C. A. Mirkin and R. L. Letsinger, *Langmuir*, 2002, **18**, 6666-6670.
94. W. J. Parak, T. Pellegrino, C. M. Micheel, D. Gerion, S. C. Williams and A. P. Alivisatos, *Nano Lett.*, 2003, **3**, 33-36.
95. S. J. Hurst, A. K. R. Lytton-Jean and C. A. Mirkin, *Anal. Chem.*, 2006, **78**, 8313-8318.
96. Z. Li, R. Jin, C. A. Mirkin and R. L. Letsinger, *Nucleic Acids Res.*, 2002, **30**, 1558-1562.
97. A. R. Herdt, S. M. Drawz, Y. Kang and T. A. Taton, *Colloid. Surface. B*, 2006, **51**, 130-139.
98. R. L. Letsinger, R. Elghanian, G. Viswanadham and C. A. Mirkin, *Bioconjugate Chem.*, 2000, **11**, 289-291.
99. J. A. Dougan, C. Karlsson, W. E. Smith and D. Graham, *Nucleic Acids Res.*, 2007, **35**, 3668-3675.
100. Y. H. Jung, K. B. Lee, Y. G. Kim and I. S. Choi, *Angew. Chem. Int. Edit.*, 2006, **45**, 5960-5963.
101. C. Sönnichsen, B. M. Reinhard, J. Liphardt and A. P. Alivisatos, *Nat. Biotechnol.*, 2005, **23**, 741-745.

102. G. L. Liu, Y. Yin, S. Kunchakarra, B. Mukherjee, D. Gerion, S. D. Jett, D. G. Bear, J. W. Gray, A. P. Alivisatos, L. P. Lee and F. F. Chen, *Nat. Nanotech.*, 2006, **1**, 47-52.
103. P. K. Jain, W. Huang and M. A. El-Sayed, *Nano Lett.*, 2007, **7**, 2080-2088.
104. S. A. Claridge, H. W. Liang, S. R. Basu, J. M. J. Fréchet and A. P. Alivisatos, *Nano Letters*, 2008, **8**, 1202-1206.
105. C. J. Loweth, W. B. Caldwell, X. Peng, A. P. Alivisatos and P. G. Schultz, *Angew. Chem. Int. Edit.*, 1999, **38**, 1808-1812.
106. D. G. Thompson, R. J. Stokes, R. W. Martin, P. J. Lundahl, K. Faulds and D. Graham, *Small*, 2008, **4**, 1054-1057.
107. S. J. Park, A. A. Lazarides, J. J. Storhoff, L. Pesce and C. A. Mirkin, *J. Phys. Chem. B*, 2004, **108**, 12375-12380.
108. S. Y. Park, A. K. R. Lytton-Jean, B. Lee, S. Weigand, G. C. Schatz and C. A. Mirkin, *Nature* 2008, **451**, 553-556.
109. S. Yamakoshi, Y. Sakai, Y. Shinohara, Y. Amemiya, N. Kanayama, T. Takarada, M. Maeda and K. Ito, *Nucl. Acid S.*, 2007, **51**, 335-336.
110. S. E. J. Bell and N. M. S. Sirimuthu, *J. Am. Chem. Soc.*, 2006, **128**, 15580-15581.
111. M. Green, F.-M. Liu, L. Cohen, P. Köllensperger and T. Cass, *Faraday Discuss.*, 2006, **132**, 269 - 280.
112. A. Barhoumi, D. Zhang, F. Tam and N. J. Halas, *J. Am. Chem. Soc.*, 2008, **130**, 5523-5529.
113. M. Procházka, P. Y. Turpin, J. Štěpánek and J. Bok, *J. Mol. Struct.*, 1999, **482-483**, 221-224.
114. G. Breuzard, J. M. Millot, J. F. Riou and M. Manfait, *Anal. Chem.*, 2003, **75**, 4305-4311.
115. D. Graham, W. E. Smith, A. M. T. Linacre, C. H. Munro, N. D. Watson and P. C. White, *Anal. Chem.*, 1997, **69**, 4703-4707.
116. K. Faulds, W. E. Smith and D. Graham, *Anal. Chem.*, 2004, **76**, 412-417.
117. K. Faulds, L. Stewart, W. E. Smith and D. Graham, *Talanta*, 2005, **67**, 667-671.
118. R. J. Stokes, A. Macaskill, P. J. Lundahl, W. E. Smith, K. Faulds and D. Graham, *Small*, 2007, **3**, 1593-1601.
119. M. B. Wabuyele and T. Vo-Dinh, *Anal. Chem.*, 2005, **77**, 7810-7815.
120. T. Vo-Dinh, *IEEE J. Sel. Top. Quant.*, 2008, **14**, 198-205.
121. K. Faulds, L. Fruk, D. C. Robson, D. G. Thompson, A. Enright, W. E. Smith and D. Graham, *Faraday Discuss.*, 2006, **132**, 261 - 268.
122. A. MacAskill, D. Crawford, D. Graham and K. Faulds, *Anal. Chem.*, 2009, **81**, 8134-8140.
123. D. Graham, D. G. Thompson, W. E. Smith and K. Faulds, *Nat. Nanotech.*, 2008, **3**, 548 - 551
124. X. Qian, X. Zhou and S. Nie, *J. Am. Chem. Soc.*, 2008, **130**, 14934-14935.
125. K. Lee and J. Irudayaraj, *J. Phys. Chem. C*, 2009, **113**, 5980-5983.
126. R. J. Stokes, A. Macaskill, J. A. Dougan, P. G. Hargreaves, H. M. Stanford, W. E. Smith, K. Faulds and D. Graham, *Chem. Commun.*, 2007, 2811-2813.
127. Y. W. C. Cao, R. Jin and C. A. Mirkin, *Science*, 2002, **297**, 1536-1540.

128. D. Graham, B. J. Mallinder, D. Whitcombe, N. D. Watson and W. E. Smith, *Anal. Chem.*, 2002, **74**, 1069-1074.
129. K. Faulds, R. Jarvis, W. E. Smith, D. Graham and R. Goodacre, *Analyst*, 2008, **133**, 1505-1512.
130. H. S. Mandal and H.-B. Kraatz, *J. Am. Chem. Soc.*, 2007, **129**, 6356-6357.
131. A. A. Vertegel, R. W. Siegel and J. S. Dordick, *Langmuir*, 2004, **20**, 6800-6807.
132. M.-E. Aubin-Tam and K. Hamad-Schifferli, *Langmuir*, 2005, **21**, 12080-12084.
133. M.-E. Aubin-Tam, H. Zhou and K. Hamad-Schifferli, *Soft Matter*, 2008, **4**, 554-559.
134. C. Palocci, L. Chronopoulou, I. Venditti, E. Cernia, M. Diociaiuti, I. Fratoddi and M. V. Russo, *Biomacromolecules*, 2007, **8**, 3047-3053.
135. W. D. Geoghegan and G. A. Ackerman, *J. Histochem. Cytochem.*, 1977, **25**, 1187-1200.
136. J. Y. Chang, H. Wu, H. Chen, Y. C. Ling and W. Tan, *Chem. Commun.*, 2005, 1092-1094.
137. C. Yu and J. Irudayaraj, *Anal. Chem.*, 2007, **79**, 572-579.
138. P. Nednoor, M. Capaccio, V. G. Gavalas, M. S. Meier, J. E. Anthony and L. G. Bachas, *Bioconjugate Chem.*, 2004, **15**, 12-15.
139. J. M. Abad, S. F. L. Mertens, M. Pita, V. M. Fernandez and D. J. Schiffrin, *J. Am. Chem. Soc.*, 2005, **127**, 5689-5694.
140. J. F. Hainfeld, W. Liu, C. M. R. Halsey, P. Freimuth and R. D. Powell, *J. Struct. Biol.*, 1999, **127**, 185-198.
141. M. Zheng, Z. Li and X. Huang, *Langmuir*, 2004, **20**, 4226-4235.
142. T. Kawano, Y. Niidome, Y. Katayama and T. Niidome, *Mol. Ther.*, 2005, **11**, S84.
143. T. Niidome, M. Yamagata, Y. Okamoto, Y. Akiyama, H. Takahashi, T. Kawano, Y. Katayama and Y. Niidome, *J. Control. Release*, 2006, **114**, 343-347.
144. M.-E. Aubin, D. G. Morales and K. Hamad-Schifferli, *Nano Letters*, 2005, **5**, 519-522.
145. K. Aslan, C. C. Luhrs and V. H. Pérez-Luna, *J. Phys. Chem. B*, 2004, **108**, 15631-15639.
146. A. Gole and C. J. Murphy, *Langmuir*, 2005, **21**, 10756-10762.
147. Z. Wang, R. Levy, D. G. Fernig and M. Brust, *J. Am. Chem. Soc.*, 2006, **128**, 2214-2215.
148. N. T. K. Thanh and Z. Rosenzweig, *Anal. Chem.*, 2002, **74**, 1624-1628.
149. D. S. Grubisha, R. J. Lipert, H.-Y. Park, J. Driskell and M. D. Porter, *Anal. Chem.*, 2003, **75**, 5936-5943.
150. S. Xu, X. Ji, W. Xu, X. Li, L. Wang, Y. Bai, B. Zhao and Y. Ozakic, *Analyst*, 2004, **129**, 63-68.
151. X. X. Han, L. J. Cai, J. Guo, C. X. Wang, W. D. Ruan, W. Y. Han, W. Q. Xu, B. Zhao and Y. Ozaki, *Anal. Chem.*, 2008, **80**, 3020-3024.
152. S. Ali, J. Magdalena, S. Jennie, J. P. Robinson and I. Joseph, in *J. Biomed. Opt.*, SPIE, 2007, p. 020502.
153. J. Anshup, S. Venkataraman, C. Subramaniam, R. R. Kumar, S. Priya, T. R. S. Kumar, R. V. Omkumar, A. John and T. Pradeep, *Langmuir*, 2005, **21**, 11562-11567.

154. E. E. Connor, J. Mwamuka, A. Gole, C. J. Murphy and M. D. Wyatt, *Small*, 2005, **1**, 325-327.
155. C. M. Goodman, C. D. McCusker, T. Yilmaz and V. M. Rotello, *Bioconjugate Chem.*, 2004, **15**, 897-900.
156. H. K. Patra, S. Banerjee, U. Chaudhuri, P. Lahiri and A. K. Dasgupta, *Nanomed.-Nanotechnol.*, 2007, **3**, 111-119.
157. P. V. AshaRani, G. Low Kah Mun, M. P. Hande and S. Valiyaveetil, *ACS Nano*, 2008, **3**, 279-290.
158. P. Gopinath, S. K. Gogoi, A. Chattopadhyay and S. S. Ghosh, *Nanotechnology* 2008, **19**, 075104.
159. U. Mahmood and R. Weissleder, *Mol. Cancer Ther.*, 2003, **2**, 489-496.
160. K. Kneipp, A. S. Haka, H. Kneipp, K. Badizadegan, N. Yoshizawa, C. Boone, K. E. Shafer-Peltier, J. T. Motz, R. R. Dasari and M. S. Feld, *Appl. Spectrosc.*, 2002, **56**, 150-154.
161. J. Kneipp, H. Kneipp, M. McLaughlin, D. Brown and K. Kneipp, *Nano. Lett.*, 2006, **6**, 2225-2231.
162. H. Morjani, J. F. Riou, I. Nabiev, F. Lavelle and M. Manfait, *Cancer Res.*, 1993, **53**, 4784-4790.
163. I. R. Nabiev, H. Morjani and M. Manfait, *Eur. Biophys. J.*, 1991, **19**, 311-316.
164. J. Kneipp, H. Kneipp, W. L. Rice and K. Kneipp, *Anal. Chem.*, 2005, **77**, 2381-2385.
165. H. W. Tang, X. B. Yang, J. Kirkham and D. A. Smith, *Anal. Chem.*, 2007, **79**, 3646-3653.
166. S. Schlücker, B. Küstner, A. Punge, R. Bonfig, A. Marx and P. Ströbel, *J. Raman Spec.*, 2006, **37**, 719-721.
167. S. Lee, S. Kim, J. Choo, S. Y. Shin, Y. H. Lee, H. Y. Choi, S. H. Ha, K. Kang and C. H. Oh, *Anal. Chem.*, 2007, **79**, 916-922.
168. X. Qian, X. H. Peng, D. O. Ansari, Q. Yin-Goen, G. Z. Chen, D. M. Shin, L. Yang, A. N. Young, M. D. Wang and S. Nie, *Nature Biotechnol.*, 2008, **26**, 83-90.
169. S. Keren, C. Zavaleta, Z. Cheng, A. de la Zerda, O. Gheysens and S. S. Gambhir, *Proc. Natl. Acad. Sci. USA*, 2008, **105**, 5844-5849.
170. G. Frens, *Nature Phys. Sci.*, 1973, **241**, 20-22.
171. J. Yguerabide and E. E. Yguerabide, *Anal. Biochem.*, 1998, **262**, 137-156.
172. F. McKenzie, A. Ingram, R. J. Stokes and D. Graham, *Analyst*, 2009, **134**, 549-556.
173. S. Uesugi, H. Miyashiro, K.-I. Tomita and M. Ikehara, *Chem. Pharm. Bull.*, 1986, **34**, 51-60.
174. A. Ono and T. Ueda, *Nucleic Acids Res.*, 1987, **15**, 219-232.
175. J. S. Lee, M. L. Woodsworth, L. J. P. Latimer and A. R. Morgan, *Nucleic Acids Res.*, 1984, **12**, 6603-6614.
176. L. E. Xodo, G. Manzini, F. Quadrifoglio, G. A. van der Marel and J. H. van Boom, *Nucleic Acids Res.*, 1991, **19**, 5625-5631.
177. U. Jakobsen, A. C. Simonsen and S. Vogel, *J. Am. Chem. Soc.*, 2008, **130**, 10462-10463.
178. K. M. L. Hertoghs, J. H. Ellis and I. R. Catchpole, *Nucleic Acids Res.*, 2003, **31**, 5817-5830.

179. A. N. Silahatoglu, N. Tommerup and H. Vissing, *Mol. Cell. Probes*, 2003, **17**, 165-169.
180. J. A. Fossella, Y. J. Kim, H. Shih, E. G. Richards and J. R. Fresco, *Nucleic Acids Res.*, 1993, **21**, 4511-4515.
181. J. R. Lakowicz, C. D. Geddes, I. G. Gryczynski, J. M. Malicka, Z. G. Gryczynski, K. Aslan, J. Lukomska, E. Matveeva, J. Zhang, R. Badugu and J. Huang, *J. Fluoresc.*, 2004, **14**, 425-441.
182. T. Nakamura and S. Hayashi, *Jpn J. Appl. Phys.*, 2005, **44**, 6833-6837.
183. S. Nath, S. K. Ghosh, S. Kundu, S. Praharaj, S. Panigrahi and T. Pal, *J. Nanoparticle. Res.*, 2006, **8**, 111-116.
184. B. C. Vidal, T. C. Deivaraj, J. Yang, H.-P. Too, G.-M. Chow, L. M. Gan and J. Y. Lee, *New J. Chem.*, 2005, **29**, 812-816.
185. L. L. Jensen and L. Jensen, *J. Phys. Chem. C*, 2008, **112**, 15697-15703.
186. M. Tsen and L. Sun, *Anal. Chim. Acta*, 1995, **307**, 333-340.
187. Q. Ye, J. Fang and L. Sun, *J. Phys. Chem. B*, 1997, **101**, 8221-8224.
188. W. E. Doering and S. Nie, *Anal. Chem.*, 2003, **75**, 6171-6176.
189. M. Xu and M. J. Dignam, *J. Chem. Phys.*, 1993, **99**, 2307-2321.
190. M. Xu and M. J. Dignam, *J. Chem. Phys.*, 1994, **100**, 197-203.
191. Z. Zhu, T. Zhu and Z. Liu, *Nanotechnology*, 2004, **15**, 357-364.
192. D. Graham, G. McAnally, J. C. Jones and W. E. Smith, *Chem. Commun.*, 1998, 1187-1188.
193. E. J. Zeman and G. C. Schatz, *J. Phys. Chem.*, 1987, **91**, 634-643.
194. F. McKenzie, V. Steven, A. Ingram and D. Graham, *Chem. Commun.*, 2009, 2872-2874.
195. K. Kneipp, A. S. Haka, H. Kneipp, K. Badizadegan, N. Yoshizawa, C. Boone, K. E. Shafer-Peltier, J. T. Motz, R. R. Dasari and M. S. Feld, *Appl. Spectrosc.*, 2002, **56**, 150-154.
196. D. Sehgal and I. K. Vijay, *Anal. Biochem.*, 1994, **218**, 87-91.
197. A. A. Deckert, K. A. Anderson, K. M. Mullaugh and C. Delaney, *J. Phys. Chem. B*, 2004, **108**, 15808-15814.
198. M. A. Gilles, A. Q. Hudson and C. L. Borders, *Anal. Biochem.*, 1990, **184**, 244-248.
199. T. A. Springer, M. L. Dustin, T. K. Kishimoto and S. D. Marlin, *Annu. Rev. Immunol.*, 1987, **5**, 223-252.
200. S. K. Bromley, W. R. Burack, K. G. Johnson, K. Somersalo, T. N. Sims, C. Sumen, M. M. Davis, A. S. Shaw, P. M. Allen and M. L. Dustin, *Annu. Rev. Immunol.*, 2001, **19**, 375-396.
201. D. Davignon, E. Martz, T. Reynolds, K. Kürzinger and T. A. Springer, *P. Natl. Acad. Sci. USA*, 1981, **78**, 4535-4539.
202. D. Casanova, D. Giaume, M. Moreau, J.-L. Martin, T. Gacoin, J.-P. Boilot and A. Alexandrou, *J. Am. Chem. Soc.*, 2007, **129**, 12592-12593.
203. R. J. Stokes, F. McKenzie, E. McFarlane, A. Ricketts, L. Tetley, K. Faulds, J. Alexander and D. Graham, *Analyst*, 2009, **134**, 170-175.
204. F. Granuccia, E. Ferreroc, M. Fotib, D. Aggujarob, K. Vettorettoc and P. Ricciardi-Castagnoli, *Microbes and Infection*, 1999, **1**, 1079-1084.

205. J. Banchereau, F. Bazan, D. Blanchard, F. Brière, J. P. Galizzi, C. van Kooten, Y. J. Liu, F. Rousset and S. Saeland, *Annu. Rev. Immunol.*, 1994, **12**, 881-926.
206. S. Satthaporn and O. Eremin, *J. R. Coll. Surg. Edinb.*, 2001, **46**, 9-19.
207. L. L. Xu, M. K. Warren, W. L. Rose, W. Gong and J. M. Wang, *J. Leukoc. Biol.*, 1996, **60**, 365-371.
208. M. W. Carr, S. J. Roth, E. Luther, S. S. Rose and T. A. Springer, *P. Natl. Acad. Sci. USA*, 1994, **91**, 3652-3656.
209. Y. Zhou, Y. Yang, G. Warr and R. Bravo, *J. Leukoc. Biol.*, 1999, **65**, 265-269.
210. J. Sharma, R. Chhabra, H. Yan and Y. Liu, *Chem. Commun.*, 2007, 477-479.
211. W. Wang, H. Liu, D. Liu, Y. Xu, Y. Yang and D. Zhou, *Langmuir*, 2007, **23**, 11956-11959.

Appendix

A1. Cell Preparation Experimental

Culture of bone marrow derived dendritic cells

Bone marrow derived dendritic cells were obtained from BALB/c mice (10 weeks of age). Briefly, the femurs were flushed with 5 mL of RPMI media (Lonza, Belgium) containing 10% v/v heat inactivated fetal bovine serum (FBS, Sigma Aldrich, Poole, UK), 1% v/v of 2 mM L-glutamine solution, 1% v/v of 100 IU/mL Penicillin-100 mg/mL Streptomycin (PAA Laboratories, GmbH, Austria) and 10% of culture supernatant from X63 myeloma cells transfected with mouse GM-CSF cDNA. The cell suspension was washed and cell concentration adjusted to 5×10^5 cells/mL before culture in 6-well plates (Corning Costar) at 37° C and 5% CO₂. Fresh medium was added to the cell cultures every 3 days generating a large number of CD11c⁺ DC largely free from granulocyte and monocyte contamination. The cells were harvested on day 10 and seeded at 5×10^5 per well in 24 well sterile tissue culture plates (Iwaki, Japan) to which 13 mm round coverslips (Scientific laboratory Supplies Ltd, Nottingham, UK) had previously been added.

In vitro cell culture

Dendritic cells were incubated for 4 hours at 37 °C and 5% CO₂ to allow the cells to adhere to the coverslips before stimulation with lipopolysaccharide (LPS 100 ng/mL, Sigma Aldrich, Poole, UK) for 24 hours. The cells were washed with serum-free RPMI (Lonza, Belgium) and incubated at 37 °C and 5% CO₂ with either the gold anti LFA-1, gold isotype control, or gold anti CD40 conjugates (0.2 nM) for 90 minutes. Following incubation with the nanoparticle conjugates, the cells were washed twice with 1x PBS, pH 7.4 to remove any extracellular nanoparticles before fixation with methanol. The dendritic cells were stained with a 10% w/v aqueous Giemsa solution (BDH, VWR International Ltd, UK) for 20 minutes and washed with PBS before

being allowed to dry and mounted onto labelled microscope slides (using DPX mountant (BDH, VWR International Ltd, UK).

Flow Cytometry

Dendritic cells were stimulated with 100 ng/mL, 200 ng/mL or 400 ng/mL lipopolysaccharide (LPS, Sigma Aldrich, Poole, UK) and incubated at 5% CO₂ and 37 °C for 24 hours. Following incubation, cells were washed in FACS buffer (5% Bovine Serum Albumin, Fraction V, (Sigma Aldrich, Poole, UK) 2 mM EDTA in PBS pH 7.4) for 5 minutes at 500 g. The cells were resuspended in purified rat anti-mouse CD16/CD32 (Fcγ111/11 receptor) monoclonal antibody (BD Biosciences, Oxford, UK) to block non-antigen specific binding of immunoglobulins to F_c receptors. Following 20 minutes incubation, cells were washed as before and stained with PE-labelled anti-LFA-1⁺ (BD Biosciences, Oxford, UK) in FACS buffer in the dark for 60 minutes at 4°C. Cells were washed as before and resuspended in 400 µL of a 10% cell fix solution (BD Biosciences, Oxford, UK) before collecting data on a FACSCanto™ (BD Biosciences, Oxford, UK). Colour compensation was set up using BD™ Compbeads and the antibodies used to stain cells. Cells were gated on forward and side scatter and the FACSDiva™ software used to analyse results.

A2. *t*- Test Calculations from Chapter 6

The SERRS intensities at 724 cm^{-1} from each pixel per cell was summed. The results for cells that had been incubated with anti LFA-1 nanoparticle conjugates and isotype control nanoparticle conjugates are shown in table A1. A *t*-test was performed to ascertain whether the mean SERRS intensity for the anti LFA-1 and isotype control conjugate cells significantly differed. It was necessary to perform an *F*-test first to determine whether the variances were significantly different as this would affect which equation to use for calculating the value of *t*.

cell number	anti LFA-1 intensity sum	isotype control intensity sum
1	931818.6	60341.72
2	121071.3	343153.2
3	346864.5	18106.46
4	248699.1	98372.58
5	400517.6	205911.2
6	1307877	32099.37
7	513745	57203.44
8	143523.6	384686.9
9	1274909	90939.27
10	804936.8	167153.9
11	1370439	360180.9
12	1799885	74501.68
13	206821.4	103052.5
14	3093697	22411.68
15	92160.92	82037.32
16	628814.5	418604.2
17	302606.6	15361.62
18	171771.8	10112.59
19	427425.7	9961.43
20	133033	7386.93
21	330710.9	8637.42
22	477698.6	8508.24
23	110934.8	139340.1
24	342533.3	125201
25	174140.8	437715
total	15756636	3280981
mean	630265.4	131239.2
s.dev.	692741.3	142505.9

Table A1. SERRS intensities from cells that had been incubated with anti LFA-1 and isotype control conjugates

F test H_0 : the population variances are equal

$$F_{calc} = \frac{s_1^2}{s_2^2} = 23.6$$

$$F_{24,24} = 2.27 \text{ (two tailed, 95 \% confidence level)}$$

$$F_{calc} > F_{crit} \therefore H_0 \text{ rejected, variances are not equal}$$

t test H_0 : the population means are equal

$$t_{calc} = \frac{(\bar{x}_1 - \bar{x}_2)}{\sqrt{\frac{s_1^2}{n_1} + \frac{s_2^2}{n_2}}} = 3.53$$

$$26 \text{ degrees of freedom calculated using: } \left\{ \frac{\left(\frac{s_1^2}{n_1} + \frac{s_2^2}{n_2} \right)^2}{\frac{(s_1^2/n_1)^2}{n_1+1} + \frac{(s_2^2/n_2)^2}{n_2+1}} \right\} - 2$$

$$t = 1.71$$

$$t_{calc} > t_{crit} \therefore H_0 \text{ rejected, means are not equal}$$

The results for cells that had been incubated with anti LFA-1 nanoparticle conjugates of which half the population had been stimulated with LPS and the other half had not been stimulated with LPS are shown in table A2. A t-test was performed to ascertain whether the mean SERRS intensity for stimulated and non-stimulated cells significantly differed. It was necessary to perform an F-test first to determine whether the variances were significantly different as this would affect which equation to use for calculating the value of t.

cell number	stimulated intensity sum	non-stimulated intensity sum
1	47826.71	0
2	43648.97	0
3	67523.13	8206.86
4	10200.74	0
5	46031.88	1514.95
6	25060.99	0
7	136573.5	0
8	17628.98	3222.88
9	49811.74	0
10	23015.09	5643.46
11	16353.69	0
12	8333.1	2686.22
13	88198.34	0
14	18752.02	1300.4
15	39941.56	3642.4
16	18700.63	0
17	47248.18	0
18	14903.94	2446.2
19	136948.2	16394.67
20	192098.4	1230.51
21	104340.9	38774.59
22	71036.46	4433.98
23	179380.4	7659.09
24	4182.13	12236.59
25	1333.58	6607.2
total	1409073	116000
mean	56362.93	4640
s.dev.	54318.1	8284.726

Table A2. *SERRS intensities of stimulated and non-stimulated cells*

F test H_0 : the population variances are equal

$$F_{calc} = \frac{s_1^2}{s_2^2} = 42.99$$

$F_{24,24} = 2.27$ (two tailed, 95 % confidence level)

$F_{calc} > F_{crit} \therefore H_0$ rejected, variances are not equal

t test H_0 : the population means are equal

$$t_{calc} = \frac{(\bar{x}_1 - \bar{x}_2)}{\sqrt{\frac{s_1^2}{n_1} + \frac{s_2^2}{n_2}}} = 4.7$$

25 degrees of freedom calculated using: $\left\{ \frac{\left(\frac{s_1^2}{n_1} + \frac{s_2^2}{n_2} \right)^2}{\frac{(s_1^2/n_1)^2}{n_1+1} + \frac{(s_2^2/n_2)^2}{n_2+1}} \right\} - 2$

$$t_{crit} = 1.71$$

$t_{calc} > t_{crit} \therefore H_0$ rejected, means are not equal

DNA Detection

Quantitative Simultaneous Multianalyte Detection of DNA by Dual-Wavelength Surface-Enhanced Resonance Raman Scattering**

Karen Faulds,* Fiona McKenzie, W. Ewen Smith, and Duncan Graham*

Quantitative identification of specific DNA sequences in a mixture without separation and at clinically relevant concentrations is a crucial requirement for the development of more effective and simpler molecular diagnostic assays. By using dual-wavelength surface-enhanced resonance Raman scattering (SERRS), we have developed a quantitative 5-plex DNA-detection system with detection limits of 10^{-12} mol dm⁻³. Five dye-labeled DNA sequences were identified by eye without separation. Calibration graphs are linear, there is no interaction between labels, indicating a high degree of multiplexing is possible. The combination of sensitivity, reliable target detection in solution, and multiple analyte detection without separations provides a new dimension for the development of more effective multiplex analytical methods for targets such as disease identification and toxicological screening.

Many methods exist for the detection of specific DNA sequences and traditionally they have focused on gel electrophoresis or, more recently, quantitative polymerase chain reaction (QPCR) based methodologies involving in situ fluorescence measurements.^[1-3] Although gel electrophoresis is accurate and widely used, it suffers from being a time-consuming and laborious process and still relies on chromatographic separation of different strands. QPCR offers many advantages over gel electrophoresis for sequence identification as most methods use homogeneous closed-tube assays, which offer the ability to detect several sequences simultaneously through deconvolution of the fluorescence emission spectra. Recently we proved that surface-enhanced resonance Raman scattering is a more sensitive technique than fluorescence for DNA-sequence detection by three orders of magnitude when using routinely available laboratory equipment.^[4] To further increase

the attractiveness of SERRS as a technique to be used in molecular biology for DNA analysis, the ability to multiplex has been examined and is reported herein.

SERRS relies on the adsorption of a colored molecule onto a roughened metal surface.^[5,6] In our case we prefer to use silver nanoparticles, as the dye adsorbed on the surface gives a resonance contribution as well as a surface enhancement from the nanoparticle surface-enhanced resonance Raman scattering is produced.^[7] This output is molecularly specific as a result of the vibrational nature of the spectroscopy, and a fingerprint spectrum of the dye label adsorbed on the surface is obtained.^[8] In a previous study we demonstrated how we could exploit the necessity for surface adsorption of specific dyes to measure enzyme activities and specificities.^[9] Excitation of a SERRS label by using a frequency close to that of the absorption maximum of the label has a very significant effect on the scattering efficiencies. Herein we demonstrate how we can exploit the resonance contribution from the label adsorbed on the metal surface to improve the multiplexing capability of SERRS for DNA sequence analysis by using a range of labels with different chromophores and two laser excitation frequencies.

The 5-plex described was carried out by means of five synthetic oligonucleotide probes, each of which incorporated a different dye label at the 5' end. The sequences used corresponded to a range of different targets. FAM, Cy5.5, and

Table 1: DNA sequences used in the multiplex study.

Target	5' Label	Sequence (5'→3') ^[a]	λ_{max} [nm]
universal reverse	FAM	XCX CXC XCT CCA CGT TTT CCC AGT CAC GAC GT	494
HPV	R6G	TGC TTC TAC ACA GTC TCC T	524
<i>E. coli</i> 157 VT2	ROX	GCG TCA TCG TAT ACA CAG GAG CAG	585
universal reverse	BODIPY TR-X	TCC ACG TTT TCC CAG TCA CGA CGT	588
universal reverse	Cy5.5	XCX CXC CXC CXC TCC ACG TTT TCC CAG TCA CGA CGT	683

[a] X = 5-(3-aminopropynyl)-2'-deoxyuridine.

[*] Dr. K. Faulds, F. McKenzie, Prof. W. E. Smith, Prof. D. Graham
Centre for Molecular Nanometrology
WestCHEM
Department of Pure and Applied Chemistry
University of Strathclyde, Glasgow G1 1XL (UK)
Fax: (+44) 141-552-0876
E-mail: Karen.faulds@strath.ac.uk
duncan.graham@strath.ac.uk

[**] This research was supported by the Royal Society of Chemistry Analytical Grand Prix Fellowship, which was awarded to D.G.

Supporting information for this article is available on the WWW under <http://www.angewandte.org> or from the author.

BODIPY TR-X were used to label a universal reverse primer, rhodamine 6G (R6G) was used to label a probe for Human papillomavirus (HPV), and ROX to label a probe to the VT2 gene of *E. coli* 157. The labels were chosen because of their different absorbance maxima (Table 1) and unique SERRS spectra.^[10,11] The DNA sequence has minimal effect on the SERRS, which indicates that these combinations of labels could be used for any 5-plex analysis. Since the FAM label is negatively charged, the oligonucleotide probe was modified to contain four positively charged modified nucleosides, 5-aminopropynyl-2'-deoxyuridine. The positively charged bases

provide a site of attraction for the probes to the negatively charged silver nanoparticles used to provide the surface enhancement.^[12] The probe labeled with Cy5.5 was also modified in a similar manner as this had been shown to improve the detection limits in previous studies.^[11]

To obtain optimal SERRS, spermine was used to neutralize the phosphate backbone of the probes and also aggregate the silver nanoparticles.^[13] The spectra obtained from each of the individual labels with two different laser excitation frequencies are shown in Figure 1. Each label gave a distinctive spectrum, thus allowing the labels to be easily distinguished from each other. However, because of the different absorbance maxima of the dyes, they will not all be in resonance at the same laser excitation frequency and this property can be exploited to produce a very sensitive and selective method for detecting each of these labels within a mixture of the others by using two different laser excitation frequencies. Figure 1a shows the spectra of the five labeled oligonucleotides when an excitation wavelength of 514.5 nm was used. Only three of the dye-labeled oligonucleotides (R6G, FAM, and ROX) gave an intense spectrum at this wavelength, which is because they are in resonance with this wavelength. Figure 1b shows the spectra of the same five dye-labeled oligonucleotides with an excitation wavelength of 632.8 nm. Again, only three of the labels gave an intense spectrum at this wavelength. In this case the labels were Cy5.5, BODIPY TR-X, and, again, ROX. This is because

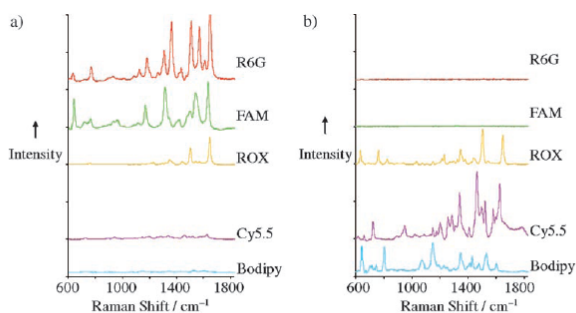


Figure 1. The individual SERRS spectra of each dye-labeled oligonucleotide at a concentration of 1.82×10^{-9} M with excitation at a) 514.5 nm and b) 632.8 nm.

Cy5.5 and BODIPY TR-X are closer to molecular resonance with the 632.8-nm than with the 514.5-nm laser light. ROX could be detected at both excitation wavelengths as, even though its absorbance maximum is at 585 nm, it also has an absorbance peak at around 530 nm which will be in resonance with the 514.5-nm laser light. Thus, it can be easily detected at both excitation wavelengths.

The multiplex spectra obtained at each excitation frequency are shown in Figure 2. Figure 2a shows the multiplex spectrum with 514.5-nm excitation; the two identifying bands from FAM and rhodamine 6G are marked on the spectrum. At 514.5 nm it was impossible to identify a band that was uniquely due to ROX, although a good spectrum was

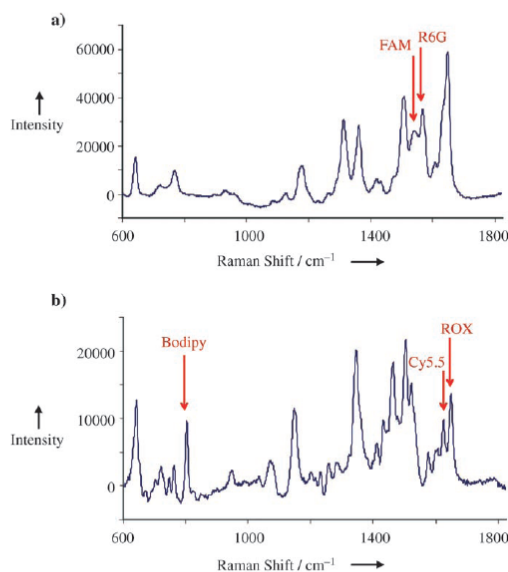


Figure 2. Multiplexed SERRS spectra of the 5-plex at a concentration of 1.82×10^{-9} M and excitation at a) 514.5 nm and b) 632.8 nm.

obtained with this excitation frequency. Figure 2b shows the multiplexed spectrum of the same mixture at 632.8-nm excitation. The identifying bands from ROX, Cy5.5, and BODIPY TR-X are marked on the spectrum. The oligonucleotide mixture was at a concentration of 1.82×10^{-9} M and the identifying bands are listed in Table 2. The bands chosen allowed simple and fast identification of the oligonucleotides in the mixture by looking for the presence of these key marker bands. The bands had sufficiently different Raman shifts to allow this multiplexed identification to be done by eye. Clearly, multiplexing could be increased by use of multivariate analysis.

To prove that this was a quantitative multiplex detection method, a series of dilutions of the mixture of the five oligonucleotides were performed and the detection limits determined (Figure 3). Six dilutions of the multiplex were analyzed; each

Table 2: Limits of detection (L.O.D.) for the oligonucleotides in a multiplex and individual assay.

Label	Band [cm ⁻¹] ^[a]	L.O.D. (multiplex) [M]	L.O.D. (individual) [M]
FAM	1539	2.91×10^{-12}	2.73×10^{-12}
R6G	1568	3.22×10^{-12}	1.17×10^{-12}
ROX	1647	1.25×10^{-11}	3.30×10^{-11}
BODIPY TR-X	802	3.08×10^{-11}	7.85×10^{-12}
Cy5.5	1625	6.70×10^{-12}	5.52×10^{-12}

[a] The single band used for identification of each oligonucleotide.

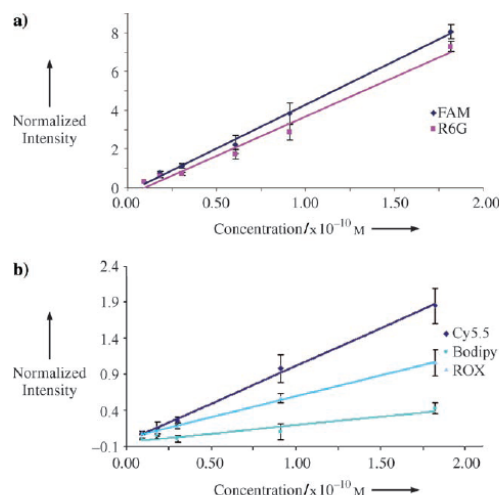


Figure 3. Dilution series of the 5-plex mixture with each dye separately identified. a) 514.5-nm and b) 632.8-nm excitation.

dilution was analyzed five times, and the average was plotted to produce the response shown. Again, two traces are shown for excitation at the two different wavelengths. We found the response to be quantitative for all five oligonucleotides within the multiplexed sampling arrangement. The gradients of the FAM- and R6G-labeled oligonucleotides were almost identical, but the gradients of the labels at 632.8-nm excitation showed differing slopes. This result shows that the sensitivity is different for the three dye-labeled oligonucleotides at this excitation wavelength; however, they could all be detected quantitatively in the mixture. The detection limits obtained for all of the labeled probes in the multiplex are very close to those published previously (Table 2) for SERRS detection of the isolated labeled oligonucleotide probes. This result clearly indicates that there is no reduction in the sensitivity of detection of these probes when used in a 5-plex and shows that through careful choice of the labels and excitation frequencies quantitative multiplexing at ultralow concentrations is possible.

This brief study indicates that it is very simple to multiplex by eye with SERRS by simply choosing the characteristics of

the dye-labeled biomolecule, in this case oligonucleotide probes, to match that of the excitation frequencies. The response is quantitative and highly sensitive and offers significant advantages over available technologies for very sensitive quantitative multiplexed analysis of labeled molecules. This has been demonstrated herein as a proof of principle experiment for oligonucleotides. To transpose this method into a molecular biological assay requires further considerations and is the subject of a current study. Further advancements could involve chemometrics to investigate the multivariate changes in spectral intensities across the whole spectrum, which would obviously be more complicated; the elegance of this approach, however, is that it can be done quite simply by eye.

Received: October 18, 2006
 Published online: January 30, 2007

Keywords: biosensors · DNA · multiplexing · Raman spectroscopy

- [1] S. Tyagi, F. R. Kramer, *Nat. Biotechnol.* **1996**, *14*, 303–308.
- [2] D. Whitcombe, J. Theaker, S. P. Guy, T. Brown, S. Little, *Nat. Biotechnol.* **1999**, *17*, 804–807.
- [3] C. T. Wittwer, M. G. Herrmann, A. A. Moss, R. P. Rasmussen, *Biotechniques* **1997**, *22*, 130–139.
- [4] K. Faulds, R. E. Littleford, D. Graham, G. Dent, W. E. Smith, *Anal. Chem.* **2004**, *76*, 592–598.
- [5] P. Hildebrandt, M. Stockburger, *J. Phys. Chem.* **1984**, *88*, 5935–5944.
- [6] C. Rodger, W. E. Smith, G. Dent, M. Edmondson, *J. Chem. Soc. Dalton Trans.* **1996**, 791–799.
- [7] C. McLaughlin, D. Graham, W. E. Smith, *J. Phys. Chem. B* **2002**, *106*, 5408–5412.
- [8] C. H. Munro, W. E. Smith, P. C. White, *Analyst* **1995**, *120*, 993–1003.
- [9] B. D. Moore, L. Stevenson, A. Watt, S. Flitsch, N. J. Turner, C. Cassidy, D. Graham, *Nat. Biotechnol.* **2004**, *22*, 1133–1138.
- [10] K. Faulds, W. E. Smith, D. Graham, *Anal. Chem.* **2004**, *76*, 412–417.
- [11] K. Faulds, L. Stewart, W. E. Smith, D. Graham, *Talanta* **2005**, *67*, 667–671.
- [12] D. Graham, W. E. Smith, A. M. T. Linacre, C. H. Munro, N. D. Watson, P. C. White, *Anal. Chem.* **1997**, *69*, 4703–4707.
- [13] D. Graham, B. J. Mallinder, W. E. Smith, *Biopolymers* **2000**, *57*, 85–91.

Evaluation of the number of modified bases required for quantitative SERRS from labelled DNA

Karen Faulds,* Fiona McKenzie and Duncan Graham

Received 31st July 2007, Accepted 6th September 2007

First published as an Advance Article on the web 11th September 2007

DOI: 10.1039/b711744b

The optimisation of the modification of DNA to facilitate quantitative detection by surface enhanced resonance Raman scattering (SERRS) detection is reported.

A number of studies have investigated the quantitative nature of the detection of labelled oligonucleotides using surface enhanced resonance Raman scattering (SERRS).^{1–3} Previous studies have shown that the nature of the dye label has a great influence on the SERRS response obtained.⁴ This is due to the requirement of adsorption of a coloured molecule onto a roughened metal surface to provide the maximum surface enhancement and also optimal resonance contribution from the overlap of the electronic transitions of the dye and the excitation frequency used in the scattering experiment. In almost all of the previous studies into the SERRS detection of labelled oligonucleotides silver nanoparticles have been used. Silver nanoparticles are traditionally prepared by the reduction of a silver salt, normally silver nitrate, using a variety of different reducing agents such as sodium borohydride, or sodium citrate.^{5–7} Nanoparticles produced in this way typically have a zeta potential of around -45 mV and as such are highly negatively charged species.⁸ This is due to the surface layer on these nanoparticles which, although not complete, is predominantly negatively charged and as such repels other nanoparticles allowing them to exist in colloidal suspension. In order to attract the species of interest onto the surface of these nanoparticles two approaches can be taken. One is to actively promote chemical adsorption through the formation of a complexing bond to the surface.^{9–11} The other approach is to use the electrostatic attraction between the negatively charged surface and a positively charged analyte.^{1,12}

In the case of DNA there is very little positive charge on either the bases or the backbone due to the hard phosphate anions which dominate this molecule resulting in DNA having an overall negative charge. In addition DNA does not contain an inherent chromophore, therefore the covalent attachment of a dye label can be used to provide a suitable resonance contribution to the commonly used visible excitation. This is directly analogous to the approach used in fluorescence detection. One of the major advantages of SERRS is that the metal surface is a very effective quencher of fluorescence and as such any fluorescent dye can be used as a SERRS label as long as it is efficiently adsorbed onto the metal surface. In terms of DNA detection this means that the extensive fluorescence chemistry which has been developed for

molecular biology over the last 20–30 years can be used for almost all SERRS experiments. Therefore, some of the original SERRS work conducted on oligonucleotides used commercially available fluorophores as a convenient label.¹² These studies found that the chemical nature of these labels had a large impact on the ability of the oligonucleotides to provide SERRS.

The dyes could be broken down into two distinct classes: positively charged dyes and negatively charged dyes. In the case of positively charged dyes it was sufficient to neutralize the phosphate backbone of the DNA through the use of spermine (a naturally occurring polyamine) which would then allow the electrostatic attraction of the species through the positively charged label.¹² In the case of the negatively charged dyes it was found that when spermine was used with the labelled oligonucleotides it was not sufficient to promote effective surface adsorption and this was attributed to the presence of the negatively charged label. In order to overcome this we introduced several modified deoxyuridine nucleosides adjacent to the negatively charged label.¹³ The modified nucleosides consisted of 5-aminopropargyl-2'-deoxyuridine which, after synthesis of the probe and attachment of the label, provided a primary aliphatic amine group which was protonated at physiological pH. This then gave rise to an area of positive charge within the DNA species. When this modified oligonucleotide was mixed with spermine, very efficient and quantitative SERRS could be obtained which was again attributed to the presence of the positively charged bases. To date the only investigation into the variation of the architecture of these probes has been to either have 6 amine modified deoxyuridines or none at all.

This study reports the effect of reducing the overall number of modified bases in the labelled oligonucleotide probe and the effect on the subsequent SERRS signal obtained. Five probes were synthesised with the same DNA sequence and a 5' FAM label. The variation came in the number of propargylamine modified bases on each probe, adjacent to the dye label, as shown in Table 1. Therefore, the difference between 6, 4, 2, 1 and 0 modified bases was assessed to ascertain how many modified bases were required to allow effective surface adsorption of the DNA on the metal surface and give the optimum SERRS signal. To achieve this we analysed each of the five DNA probes by obtaining the SERRS signal of different concentrations of each probe over a range of concentrations spanning 2 orders of magnitude. This allowed the graph of the concentration dependence of the signal of each probe to be obtained, as shown in Fig. 1 (each point is the average of 5 replicate measurements). The graph shows that the data obtained had an approximately linear concentration dependence and it can

Centre for Molecular Nanometrology, Department of Pure and Applied Chemistry, University of Strathclyde, 295 Cathedral Street, Glasgow, UK G1 1XL. E-mail: Karen.faulds@strath.ac.uk; Fax: +44 (0)141 552 0846; Tel: +44 (0)141 548 2507

Table 1 Sequences of bases in the modified oligonucleotides

Number of propargylamines	Sequence 5' → 3' ^a
0	FAM TCC ACG TTT TCC CAG TCA CGA CGT
1	FAM XC TCC ACG TTT TCC CAG TCA CGA CGT
2	FAM XCXC TCC ACG TTT TCC CAG TCA CGA CGT
4	FAM XCXCXCXC TCC ACG TTT TCC CAG TCA CGA CGT
6	FAM XCXCXCXCXCXC TCC ACG TTT TCC CAG TCA CGA CGT

^a X denotes propargylamine modification.

be clearly seen that the intensity of the SERRS signal obtained increases with the number of propargylamine modifications present.

The data can equally be presented in a convenient bar chart form where it becomes clear that the largest signals occur at the higher concentration although there is some signal obtained from the unmodified FAM labelled oligonucleotide (Fig. 2). The small signal which is obtained from the unmodified FAM can be attributed to the neutralisation effect of the spermine aggregating agent on the phosphate backbone of the DNA and the negatively charged label, allowing some of the labelled oligonucleotide to come down on the metal surface and give a signal. However, when propargylamine modified bases are added the signal starts to increase, in fact the addition of only one modified base more than doubles the signal obtained. This increase in signal continues with the addition of a second modified base with the largest increases observed when the probes are modified with 6 or 4 modified bases.

As the concentration is reduced the difference between 6 and 4 modifications remains very similar and as such there is no real need to having 6 modified bases since 4 will give the same analytical response. Indeed, at lower concentrations 2 modified bases were sufficient to generate a very similar response to that obtained from the 4 or 6 modified base oligonucleotides.

The detection limits obtained for each of the labelled oligonucleotides are given in Table 2. It can be seen that improved detection limits were achieved immediately upon the addition of only one propargylamine base, with a 3-fold increase in signal intensity. The detection limit obtained for the addition of 1 or 2 and 4 or 6 propargylamine bases are the same owing to the slope of the calibration lines being the same. However, it can be clearly seen that the increase in signal intensity obtained upon addition of 2 modified bases is the most dramatic, with 5 times the signal intensity of the unmodified probe. Therefore, the addition of 2 propargylamine bases is the preferred modification to achieve the best increase in signal intensity and detection limit offset against the increase in cost associated with the addition of additional bases.

This is a significant finding since the addition of modified bases add complexity and, perhaps more importantly, cost to these types of analytical probes. Reducing the amount of propargylamine modifications on a probe sequence simplifies and significantly lowers the cost of the probe. In order to maximise the multiplexing potential of SERRS a large library of available dyes is required and as such negatively charged dyes are necessary as much as positively charged dyes. Although the amount of required modified bases may vary depending on the dye label used, these results indicate that by reducing the number of modified bases to 2, an improvement in SERRS response is possible and allows much simpler probe design for future SERRS based experiments.

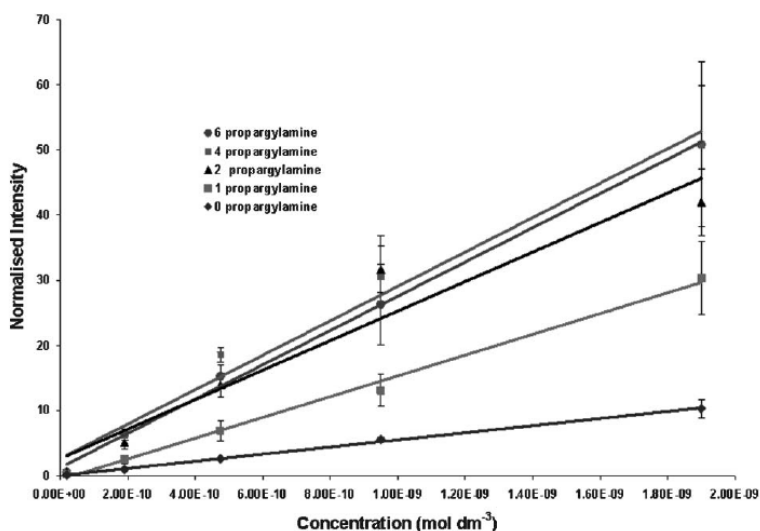


Fig. 1 Concentration dependence of the signal obtained from a FAM labelled oligonucleotide which has been modified with 0, 1, 2, 4 or 6 propargylamine modified bases.

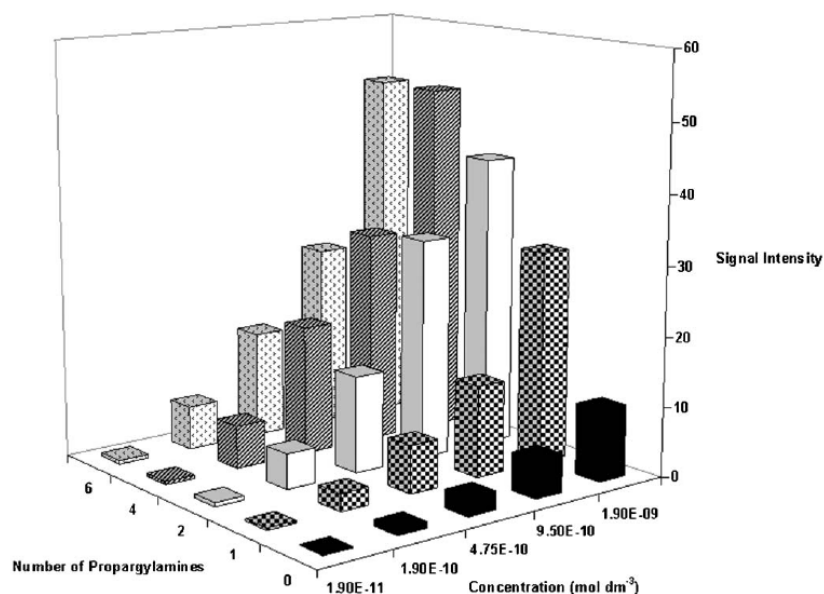


Fig. 2 Concentration dependence of the signal obtained from a FAM labelled oligonucleotide which has been modified with 0, 1, 2, 4 or 6 propargylamine modified bases expressed as a bar chart.

Table 2 Limit of detection of the 5 labelled oligonucleotides

Number of propargylamines	Limit of detection/mol dm ⁻³
0	7.42×10^{-12}
1	1.86×10^{-12}
2	1.86×10^{-12}
4	1.24×10^{-12}
6	1.24×10^{-12}

Notes and references

- 1 K. Faulds, W. E. Smith and D. Graham, *Anal. Chem.*, 2004, **76**, 412.
- 2 K. Faulds, L. Stewart, W. E. Smith and D. Graham, *Talanta*, 2005, **67**, 667.
- 3 R. J. Stokes, A. Macaskill, P. J. Lundahl, W. E. Smith, K. Faulds and D. Graham, *Small*, 2007, **3**(9), 1593.

- 4 D. Cunningham, R. E. Littleford, W. E. Smith, P. J. Lundahl, I. Khan, D. W. McComb, D. Graham and N. Laforest, *Faraday Discuss.*, 2006, **132**, 135.
- 5 P. C. Lee and D. J. Meisel, *J. Phys. Chem.*, 1982, **86**, 3391.
- 6 C. H. Munro, W. E. Smith, M. Garner, J. Clarkson and P. C. White, *Langmuir*, 1995, **11**, 3712.
- 7 K. Cermakova, O. Sestak, P. Matejka, V. Baumruk and B. Vlckova, *Collect. Czech. Chem. Commun.*, 1993, **58**, 2682.
- 8 K. Faulds, R. E. Littleford, D. Graham, G. Dent and W. E. Smith, *Anal. Chem.*, 2004, **76**, 592.
- 9 R. Brown, W. E. Smith and D. Graham, *Tetrahedron Lett.*, 2003, **44**, 1339.
- 10 L. Fruk, A. Grondin, W. E. Smith and D. Graham, *Chem. Commun.*, 2002, 2100.
- 11 D. Graham, L. Fruk and W. E. Smith, *Analyst*, 2003, **128**, 692.
- 12 D. Graham, W. E. Smith, A. M. T. Linacre, C. H. Munro, N. D. Watson and P. C. White, *Anal. Chem.*, 1997, **69**, 4703.
- 13 D. Graham, B. J. Mallinder and W. E. Smith, *Angew. Chem., Int. Ed.*, 2000, **39**, 1061.

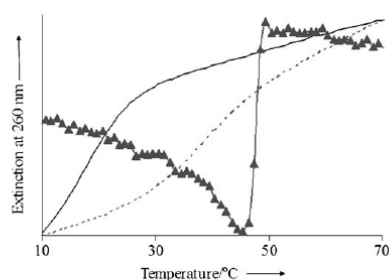


Figure 2. UV melting curve obtained at 260 nm for DNA and LNA chimera duplexes. Solid line: DNA–DNA duplex (A); dotted line: LNA–DNA duplex (B); triangles: nanoparticle-modified LNA/DNA duplex (C).

The presence of the nanoparticles results in the observation of an optical signature associated with the change in plasmon resonance upon hybridization and not due to the hypochromicity of the DNA. As such, it is hard to say whether the nanoparticles are stabilizing the interaction between the oligonucleotides, or whether the LNA is affecting the melting temperature of the gold conjugates after thermal dissociation of the probes from the target DNA has occurred. Mirkin et al. have suggested that an increased dielectric afforded by the nanoparticle probes results in stabilization of the duplex DNA interconnects.^[9] Interestingly, modification of just one LNA probe does not produce an increased thermal stability and melting curves measured at 260 nm produce nonsigmoidal curves with very broad transitions (data not shown). This suggests that if nanoparticles do confer stabilization towards the duplex, it involves interparticle interactions. At this stage, one may assume that together the LNA and coupling nanoparticles offer a synergistic stabilization towards the oligonucleotide conjugates. Melting experiments of analogous DNA probes were conducted to determine if the extent of this synergy was limited to only LNA-gold conjugates, the results of which are shown in Table 1. LNA-functionalization of gold nanoparticles confers an additional 3.2 °C stabilization towards the resultant duplex compared with DNA-functionalized nanoparticles. It appears that the stabilizing effect of localized oligonucleotide concentration on the nanoparticle surface appears to have been enhanced through the use of LNA, leading to a greater stability than expected. This is a significant observation as similar DNA-gold nanoparticle systems do not exhibit such synergistic improvements in stability.

Table 1. A comparison of melting temperatures between Au-conjugated DNA and LNA probes. ΔT_m values for the Au-conjugate duplex are in reference to the unmodified duplex. ΔT_m values for the mismatched sequences are in reference to the Au-conjugate duplex.

	DNA Probes [°C]	ΔT_m [°C]	LNA Probes [°C]	ΔT_m [°C]
Unmodified duplex	19.0		38.5	
Au-conjugate duplex	24.5	5.5	47.2	8.7
Probe-head mismatch	24.2	-0.3	45.1	-2.1
Midprobe mismatch	19.3	-5.2	42.2	-5.0
Probe-tail mismatch	15.3 ^[1]	-9.2	27.1	-20.1

Melting experiments of the LNA probes with noncomplementary DNA were also performed. The target DNA contained single base-pair mismatches at different locations in the sequence (Figure 1). A base-pair mismatch at the probe tail (D), that is, the middle of the target sequence, resulted in the largest difference in melting temperature compared with complementary DNA and a mismatch at the probe head (E) that gave the least difference (Figure 3). DNA containing two base mismatches (one mismatch on each probe) (G) resulted in the lowest melting temperature of all the duplex systems, giving rise to a significant decrease of 28 °C.

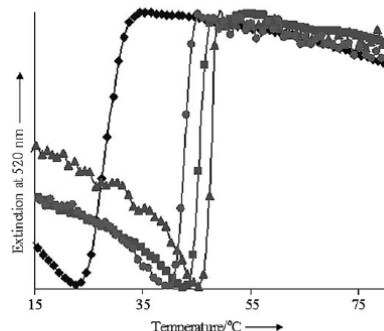


Figure 3. Melting curves obtained at 520 nm for LNA chimera duplexes incorporating single base-pair mismatches. Triangles: complementary DNA target (C); squares: probe-head mismatch (E); circles: midprobe mismatch (F); diamonds: probe-tail mismatch (D).

There are several factors affecting these observed thermal stabilities. Firstly, the base-pair mismatch at the probe tail is between a C–G pair. Due to the increased number of hydrogen bonds between C–G compared to A–T, it is likely that a mismatch between these bases will result in an overall lower melting temperature. The other mismatches (probe head and midprobe) occur between A–T which may partly explain the modest decrease in the complementary strands melting temperature. The location of the base mismatches also has a significant effect since both probe head and midprobe mismatches involve A–T pairing but the midprobe mismatch exhibits an additional 3 °C destabilization. It is possible that this is attributable to partial denaturation of the duplex closest to the nanoparticle even when the bases are complementary, and therefore base substitution in this region will have little effect. It has been suggested that this denaturation is caused by secondary interactions between the oligonucleotide and gold nanoparticle surface,^[10] although it is unlikely that this is the cause of the observed differences in this study since all oligonucleotides contained a polyadenine

linker and incorporated the same probe sequences. A probable rationalization is that the nanoparticle sterically hinders the incoming DNA from targeting the bases in close proximity to the gold surface.^[11] The immense decrease in melting temperature involving target DNA with two base mismatches is likely to be an additive effect of the midprobe and near-end-probe mismatches, one of which occurs between a C–G base-pair.

This pattern of destabilization caused by mismatches in different regions of the sequence is in agreement with duplex systems utilizing DNA-functionalized nanoparticles,^[10,12] although LNA-functionalized nanoparticles exhibit much greater discrimination between complementary and noncomplementary DNA targets, as illustrated by the extensive drop of 20 °C for a probe-tail base-pair mismatch; a mismatch in the analogous DNA probe resulted in less than a 10 °C decrease (Table 1). The LNA conjugates were also superior to the DNA conjugates for probe-head mismatches. A probe-head mismatch for the LNA probes gave rise to a difference in 2.1 °C of the melting temperature, allowing straightforward differentiation from the complementary system, whereas the same probe mismatch in the DNA probes resulted in only a 0.3 °C decrease, which would be difficult to distinguish from a fully complementary duplex.

This is the first report of gold-nanoparticle functionalization with LNA and demonstrates how these conjugates display remarkable binding affinity and selectivity towards DNA, more so than DNA itself. An interesting synergistic effect between the gold and LNA is proposed to explain the increase in stability displayed by these LNA–gold nanoparticle conjugates. The use of LNA/DNA chimeras offers the enhanced stability of duplexes formed using gold-nanoparticle conjugates and offers exquisite discrimination between mismatch and complementary target DNA. This offers a significant improvement over existing DNA–gold nanoparticles and illustrates the immense potential for these nanoconjugates in bioanalytical and diagnostic applications.

Experimental Section

The gold nanoparticles were prepared via citrate reduction of HAuCl₄. The concentration of the gold nanoparticles was increased by centrifugation and resuspension to obtain a final concentration of 37.5 nM. Purified thiol-capped LNA/DNA chimeras with a 20 adenine linker between the thiol group and the DNA sequence (Eurogentec, Belgium) were added to the aqueous nanoparticle suspension (final concentration of oligonucleotide 3 μM). After 24 h, the suspension was brought to 10 mM phosphate (NaH₂PO₄/Na₂HPO₄) by addition of 60 mM pH 7 buffer. Following a further 24 h, the suspension was brought to 0.1 M NaCl by several additions of 2 M NaCl solution over 48 h. The nanoparticles were centrifuged to remove excess oligonucle-

otide and were resuspended in 0.3 M PBS. The final concentration of the LNA/DNA gold conjugates, obtained using UV/Vis spectroscopy, was 10–100 nM. DNA oligonucleotides (ATD Bio, Southampton) conjugated to gold nanoparticles were prepared by an identical method.

Unmodified oligonucleotides were hybridized in a 1:1 ratio (100 nM) in 0.3 M PBS. The nanoparticle-labeled duplex was prepared by mixing the target single-stranded DNA (100 nM) with the two oligonucleotide probes (1 nM) in 0.3 M PBS buffer. The oligonucleotide sequences used are shown in Figure 1. The melting experiments were conducted by monitoring the change in absorbance at 260 nm and 520 nm, using a Varian CaryWin UV/Vis spectrometer.

Keywords:

DNA · gold · hybridization · nanoparticles

- [1] G. Yao, M. S. John, W. Tan, in *Fluorescence Sensors and Biosensors* (Ed.: R. B. Thompson), CRC Press, Boca Raton, FL **2006**, pp. 67–93.
- [2] W. Fritzsche, T. A. Taton, *Nanotechnology* **2003**, *14*, 63–73.
- [3] G. L. Lui, Y. Yin, S. Kunchakarra, B. Mukherjee, D. Gerion, S. D. Jett, D. G. Bear, J. W. Gray, A. P. Alivisatos, L. P. Lee, F. F. Chen, *Nat. Nanotechnol.* **2006**, *1*, 47–52.
- [4] C. Sönnichsen, B. M. Reinhard, J. Liphardt, A. P. Alivisatos, *Nat. Biotechnol.* **2005**, *23*, 741–745.
- [5] a) P. S. Miller, M. P. Reddy, A. Murakami, K. R. Blake, S.-B. Lin, C. H. Agris, *Biochemistry* **1986**, *25*, 5092–5097; b) W. T. Wiesler, M. H. Caruthers, *J. Org. Chem.* **1996**, *61*, 4272–4281; c) S. M. Freier, K.-H. Altmann, *Nucleic Acids Res.* **1997**, *25*, 4429–4443; d) L. Kibler-Herzog, G. Zon, B. Uznanski, G. Whittier, W. D. Wilson, *Nucleic Acids Res.* **1991**, *19*, 2979–2986; e) S. Gryaznov, J.-K. Chen, *J. Am. Chem. Soc.* **1994**, *116*, 3143–3144; f) P. E. Nielsen, *Acc. Chem. Res.* **1999**, *32*, 624–630.
- [6] J. Wengel, *Acc. Chem. Res.* **1999**, *32*, 301–310.
- [7] M. Petersen, C. B. Nielsen, K. E. Nielsen, G. A. Jensen, K. Bondensgaard, S. K. Singh, V. K. Rajwanshi, A. A. Koshkin, B. M. Dahl, J. Wengel, J. P. Jacobsen, *J. Mol. Recognition* **2000**, *13*, 44–53.
- [8] G. T. Walker, *Nucleic Acids Res.* **1988**, *16*, 3091–3099.
- [9] R. Jin, G. Wu, Z. Li, C. A. Mirkin, G. C. Shatz, *J. Am. Chem. Soc.* **2003**, *125*, 1643–1654.
- [10] N. C. Harris, C.-H. Kiang, *J. Phys. Chem. B* **2006**, *110*, 16393–16396.
- [11] L. M. Demers, C. A. Mirkin, R. C. Mucic, R. A. Reynolds, R. L. Letsinger, R. Elghanian, G. Viswanadham, *Anal. Chem.* **2000**, *72*, 5535–5541.
- [12] J. J. Storhoff, R. Elghanian, R. C. Mucic, C. A. Mirkin, R. L. Letsinger, *J. Am. Chem. Soc.* **1998**, *120*, 1959–1964.

Received: March 29, 2007

Revised: August 8, 2007

Published online on October 12, 2007

LNA functionalized gold nanoparticles as probes for double stranded DNA through triplex formation†

Fiona McKenzie, Karen Faulds and Duncan Graham*

Received (in Cambridge, UK) 7th February 2008, Accepted 29th February 2008

First published as an Advance Article on the web 20th March 2008

DOI: 10.1039/b802163e

Nanoparticle modified LNA probes have been used for colorimetric identification of double stranded DNA via parallel triplex formation, eliminating the need for prior denaturation of the target duplex.

Over the last decade there has been a significant amount of research dedicated to the properties and applications of DNA functionalized gold nanoparticles. DNA in the form of synthetic oligonucleotides has been conjugated to the surface of gold nanoparticles and used in a variety of different studies including hybridizations for specific sequences,^{1,2} assembly of 3-dimensional aggregates,^{3,4} immobilization onto surfaces and sensing of protein species via DNA protein interactions.⁵ The protein interactions aside, the majority of these functionalized gold nanoparticles have been used to hybridize to single stranded DNA sequences using Watson Crick base pairing. This has resulted in excellent sensitivity and sequence specificity due to the discriminatory effect of the gold nanoparticles on the ability of the oligonucleotide sequences to hybridise the DNA target. Sharp melting transitions over 2–3 °C have been obtained and in some cases the combination of gold nanoparticles hybridizing to specific DNA sequences coupled with a highly sensitive silver reduction has resulted in detection of DNA without the use of the polymerase chain reaction.⁶

DNA in its natural state is double stranded and as such it is attractive to try and develop methodologies that can detect double stranded DNA and hence do not require denaturation into single strands as is required in most commonly used approaches. Triplex forming oligonucleotides (TFOs) have been reported many times in the literature;^{7–9} however, they have never been reported as conjugated to gold nanoparticles for use in the detection of a specific double stranded DNA sequence. Previous work has used gold nanoparticles conjugated to oligonucleotides to assess the behaviour and stability of DNA triple helices but used as a self complementary loop sequence which was attached to one gold nanoparticle and the triplex forming oligonucleotide attached to another gold nanoparticle.¹⁰ In a similar study, Jung *et al.* reported the use of DNA functionalized gold nanoparticles to examine the proton fuelled reversible assembly of triplex formation.¹¹ Both of these studies used the interaction of the gold nanoparticles

and the resulting change in plasmon resonance when the nanoparticles are pulled closer together on triplex formation. These approaches are not useful for the detection of a specific duplex since they rely on one of the target DNA sequences being modified with gold nanoparticles. In addition, these studies used unmodified DNA and as such required an acidic pH to form the triple helices through the protonation of the deoxycytidine residues. An alternative to using acidic conditions is to replace some of the DNA nucleosides with locked nucleic acids (LNA). Investigations to find the optimum number of LNA nucleotide modifications per oligonucleotide have shown that one modification every 2–3 bases to be ideal.¹² This ratio of LNA to DNA nucleotides yields the greatest thermal stabilities, whereas fully modified LNA oligonucleotides inhibit triplex formation.¹³ Further to this, the 5 position of deoxycytidine can be methylated to increase the p*K*_a and thus promote the protonation potential at neutral pH. This allows the formation of a triple helix at room temperature under normal physiological conditions.^{12–14}

In a recent study, we have demonstrated the ability of LNA functionalized gold nanoparticles to provide excellent sequence selectivity compared to DNA functionalized gold nanoparticles for duplex formation.¹⁵ Here, we report the advancement of that investigation by using the LNA functionalized gold nanoparticles in a split probe arrangement to detect a sequence of duplex DNA through triple helix formation. The LNA functionalized gold nanoparticles were synthesized as previously reported¹⁵ and used 20 adenine spacers onto the surface of the gold nanoparticles, which were calculated to be 13 nm in diameter using TEM measurements. Seferos *et al.* have calculated the number of LNA oligonucleotides for 13 nm gold nanoparticles to be approximately 205 strands per particle.¹⁶ The target chosen for detection was that of the mouse nitric oxide synthase (NOS) gene, where a region of purine residues was located. It should be noted that triplex formation is optimal when there is a polypurine target; however, recent studies have indicated that specially designed base analogues targeted directly against runs of mixed purines and pyrimidines will allow triplex formation from a greater range of sequences,¹⁷ however, as yet these modified nucleosides are not commercially available.

A 14 base target was chosen from the mouse gene and two 7-mer LNA modified probes were synthesized as shown in Fig. 1. Three LNA bases were used per probe and each was synthesized with an alkyl thiol, which was used to immobilise the LNA probes onto the gold nanoparticles. All the deoxycytidine residues were methylated at the 5 position

Centre for Molecular Nanometrology, WestCHEM, 295, Cathedral Street, Glasgow, UK. E-mail: Duncan.Graham@strath.ac.uk; Fax: +44(0)141 552 0876; Tel: +44(0)141 548 4701

† Electronic supplementary information (ESI) available: UV-Vis melting profiles and experimental details. See DOI: 10.1039/b802163e

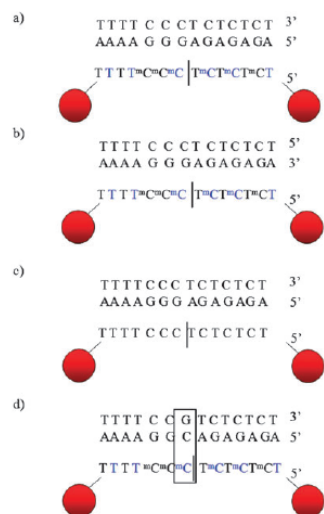


Fig. 1 (a) Nanoparticle-modified parallel LNA oligonucleotide sequences used for triplex formation with double stranded DNA; (b) and (c) control samples incorporating nanoparticle-modified anti-parallel LNA sequences and parallel DNA sequences, respectively; (d) parallel LNA sequences with mismatch target DNA. The boxed region indicates the single base pair mismatch. The linkage between gold nanoparticles and DNA–LNA sequence represents 20 adenine bases. Blue letters denote LNA bases. ^mC represents 5-methyldeoxycytosine.

including those of the DNA to increase protonation and hence triplex formation at physiological pH. Fig. 1a shows the duplex targeted by the triplex forming split probes to form the parallel triplex through the Hoogsteen base pairing bringing the gold nanoparticles into close proximity. Fig. 1b represents the LNA probes mixed with the reverse double stranded DNA sequence. This combination of DNA target sequence and anti-parallel probe sequence is the same as would be used for DNA sequence detection where denaturation is required. Fig. 1c shows analogous DNA nanoparticle probes of parallel sequence to the target duplex.

The visual colour change of the nanoparticles and the corresponding extinction spectra on addition of the double stranded DNA is shown in Fig. 2. DNA addition takes place at room temperature and the samples are not heated and cooled to form the resultant hybrids. Addition of the double stranded DNA to the triplex forming LNA probes clearly shows aggregation of the nanoparticles, illustrated by a red shift in the plasmon resonance peak (Fig. 2a), accompanied by a dramatic colour change from red to purple (Fig. 2b). Melting curves conducted at 520 nm and 260 nm wavelengths (shown in the ESI†) illustrate a melting temperature of 37 °C, which is consistent with the observation of hybridisation-induced aggregation of the nanoparticles at room temperature. Use of analogous DNA probes to hybridise to the target duplex did not result in any nanoparticle aggregation, indicating that the LNA and 5-methyldeoxycytidine modifications are an essential requirement for triplex formation under the conditions used. The LNA probes were also added to a duplex of reverse sequence (Fig. 1b). Probe hybridisation and subsequent

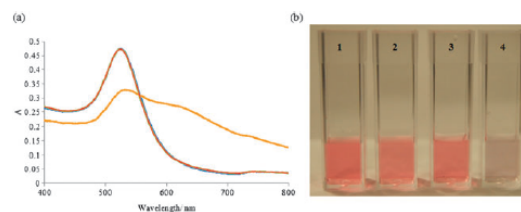


Fig. 2 Extinction spectra (a) and corresponding photograph of nanoparticle probes obtained 1 hour after sample preparation (b). Red line/cuvette 1: LNA probes before double stranded DNA addition; blue line/cuvette 2: DNA probes after double stranded DNA addition (Fig. 1c); green line/cuvette 3: LNA probes after addition of reverse sequence double stranded DNA (Fig. 1b); orange line/cuvette 4: LNA probes after double stranded DNA addition (Fig. 1a).

aggregation of the nanoparticles would only be anticipated if the probes formed an anti-parallel triplex or were able to invade the complementary DNA strands and hybridise to the target strand through Watson Crick base pairing. Nanoparticle aggregation from the sequences shown in Fig. 1b was observed but only after a time period of 24 hours had lapsed. The time limitation associated with using anti-parallel probes emphasises the advantage of using the parallel LNA TFOs for targeting double stranded DNA. Repetition of the experiment using analogous DNA nanoparticle probes (Fig. 1c) did not result in nanoparticle aggregation indicating the hybridisation properties observed are unique to the LNA nanoparticle probes under the conditions used.

The sequence selectivity of the TFO LNA probes was investigated by using target double stranded DNA that incorporated a single base pair mismatch (Fig. 1d). The mismatch target DNA was added at room temperature and the extinction spectrum was monitored, as shown in Fig. 3.

Addition of the complementary target results in complete aggregation of the nanoparticles within 30 minutes, whereas addition of the mismatch target has a negligible effect on the plasmon resonance of the nanoparticle probes within the same time frame. After an hour at room temperature, the mismatch target can clearly be differentiated from the complementary target due to the large colorimetric difference between the two samples (Fig. 4).

In summary the ability of split LNA probes conjugated to nanoparticles to selectively form a triplex and hence target a region of double stranded DNA without denaturation has

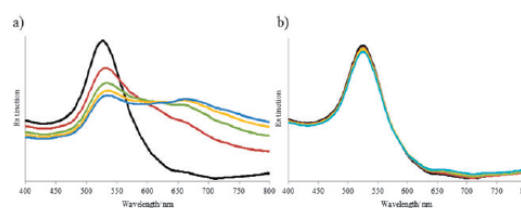


Fig. 3 Extinction spectra of (a) complementary triplex and (b) mismatch triplex monitored over 30 minutes at room temperature. Black line: 0 minutes; red: 6 minutes; green: 12 minutes; orange: 18 minutes; blue: 24 minutes.



Fig. 4 Photograph of nanoparticle probes obtained 1 hour after addition of double stranded DNA. Left cuvette: complementary target; right cuvette: target incorporating a single base pair mismatch.

been demonstrated. This is the first such demonstration to our knowledge and indicates that there is no need to denature double stranded DNA if targeting a polypurine region of the duplex. Use of specialist modified nucleosides will allow this approach to be used to target almost any region of double-stranded DNA and opens up the possibility of a very simple colorimetric indicator of the presence of sufficient quantities of double-stranded DNA in a very sequence specific manner.

Notes and references

1 J. J. Storhoff, R. Elghanian, R. C. Mucic, C. A. Mirkin and R. L. Letsinger, *J. Am. Chem. Soc.*, 1998, **120**, 1959–1964.

- 2 R. Elghanian, J. J. Storhoff, R. C. Mucic, R. L. Letsinger and C. A. Mirkin, *Science*, 1997, **277**, 1078–1081.
- 3 J. J. Storhoff and C. A. Mirkin, *Chem. Rev.*, 1999, **99**, 1849–1862.
- 4 A. P. Alivisatos, K. P. Johnsson, X. G. Peng, T. E. Wilson, C. J. Loweth, M. P. Bruchez and P. G. Schultz, *Nature*, 1996, **382**, 609–611.
- 5 V. Pavlov, Y. Xiao, B. Shlyahovsky and I. Willner, *J. Am. Chem. Soc.*, 2004, **126**, 11768–11769.
- 6 J. J. Storhoff, S. S. Marla, P. Bao, S. Hagenow, H. Mehta, A. Lucas, V. Garimella, T. Patno, W. Buckingham, W. Cork and U. R. Muller, *Biosens. Bioelectron.*, 2004, **19**, 875–883.
- 7 S. Buchini and C. J. Leumann, *Curr. Opin. Chem. Biol.*, 2003, **7**, 717–726.
- 8 D. Prascuth, A. L. Guicysse and C. Helene, *Biochim. Biophys. Acta*, 1999, **1489**, 181–206.
- 9 M. M. Seidman and P. M. Glazer, *J. Clin. Invest.*, 2003, **112**, 487–494.
- 10 D. Murphy, R. Eritja and G. Redmond, *Nucleic Acids Res.*, 2004, **32**, e65.
- 11 Y. H. Jung, K. B. Lee, Y. G. Kim and I. S. Choi, *Angew. Chem., Int. Ed.*, 2006, **45**, 5960–5963.
- 12 H. Torigoe, Y. Hari, M. Sekiguchi, S. Obika and T. Imanishi, *J. Biol. Chem.*, 2001, **276**, 2354–2360.
- 13 S. Obika, T. Uneda, T. Sugimoto, D. Nanbu, T. Minami, T. Doi and T. Imanishi, *Bioorg. Med. Chem.*, 2001, **9**, 1001–1011.
- 14 B. W. Sun, B. R. Babu, M. D. Sorensen, K. Zakrzewska, J. Wengel and J. S. Sun, *Biochemistry*, 2004, **43**, 4160–4169.
- 15 F. McKenzie, K. Faulds and D. Graham, *Small*, 2007, **3**, 1866–1868.
- 16 D. S. Seferos, D. A. Giljohann, N. L. Rosi and C. A. Mirkin, *ChemBioChem*, 2007, **8**, 1230–1232.
- 17 D. A. Rusling, V. E. C. Powers, R. T. Ranasinghe, Y. Wang, S. D. Osborne, T. Brown and K. R. Fox, *Nucleic Acids Res.*, 2005, **33**, 3025–3032.

SERRS coded nanoparticles for biomolecular labelling with wavelength-tunable discrimination†‡

Fiona McKenzie,§ Andrew Ingram,§ Robert Stokes and Duncan Graham*

Received 8th August 2008, Accepted 14th November 2008

First published as an Advance Article on the web 8th December 2008

DOI: 10.1039/b813821d

The preparation and use of tri-functional linkers for surface complexation to both gold and silver nanoparticles is reported. These molecules confer excellent stability towards nanoparticles ensuring particle monodispersity in biological buffers, and also incorporate dyes to allow use of the functionalised nanoparticles as SERRS reporters. Biomolecule conjugation and quantitation has been illustrated using Alexafluor 680 labelled streptavidin. Variation of the chromophore has been introduced, which allows for exquisite control of the SERRS by manipulation of laser wavelength. This demonstrates the potential of SERRS functionalised nanoparticles for multiple, simultaneous monitoring of excitation events, an area of research where the capability of molecular fluorophores and quantum dots is limited.

Introduction

Spectroscopic labels for biological molecules have an essential role in efforts to further understand and explore the complex spatiotemporal interaction of biological entities. Fluorescence labelling techniques are the most widely used,^{1,2} but molecular fluorophores can suffer from photobleaching and relatively broad emission spectra are obtained, potentially limiting the number of species that can be studied simultaneously. Quantum dots are attracting increasing interest,^{3,4} although issues of cellular toxicity remain.^{5,6}

Surface enhanced Raman scattering (SERS) and surface enhanced resonance Raman scattering (SERRS) offer sensitivity equivalent to molecular fluorophores or quantum dots,^{7–9} yet the ability to discriminate multiple analytes in a single mixture is greatly improved due to the information-rich nature of the vibrational spectra. The use of dye reporters in SERRS offers a significant advantage as characteristic bands associated with the chromophore are enhanced over the other materials in the matrix, allowing facile identification. Previously reported examples of this are the coupled N=N modes observed in the spectra of the SERRS azo dyes,^{10,11} and the unique carbonyl modes of the squarylium type reporter.¹² Furthermore, by adjustment of excitation wavelength, multiple components in a mixture can be identified by their wavelength selectivity, thus exploiting the resonance enhancement capability of SERRS.^{13,14}

There are 3 broad classes in which SE(R)RS has been used as an analytical tool for bioanalysis. The molecular SE(R)RS label may be directly attached to the biomolecule followed by addition of the sample to a colloidal solution, commonly gold or silver, and spectroscopic interrogation. This method has been used for quantitative DNA detection,^{15,16} DNA genotyping¹⁷ and molecular sentinels.¹⁸ Alternatively a SE(R)RS active species can be generated *in-situ* by enzymatic action upon an inactive substrate, a technique successfully employed in the detection of lipases,¹⁹ phosphatase²⁰ and peroxidase in conjunction with an immunoassay.²¹ Again this method requires the analyte to be placed in a colloidal suspension prior to analysis, although the reaction can also be performed in colloid.¹⁹

A more elegant approach is to pre-functionalise gold or silver nanoparticles with a reporter molecule incorporating an additional reactive group to enable analyte attachment. A subsequent colloidal addition step is not necessary as all the components for SE(R)RS detection are included in the so-called SE(R)RS tag. Furthermore each functionalised nanoparticle can have multiple reporters, and theoretically greater sensitivity than an analyte labelled with a single Raman reporter. The earliest examples of this concept were by Porter and co-workers,²² who prepared functionalised gold nanoparticles for antibody conjugation by surface complexation of simple non-resonant thiolated molecules, and subsequent co-absorption of antibodies by a mixture of ionic and hydrophobic interactions. Latterly Porter and co-workers have used gold nanoparticles modified with a bis-succinimidyl nitrobenzoic acid disulfide derivative, a non-resonant reporter which also doubles as a means of covalent antibody attachment, in contrast to their earlier non-specific adsorption approach.²³ By this method Porter was able to report femtomolar levels of PSA detection in an immunoassay format. Colloidal stability is a commonly encountered problem, as aggregation or agglomeration can occur upon surface complexation, or changes in ionic strength of the colloidal medium. To overcome this, a number of encapsulation strategies have been explored. Natan and co-workers employed a glass encapsulation

Department of Pure and Applied Chemistry, WestCHEM, University of Strathclyde, Thomas Graham Building, 295 Cathedral Street, Glasgow, UK G1 1XL. E-mail: Duncan.Graham@strath.ac.uk; Fax: +44 (0)141 548 4822; Tel: +44 (0)141 548 4701

† This paper is part of a joint web theme in *Journal of Materials Chemistry* and *Analyst* on Materials for Detection. Guest editor Charles Martin.

‡ Electronic supplementary information (ESI) available: UV-visible spectra of linker materials, and SERRS signal stability of nanoparticle conjugates. See DOI: 10.1039/b813821d

§ These authors contributed equally to this work.

strategy to afford improved stabilisation to the nanoparticles.²⁴ Both gold and silver nanoparticles were tagged with non-resonant reporters, followed by glass encapsulation. This core-shell approach affords particles which are non-aggregating and can be used in a broad range of solvents. Doering and Nie have prepared Raman tagged nanoparticles using a similar core-shell approach.²⁵ In this case, fluorescent dyes were anchored to gold nanoparticles *via* isothiocyanate moieties, followed by silica encapsulation which offers SERRS active particles resistant to agglomeration, stable in a range of organic solvents and with enhancement factors reportedly large enough to facilitate single particle or single molecule detection.

A number of single-step functionalisation procedures have been developed to circumvent the need for a two-step functionalisation then encapsulation strategy, as detailed above. One of which is Raman label-induced controlled aggregation. Su *et al.*²⁶ synthesised gold and silver nanoparticles with concomitant addition of Raman reporter molecules to form controlled aggregates of nanoparticles around the Raman reporters. These pre-formed aggregates were then stabilised by addition of BSA, and can be used for bio-molecular labelling through electrostatic attachment. A second approach by Cormack *et al.*²⁷ incorporated a resonance Raman reporter, which doubled as a surface seeking group, into a styrene/maleic anhydride copolymer backbone, thus providing a Raman reporter, surface complexing group and polymer encapsulation for stability in one macromolecule. These nanoparticle macromolecule conjugates had enhanced stability to salt-induced aggregation, and successful conjugation to oligonucleotide *via* activated carboxyl groups on the macromolecule surface was demonstrated.

Progression from *in-vitro* to *in-vivo* imaging using functionalised gold nanoparticles has been recently demonstrated by Nie and co-workers.²⁸ Nie used organic dyes conjugated to gold nanoparticles as Raman reporters, with thiolated poly(ethylene glycol) subsequently added to stabilise the conjugate. The authors noted that the thiolated PEG did not displace the dye molecules, but improved nanoparticle stability to the extent that the particles remained stable in very harsh conditions including 0.1 M HCl or 0.1 M NaOH. When conjugated to tumour targeting antibodies, the nanoparticles were able to selectively bind to EGF receptors in human cancer cells.

This paper reports the synthesis of two tri-functional SERRS labels containing dyes of variable excitation wavelengths. These linkers can be used to form SERRS functionalised gold or silver nanoparticles which are stable without an additional polymer shell being added and exploit the extra sensitivity of resonance Raman spectroscopy. They remain monodisperse in solution, providing detectable SERRS in this monodisperse state, and also upon surface immobilisation.

Experimental

Chemical synthesis

¹H, ¹³C NMR were recorded on a Bruker DPX 400 spectrometer with the appropriate solvent peak as a reference. *J* values are quoted in Hertz. Elemental analyses were performed as a University service using a Perkin-Elmer 240 elemental analyser. High resolution mass spectra were obtained from the EPSRC mass spectrometry service, Swansea.

3-[2-(2-(2-[6-*tert*-Butoxycarbonylamino-2-(9H-fluoren-9-ylmethoxycarbonylamino)-hexanoylamino]-ethoxy)-ethoxy)-ethoxy]-propionic acid *tert*-butyl ester 2. *N_α*-Fmoc-*N_ε*-Boc-L-lysine (1.000 g, 2.1 mmol), and *tert*-butyl-12-amino-4,7,10-trioxadodecanoate (0.580 g, 2.1 mmol) were dissolved in DCM (10 mL). *N,N*-Dicyclohexylcarbodiimide (0.480 g, 2.3 mmol) was added, and the reaction mixture left to stir for 18 h at room temperature. Dicyclohexylurea precipitate was removed by filtration, the filtrate was collected and the solvent removed at reduced pressure. The residue was purified by silica gel chromatography, eluting with 40% ethyl acetate in petroleum ether, increasing to 90% ethyl acetate to afford the title compound as a sticky gum (1.208 g, 78%); (Found: C, 64.5; H, 8.1; N, 5.5. C₃₉H₅₇N₃O₁₀ requires C, 64.4; H, 7.9; N, 5.8%); δ_H(400 MHz; CDCl₃) 1.25 (2H, m, CH₂), 1.39 (9H, s, 3 × CH₃) 1.39 (9H, s, 3 × CH₃), 1.67–1.85 (4H, m), 2.49 (2H, t, *J* 6.5, CH₂), 3.10 (2H, br, CH₂), 3.4–3.8 (14H, m), 4.15 (1H, m, CH), 4.20 (1H, t, *J* 6.8, CH), 4.40 (2H, t, *J* 6.8, CH₂), 4.7 (1H, br, NH), 5.60 (1H, br, NH), 6.65 (1H, br, NH), 7.32 (2H, dd, *J* 7.4, 7.4, ArH), 7.41 (2H, dd, *J* 7.4, 7.4, ArH), 7.61 (2H, d, *J* 7.3, ArH), 7.77 (2H, d, *J* 7.5, ArH); δ_C(100 MHz; CDCl₃) 22.5, 24.9, 25.6, 28.1, 28.1, 28.4, 28.4, 28.4, 33.8, 36.2, 39.3, 47.2, 54.9, 66.8, 66.9, 69.5, 69.6, 70.3, 70.4, 70.5, 80.6, 81.0, 125.1, 125.1, 127.1, 127.1, 127.1, 127.1, 127.7, 127.7, 127.7, 141.2, 141.3, 143.8, 143.8; *m/z* 728.4117 [M + H]⁺. C₃₉H₅₈N₃O₁₀ requires 728.4121).

3-[2-(2-(2-[6-*tert*-Butoxycarbonylamino-2-(5-1,2-dithiolan-3-ylpentylamino)-hexanoylamino]-ethoxy)-ethoxy)-ethoxy]-propionic acid *tert*-butyl ester 3. Lysine derivative 2 (0.505 g, 1 mmol) was dissolved in acetonitrile (16 mL) and piperidine (4 mL) was then added. The mixture was left to stir at room temperature for 2 h, then piperidine and acetonitrile were removed at reduced pressure. The residue was taken up in DCM (10 mL), and thioctic acid (0.206 g, 1 mmol) and *N,N*-dicyclohexylcarbodiimide (0.225 g, 1.2 mmol) were added, and the reaction mixture left to stir for 18 h at room temperature. Dicyclohexylurea precipitate was removed by filtration, the filtrate was collected and the solvent removed at reduced pressure. The residue was purified by silica gel chromatography, eluting with ethyl acetate, increasing to 10% methanol in ethyl acetate to afford the title compound as a yellow oil (0.410 g, 60%); (Found: C, 52.0; H, 8.5; N, 6.4. C₃₉H₅₇N₃O₁₀ requires C, 52.7; H, 8.1; N, 6.6%); δ_H(400 MHz; CDCl₃) 1.25 (2H, m, CH₂), 1.43 (9H, s, 3 × CH₃), 1.45 (9H, s, 3 × CH₃), 1.5–1.85 (11H, m), 1.9 (1H, m, CH), 2.26 (2H, t, *J* 7.1, CH₂), 2.48 (1H, m, CH), 2.52 (2H, t, *J* 6.5, CH₂), 3.0–3.2 (4H, m, CH), 3.45 (2H, t, *J* 6.9, CH₂), 3.5–3.7 (10H, m), 3.73 (2H, t, *J* 6.5, CH₂), 4.41 (1H, dd, *J* 7.6, 7.4, CH), 4.7 (1H, Br, NH), 6.30 (1H, d, *J* 7.6, CH), 6.65 (1H, t, *J* 5.4, NH); δ_C(100 MHz; CDCl₃) 21.5, 24.3, 27.0, 27.4, 27.4, 27.4, 27.8, 27.8, 27.8, 28.6, 31.4, 33.6, 35.1, 35.1, 35.2, 37.4, 38.2, 39.1, 39.2, 51.8, 55.3, 65.8, 68.5, 69.2, 69.3, 69.4, 69.5, 77.9, 79.6, 155.1, 169.9, 170.8, 171.7; *m/z* 694.3762 [M + H]⁺. C₃₂H₆₀N₃O₉S₂ requires 694.3765).

4-(4-Dimethylamino-naphthalen-1-ylazo)-benzoic acid 4. *para*-Aminobenzoic acid (2.000 g, 14.6 mmol) was dissolved in 50% HCl (5 mL) and cooled to 0 °C. Sodium nitrite (1.209 g, 17.5 mmol) dissolved in 1 mL H₂O was added dropwise to the solution which was left to stir at 0 °C for 30 min. *N,N*-dimethyl-1-aminonaphthalene (2.497 g, 14.6 mmol) was dissolved in sodium

acetate buffer (100 mL, 1 M, pH 6) and methanol (~10 mL) to aid solubility. To this solution the diazotised aminobenzoic acid was added dropwise, at which point a red precipitate was seen to form. The reaction mixture was left to stir overnight at room temperature, then filtration afforded the title compound as a red solid (4.105 g, 90%); (Found: C, 71.1; H, 5.8; N, 13.0. $C_{39}H_{57}N_3O_{10}$ requires C, 71.5; H, 5.4; N, 13.2%; δ_H (400 MHz; DMSO) 2.99 (6H, s, 2 \times CH₃), 7.15 (1H, d, *J* 8.6, ArH), 7.62 (1H, dd, *J* 7.5, 7.5, ArH), 7.69 (1H, dd, *J* 7.5, 7.5, ArH), 7.89 (1H, d, *J* 8.4, ArH), 8.03 (2H, d, *J* 8.4, ArH), 8.13 (2H, d, *J* 8.7, ArH), 8.18 (1H, d, *J* 8.2, ArH), 8.94 (1H, d, *J* 8.3, ArH); δ_C (100 MHz; DMSO) 44.4, 44.4, 112.9, 113.0, 122.4, 123.2, 124.7, 125.5, 127.0, 127.3, 130.6, 132.8, 134.2, 141.3, 155.1, 155.1, 166.8; *m/z* 320.1395 ([M + H]⁺. $C_{19}H_{18}N_3O_2$ requires 320.1394).

3-(2-[2-(2-(2-(5-1,2-Dithiolan-3-yl-pentanoylamino)-6-[4-(4-dimethylamino-naphthalen-1-ylazo)-benzoylamino]-hexanoylamino)-ethoxy]-ethoxy]-ethoxy)-propionic acid 5. 3 (0.693 g, 1 mmol) was dissolved in DCM (3 mL) and cooled to 0 °C. TFA (3 mL) was slowly added, and the reaction mixture allowed to warm to room temperature, and left to stir for 2 h. TFA and DCM were then removed at reduced pressure, and the residue re-suspended in anhydrous DCM and DIPEA (0.5 mL, 3 mmol). A mixture of **4** (0.319 g, 1 mmol), *N*-hydroxysuccinimide (0.115 g, 1 mmol) and *N,N*-dicyclohexylcarbodiimide (0.206 g, 1 mmol) in 10 mL DCM, which had been pre-reacted for 2 h, was then added and the combined mixture left to stir overnight at room temperature. The solvents are then removed at reduced pressure, and the residue purified by column chromatography, eluting with 9 : 1 : 1 DCM, MeOH and AcOH respectively to afford the title compound as a red gum (0.421 g, 49%). (Found: C, 59.7; H, 7.0; N, 10.1. $C_{39}H_{57}N_3O_{10}$ requires C, 59.7; H, 6.8; N, 10.2%; δ_H (400 MHz; CDCl₃) 1.2–1.9 (14H, m), 2.26 (2H, t, *J* 7.6, CH₂), 2.41 (1H, m, CH), 2.5–2.7 (3H, m), 3.0 (6H, s, 2 \times CH₃), 3.09 (1H, m, CH), 3.5–3.7 (14H, m), 4.60 (1H, d, *J* 6.2, CH), 6.89 (1H, d, *J* 8.1, ArH), 7.05–7.08 (2H, m, 2 \times ArH), 7.56 (1H, dd, *J* 7.4, 7.4 ArH), 7.62 (1H, dd, *J* 7.5, 7.5, ArH), 7.89 (1H, d, *J* 8.3, ArH), 8.2–8.3 (2H, m, 2 \times ArH), 8.98 (1H, d, *J* 7.9, ArH); δ_C (100 MHz; CDCl₃) 17.9, 22.7, 25.3, 25.6, 28.7, 30.1, 31.0, 31.5, 32.2, 34.8, 35.7, 39.3, 41.7, 42.1, 44.8, 45.2, 45.2, 52.8, 53.4, 67.0, 69.5, 69.5, 70.0, 70.0, 70.3, 112.8, 113.0, 122.6, 128.0, 158.9, 167.5, 172.9, 174.0, 176.0; *m/z* pending.

3-[2-(2-[2-[6-*tert*-Butoxycarbonylamino-2-(7-[1-ethyl-3,3-dimethyl-1,3-dihydro-benzindolylidene]-hepta-1,3,5-trienyl)-1,1-dimethyl-1*H*-benz[e]indolium-hexanoylamino]-ethoxy)-ethoxy]-ethoxy]-propionic acid *tert*-butyl ester 6. Lysine derivative **2** (0.117 g, 1 mmol) was dissolved in acetonitrile (16 mL) and piperidine (4 mL) was then added. The mixture was left to stir at room temperature for 2 h, then piperidine and acetonitrile were removed at reduced pressure. The residue was taken up in DCM (10 mL), and indocyanine green carboxylate²⁹ (0.100 g, 0.16 mmol) and *N*-(3-dimethylamino-propyl)-*N'*-ethylcarbodiimide hydrochloride (0.062 g, 0.32 mmol) were added, and the reaction mixture left to stir for 18 h at room temperature. The solvent was removed at reduced pressure and the residue was purified by silica gel chromatography, eluting with ethyl acetate, increasing to 5% methanol in DCM to afford the title compound as a green oil (0.110 g, 51%); δ_H (400 MHz; CDCl₃) 1.2–1.4 (6H, m), 1.43 (18H, s, 6 \times CH₃), 1.5–2.0 (19H, m), 2.4–2.6 (6H,

m), 3.12 (2H, t, *J* 6.8, CH₂), 3.4–3.8 (12H, m), 4.1–4.4 (6H, m), 4.43 (2H, d, *J* 8.1, CH₂), 6.15 (1H, d, *J* 13.1, CH), 6.22 (1H, d, *J* 13.2, CH), 6.64 (1H, t, *J* 13.1, CH), 6.74 (1H, t, *J* 12.9, CH), 7.08 (1H, dd, *J* 7.2, 7.2, ArH), 7.22 (1H, d, *J* 8.9, ArH), 7.3–7.5 (3H, m, 3 \times ArH), 7.53 (2H, dd, *J* 7.2, 7.2, 2 \times ArH), 7.6–7.7 (2H, m, 2 \times ArH), 7.8–7.9 (4H, m, 4 \times ArH), 8.05 (2H, dd, *J* 8.4, 3.0, 2 \times ArH); *m/z* 1110.6898 ([M + H]⁺. $C_{67}H_{92}N_5O_9$ requires 1110.6890).

3-(2-[2-(2-(2-(5-1,2-Dithiolan-3-yl-pentanoylamino)-6-[7-[1-ethyl-3,3-dimethyl-1,3-dihydro-benzindolylidene]-hepta-1,3,5-trienyl)-1,1-dimethyl-1*H*-benz[e]indolium]-hexanoylamino)-ethoxy)-ethoxy]-ethoxy)-propionic acid 7. **6** (0.111 g, 0.1 mmol) was dissolved in DCM (3 mL) and cooled to 0 °C. TFA (3 mL) was slowly added, and the reaction mixture allowed to warm to room temperature, and left to stir for 2 h. TFA and DCM were then removed at reduced pressure, and the residue re-suspended in anhydrous DCM and DIPEA (0.05 mL, 0.3 mmol). A mixture of thioctic acid (0.021 g, 0.1 mmol), *N*-hydroxysuccinimide (0.012 g, 0.1 mmol) and *N,N*-dicyclohexylcarbodiimide (0.021 g, 0.1 mmol) in 10 mL DCM, which had been pre-reacted for 2 h, was then added and the combined mixture left to stir overnight at room temperature. The solvents are then removed at reduced pressure, and the residue purified by column chromatography, eluting with 9 : 1 : 1 DCM, MeOH and AcOH respectively to afford the title compound as a red gum (0.051 g, 41%); δ_H (400 MHz; CDCl₃) 1.2–1.9 (24H, m), 1.94 (12H, s, 4 \times CH₃), 2.21 (2H, t, *J* 7.1, CH₂), 2.33 (2H, t, *J* 7.3, CH₂), 2.40 (1H, m), 2.61 (4H, m), 2.9–3.1 (3H, m), 3.2–3.7 (13H, m), 4.1–4.4 (4H, m), 4.37 (1H, d, *J* 6.9, CH₂), 6.13 (1H, d, *J* 13.1, CH), 6.25 (1H, d, *J* 13.2, CH), 6.57 (2H, m, 2 \times CH), 7.08 (1H, dd, *J* 7.2, 7.2, ArH), 7.31 (1H, d, *J* 8.9, ArH), 7.3–7.5 (3H, m, 3 \times ArH), 7.60 (2H, dd, *J* 7.2, 7.2, 2 \times ArH), 7.6–7.7 (2H, m, 2 \times ArH), 7.8–7.9 (4H, m, 4 \times ArH), 8.05 (2H, dd, *J* 8.2, 3.1, 2 \times ArH); *m/z* 1142.6065 ([M + H]⁺. $C_{66}H_{88}N_5O_8S_2$ requires 1142.6069).

Preparation of functionalised nanoparticles

Gold nanoparticles were prepared by the Turkevich method.³⁰ HAuCl₄ was reduced using citrate to afford colloidal gold of approximately 13 nm diameter. To prepare azo dye-gold conjugates, 100 μ L of **5**, 10⁻³ M was added to 1 mL of gold colloid, 4.5 nM. To prepare near-IR gold conjugates, 200 μ L of **7**, 10⁻⁴ M in 60 mM phosphate, pH 8.5 was added. The samples were left to incubate for 4 h then centrifuged for 20 min at 5000 rpm. The supernatant was discarded and the pellet resuspended to 500 μ L in 10 mM phosphate buffer, pH 7.7.

Silver nanoparticles were made by the Lee method.³¹ AgNO₃ was reduced using citrate to afford colloidal silver of approximately 35 nm diameter. To prepare azo dye-silver conjugates, 50 μ L of **5**, 10⁻³ M was added to 1 mL of colloid, 0.4 nM, to prepare near-IR silver conjugates, 100 μ L of **7**, 10⁻⁴ M in 60 mM phosphate, pH 8.5 was added. The samples were left to incubate for 4 h then centrifuged for 20 min at 3500 rpm. The supernatant was discarded and the pellet resuspended to 500 μ L in 10 mM phosphate buffer, pH 7.7.

Bioconjugation protocol

The linker-functionalised nanoparticles were centrifuged to form a pellet and resuspended in 1 mL phosphate buffer, pH 7.6

containing 10 μL EDC (Aldrich), 2 mg mL^{-1} , 10 μL sulfoNHS (Apollo scientific), 2 mg mL^{-1} , and 10 μL streptavidin-Alexafluor 680 conjugate (Aldrich 2 mg mL^{-1}). The reaction mixture was shaken for 16 h. The samples were then centrifuged for 20 min (gold) at 5000 rpm or 10 min at 3500 rpm (silver). The supernatant was discarded and the pellet resuspended to 500 μL in PBS.

Biomolecule quantitation

Bioconjugated nanoparticle concentration was determined by UV-visible spectroscopy (molar extinction coefficients are $2.87 \times 10^{10} \text{ M}^{-1} \text{ cm}^{-1}$ for silver at 400 nm³² and $2.7 \times 10^8 \text{ M}^{-1} \text{ cm}^{-1}$ for gold at 520 nm³³). To ascertain the biomolecule concentration, the conjugate was diluted to 1 mL in 10 mM pH 8.5 phosphate buffer containing DTT to give a final DTT concentration of 250 mM. For gold nanoparticles labelled with 7, the conjugate was diluted to 1 mL in 10 mM pH 7.6 phosphate buffer containing 0.1 mg mL^{-1} trypsin. All samples were left overnight at room temperature and then centrifuged twice at 5000 rpm for 20 min. The supernatants were analysed by fluorescence spectroscopy using 679 nm excitation wavelength. The concentration of streptavidin was determined using a calibration line prepared from standard solutions.

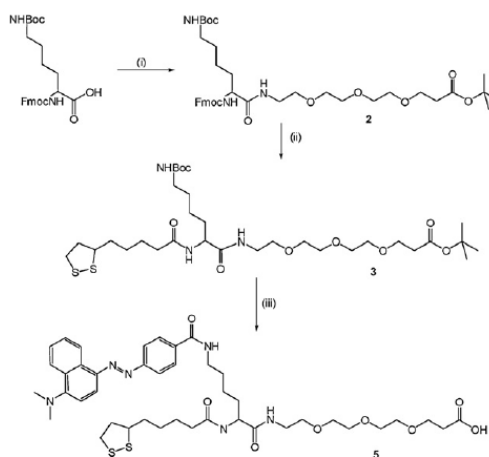
SERRS analysis

Solution-based samples were conjugates diluted in $1 \times \text{PBS}$ to give a concentration of 2 nM gold or 0.2 nM silver. The samples were analysed in microtitre plates using $20\times$ long-working distance objective at various wavelengths. All spectra were baseline corrected using GRAMS software and normalised. Spectra were recorded using the laser excitation sources described below, using 180° backscattering from a 96-well microtitre plate.

SERRS maps were created by deposition of 0.5 μL (10^{-3} M) of each sample (Au-Azo, Ag-Azo, Au-NIR and Ag-NIR) onto a SiO_x substrate. Spectra were collected from map points across the area of the slide in increments of 50 μm using Renishaw InVia Raman inverted and upright microscope systems (Renishaw, Wootton-under-Edge, UK). Four excitation sources were used at 514.5 nm ($\sim 6 \text{ mW}$), 632.8 nm (HeNe, $\sim 30 \text{ mW}$), 785 nm ($\sim 180 \text{ mW}$) and 830 nm (diodes, $\sim 170 \text{ mW}$). Power was attenuated using neutral density filters to that described for each experiment. Line mapping was performed using a Streamline[®] Raman mapping system (Renishaw, UK). SERRS maps were coloured by integrating the area under a single peak that was characteristic for each reporter, at each wavelength.

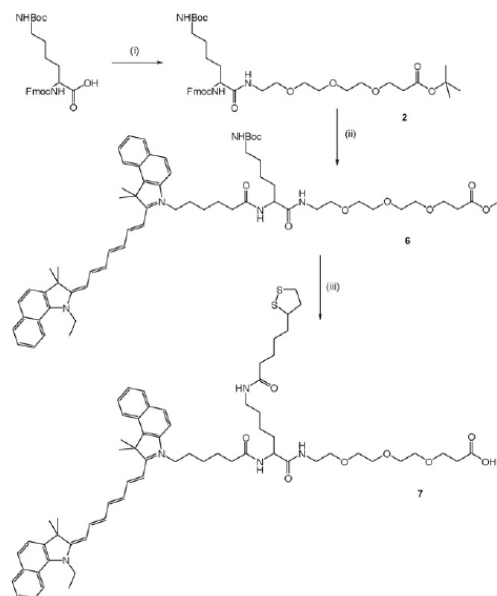
Results and discussion

The SE(R)RS labels were synthesised around a lysine core, so chosen as it has three reactive groups, all of which can be functionalised by adaptation of peptide coupling chemistry. The use of peptide coupling chemistry was advantageous due to the breadth of coupling agents available and well-established protecting group strategies. The reaction, as detailed in Schemes 1 and 2, first required the attachment of a protected oligo(ethylene glycol) which has been reported to reduce non-specific protein adsorption of protein on to nanoparticles³⁴ and to improve



Scheme 1 Reagents and conditions: (i) *tert*-butyl-12-amino-4,7,10-trioxadodecanoate, DCC; (ii) (a) piperidine, (b) thioctic acid, DCC; (iii) (a) 50% TFA/DCM, (b) 4, DCC, DIPEA.

aqueous solubility.³⁵ Thioctic acid was used as a surface complexing group as it has been shown to offer enhanced stability on both gold and silver nanoparticles in comparison to mono-thiols.³⁶ Amidation of thioctic acid can be achieved at either the α or γ nitrogen of lysine as required. Incorporation of a chromophore can then be accomplished at the remaining amine, in



Scheme 2 Reagents and conditions: (i) *tert*-butyl-12-amino-4,7,10-trioxadodecanoate, DCC; (ii) (a) piperidine, (b) indocyanine green,^{29,40} DCC; (iii) (a) 50% TFA/DCM, (b) thioctic acid, DCC, DIPEA.

this case an azo dye for **5**, or a cyanine-based dye for **7**. For this study the dyes were custom made; however, a wide range of amine reactive dyes commonly used for labelling biological entities are commercially available. Conventionally, the nanoparticle surface complexing group of the dye label (or the ability of the dye label to adhere to the nanoparticle surface) should be considered when selecting SERRS reporters, but for these trifunctional linkers, the chromophore will be placed on a ready-made scaffold for nanoparticle adhesion meaning fewer limitations on chromophore selection.

The chromophores in **5** and **7** were chosen to be significantly different in both molecular structure and wavelength at which they absorb light. This is to ensure that discriminable SERRS spectra can be obtained at a single wavelength. Additionally, dyes of varying absorption maxima permit wavelength selectivity of SERRS by exploiting the resonance enhancement effect of Raman scattering. By choosing two dyes of varying wavelength, it was intended that detection of **5** would be facilitated using short-wavelength laser excitation and detection of **7** by long-wavelength laser excitation.

Of further consideration when preparing linker **7** was the possibilities afforded by a dye that absorbs in the near-IR region of the electromagnetic spectrum for *in-vivo* imaging. Spectroscopic analyses can be performed in this region without interferences such as autofluorescence from proteins or heme group absorptions,³⁷ as recently illustrated by Nie and co-workers.²⁸

Spectroscopic characteristics

The solution and surface-based SERRS analysis of the linkers is illustrated in Fig. 1 and 2, respectively. Several trends can be observed in these data. Most apparent is the significantly higher SERRS intensity from the Ag composite materials when compared to the Au equivalents, even with Au nanoparticles present at a ten-fold higher concentration. The reasons for this are well established and include the relative size of the nanoparticles (Au = 13 nm diameter, Ag ≈ 35 nm diameter), and the fact that the surface plasmon electrons are more polarisable at these wavelengths of excitation. In addition the Au particles

perform poorly at 514.5 nm due to the close proximity of inter-band transition in the blue, despite the fact that the surface plasmon resonance maximum (~520 nm) is close in energy to the excitation source.¹⁴

Both materials yield a number of distinct SERRS lines when examined with a range of wavelengths (514.5–830 nm). A typical SERRS analysis reports a number of characteristic resonant vibrational modes that correspond to azo and coupled azo stretching vibrations with deformations of the conjugated ring systems.¹⁹ It is notable that both materials exhibit easily identifiable vibrational modes (that have large scattering cross-sections) in the region 400–900 cm⁻¹. This is a key region in SERRS analysis as it is often considerably less cluttered in terms of background scattering than the equivalent 900–1600 cm⁻¹ spectroscopic region.

The effect of the resonance and vibronic selectivity can also be seen in Fig. 1 and 2. The azo linker **5** ($\lambda_{\text{max}} = 462$ nm) performs very well using 514.5 nm excitation, whilst the optimum performance for the near-IR linker **7** ($\lambda_{\text{max}} = 712$ nm) is found using the 785 nm excitation line. Excitation at 632.8 nm allows identification of both of the dye-labelled linkers (Fig. 2). The superimposed spectra illustrate that the near-IR and azo linker have at least one scattering band that does not coincide with bands from the other linker meaning that at this wavelength, these linkers can be used simultaneously for multiplexing purposes. The wavelength selectivity of the linkers is advantageous as it means that an increased number of dye labels can be used in multiplexed analysis with reduced spectral interference from each other if multiple excitation wavelengths are used. This has been demonstrated by Faulds *et al.* using dye-labelled oligonucleotides.¹³ It should be noted that the spectral profiles of the linkers may differ at other wavelengths due to vibronic selectivity effects. The near-IR linker shows evidence of such across the red and near-IR region. The absorbance spectrum for this material is broad and will comprise a number of potential electronic excited states suitable for resonance enhancement, each possessing its own resonance excitation profile. When the laser wavelength is close to a suitable strongly allowed transition, the corresponding Raman scattering will be enhanced significantly. This is apparent

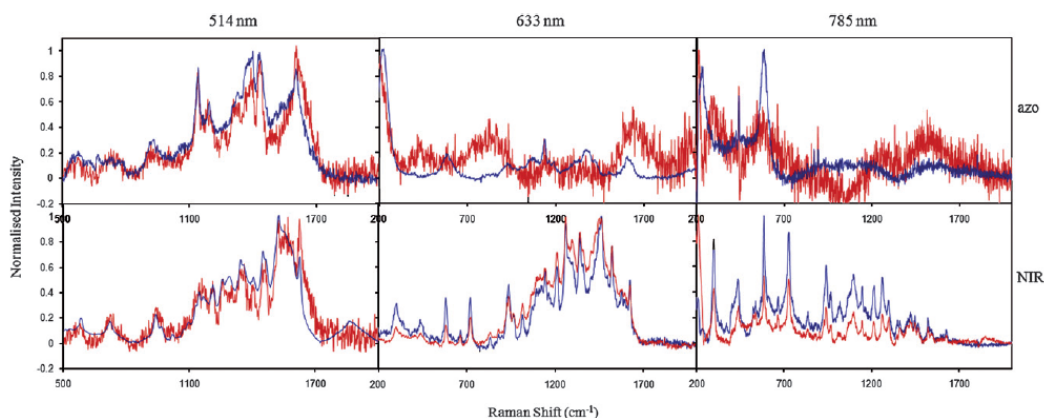


Fig. 1 SERRS spectra of NIR and azo labelled gold (red) and silver (blue) nanoparticles at 514.5, 632.8 and 785 nm.

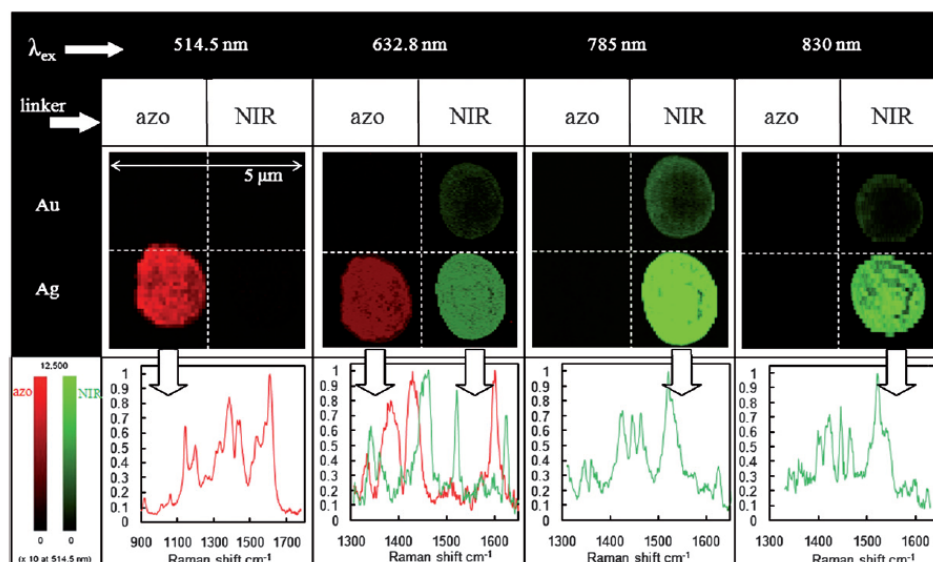


Fig. 2 SERRS intensity maps of 5 (azo) and 7 (NIR) functionalised nanoparticles on SiO_x surfaces at four wavelengths of excitation (λ_{ex}). Sample spots are approximately 1 mm in diameter. [Map step sizes for 632.8, 785 and 830 nm are 50 μm , step size for 514.5 nm is 200 μm .] The intensity of the false colour maps area based on the maximum signal to background based on the integrated area under common SERRS peaks (units are Y-axis/CCD counts under normal gain). Spectra are baseline corrected and normalised for direct comparison.

in the data where the ratios between some peaks vary between wavelengths, e.g. near-IR linker at 632.8 and 785 nm.

It should also be borne in mind that the sensitivity of the detector and grating is not linear with wavelength. For example, the sensitivity of 785 and 830 nm Raman spectroscopy decreases rapidly towards longer wavelengths (also larger Stokes shifts). This effect is apparent when comparing the relative intensities of peaks from these materials (Fig. 2).

The study presented in Fig. 2 is intended to simulate the response from the materials in thin layers in a biosensor array application. The Raman maps were recorded using the minimal exposure times (~ 50 ms per spectrum) that would be required to scan large areas of an array in comparable time to equivalent fluorescent markers. Even at this short accumulation time, the spectral contrast is still sufficiently high to generate false colour maps based on the intensity of the spectral response. It is worth noting that due to the resonance enhancement effect the spectral lines from the reporter are generally enhanced to a greater degree than the surrounding matrix.

Bioconjugation of functionalised nanoparticles

Bioconjugation can be accomplished *via* the carboxylic acid moiety using well-established protocols.³⁸ Separation of the nanoparticle–biomolecule conjugate from excess biomolecule and coupling reagent can be simply achieved by centrifugation. Colloidal material will concentrate to a pellet after centrifugation whereas unreacted biomolecule and coupling agent remain in the supernatant and can thus be removed. The pellet of colloid can then be diluted to a desired concentration using the medium of

choice: not only a useful method of concentrating or diluting samples as desired but also an effective method for buffer exchange. The number of biological molecules conjugated to a nanoparticle will vary depending on the individual species; however, for this study an approximate value for Alexafluor 680 labelled streptavidin was established using a modified protocol developed by Demers *et al.* for quantification of nanoparticle-bound DNA strands.³⁹ The streptavidin was conjugated to the nanoparticle using the method outlined above, followed by DTT-induced surface cleavage of the complex and subsequent quantification of total streptavidin present using fluorimetry (Table 1). By this method it was determined that the average number of streptavidin molecules per nanoparticle was 0.7 when using azo linker 5 with gold and 10.6 with silver. It was not possible to use DTT to displace 7 from gold, presumably due to the stability of the complex. Instead, trypsin was used to hydrolyse the peptide bonds throughout the streptavidin molecule, subsequently releasing the Alexafluor label from the nanoparticle conjugate into the bulk solution. Protein quantitation using this method was estimated to be 0.3 streptavidin molecules per gold nanoparticle. It was possible to displace near-IR linker 7 from silver using DTT, and a determination of 3.6

Table 1 The estimated number of Alexafluor 680 labelled streptavidin molecules per nanoparticle

Au azo	0.7
Ag azo	10.6
Au near-IR	0.3
Ag near-IR	3.6

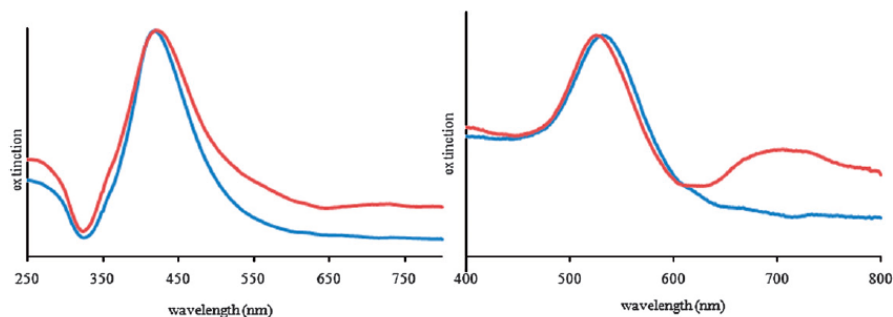


Fig. 3 UV-visible spectra for (left) Ag nanoparticles with 5 (blue) in 0.5 M NaCl, 10 mM phosphate pH 7 and 7 (red) in 0.5 M NaCl, 10 mM phosphate pH 7; (right) Au nanoparticles with 5 (blue) and 7 (red) in 0.5 M NaCl, 10 mM phosphate, pH 7.

protein molecules per nanoparticle was made. The difference between numbers of surface-bound streptavidin on gold and silver nanoparticles is comparable for the near-IR linker and azo linker, which is also comparable with the difference in surface area of 13 nm (gold nanoparticle diameter) and 35 nm (silver nanoparticle diameter) spheres.

Nanoparticle stability

Citrate-reduced nanoparticles were used in this study featuring an average size of 13 nm for gold and 35 nm for silver. Upon complexation to each linker, the nanoparticles retain their monodispersity when viewed in polarised light microscopy. When illuminated using polarised white light and viewed using a crossed analyser the nanoparticles appear to scatter predominantly at the single particle surface plasmon resonance frequency (*i.e.* 520 nm for the gold nanoparticles). The lack of larger slower moving aggregates scattering a significantly greater proportion of light indicates that the particles remain monodisperse after the surface binding has occurred. The linker-functionalised nanoparticles remain in a monodisperse state when placed in $1 \times$ PBS (0.137 M NaCl, 10 mM phosphate, 2.7 mM KCl), meaning that they are stable in conditions necessary for bioconjugation work, and upon bioconjugation are stable in 0.5 M NaCl, 10 mM phosphate, with the exception of near-IR dye-labelled silver nanoparticles which have only been shown to be stable in $1 \times$ PBS (Fig. 3). A second absorption maximum at approximately 700 nm is present in the UV-visible spectrum of nanoparticles labelled with 7, corresponding to the near-IR chromophore. This is more apparent in the gold nanoparticle spectrum as the extinction coefficient of the dye is more comparable with gold nanoparticles than for silver nanoparticles.

The unambiguous SERRS signal for each nanomaterial is stable in solution over several weeks. The SERRS signal is also stable over extended periods of repeated spectral accumulations (*e.g.* 200 s).[‡] In solution, spectra are typically recorded using a $20 \times / 0.4$ objective creating a voxel with an aspect ratio of approximately 3 : 1. The spot diameter is $\sim 0.6 \times$ WL/NA. At 632.8 nm, the laser power with no laser attenuation (20.1 mW) is not sufficient to cause significant photobleaching of the materials over short periods (up to 200 s). Damage from localised heating

(caused by nanoparticle surface plasmon resonance) is also negligible as this energy is lost to the surrounding medium.

Conclusions

The synthesis of novel gold and silver complexing substrates has been accomplished. These substrates confer excellent stability to the nanoparticles, allowing for maintenance of monodispersity in biological media with functionality incorporated for facile conjugation of biological entities. Biomolecular conjugation has been illustrated for streptavidin, and an estimation of biomolecular surface coverage has been made for both silver and gold nanoparticles. By incorporation of dyes into each linker it has been possible to exploit the wavelength dependence of these dyes allowing for simultaneous discrimination of coded nanoparticles. These nanoparticles offer excellent opportunities for use in a wide range of analytical and bioanalytical applications.

References

- 1 A. Castro and J. G. K. Williams, *Anal. Chem.*, 1997, **69**, 3915–3920.
- 2 M. Schena, D. Sharon, R. W. Davis and P. O. Brown, *Science*, 1995, **270**, 467–470.
- 3 M. Bruchez, M. Moronne, P. Gin, S. Weiss and A. P. Alivisatos, *Science*, 1998, **281**, 2013–2016.
- 4 W. C. W. Chan and S. M. Nie, *Science*, 1998, **281**, 2016–2018.
- 5 A. M. Derfus, W. C. W. Chan and S. N. Bhatia, *Nano Lett.*, 2004, **4**, 11–18.
- 6 C. Kirchner, T. Liedl, S. Kudera, T. Pellegrino, A. M. Javier, H. E. Gaub, S. Stolzle, N. Fertig and W. J. Parak, *Nano Lett.*, 2005, **5**, 331–338.
- 7 P. Hildebrandt and M. Stockburger, *J. Phys. Chem.*, 1984, **88**, 5935–5944.
- 8 K. Kneipp, Y. Wang, R. R. Dasari and M. S. Feld, *Appl. Spectrosc.*, 1995, **49**, 780–784.
- 9 K. Kneipp, Y. Wang, H. Kneipp, L. T. Perelman, I. Itzkan, R. Dasari and M. S. Feld, *Phys. Rev. Lett.*, 1997, **78**, 1667–1670.
- 10 D. Graham, C. McLaughlin, G. McAnally, J. C. Jones, P. C. White and W. E. Smith, *Chem. Commun.*, 1998, 1187–1188.
- 11 G. McAnally, C. McLaughlin, R. Brown, D. C. Robson, K. Faulds, D. R. Tackley, W. E. Smith and D. Graham, *Analyst*, 2002, **127**, 838–841.
- 12 R. J. Stokes, A. Ingram, J. Gallagher, D. R. Armstrong, W. E. Smith and D. Graham, *Chem. Commun.*, 2008, 567–569.
- 13 K. Faulds, F. McKenzie, W. E. Smith and D. Graham, *Angew. Chem., Int. Ed.*, 2007, **46**, 1829–1831.
- 14 R. J. Stokes, A. Macaskill, P. J. Lundahl, W. E. Smith, K. Faulds and D. Graham, *Small*, 2007, **3**, 1593–1601.

- 15 D. Graham, W. E. Smith, A. M. T. Linacre, C. H. Munro, N. D. Watson and P. C. White, *Anal. Chem.*, 1997, **69**, 4703–4707.
- 16 K. Faulds, W. E. Smith and D. Graham, *Anal. Chem.*, 2004, **76**, 412–417.
- 17 D. Graham, B. J. Mallinder, D. Whitcombe, N. D. Watson and W. E. Smith, *Anal. Chem.*, 2002, **74**, 1069.
- 18 M. B. Wabuyeale and T. Vo-Dinh, *Anal. Chem.*, 2005, **77**, 7810–7815.
- 19 A. Ingram, R. J. Stokes, J. Redden, K. Gibson, B. Moore, K. Faulds and D. Graham, *Anal. Chem.*, 2007, **79**, 8578–8583.
- 20 C. M. Ruan, W. Wang and B. H. Gu, *Anal. Chem.*, 2006, **78**, 3379–3384.
- 21 X. Dou, T. Takama, Y. Yamaguchi, H. Yamamoto and Y. Ozaki, *Anal. Chem.*, 1997, **69**, 1492–1495.
- 22 J. Ni, R. J. Lipert, G. B. Dawson and M. D. Porter, *Anal. Chem.*, 1999, **71**, 4903–4908.
- 23 D. S. Grubisha, R. J. Lipert, H. Y. Park, J. Driskell and M. D. Porter, *Anal. Chem.*, 2003, **75**, 5936–5943.
- 24 S. P. Mulvaney, M. D. Musick, C. D. Keating and M. J. Natan, *Langmuir*, 2003, **19**, 4784–4790.
- 25 W. E. Doering and S. Nie, *Anal. Chem.*, 2003, **75**, 6171.
- 26 X. Su, J. Zhang, L. Sun, T. Koo, S. Chan, N. Sundararajan, M. Yamakawa and A. Berlin, *Nano Lett.*, 2005, **5**, 49–54.
- 27 P. Cormack, A. Hernandez, R. A. Prasath, F. McKenzie, D. Graham and W. E. Smith, *Chem. Commun.*, 2008, 2517–2519.
- 28 X. M. Qian, X. H. Peng, D. O. Ansari, Q. Yin-Goen, G. Z. Chen, D. M. Shin, L. Yang, A. N. Young, M. D. Wang and S. M. Nie, *Nat. Biotechnol.*, 2008, **26**, 83–90.
- 29 T. Hirata, H. Kogiso, K. Morimoto, S. Miyamoto, H. Taue, S. Sano, N. Muguruma, S. Ito and Y. Nagao, *Bioorg. Med. Chem.*, 1998, **6**, 2179–2184.
- 30 J. Turkevich, P. C. Stevenson and J. Hillier, *Discuss. Faraday Soc.*, 1951, **11**, 55–74.
- 31 P. C. Lee and D. Meisel, *J. Phys. Chem.*, 1982, **86**, 3391–3395.
- 32 J. Yguerabide and E. E. Yguerabide, *Anal. Biochem.*, 1998, **262**, 137–156.
- 33 R. C. Jin, G. S. Wu, Z. Li, C. A. Mirkin and G. C. Schatz, *J. Am. Chem. Soc.*, 2003, **125**, 1643–1654.
- 34 C. Palegrosdemange, E. S. Simon, K. L. Prime and G. M. Whitesides, *J. Am. Chem. Soc.*, 1991, **113**, 12–20.
- 35 W. P. Wueling, S. M. Gross, D. T. Miles and R. W. Murray, *J. Am. Chem. Soc.*, 1998, **120**, 12696–12697.
- 36 J. A. Dougan, C. Karlsson, W. E. Smith and D. Graham, *Nucleic Acids Res.*, 2007, **35**, 3668–3675.
- 37 U. Mahmood and R. Weissleder, *Mol. Cancer Ther.*, 2003, **2**, 489–496.
- 38 G. T. Hermanson, *Bioconjugate Techniques*, Academic Press, London, 1996.
- 39 L. M. Demers, C. A. Mirkin, R. C. Mucic, R. A. Reynolds, R. L. Letsinger, R. Elghanian and G. Viswanadham, *Anal. Chem.*, 2000, **72**, 5535–5541.
- 40 S. Ito, N. Muguruma, Y. Kakehashi, S. Hayashi, S. Okamura, H. Shibata, T. Okahisa, M. Kanamori, S. Shibamura, K. Takesako, M. Nozawa, K. Ishida and M. Shiga, *Bioorg. Med. Chem. Lett.*, 1995, **5**, 2689–2694.

Rapid cell mapping using nanoparticles and SERRS

Robert J. Stokes,^a Fiona McKenzie,^a Emma McFarlane,^b Alastair Ricketts,^a Laurence Tetley,^c Karen Faulds,^a James Alexander^b and Duncan Graham^{*,a}

Received 1st September 2008, Accepted 29th October 2008

First published as an Advance Article on the web 19th November 2008

DOI: 10.1039/b815117b

Bone marrow-derived immune cells (macrophages) treated with gold and silver nanoparticles before fixation and dye staining have been analysed by multiple wavelength line scanning surface enhanced resonance Raman scattering (SERRS) mapping. The method yields high selectivity and sensitivity within short analysis times, identifying nanoparticle aggregates in secondary lysosomes. Using routine cell stains, the output from fluorescence, Raman and SERRS is quantified at four wavelengths of excitation, demonstrating the potential at longer biologically compatible wavelengths of using nanoparticles with cell stains for superior cell mapping.

Introduction

There is a growing need for new methods for cellular analysis that combine high speed with high resolution and sensitivity. The ability of a technique to identify multiple targets within a cell at low concentrations is also highly desirable. Surface enhanced Raman scattering (SERS) is a technique that could offer this and arises when a target molecule is adsorbed onto a suitably roughened metal surface, resulting in an enhancement of the signal intensity (10^5 – 10^6).¹ A significant additional resonance enhancement is observed when the exciting laser line is close to the maximum absorbance of the metal nanoparticle surface plasmon and a suitable vibronic transition of the molecular chromophore. Surface enhanced resonance Raman scattering (sometimes given the distinction 'SERRS') is a highly sensitive spectroscopic technique that is finding an increasing number of applications in biodiagnostics including gene probes^{2,3} and DNA detection.⁴

Recently, Nie and co-workers demonstrated an elegant application of SERS by the *in vivo* targeting of tumour cells in mice.⁵ In this case, nanoparticles with embedded dye labels were functionalised with a single-chain variable-fragment (ScFv) antibody to target the over-expression of epidermal growth factor in malignant cells. Importantly, the same study reports the considerable increase in 'brightness' in the red near-IR window, achieved by using the SERRS method over quantum dots. Spatial resolution of SERS or SERRS from a variety of samples can be performed by using near-field or confocal scanning,⁶ tip-enhanced Raman scattering (TERS),⁷ Raman mapping,⁸ or Raman imaging.⁹ Kneipp *et al.* have previously used SERS as an effective method to probe cellular compartments¹⁰ and to visualise the distribution of the dye indocyanine green.¹¹ Raman

point mapping has recently been shown to be an effective method for the analysis of human osteosarcoma cells using gold nanoparticles and the dye Rhodamine 6G.¹² In this study, we present the application of multiple wavelength fast line scanning SERRS to the analysis of immune system cells treated with staining materials routinely used by life scientists. The use of fast line scanning combined with metallic nanoparticles as the surface for enhancing the Raman scattering produces a highly efficient mapping of cells and reduces the overall collection time for the analysis of a single cell by a factor of 15 compared to single point mapping.

Results and discussion

The cell stains methylene blue and the eosin derivative, known collectively as Giemsa, were selected as the reporter molecules in this study. The cell stain Giemsa was chosen as it comprises two components with similar molar extinction coefficients, methylene blue (MB, $\lambda_{\max} = 660$ nm, $\epsilon \approx 75\,000$ M cm⁻¹) and eosin Y (EY, $\lambda_{\max} = 525$ nm, $\epsilon \approx 112\,000$ M cm⁻¹). MB does not exhibit considerable fluorescence and has a structure suited to Ag and Au surface binding. The fluorescein derivative eosin is fluorescent and has a quantum yield of approx. 0.67. As common materials in cellular and molecular biology with several applications, these dyes are often used as stains to target the phosphate backbone of nucleic acids, particularly in adenine-thymine-rich regions.

A major advantage of the SERRS approach is that the excitation wavelength (λ_{ex}) can be selected anywhere in the optical range. In addition, it has been recently shown how intelligent dye reporter design¹³ and wavelength selectivity¹⁴ can increase the potential for multiple target detection within a mixture. A range of dyes have been reported that are effective at longer wavelengths using both silver and gold nanoparticles as the enhancing substrate.¹⁵ The limits of detection reported in these examples are significantly lower than using conventional fluorescence methods. Although highly sensitive, the optimal λ_{ex} for equivalent quantum dot-based approaches is often in the blue or near-UV, especially if multiple targets are to be analysed. Therefore the use of SERRS and λ_{ex} in the red or near-infra-red (NIR)¹⁶ can

^aCentre for Molecular Nanometrology, WestCHEM, Department of Pure and Applied Chemistry, University of Strathclyde, 295 Cathedral Street, Glasgow, UK G1 1XL. E-mail: duncan.graham@strath.ac.uk; Tel: +44(0)141 548 4701

^bStrathclyde Institute of Pharmacy and Biomedical Sciences, University of Strathclyde, The John Arbuthnot Building, 27 Taylor Street, Glasgow, UK G4 0NR

^cDivision of Infection & Immunity, IBSL, Joseph Black Building, University of Glasgow, Glasgow, UK G12 8QQ

reduce background fluorescence and increase sample depth penetration due to lower background scattering intensity (I_{scat}) since $I_{\text{scat}} \propto 1/\lambda^4$. The red-NIR spectral window (600–1200 nm) is ideal for analysis of real biological samples as the balance between minimal absorbance from haem groups (shorter λ) and water (longer λ IR) is optimal.

Bone marrow-derived murine macrophages¹⁷ were incubated with gold (13 nm) and silver (35 nm) nanoparticles for 2, 4, 6 and 24 hours at 37 °C, 5% CO₂ before being fixed (100% methanol or 4% paraformaldehyde) and stained (Giemsa or only methylene blue). Analysis of the time course by polarized light microscopy indicated that a substantial number of both the silver and the gold nanoparticles had been internalized by endocytosis. This was confirmed by transmission electron microscopy (TEM, shown in Fig. 1). Two hours post-treatment, nanoparticles were identified as having been endocytosed into transparent vacuoles near the macrophage plasma membrane. Furthermore, by this time, nanoparticles were also located within electron-dense vacuoles towards the centre of the cell and often near the nucleus. The darker matrix vacuoles containing nanoparticles are typical of phagosome maturation as a result of lysosome fusion.

The transmission polarized light images shown in Fig. 2(A, A1 and C1) were recorded using polarized white light illumination and an analyzer to view the scattered light from the sample (Eclipse SE2000, Nikon, Japan). The internalized nanoparticles appear coloured in high contrast due to the fact that they scatter light very efficiently at the frequency of the surface plasmon

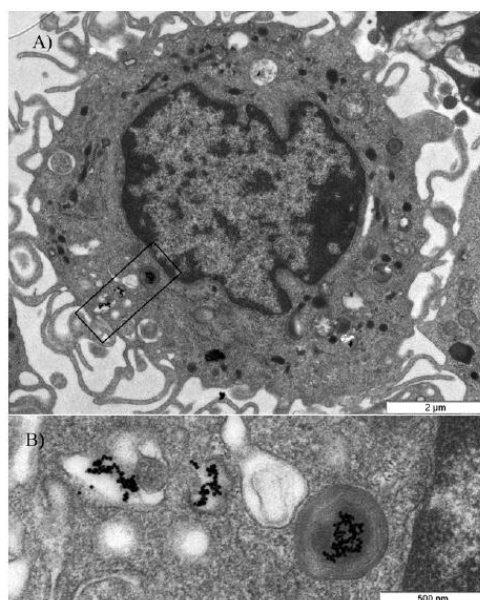


Fig. 1 TEM of macrophage after 2 hours of incubation with gold nanoparticles. (A) Transverse section of a macrophage showing uptake of nanoparticles into vacuoles near the cell surface (transparent matrix) and also in a mature phagosome (darker matrix) near the nucleus in the centre of the cell. (B) Detail is seen in the lower panel, an enlargement of the rectangular area outlined in the upper panel.

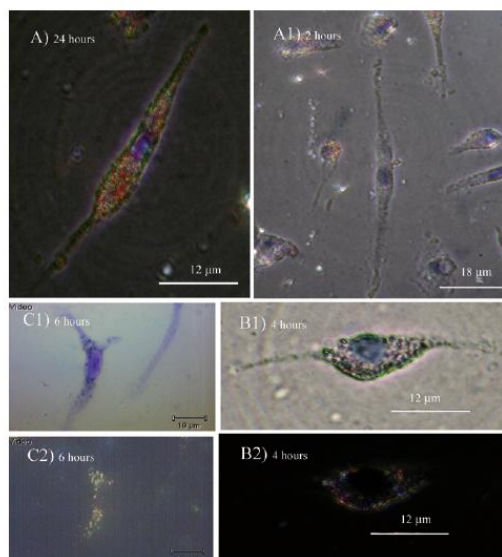


Fig. 2 Nanoparticle time course studies. (A) Transmission polarized light microscope image of a macrophage cell after 24 hours of incubation with citrate-reduced Ag nanoparticles and stained with methylene blue. Areas of colour indicate the presence of nanoparticles scattering the polarized white light at plasmon resonant frequencies. (A1) As (A) except that the incubation time was reduced to 2 hours. (B1) Bright-field image of macrophage cell incubated with silver nanoparticles for 4 hours and stained with Giemsa. (B2) Dark-field image of the same cell as in (B1) recorded with illumination from a masked high NA condenser (0.9). The nanoparticles show up as brightly scattering points in the image. (C1) Macrophage incubated for 6 hours with silver nanoparticles and stained with methylene blue. (C2) Polarized light microscope image of the same cell shown in (C1).

resonance maximum, up to 10^6 – 10^8 times more than an equivalent fluorophore. The dark-field image shown below in Fig. 2(B1) was recorded in the conventional manner using a high NA masked condenser (Leica, Germany). Although this method has less overall light throughput there is significantly less background scattering from the cell walls and other features. Nonetheless, using both contrast methods both Au and Ag nanoparticles were clearly visible within the cytoplasm of the cell. The imaging also indicates that the nanoparticles do not cross the nuclear membrane as this area primarily retains the blue colouration of the stain when viewed in polarized transmission. This distribution was also confirmed by TEM (Fig. 1).

More detailed and sensitive distribution information was obtained by a SERRS analysis of the cells. As the samples contained both nanoparticles and dye labels, strong SERRS spectra could be obtained using suitable combinations of metal nanoparticle, dye λ_{max} and λ_{ex} .¹⁵ The effective combination of these parameters is critical for obtaining the most sensitive results. For example, MB ($\lambda_{\text{max}} = 660$ nm) and Giemsa (MB and eosin, $\lambda_{\text{max}} = 525$ nm) provided strong SERRS spectra from within cells incubated with silver nanoparticles at 514.5, 632.8, 785 and 830 nm λ_{ex} .

Conventional Raman point mapping or scanning provides an efficient means of both spectral acquisition and analysis. The method is information-rich as a complete vibrational spectrum is recorded for each pixel in the map as the focused laser spot is rastered across the sample area. Practically the technique is slow, especially if longer accumulation times are required for low concentration samples. Raman line mapping significantly decreases the time required to record an image by line focusing the laser and recording spectra across the full area of the charge coupled device (CCD). Owing to the high efficiency of the SERRS method, minimal exposure times could be applied, thus recording up to 1000 spectra per minute. An equivalent point mapping experiment using the same exposure time would record approx. 30 spectra per minute. Line mapping is compromised by reduced resolution along the laser line, although this can be traded against Y binning and scanning speed. The application of line mapping has several other distinct advantages. Since the laser is (line) defocused and scanned rapidly across the sample, the power density on any one area of the cell is lessened by a factor of 40–60 times, when compared to an equivalent like-for-like response in scanning confocal or point mapping. This reduces the effect of photobleaching which can be observed in identical point mapping experiments. In addition, the effective accumulation time for each point is increased.

Although Raman mapping data are often presented in two dimensions it is important to consider the fact that the spectra are collected from a three-dimensional voxel. For single point Raman mapping, the minimum spot size (S) is given by the approximation: $S = 0.61 \lambda_{\text{ex}}/\text{NA}$, with the confocal aspect ratio being approximately 3 : 1 in this case. Normally, increasing the confocality by a factor of 5 (high confocality) much of the out-of-focus scattering is rejected but the SERRS throughput is reduced dramatically. The SERRS collection efficiency in line mapping mode at varying focal depths was investigated and is shown below in Fig. 3. The sample cell depth (when sandwiched between coverslips) was measured using z -drive focusing to be approximately 25 μm , with 0 μm being set at the coverslip surface. In

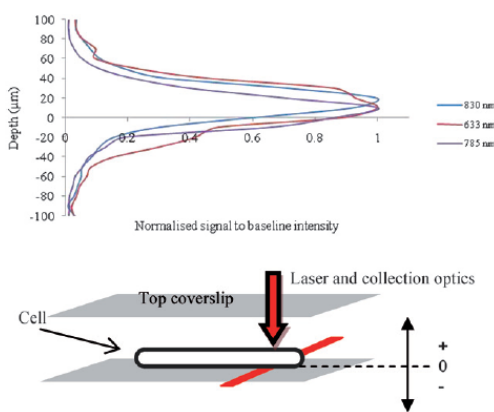


Fig. 3 SERRS signal to focal depth profile through a fixed macrophage cell (cell $z \approx 25 \mu\text{m}$) [100 \times /0.75 objective] and schematic of SERRS collection set-up.

a standard confocal set-up, the majority of the SERRS signal arises from within an area of the cell +5 to +20 μm above the cover slip plane (set as 0 μm). This study confirms our TEM observations illustrating that the majority of the SERRS signals originated from within the cell rather than being concentrated at receptors on the surface.

Examples of SERRS maps obtained from macrophages treated with nanoparticles, fixed, and Giemsa-stained are shown in Fig. 4. The false colour SERRS maps were created by analysis of the spectrum recorded at each pixel. The SERRS intensity was calculated by integrating the area under a known peak in the SERRS spectra of methylene blue or Giemsa (shown in Fig. 4(A)). Control experiments were performed to better understand the strength and distribution of the SERRS signals. Fig. 4(B) shows the mapped fluorescence response from control cells that have been stained using the same procedure but have not been treated with nanoparticles. The fluorescence response of the (predominantly eosin) component was recorded by measuring the absolute intensity at a fixed point in the Stokes region. The fluorescent signal intensity observed was relatively even across the cells examined, with some cells showing significantly higher intensity from the nucleus. Using 632.8 nm λ_{ex} , weak resonance Raman scattering (from the MB component) was detected from the stained control cells with the signal again being concentrated around the nucleus (data not shown).

Analysis of the cells that had been incubated with nanoparticles (NP) revealed that the Raman signals from the MB component of the Giemsa stain were significantly enhanced. In the case of silver nanoparticles at 632.8 nm λ_{ex} , the intensity recorded in some pixels (500 nm width) of the maps increased by up to 20-fold. In addition, the signal intensity in the SERRS maps is no longer evenly distributed throughout the cytoplasm. Instead, the signals follow similar distribution patterns to the Rayleigh scattering observed using polarized and dark-field contrast (Fig. 2) and TEM (Fig. 1), with higher signals from the cytoplasm and relatively little from the nuclei. The relative fluorescence, resonance Raman and SERRS intensities observed in this study are summarised in Table 1. This highlights the effectiveness of SERRS at longer λ_{ex} . The UV/visible extinction of Giemsa, relative to the position of each laser excitation is shown in Fig. 5 below.

The signal-to-background ratio increases with longer λ_{ex} when using silver nanoparticles. This is due to the weaker background contribution from fluorescence and general light scattering in the optical path at longer wavelengths. The resonance contribution for many vibronic states will decay in an approximately Lorentzian fashion as the wavelength of the excitation source is moved away from the optimum. However, the surface enhancement provided by the nanoparticles is available over larger wavelength ranges and at longer wavelengths. This may be due to the presence of aggregates of nanoparticles contained within vesicles as demonstrated by TEM. Larger aggregates are known to afford longer wavelength surface plasmon resonances in addition to stronger electric field gradient junctions between particles. Examination of Fig. 5 and gold nanoparticles were found to be relatively ineffective SERRS substrates in this study using 514.5 nm λ_{ex} due to the proximity of the interband absorbance region. However, we found that using the same dye, gold nanoparticles were highly

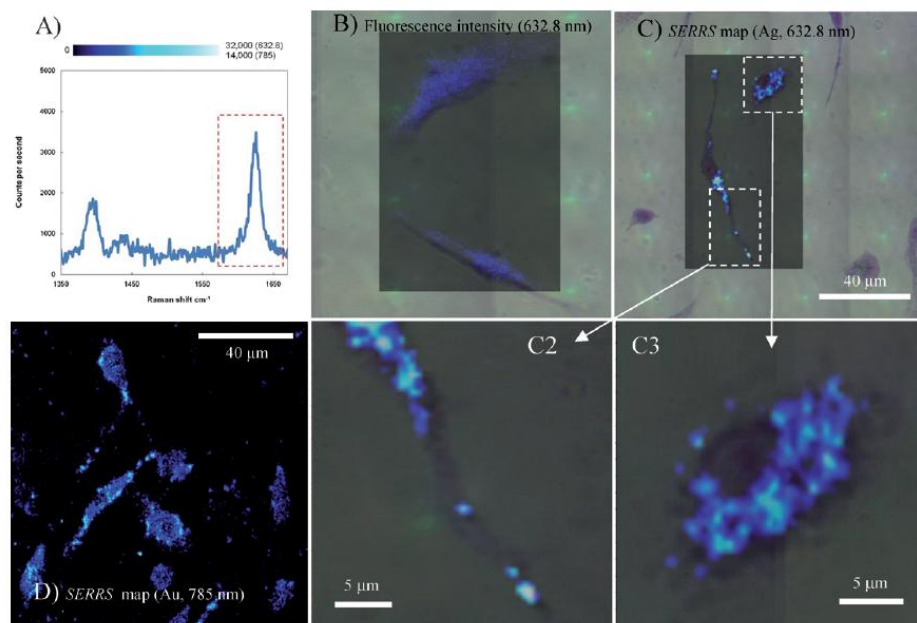


Fig. 4 (A) Individual SERS spectrum from within cells (632.8 nm, 1×1 s, 0.7 mW). This peak is measured relative to the baseline to dictate the intensity of the colour in the SERS maps. (B) Macrophage cell stained with Giemsa, false colour map based on *fluorescence* intensity recorded by spectrometer (632.8 nm λ_{ex}). No nanoparticles were added. (C–C3) Streamline SERS maps over white light image of macrophages recorded after 4 hours of incubation with Ag nanoparticles (Giemsa stain) (632.8 λ_{ex}). (D) Streamline SERS map of macrophages recorded after 4 hours of incubation with Au nanoparticles (Giemsa stain) (785 nm λ_{ex}). Originally recorded at $1000\times$ magnification, the effective accumulation time per pixel is 2 seconds.

Table 1 Relative signal intensities from mapping methods

Method	Control ^a	Ag NP ^b	Au NP ^b
Fluorescence			
λ_{ex} 514.5 nm	4165		
λ_{ex} 632.8 nm	4012		
λ_{ex} 785 nm	833		
λ_{ex} 830 nm	—		
Resonance Raman			
λ_{ex} 514.5 nm	1037		
λ_{ex} 632.8 nm	255		
SERS			
λ_{ex} 514.5 nm ^c		2040	—
SERS			
λ_{ex} 632.8 nm		6426	3366
SERS			
λ_{ex} 785 nm		2635	6613
SERS			
λ_{ex} 830 nm		1037	748

^a Fixed Giemsa-stained cells not exposed to nanoparticles. ^b NB: fluorescence and Raman signals were calculated by different digital analysis methods and cannot be compared directly (see Experimental section). ^c Point mapping only. All others are fast line mapping.

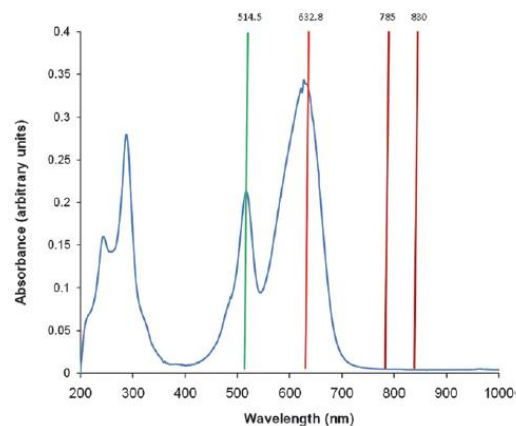


Fig. 5 UV/visible spectrum of Giemsa cell stain showing the relative positions of the laser lines used.

effective at 632.8, 785 and 830 nm λ_{ex} . It was possible to detect low levels of gold nanoparticles in the stained cells after only short accumulation times (2 s effective per pixel, *ca.* 6 min per cell using 500 nm Y step size).

Conclusions

Fast line mapping combined with the high Raman scattering efficiency from areas of the sample where nanoparticles are present results in an efficient, highly sensitive analytical

technique. The further development of this method using biologically functionalised nanoparticles to target activity in cells is in progress and will be reported shortly. More efficient, accurate and sensitive analysis of the biology of cells, such as macrophages, which play significant roles in infectious and inflammatory disease, will create the potential to identify more and better therapeutic targets for disease intervention.

Experimental

Cell culture

Bone marrow-derived macrophages were obtained from BALB/c mice. Briefly, the femurs were flushed with 5 ml of Dulbecco's Modified Eagle Medium (D-MEM; Invitrogen, Paisley, UK) substituted with 10% v/v heat inactivated fetal bovine serum (Sigma Aldrich, Poole, UK), 1% v/v of 2 mM L-glutamine solution, 1% v/v of 100 IU/ml Penicillin-100 µg/ml Streptomycin (PAA Laboratories, GmbH, Austria) and 30% v/v L-cell conditioned media and the resultant cell suspension was incubated at 37 °C and 5% CO₂. The cells were harvested on day 10, suspended in serum-free media (RPMI 1640; Lonza, Belgium) supplemented with 1% v/v of 2 mM L-glutamine solution and 1% v/v of 100 IU/ml Penicillin-100 µg/ml Streptomycin (PAA Laboratories, GmbH, Austria) and seeded at 1×10^4 to 1×10^5 per well in 24-well sterile tissue culture plates (Iwaki, Japan) to which 13 mm round coverslips (Scientific Laboratory Supplies Ltd, Nottingham, UK) had previously been added. Macrophages were incubated overnight at 37 °C and 5% CO₂ to allow the cells to adhere to the coverslips. Macrophages were washed with serum-free media and incubated at 37 °C and 5% CO₂ with gold or silver colloid (used at 1–10 µl/ml) for 2–24 hours. Colloid was prepared by centrifuging 1 ml aliquots of gold or silver at 13 000 rpm for 15 minutes and resuspending the resultant pellet in 500 µl of molecular grade water (Sigma Aldrich, Poole, UK). Following incubation with colloid, the cells were washed twice with $1 \times$ phosphate buffered saline (PBS, pH 7.4) to remove any extracellular colloid before fixation with 4% paraformaldehyde. Macrophages were stained with either methylene blue or a 10% w/v aqueous Giemsa solution (BDH, VWR International Ltd, UK) for 20 minutes and washed with PBS before being allowed to dry and mounted onto labeled slides ($26 \times 76 \times 1.0$ mm microscope slides; Thermo Electron Corporation, Cheshire, UK) using DPX Mountant (BDH, VWR International Ltd, UK).

SERRS Spectroscopy and line mapping

SERRS mapping was performed using Renishaw *InVia* Raman inverted and upright microscope systems (Renishaw, Wotton-under-Edge, UK), equipped with $100\times/0.75$ and $50\times/0.5$ long working distance objectives. Four excitation sources were used at 514.5 nm (ca. 6 mW), 632.8 nm (HeNe, ca. 30 mW), 785 nm (ca. 180 mW) and 830 nm (diodes, ca. 170 mW). Power was attenuated using neutral density filters to that described for each experiment. Line mapping was performed using a Streamline Raman mapping system (Renishaw, UK). The reduction in power density using the line focusing optics was between 40 to 60 times depending on the wavelength of excitation used. SERRS

maps were coloured by integrating the area under single characteristic peaks. Fluorescence intensity is recorded as intensity at a fixed point in the Stokes region normally free from Raman bands (e.g. ca. 1700–1900 cm⁻¹). The detector used at 632.8, 785 and 830 nm was a deep-depletion RenCAM CCD. SERRS intensities were corrected in Table 1 for objective NA and for the wavelength dependent response of the detector and grating using a calibration source. Two gratings were used in the experiments for spectral dispersion. These were 1800 lines/mm (514.5 and 632.8 nm) and 1200 lines/mm (632.8, 785 and 830 nm). The response was normalized using a combination of a white light and neon calibration source. This allowed a direct comparison of the efficiency of the technique at four wavelengths.

Dark-field and polarized light microscopy

Dark-field microscope images were recorded using an inverted microscope equipped with a masked condenser NA = 0.9 (S1; Leica, Germany) and long working distance objectives with appropriate NA values. Polarized light images were recorded using an inverted microscope (Eclipse TE2000, Nikon, Japan) equipped with a polarized xenon arc white light source. The transmitted light was collected using a $\approx 60\times$ objective (Nikon, Japan) and an analyzing polarizer. The total optical magnification in the original images was $900\times$.

Transmission electron microscope imaging

Cells were harvested after nanoparticle incubation, fixed in phosphate buffered 2% glutaraldehyde for 40 mins, followed by aqueous 1% osmium tetroxide and 2% uranyl acetate en bloc staining, dehydration in ethanol and finally embedding in Epon/Araldite resin. After polymerizing at 60 °C for 48 hours, sections were cut and imaged after lead and uranyl staining. Images were recorded on a 2K Proscan CCD on a Zeiss 912 AB energy filtering transmission EM, contrast enhanced using zero-loss imaging mode.

References

- 1 M. Moscovits, *Rev. Mod. Phys.*, 1985, **57**(3), 783.
- 2 T. Vo-Dinh, K. Houck and D. L. Stokes, *Anal. Chem.*, 1994, **66**(20), 3379.
- 3 L. R. Allain and T. Vo-Dinh, *Anal. Chim. Acta*, 2002, **469**, 149.
- 4 Y. C. Cao, R. Jin and C. A. Mirkin, *Science*, 2002, **297**(5586), 1536.
- 5 X. Quian, X.-H. Peng, D. O. Ansari, Q. Yin-Goan, G.-Z. Chen, D. M. Shin, L. Yang, A. N. Young, M. D. Wang and S. Nie, *Nat. Biotechnol.*, 2008, **26**(1), 83.
- 6 P. Anger, A. Feltz, T. Berghaus and A. J. Meixner, *J. Microsc. (Oxf.)*, 2005, **209**(3), 162.
- 7 B. Ren, B. Pettinger, G. Picardi, R. Schuster and G. Ertl, *Angew. Chem., Int. Ed.*, 2005, **44**(1), 139.
- 8 K. Kneipp, A. S. Haka, H. Kneipp, K. Badizadegan, N. Yoshizawa, C. Boone, K. E. Shafer-Peltier, J. T. Motz, R. R. Dasari and M. S. Feld, *Appl. Spectrosc.*, 2002, **56**(2), 150.
- 9 M. B. Wabuyele, F. Yan, G. D. Griffin and T. Vo-Dinh, *Rev. Sci. Instrum.*, 2005, **76**, 63710.
- 10 J. Kneipp, H. Kneipp, M. McLaughlin, D. Brown and K. Kneipp, *Nano Lett.*, 2006, **6**(10), 2225.
- 11 J. Kneipp, H. Kneipp, W. L. Rice and K. Kneipp, *Anal. Chem.*, 2005, **77**(8), 2381.
- 12 H.-W. Tang, X. B. Yang, J. Kirkham and D. A. Smith, *Anal. Chem.*, 2007, **79**(10), 3646.
- 13 R. J. Stokes, A. Ingram, J. Gallagher, D. R. Armstrong, W. E. Smith and D. Graham, *Chem. Commun.*, 2008, 567.

-
- 14 K. Faulds, F. McKenzie and D. Graham, *Angew. Chem., Int. Ed.*, 2007, **46**, 1829.
- 15 R. J. Stokes, A. Macaskill, P. J. Lundahl, K. Faulds, W. E. Smith and D. Graham, *Small*, 2007, **3**(9), 1593.
- 16 K. Kneipp, H. Kneipp, I. Itzkan, R. R. Dasari and M. S. Feld, *Chem. Rev.*, 1999, **99**, 2957.
- 17 J. Caamano, J. Alexander, L. Craig, R. Bravo and C. A. Hunter, *J. Immunol.*, 1999, **163**, 4453.

Quantitation of biomolecules conjugated to nanoparticles by enzyme hydrolysis†

Fiona McKenzie,‡ Victoria Steven,‡ Andrew Ingram and Duncan Graham*

Received (in Cambridge, UK) 23rd December 2008, Accepted 16th March 2009

First published as an Advance Article on the web 31st March 2009

DOI: 10.1039/b823057a

A novel method for quantifying biomolecules immobilised onto gold and silver nanoparticles is reported; fluorescent-labelled antibodies and DNA are hydrolysed on the surface of the nanoparticles by the addition of trypsin and DNase I, respectively, resulting in the release of the quantifiable fluorescent label into the bulk solution.

Noble metal nanoparticles are finding much use in bioanalytical applications due to their near-field and far-field optical properties. Their intense colours, arising from their capacity to strongly absorb and scatter light at the plasmon resonance wavelength, renders them highly suitable as staining and visualisation agents^{1,2} and for sensing in plasmon resonance^{3,4} and SERS detection techniques;^{5,6} whilst their inert nature and ability to be naturally internalised by cells means they are finding use in the delivery of molecules.^{7,8}

Nanoparticles can be functionalised with a variety of biomolecules including proteins,⁹ antibodies^{10,11} and DNA¹² using several different conjugation techniques such as electrostatic adsorption,^{13,14} thiol-gold interactions¹² and *via* nanoparticle surface ligands.^{15,16} However, it is important that the resultant conjugate is adequately characterised for each method and specific biomolecule. Protein structures are susceptible to denaturation and nanoparticle conjugation has been shown to affect the protein structure,^{17,18} whilst excessive biomolecule coverage can reduce functionality due to steric crowding.¹⁹ In addition to controlling biomolecule coverage to maintain functionality, it is important to quantify numbers of adsorbed biomolecules to determine the response per immobilised biomolecule.

Characterisation has been achieved for protein nanoparticle conjugates using fluorescence resonance energy transfer (FRET),²⁰ stepwise photobleaching,²¹ and adsorption isotherms.¹⁷ Absorption spectroscopy has also been used for quantitation of immobilised protein molecules by subtracting the nanoparticle contribution from the extinction spectrum of the conjugated nanoparticles¹⁸ and also by analysis of protein concentration remaining in the bulk solution following conjugation to nanorods.¹⁰ This method is less than ideal as it requires post-analysis data correction or observation of a decrease in the extinction intensity. Demers *et al.* developed a method for quantifying numbers of single stranded DNA

molecules on gold nanoparticles by incorporating a fluorescent label at the terminus of the DNA sequence.¹⁹ DTT was used to displace the surface-bound strands allowing quantitation by fluorescence spectroscopy. This technique is simple and sensitive however it relies on the competition of ligands for the nanoparticle surface and in cases where both types of ligands (the DNA and the displacing molecule) have a similar affinity for the surface, an equilibrium may be established where displacement of the fluorescent-labelled biomolecule is not entirely efficient.

This communication presents a method for quantifying biomolecules attached to gold and silver nanoparticles which utilises enzyme hydrolysis of the biomolecular structure. Only one bond needs to be hydrolysed to release the fluorescent label into the bulk solution and therefore 100% efficiency of the enzyme is not required for this method to be effective. Since this is not a displacement technique, it is not reliant on which species has a greater affinity for the nanoparticle surface which provides greater flexibility in terms of the range of surface-bound species that can be quantified. This method may be applied to any fluorophore-labelled biomolecule. To demonstrate this, we have used a fluorescein isothiocyanate labelled anti leukocyte function associated antigen-1 (LFA-1) and FAM labelled thiol-DNA.

The anti LFA-1 was conjugated to gold and silver nanoparticles using a cyclic disulfide linker incorporating a surface-enhanced resonance Raman scattering (SERRS) active near-infrared chromophore (Fig. 1).²² Addition of DTT to anti LFA-1 FITC conjugated to gold, for use in the Demers quantitation method,¹⁹ did not induce aggregation of the nanoparticles which is the usual indication that the DTT has displaced the biomolecule and has rendered them unstable in the conjugation buffer. Fig. 2 illustrates the extinction spectrum for gold nanoparticles modified with the linker that had been incubated with DTT. The λ_{max} and peak width for the plasmon resonance extinction remains relatively

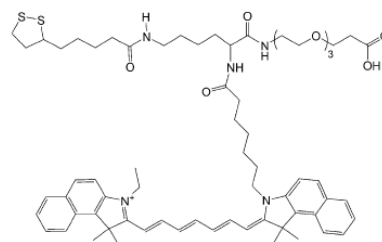


Fig. 1 Cyclic disulfide linker used to conjugate biomolecules to nanoparticle surfaces.

Centre for Molecular Nanometrology, WestCHEM, Pure and Applied Chemistry, University of Strathclyde, 295 Cathedral Street, Glasgow, UK G1 1XL, E-mail: duncan.graham@strath.ac.uk;

Tel: +44 (0)141 548 4701

† Electronic supplementary information (ESI) available: Experimental details. See DOI: 10.1039/b823057a

‡ These authors contributed equally to this work.

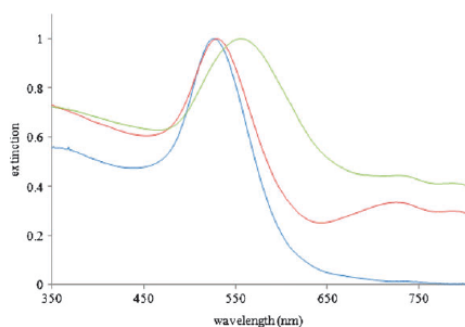


Fig. 2 UV-visible spectra of unmodified gold nanoparticles (blue), linker-modified nanoparticles incubated with DTT in 0.1 M PBS (red), and linker-modified nanoparticles incubated with trypsin in 0.1 M PBS (green). The broad absorbance ~ 700 nm corresponds to the near-infrared linker.

unchanged, confirming that the nanoparticles still exist in a monodisperse state. It was therefore assumed that due to the stability of the resultant conjugate afforded by the cyclic disulfide linker, the DTT was unable to displace the biomolecule. There has been significant effort to develop surface complexing linkers to improve the stability of biomolecule conjugates in bioapplications, therefore it is important that a technique can be employed that is sufficient in characterising these superior particles. DTT was substituted with trypsin, an enzyme that hydrolyses peptide backbones following lysine and arginine residues. In this approach, the fluorescent label is released upon digestion of the biomolecule instead of the entire biomolecule, including the surface complexing group, being

displaced from the surface (Fig. 3). The addition of trypsin to linker-modified nanoparticles results in a shift and broadening of the plasmon resonance peak (Fig. 2), presumably due to neutralisation of the repulsive electrostatic charges on the nanoparticle surface.

Comparison of the concentration of nanoparticles and fluorescent label allows quantitation of the number of biomolecules per nanoparticle. This is shown for anti LFA-1 FITC on gold nanoparticles in Fig. 4. The number of anti LFA-1 FITC molecules per 13 nm Au nanoparticle was found to be 0.21 ± 0.02 (Table 1). This suggests that some nanoparticles are not functionalised with antibody which is consistent with data that indicates polyvalent biomolecule functionalisation follows a Poisson distribution.²⁰ To corroborate this technique, the DTT displacement method was also performed for anti LFA-1 FITC conjugated to silver nanoparticles. Silver nanoparticles functionalised with protein *via* the cyclic disulfide linker are less stable than the analogous gold nanoparticles and therefore the linker may be displaced from the surface.²² The number of anti LFA-1 FITC molecules per 35 nm silver nanoparticle, using the DTT displacement method, was found to be 1.82 ± 0.10 . This was in close agreement with the number calculated using the trypsin hydrolysis method: 1.85 ± 0.50 (Table 1).

The technique was also applied to DNA functionalised nanoparticles. Quantitation of FAM labelled DNA strands on gold nanoparticles was achieved using the endonuclease, DNase I. DNase I catalyses the hydrolysis of phosphodiester linkages in the DNA backbone, preferentially adjacent to pyrimidine nucleotides. Hydrolysis of any bond along the DNA molecule will allow the release of the fluorescein label into the bulk solution. Again, the calculated number of DNA

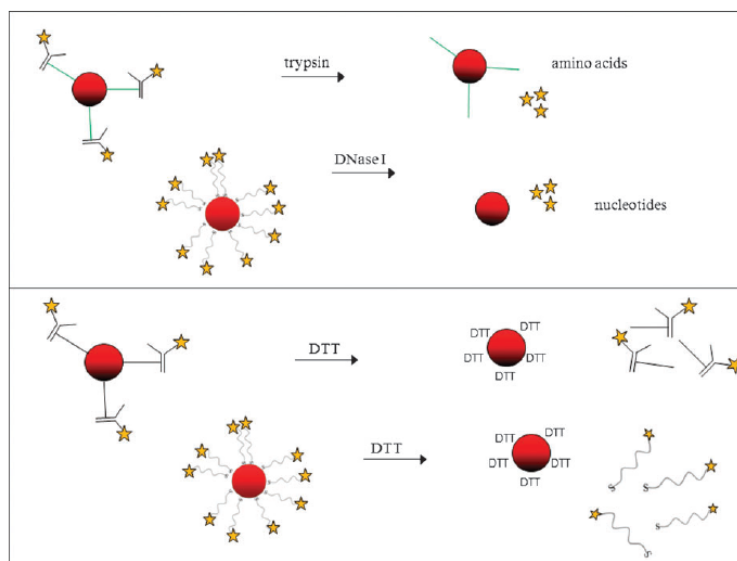
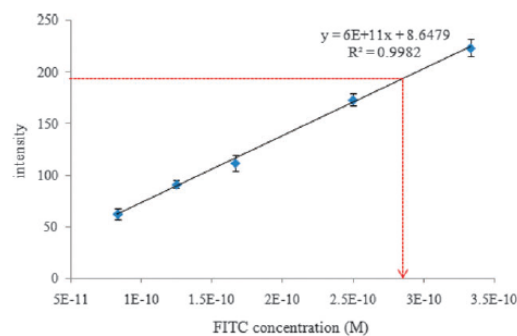


Fig. 3 Enzyme hydrolysis method (top): the trypsin and DNase I will hydrolyse the antibodies and DNA, respectively, leaving the surface linker in-tact with the nanoparticle surface. DTT displacement method (bottom): the DTT has a higher affinity for the nanoparticle surface than the linkers and biomolecules so it will displace them.



sample	fluorescence intensity	FITC concentration using calibration equation	concentration prior to sample dilution	nanoparticle concentration	antibodies per nanoparticle
A	205.84	3.29×10^{-10}	9.13×10^{-10}	3.87×10^{-9}	0.23
B	155.83	2.45×10^{-10}	6.81×10^{-10}	3.26×10^{-9}	0.21
C	184.21	2.93×10^{-10}	8.13×10^{-10}	4.21×10^{-9}	0.19
D	168.02	2.66×10^{-10}	7.38×10^{-10}	3.61×10^{-9}	0.20
E	195.19	3.11×10^{-10}	8.64×10^{-10}	4.05×10^{-9}	0.21

Fig. 4 Calibration graph for FITC-labelled anti LFA-1 illustrating the intensity for unknown sample C. The anti LFA-1 FITC concentration was determined for each sample using the calibration equation. Evaluation of the number of antibodies per nanoparticle was achieved by dividing the value for the antibody concentration by the nanoparticle concentration.

Table 1 Calculated number of FITC labelled anti LFA-1 molecules and FAM labelled oligonucleotides immobilised onto Au and Ag nanoparticles

Method	Number of antibodies per Au NP	Number of antibodies per Ag NP	Number of oligonucleotides per Au NP
Enzyme hydrolysis	0.21 ± 0.02	1.85 ± 0.50	24.52 ± 1.26
DTT displacement	Not possible	1.82 ± 0.10	24.47 ± 1.49

strands adsorbed onto the nanoparticles using the enzyme digestion method was consistent with the values obtained using the DTT displacement method (Table 1).

In summary, we have presented a novel enzyme-based technique for quantifying biomolecules on nanoparticles. It allows quantitation when complexing groups of high surface affinity are used for conjugation of the biomolecule and displacement methods are unsuitable. It is possible that the accessibility of the incoming enzyme may be hindered for nanoparticles with high biomolecule surface coverage and as such may affect the efficiency of hydrolysis. However, the similarity between the calculated quantitation values for our nanoparticle conjugates indicates that the enzyme hydrolysis method technique is equally as effective for quantifying biomolecules on nanoparticles as the DTT displacement method and supersedes it in circumstances where biomolecules are unable to be displaced.

Notes and references

- I. O. Ellis, J. Bell and J. D. Bancroft, *J. Histochem. Cytochem.*, 1988, **36**, 121–124.
- M. De Waele, W. Renmans, E. Segers, V. De Valck, K. Jochmans and B. Van Camp, *J. Histochem. Cytochem.*, 1989, **37**, 1855–1862.

- N. Nath and A. Chilkoti, *J. Fluoresc.*, 2004, **14**, 377–389.
- A. J. Haes, D. A. Stuart, S. M. Nie and R. P. Van Duyne, *J. Fluoresc.*, 2004, **14**, 355–367.
- S. Nie and S. R. Emory, *Science*, 1997, **275**, 1102.
- K. Kneipp, Y. Wang, H. Kneipp, L. T. Perelman, I. Itzkan, R. R. Dasari and M. S. Feld, *Phys. Rev. Lett.*, 1997, **78**, 1667–1670.
- P. Ghosha, G. Hana, M. Dea, C. K. Kima and V. M. Rotello, *Adv. Drug Delivery Rev.*, 2008, **60**, 1307–1315.
- D.-R. Chen, C. H. Wendt and D. Y. H. Pui, *J. Nanopart. Res.*, 2000, **2**, 133–139.
- M.-E. Aubin-Tam and K. Hamad-Schifferli, *Biomed. Mater.*, 2008, **3**, 1–17.
- C. X. Yu and J. Irudayaraj, *Anal. Chem.*, 2007, **79**, 572–579.
- J. Y. Chang, H. M. Wu, H. Chen, Y. C. Ling and W. H. Tan, *Chem. Commun.*, 2005, 1092–1094.
- R. Elghanian, J. J. Storhoff, R. C. Mucic, R. L. Letsinger and C. A. Mirkin, *Science*, 1997, **277**, 1078–1081.
- L. A. Dykman, V. A. Bogatyrev, B. N. Khlebtsov and N. G. Khlebtsov, *Anal. Biochem.*, 2005, **341**, 16–21.
- W. D. Geoghegan and G. A. Ackerman, *J. Histochem. Cytochem.*, 1977, **25**, 1187–1200.
- R. L. Letsinger, R. Elghanian, G. Viswanadham and C. A. Mirkin, *Bioconjugate Chem.*, 2000, **11**, 289–291.
- J. A. Dougan, C. Karlsson, W. E. Smith and D. Graham, *Nucleic Acids Res.*, 2007, **35**, 3668–3675.
- A. A. Vertegel, R. W. Siegel and J. S. Dordick, *Langmuir*, 2004, **20**, 6800–6807.
- M.-E. Aubin-Tam, H. Zhou and K. Hamad-Schifferli, *Soft Matter*, 2008, **4**, 554–559.
- L. M. Demers, C. A. Mirkin, R. C. Mucic, R. A. Reynolds, R. L. Letsinger, R. Elghanian and G. Viswanadham, *Anal. Chem.*, 2000, **72**, 5535–5541.
- T. Pons, I. L. Medintz, X. Wang, D. S. English and H. Mattoussi, *J. Am. Chem. Soc.*, 2006, **128**, 15324–15331.
- D. Casanova, D. Giaume, M. Moreau, J.-L. Martin, T. Gacoïn, J.-P. Boilot and A. Alexandrou, *J. Am. Chem. Soc.*, 2007, **129**, 12592–12593.
- F. McKenzie, A. Ingram, R. J. Stokes and D. Graham, *Analyst*, 2009, **134**, 549–556.

Controlled assembly of SERRS active oligonucleotide–nanoparticle conjugates†

Fiona McKenzie and Duncan Graham*

Received (in Cambridge, UK) 2nd July 2009, Accepted 20th August 2009

First published as an Advance Article on the web 2nd September 2009

DOI: 10.1039/b913140j

A novel method for the preparation of SERRS active oligonucleotide–nanoparticle conjugates is described, offering significant advantages over previously reported techniques in terms of versatility and ease of preparation.

In recent years, several strategies have emerged for the rational assembly of nanomaterials, in particular metal nanoparticles.^{1–4} One effective route for assembly utilises oligonucleotides due to their favourable properties.^{5–10} A great degree of control can be exerted over the interparticle distance due to the ability to synthesise oligonucleotide sequences of discrete lengths in an automated fashion, and the oligonucleotides can be programmed to assemble by manipulation of the temperature, electrolyte concentration and pH.^{8,10,11} Another advantage for the use of oligonucleotides is their inherent molecular recognition properties meaning they can pose as both the scaffold and the linker for construction of the assembly. It is for these reasons that oligonucleotides have become ideal candidates for generating nanoparticle assemblies and hence have attracted particular interest in this field.

One of the most effective approaches to monitoring the formation of nanoparticle networks is to exploit the striking optical properties of nanoparticles. The plasmon resonance wavelength of metallic nanoparticles red-shifts upon aggregation meaning assembly can be observed by extinction spectroscopy and colorimetrically by eye. Another approach is to exploit the near-field electromagnetic properties of metallic nanoparticles. Aggregated gold and silver nanoparticles are often used in surface enhanced (resonance) Raman scattering (SE(R)RS) applications to this effect. Electromagnetic coupling between adjacent nanoparticle spheres generates intense electromagnetic fields at the interparticle junctions; which ultimately results in large surface enhancement of Raman signals if a Raman-active analyte has been adsorbed onto the nanoparticle surface.

Assembly of oligonucleotide-modified nanoparticles has been monitored using SERRS previously by Graham and co-workers¹² and Nie and co-workers.¹³ Both methods involve labelling the nanoparticles with the SERRS active dye and then functionalising any remaining surface sites with thiol-modified oligonucleotides. The dye-labelling step is potentially hazardous as many commercially available dyes

incorporate positive charges and are hydrophobic in nature which is likely to induce irreversible aggregation of the nanoparticles. To avoid this problem, caution is required to control the surface coverage of the dye on the nanoparticle surface and the dye selection is limited. Qian *et al.* required adsorption of poly(ethylene)glycol (PEG) to aid stability of the nanoparticles¹⁵ and Graham *et al.* used an electrostatically neutral dye.¹² Here we report an approach for the preparation of dye-labelled oligonucleotide-functionalised silver nanoparticles that overcomes the stability issues associated with the aforementioned methods. The concentration of the dye does not necessarily need to be controlled and a wide variety of dye labels may be used, which is a significant advantage in terms of the multiplexing capabilities of the method.

Citrate-reduced silver nanoparticles were functionalised with thiol-modified locked nucleic acid (LNA) oligonucleotide sequences. The ribose sugars were modified to LNA as this significantly increases the melting temperature of the duplex.¹⁴ The SERRS measurements need to be performed at temperatures below the melting temperature and so the use of LNA allows shorter oligonucleotide sequences to be analysed at room temperature. It should be noted that a PEG spacer has been incorporated into the oligonucleotide sequences adjacent to the thiol modification. It has been reported that oligonucleotides featuring PEG spacers give rise to increased surface coverages compared to nucleotide spacer regions¹⁵ and so will significantly aid nanoparticle stability against non-specific aggregation which is a valuable asset in the preparation of the dye-labelled nanoparticle conjugates. Following oligonucleotide functionalisation, the nanoparticles were incubated with an aqueous solution of the SERRS active dye. To illustrate the versatility of this labelling method, four dyes were used utilising different means of surface attachment (ESI†): TAMRA isothiocyanate (ITC) and ROX ITC bind to the surface through the isothiocyanate moiety;¹⁶ Victoria Blue adsorbs *via* an electrostatic interaction with the nanoparticle's negatively charged citrate surface layer¹⁷ and the azo dye, 3,5-dimethoxy-4-(6'-azobenzotriazolyl)phenylamine, herein referred to as DABT PA, adsorbs through the benzotriazole group.¹⁸ By labelling the nanoparticle post-oligonucleotide functionalisation it means that the nanoparticles have already been afforded steric and electrostatic protection and therefore are more amenable to further modification. The stability of the dye-labelled DNA functionalised nanoparticles was assessed by inspection of the plasmon resonance peak wavelength and width in the UV-visible spectrum (ESI†), which is indicative of the monodispersity of the sample. The assembly design involves a split-probe arrangement as shown in Fig. 1. The melting temperature of the duplex is 45 °C and so upon addition of the

Centre for Molecular Nanometrology, Pure and Applied Chemistry, University of Strathclyde, 295 Cathedral Street, Glasgow, UK G1 1XL. E-mail: Duncan.Graham@strath.ac.uk

† Electronic supplementary information (ESI) available: Experimental; SERRS intensity time study; dye chemical structures; UV-visible spectrum of DNA nanoparticles. See DOI: 10.1039/b913140j

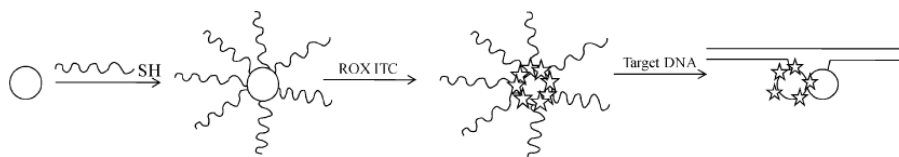


Fig. 1 Preparation and hybridisation of the dye-labelled LNA-functionalised silver nanoparticles in a head-to-head orientation. Only one of the oligonucleotide-nanoparticles is labelled with ROX ITC.

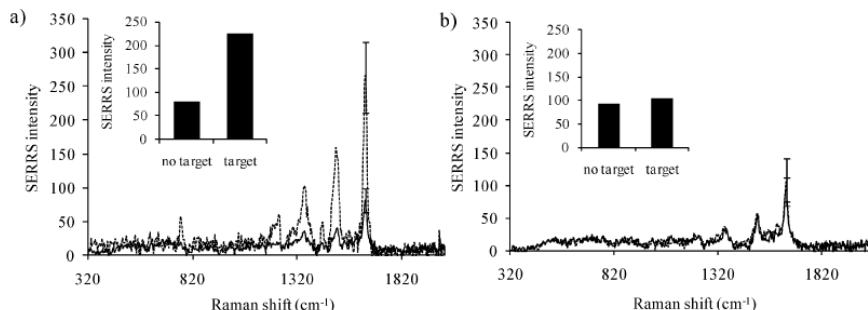


Fig. 2 SERRS spectra of ROX ITC labelled LNA oligonucleotide-silver conjugates before (solid line) and 5 minutes after (dotted line) the addition of (a) complementary target DNA sequence and (b) non-complementary DNA sequence. The probes were hybridised in a head-to-head format. The insets illustrate the SERRS intensities at 1647 cm^{-1} as bar graphs. Error bars represent the standard deviation of 5 replicate SERRS analyses.

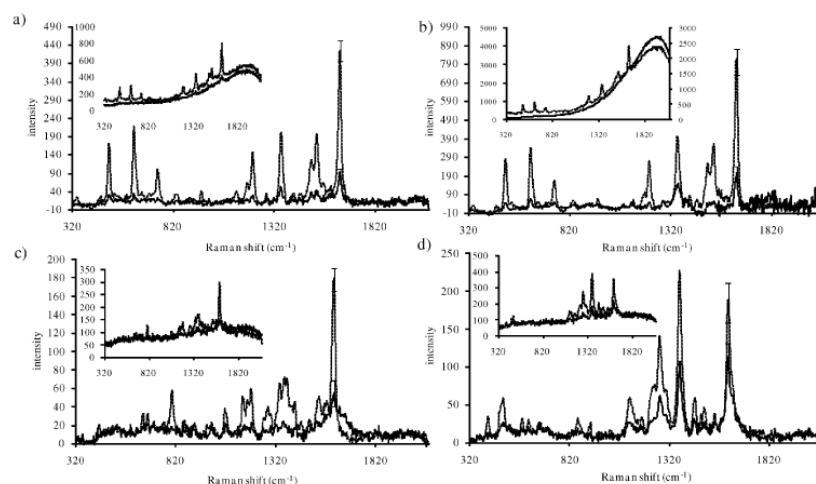


Fig. 3 SERRS spectra of LNA nanoparticle probes before (solid line) and 5 minutes after the addition of the complementary target (dotted line). (a) A single probe was labelled with TAMRA ITC; (b) both probes were labelled with TAMRA ITC; (c) a single probe was labelled with Victoria Blue; (d) a single probe was labelled with DABT PA. The probes were hybridised in a head-to-head format. The inset graphs illustrate the non-baseline corrected spectra. Error bars represent the standard deviation of 5 replicate SERRS analyses.

target DNA at room temperature, the probes hybridise to the target inducing aggregation of the nanoparticles.

There is a significant increase in SERRS intensity as early as 5 minutes following the addition of the target DNA (Fig. 2). This is due to the creation of intense electromagnetic fields, ‘hot-spots’, at the junctions of aggregated nanoparticles.¹⁹ Aggregation of the nanoparticles also brings the nanoparticle plasmon wavelength in resonance with the laser excitation and the absorption maximum of the dye label (ESI^+) which will contribute to an increased SERRS output. To illustrate that

the observed increase in SERRS intensity is the result of a specific Watson-Crick hydrogen bonding interaction between the oligonucleotide probes and the target sequence, the probes were also incubated with a non-complementary sequence. No increase in SERRS intensity was observed following the 5 minute incubation period (Fig. 2). This indicates that the nanoparticles must undergo hybridisation-induced aggregation before an increase in SERRS is recorded.

The spectra obtained from hybridisation of the nanoparticle probes labelled with other SERRS active dyes with the target

sequence are shown in Fig. 3. An increase in SERRS intensity was recorded for all dye labels although the magnitude of the increase is somewhat poorer for the azo dye, DABT PA. This is because DABT PA gives rise to well-defined SERRS spectra even when the nanoparticles are unaggregated, presumably because its absorption maximum wavelength (435 nm) is approximately coincident with the plasmon resonance wavelength of monodisperse silver nanoparticles (410 nm). The duplex was also assembled where both the nanoparticle probes were labelled with the reporter dye, and not just the one probe as shown in Fig. 1. The spectra for nanoparticle duplexes that had been labelled with TAMRA ITC at only one probe and both probes are shown in Fig. 3a and b. Although the absolute SERRS intensity is higher for the double labelled duplex, there is no significant difference between the positive and negative signal, indicating that labelling only one probe with the SERRS dye is as effective as labelling both. This is advantageous as it improves ease of preparation and has economical benefits.

The dye spectra shown in Fig. 2 and 3 were obtained using a head-to-head probe alignment as shown in Fig. 1. This probe orientation was chosen as hybridisation causes the nanoparticles to assemble closer together than the other orientations (Fig. 4). Electromagnetic coupling effects have been shown to decay exponentially as the interparticle distance grows larger;²⁰ therefore it is beneficial to reduce the interparticle distance as much as possible. Indeed, the head-to-head probe orientation has proven to be effective in producing large discriminations between signals corresponding to the absence

and presence of target DNA; however it is necessary to ascertain if this probe orientation is a crucial requirement in the assay design for successful signal activation. The SERRS spectra for the three duplexes of differing probe orientations are illustrated in Fig. 4. There appears to be no detrimental effect on the SERRS intensities when the other orientations are used. This is an interesting result as it indicates that there is not a strong dependence on interparticle distance on the electromagnetic coupling effect for these assemblies. However, it should be noted that the nanoparticle probes hybridise to form 3-dimensional networks and that the nanoparticles are not tethered to the probes through a rigid linker. The observed signal is the result of many electromagnetic coupling events and possibly is more representative of a small number of nanoparticles interacting over a shorter distance than the bulk majority.

In conclusion, we have detailed the preparation and use of dye-labelled oligonucleotide-functionalised silver nanoparticle probes for monitoring the assembly of a nanoparticle network using SERRS. The method for probe preparation has significant advantages over previous methods detailed in the literature in terms of versatility and ease of preparation. The SERRS output is also not restricted to a particular probe orientation, further illustrating the flexibility of this approach. Due to the specificity of the probes for the target, this method may also find use in diagnostic applications.

Notes and references

- 1 M. Brust, D. Bethell, D. J. Schffrin and C. J. Kiely, *Adv. Mater.*, 1995, **7**, 795–797.
- 2 W. Shenton, S. A. Davis and S. Mann, *Adv. Mater.*, 1999, **11**, 449–452.
- 3 S. Connolly and D. Fitzmaurice, *Adv. Mater.*, 1999, **11**, 1202.
- 4 J. J. Storhoff and C. A. Mirkin, *Chem. Rev.*, 1999, **99**, 1849–1862.
- 5 A. P. Alivisatos, K. P. Johnsson, X. G. Peng, T. E. Wilson, C. J. Loweth, M. P. Bruchez and P. G. Schultz, *Nature*, 1996, **382**, 609–611.
- 6 C. J. Loweth, W. B. Caldwell, X. H. Peng and A. P. Alivisatos, *Angew. Chem., Int. Ed.*, 1999, **38**, 1808–1812.
- 7 S. J. Park, A. A. Lazarides, J. J. Storhoff, L. Pesce and C. A. Mirkin, *J. Phys. Chem. B*, 2004, **108**, 12375–12380.
- 8 Y. H. Jung, K. B. Lee, Y. G. Kim and I. S. Choi, *Angew. Chem., Int. Ed.*, 2006, **45**, 5960–5963.
- 9 S. Xiao, F. Liu, A. E. Rosen, J. F. Hainfeld, N. C. Seeman, K. Musier-Forsyth and R. A. Kiehl, *J. Nanopart. Res.*, 2002, **4**, 313–317.
- 10 C. A. Mirkin, R. L. Letsinger, R. C. Mucic and J. J. Storhoff, *Nature*, 1996, **382**, 607–609.
- 11 R. C. Jin, G. S. Wu, Z. Li, C. A. Mirkin and G. C. Schatz, *J. Am. Chem. Soc.*, 2003, **125**, 1643–1654.
- 12 D. Graham, D. G. Thompson, W. E. Smith and K. Faulds, *Nat. Nanotechnol.*, 2008, **3**, 548–551.
- 13 X. Qian, X. Zhou and S. Nie, *J. Am. Chem. Soc.*, 2008, **130**, 14934–14935.
- 14 J. Wengel, *Acc. Chem. Res.*, 1999, **32**, 301–310.
- 15 S. J. Hurst, A. K. R. Lytton-Jean and C. A. Mirkin, *Anal. Chem.*, 2006, **78**, 8313–8318.
- 16 W. E. Doering and S. Nie, *Anal. Chem.*, 2003, **75**, 6171–6176.
- 17 C. H. Munro, W. E. Smith, M. Garner, J. Clarkson and P. C. White, *Langmuir*, 1995, **11**, 3712–3720.
- 18 D. Graham, G. McAnally, J. C. Jones and W. E. Smith, *Chem. Commun.*, 1998, 1187–1188.
- 19 J. M. McMahon, A.-I. Henry, K. L. Wustholz, M. J. Natan, R. G. Freeman, R. P. Van Duyne and G. C. Schatz, *Anal. Bioanal. Chem.*, 2009, **394**, 1819–1825.
- 20 Z. Zhu, T. Zhu and Z. Liu, *Nanotechnology*, 2004, **15**, 357–364.

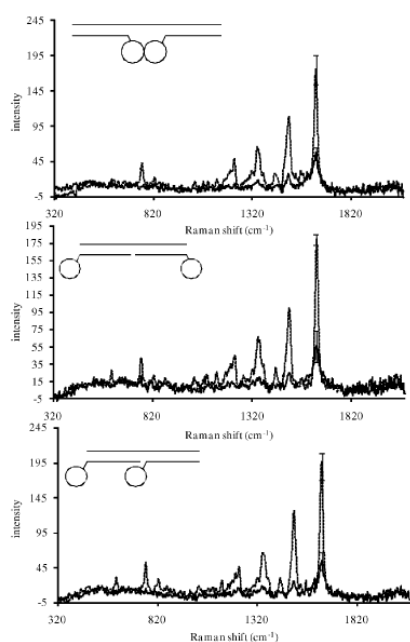


Fig. 4 SERRS spectra of ROX ITC-labelled LNA nanoparticle probes in different probe orientations before (solid line) and 5 minutes after the addition of the complementary target (dotted line).